Department of Chemical Engineering

The Settling of Spheres in Viscoplastic Fluids

Monica Gumulya

This thesis is presented for the Degree of
Doctor of Philosophy
of
Curtin University of Technology

November 2009

Declaration

To the best of my knowledge and belief this thesis contains no material previously published by any other person except where due acknowledgement has been made.

This thesis contains no material which has been accepted for the award for any other degree or diploma at any other university.

Signature:

Date:

LIST OF PUBLICATIONS

Journals

Gumulya, M. M., Horsley, R. R., & Wilson, K. C. (2007). The settling of consecutive spheres in viscoplastic fluids. *International Journal of Mineral Processing, 82*(2), 106-115.

Lichti, D. D., Gumulya, M. M., & Horsley, R. R. (2009). Determination of trajectories of metallic spheres settling in non-Newtonian fluids. *The Photogrammetric Record, 24*(125), 37-50.

Seminars

Gumulya, M. M. The settling of consecutive spheres in viscoplastic fluids. Curtin Engineering Faculty Research Colloquium. Curtin University of Technology, June 6, 2007, Perth, Australia.

ABSTRACT

In this thesis, several significant contributions have been made towards the understanding of the flow behaviour of viscoplastic fluids and the settling behaviour of particles in these fluids. The attainment of this knowledge is highly crucial for the development of large-scale simulations of the movement of particles in tertiary grinding circuits, through which effective cost and resource saving strategies for the design and operation of these highly resource-demanding unit processes could be developed.

To achieve the underlying objective of this thesis, the settling-sphere problem was approached using both experimental and numerical techniques. Experimentally, the flow behaviour of the viscoplastic slurries was represented by viscoplastic (aqueous) solutions of polyacrylamide. The settling behaviour of two spheres, using two different configurations of initial sphere positions, was then examined. In the first configuration, the two spheres are vertically-aligned, i.e. one sphere is released following the flow path of another sphere that has been released some time earlier into the fluid medium. In the second configuration, the two spheres are horizontally aligned, with a set distance apart, and released simultaneously into the viscoplastic solution. One of the major accomplishments achieved during the design of these experiments was the development of a stereo-photogrammetry sensor system, through which the 3D movement of spheres falling through the fluid could be determined to within ~ 1.5 mm accuracy.

The numerical part of this study was conducted using Computational Fluid Dynamics (CFD) technique. Based on the Volume of Fluid (VOF) method, the settling particles were represented by fluids of very high viscosity (~ 400 – 1000 Pa.s). By implementing appropriate discretisation and approximation methods, the effects of numerical smearing and diffusion, as well as the level of deformation in the settling particles, could be minimised. A time-dependent estimation of the flow behaviour of the test fluids was then developed and implemented into this numerical scheme, using a series of User Defined Functions (UDFs).

The development of the UDFs in the CFD analysis was based on the results of the rheometric assessment of the test fluids, through which it was found that these solutions possess a level of time dependency resulting from both thixotropy and elasticity. A new fluid model was thus developed, based on a scalar parameter that represents the integrity of the structural network configuration, resulting from the hydrogen bonding between the polyacrylamide and water molecules in the fluid. Although the resulting fluid model does not exclusively feature a yield stress value, the results of a series of dynamic analyses conducted on this model were found to be similar to those found experimentally, in which fluids that were initially 'undisturbed' or intact in structure have been found to require the application of stresses that are significantly larger in magnitude for the initiation of its deformation than in cases where the structure of the fluid is already deformed. Due to these dynamic characteristics, in which the fluid model seems to feature yield stress-like quality that dissipates once the 'structure' of the fluid has been deformed due to the application of shear, this fluid model was termed 'semi-viscoplastic'.

Using the analytical techniques outlined above, two significant contributions were made towards the understanding of the settling behaviour of particles in viscoplastic fluids. First, the settling velocity of particles falling in the fluid medium was found to be highly dependent on the structural condition of the fluid, i.e. whether it has recently been subjected to shear or whether sufficient time has been allowed for the fluid to recover its original viscous parameters. Based on this finding, a new generalised correlation was developed, through which predictions of the settling velocity of particles falling in fluids of various structural conditions can be made with much greater accuracy than before. The second contribution was in the understanding of the interaction tendencies between spheres that are settling in close proximity to each other. Through experimental and numerical analyses, it was found that the interaction tendencies of the particles are highly dependent on the elastic properties of the fluids. Correlations relating the tendencies of the spheres to interact with the elastic and viscous properties of the fluid were then developed. Through both of these contributions, aspects that are critical for the understanding of the motion of solid bodies in grinding circuits have been addressed.

ACKNOWLEDGEMENTS

I would like to firstly express my deepest gratitude towards my supervisor, Emeritus Professor Richard Horsley, for his unconditional support and encouragement in conducting this project. It is due to his encouragement that I decided to undertake this ambitious project a few years ago, and without his perseverance and guidance, I would not be able to complete the formidable task of completing this PhD thesis.

I would also like to thank Associate Professor Vishnu Pareek for the opportunity to undertake this work under his supervision, as well as his guidance in my understanding of CFD. His continual encouragement and assurance throughout this PhD project were invaluable to me.

My deepest gratitude also goes towards Dr. Derek Lichti, for his help in the design of the stereo-photogrammetry system. This system is highly crucial for the experimental part of this thesis, so without his help, I would not be able to complete this project. I'm very sorry for the delay in writing up those promised research papers – they will be done as soon as I get this thesis completed!

I would like to thank Professor Ken Wilson, for his continuous feedback and ideas during the early stages of this project. Through this contribution, Professor Wilson has guided me in developing a level of technical curiosity and confidence in tackling scientific analyses. I am also deeply grateful for the guidance of Professor John Reizes during the period of my CFD work. His patience and intelligence in explaining the various difficult concepts of CFD, despite the fact that we have actually never met face to face, have given me inspiration and enlightenment in solving the numerous problems of this thesis.

Many other individuals have contributed towards the completion of my PhD. The support given by the technical staff in the Faculty of Engineering in resolving various issues related with my experiments, notably Mr. John Murray, Mr. Jeff Pickles, Mr. Derek Oxley, and Ms. Karen Haynes, were highly invaluable to me. I

would also like to especially acknowledge the help of Mr. Peter Bruce, for his design and construction of the ball droppers. Without his skills and talents in developing these instruments, I would not be able to perform all those experiments. The help of the secretarial staff, namely Ms. Brenda Tipping, Ms. Jann Bolton, Ms. Simret Habtemariam, Ms. Naomi Tokisue, and Ms. Zalila Abdul Rahman, is also highly appreciated. I would like to thank the support of the IT staff in Faculty of Engineering, especially Mr. Glenvill Abeywickrema and Ms. Alison Lynton, in resolving numerous computer related issues, particularly relating to the cluster! Finally, I'd like to thank the numerous project students that we've had over the years, without whose help, I would not be able to perform the numerous experiments that were required for this thesis: Debby Chua, Edmund Yap, Wahono Fok, and Dustin Browne, thank you all very much!

I wish to acknowledge the financial support of the Australian government, Curtin University, the School of Engineering, as well as the Department of Chemical Engineering, throughout the various stages of my PhD course. My particular thanks to Professor Moses Tade and Professor Ming Ang for their unconditional support, even when it seems that this project would take forever to finish.

Finally, I would like to thank my family and friends, particularly my parents and my sister, for supporting me throughout the difficult journey that we have all faced, particularly this year. Their prayers, dedication, love and support have given me the strength, not only in completing this formidable task of completing this thesis, but also in handling the various challenges in life.

Monica Gumulya

Curtin University of Technology
Perth, Australia
November, 2009

TABLE OF CONTENTS

LIST OF TABLES

Table A-1: The calibration parameters of the cameras used for the stereo-photogrammetry system..... 271

Table A-2: The resolved 3D co-ordinates (x, y, z) of one of the spheres (sphere A) in an experiment involving two chrome steel spheres (6.35 mm diameter) in 1.0% Floxit solution. (X_1, Y_1) and (X_2, Y_2) represent the 2D co-ordinates of sphere A from the perspectives of cameras 1 and 2, respectively..... 272

Table A-3: Error analysis of the stereo-photogrammetry system, indicated by the discrepancies in the resolved 3D co-ordinates presented in Table A-1 with the co-ordinates calculated based on: (I) (X_1+1.5875, Y_1) and (X_2, Y_2); (II) (X_1, Y_1) and (X_2+1.5875, Y_2); (III) (X_1+1.5875, Y_1) and (X_2+1.5875, Y_2)..... 272

LIST OF FIGURES

NOMENCLATURE

Symbol	Meaning	Page no. of first use
a, b, c	Constants	16
A	Surface area of sphere	202
$\vec{A}$	Combined form of the direction vector with the surface area of a control volume	131
A_P	Area affected by the drag force (m^2)	36
Bi_{HB}	Bingham number, calculated based on the fit parameters of the Herschel-Bulkley model	43
c	Focal length of camera	73
C_1, C_2	Fit parameters for the calculation of equivalent viscosity (-)	187
C_D	Drag coefficient (-)	36
C_{D0}	The drag coefficient of the first sphere the settling experiment of two consecutive spheres (-)	51
d	Characteristic linear size of the experiment (m)	19
d	Diameter of column (m)	46
D	Diameter of sphere (m)	37
d_0	Initial distance between two spheres (in the experiment of horizontally-aligned spheres) (m)	69
De	Deborah number (-)	19
d_H	Horizontal distance between two spheres (in the experiment of two horizontally-aligned spheres) (m)	78
E	Elastic modulus (Pa)	20
E′	Tensile storage modulus (Pa)	18
E″	Tensile loss modulus (Pa)	18
El	Elasticity number	46
f	face enclosing control volume v	132
$\vec{F}$	Gravitational and external body forces (momentum equation)	128
F_D	Drag force (N)	36

FW_{12}	Submerged weight of two aggregated spheres (kg)	202
g	Acceleration due to gravity (m/s^2)	35
G	Shear modulus (Pa)	25
G′	Shear storage modulus (Pa)	18
G″	Shear loss modulus (Pa)	18
H	Distance from the inside face of the column to an object (m)	74
J_0	Recoverable compliance of fluid	110
k	Constant	14
k_1, k_2	Rate constants of structural breakdown and build-up in the microstructural/kinetic approach for thixotropy	24
(k_1, k_2, k_3)	Constants representing the radial distortion of the cameras due to imperfections in the lenses	73
k_N	Constant for the power-law fit of the first normal stress of the fluid	112
ℓ	The distance between the centre gravities of two settling spheres (m)	51
ℓ_C	Vertical distance required for two spheres to attract and converge (in the experiment of horizontally-aligned spheres) (m)	219
L	Distance from the camera perspective centre to the outside of the column (m)	74
m	Power constant	14
$\dot{m}$	Rate of mass transfer (kg/m^3)	129
m_N	Power constant for the power-law fit of the first normal stress of the fluid	112
n	Constant	16
n	Number of bonds or links between particles (direct microstructural model of thixotropy) (-)	24
N	Number of measurements	95
N	Fit parameter (-)	187
n_0	Number of bonds of links between particles in an undisturbed structure (direct microstructural model of thixotropy) (-)	24

n_1, n_2, n_3	Refraction indices of air, Perspex, and Floxit solution, repectively	74
N_1	First normal stress function, $\tau_{11} - \tau_{22}$ (Pa)	18
N_2	Second normal stress function, $\tau_{22} - \tau_{33}$ (Pa)	18
n_{crit}	Critical value of the number of bonds between the particles, above which no flow would occur (direct microstructural/kinetic approach for thixotropy) (-)	24
p	Pressure (Pa)	35
P	Parameter representing the level of plasticity of a fluid material (-)	107
(P_1, P_2)	Constants representing the decentring (or tangential) distortion of the cameras due to imperfections in the lenses	73
Q	Amount of fluid displaced due to the settling movement of a sphere (m^3/s)	230
Q_A	Modified dynamic parameter for the calculation of drag coefficient of a sphere settling in yield-stress fluid	43
r	2D radial position of an object from the principal point of a camera	74
r	Polar co-ordinates of the spheres on the horizontal axes	211
R	Radius of the cone (m)	28
R	Radius of sphere (m)	36
R_{ij}	Rotation matrix with element i,j (photogrammetry)	73
Re	Reynolds number (-)	28
Re*	Shear Reynolds number (-)	44
Re_{PL}	Reynolds number, calculated based on the power-law fluid model (-)	37
Re_R	Rotational Reynolds number (rheometer) (-)	28
Reff	Effective cone-and-plate radius (rheometer)	29
S	Source or sink term of the momentum conservation equation	131
t	Time (s)	19
t	Time lapse since the fluid was sheared by the settling movement of a preceding sphere (in the experiment of two	55

	vertically-aligned spheres) (s)	
T	Measured torque in rheometer (N.m)	28
t*	Dimensionless form of the t (in the experiment of two vertically-aligned spheres) (-)	55
t_C	Column wall thickness (m)	74
T_{act}	Actual torque in rheometer (N.m)	28
v	Control volume	130
V	Velocity (m/s)	19
V*	Shear velocity (m/s)	44
V_2	Settling velocity of the second (trailing) sphere (in the experiment of two vertically-aligned spheres) (m/s)	55
V_H	Rate of convergence between two settling spheres (in the experiment of two horizontally-aligned spheres) (m/s)	229
V_t	Terminal velocity (m/s)	45
W_D	Hydraulic diameter of column (m)	152
We	Weissenberg number (-)	19
We_G	Representative Weissenberg number of the sheared fluid within the gap between two settling spheres (-)	232
(x, y, z)	3D Coordinates of an object	73
(x_0, y_0, z_0)	3D Coordinates of the camera perspective centre in the object frame	73
(X, Y)	Photo-coordinates of an object in the image frame	73
(X_P, Y_P)	Photo-coordinates of the projection of the camera perspective centre in the image frame	73
Y	Drag correction factor for particles settling in non-Newtonian fluids (-)	37
Y_G	Critical ratio of fluid yield stress over the buoyant weight of the particle, below which the particle would not settle (-)	41

Greek letters

Symbol	Meaning	Page no. of first use
α	Cone angle of rheometer (degrees)	27
α	Rheogram shape factor (-)	52
α	Volume fraction	125
β	Constant that takes into account the path interference created due to the orientation of two aggregated spheres, for the calculation of mean surficial stress ($\bar{\tau}_{12}$) (-)	52
$\beta_{identical}$	Constant that takes into account the path interference created due to the orientation of two aggregated (identical spheres) (-)	204
tan δ	Loss tangent (-)	18
δr	Refraction correction factor for the 2D radial position of the object from the principal point of a camera	74
δR	Radius error in cone-and-plate rheometer	29
Δx	Width of control volume or mesh (m)	133
ε	Regularisation parameter (-)	22
ε	Under-relaxation parameter (-)	141
η_0	Zero shear viscosity (SAOS measurement) (Pa.s)	110
θ_1, θ_2, θ_3	Angle between the point ray of an object and the surface normal at a media interface (^{o})	74
γ	Shear strain (-)	19
γ_e	Elastic strain (-)	25
$\dot{\gamma}$	Shear rate (1/s)	13
$\dot{\gamma}_G$	Average shear rate within the gap between two settling spheres (1/s)	231
$\dot{\gamma}_{min}$	Estimated minimum rate of shear due to the movement of a particle through a column (1/s)	152
Γ	Diffusion coefficient	131

φ	Characteristic relaxation time due to fluid elasticity (s)	19
φ	Scalar variable	131
κ	Rate of deformation in structure parameter, λ (-)	25
λ	Scalar variable, representing the integrity in the structure of a material or the extent of breakdown in structure (-)	25
$\bar{\lambda}_0$	Representative fluid structure parameter below a settling sphere (-)	183
λ_{ss}	Fluid structure parameter when sheared under steady-state conditions (-)	92
$\bar{\lambda}_{eff}$	Representative fluid structure parameter surrounding a settling sphere (-). This parameter reflects the equivalent viscosity of the fluid, μ_{eq}.	185
$\bar{\lambda}_{ss}$	Representative fluid structure parameter above a settling sphere (-)	183
μ	Viscosity (Pa.s)	13
μ_0	Limiting zero shear viscosity (Pa.s)	16
μ_s	Viscosity representing the 'solid' phase (Pa.s)	147
μ_A	Apparent (regularised) viscosity (Pa.s)	22
μ_C	Viscosity constant for Casson equation (Pa.s)	16
μ_{eq}	Equivalent Newtonian viscosity (Pa.s)	44
μ_N	Newtonian viscosity (Pa.s)	13
μ_{ss}	Fluid viscosity, measured under steady-state conditions (Pa.s)	92
μ_∞	Limiting high shear viscosity (Pa.s)	16
Ω	Rotational speed of the rheometer spindle (rad/s)	28
Ω	A variable for the calculation of β and $\bar{\tau}_{12}$ (-)	52
ρ	Density (kg/m^3)	28
ρ_s	Density of particle (kg/m^3)	41
ρ_f	Density of fluid (kg/m^3)	41
τ_{11}, τ_{22}, τ_{33}	Normal stresses in Cartesian coordinates (Pa)	18

τ	Shear stress (Pa)	2
τ_C	Casson yield stress (Pa)	16
τ_{HB}	Herschel-Bulkley yield stress (Pa)	16
τ_{ss}	Shear stress, measured under steady-state conditions (Pa)	91
τ_Y	Yield stress (Pa)	14
$\bar{\tau}$	Mean surficial shear stress (Pa)	45
$\bar{\tau}_{12}$	Mean surficial shear stress of two aggregated spheres (sphere 1 and 2) (Pa)	52
θ	Characteristic relaxation time in the viscous deformation of the fluid (s)	25
ω	Angular frequency (rad/s)	110
$(\omega, \varphi, \kappa)$	Rotational angles of the camera perspective centre around the X, Y, and Z axes, respectively	73
ψ_1	First normal stress coefficient ($Pa.s^2$)	18
ψ_2	Second normal stress coefficient ($Pa.s^2$)	18

Acronyms

CR = Controlled rate

CS = Controlled stress

CD = Controlled deformation

SAOS = Small amplitude oscillatory shear

3D = Three dimensional

2D = Two dimensional

CFD = Computational fluid dynamics

UDF = User defined functions

LVE = Linear visco-elasticity

FE = Finite element

FV = Finite volume

FD = Finite difference

PIV = Particle image velocimetry

LSE = Least squares estimation

RSQ = Pearson correlation coefficient (R^2)

SSE = Sum of squared error

MPM = Macroscopic particle model

CV = Control volume

PRESTO! = Pressure staggering option

PLIC = Piecewise linear interface construction

SIMPLE = Semi-implicit method of pressure-linked equations

SG = Specific gravity

Chapter 1 Introduction

1.1 Background

In the mineral processing industry, one of the customary stages of processing is the grinding and milling of mineral ores. At this stage, mined rocks, which have been primarily reduced in size through a series of crushing processes, undergo further reductions in size as they go through several stages of grinding and milling. Depending on the characteristics of the ores and rocks, as well as the required product size, equipment of various configurations and capacity can be used for this operation, most common of which are the rod, ball and stirred mills. In these pieces of equipment, rock particles, which are mixed with a suspending fluid medium (normally water), are subjected to compression, chipping and abrasion forces, as particles fall and collide with each other during the tumbling motion of the milling equipment.

The process of grinding has generally been accepted to be highly effective in reducing the sizes of mineral rocks and particles. Herbst et al. (2003) have noted that products as fine as 300 μm can be obtained from a primary grinding circuit, whereas product sizes of a few microns can be obtained after several stages of grinding and milling. However, these processes have also been known to have very low levels of efficiency and are highly demanding in both energy and resource requirements, e.g. in water consumption. Energy requirements of 5 – 25 kWh/tonne for a primary grinding circuit have been noted by Herbst et al. (2003), whereas in processes where very fine product sizes are required (± 1-2 μm), the energy consumption can be as high as 50 kWh/tonne. In turn, the efficiency of these processes generally ranges from 1 – 15% (Herbst et al., 2003). The improvement of the efficiency of these processes, therefore, is an imperative endeavour, which, if accomplished, can lead to significant reductions in the costs involved with the processes of the recovery and refinement of minerals.

To improve the efficiency of grinding processes, a detailed understanding of the motion of rocks and particles falling in the slurry medium is necessary. This is, therefore, the general aim of this research. Through this knowledge, the forces produced through the collision of particles, and the subsequent reduction in particle size, can be determined. Effective design of the milling equipment, as well as the control of its operational parameters, can then be developed based on the results of these calculations.

Most of the slurries and suspensions of fine particles that are utilised in mineral processing plants possess viscoplastic flow characteristics. The viscoplastic flow behaviour is unique in that a critical or minimum amount of force is required to deform the structure of the medium before it starts to flow. This condition of criticality is commonly termed as the yield stress. A typical example of this fluid flow behaviour can be seen in Figure 1-1, in which the rate of deformation exhibited by a sludge-type of material, as a function of the shear forces applied to it, has been presented. As can be seen in this graph, when the material is subjected to relatively low values of shear stress (τ < 13.0 Pa), no significant levels of deformation (represented here by shear rate) was produced. At higher values of shear stress, the material starts to flow and undergoes significantly higher rates of deformation.

To illustrate this flow behaviour, numerous fluid models have been proposed in the past, the most prominent of which include those of Bingham (1922), Herschel and Bulkley (1926), as well as Casson (1959). All of these models feature a constant value of yield stress, i.e. in cases where the fluid is subjected to shear stresses that are below this yield value, the rate of deformation is set to zero. The use of these fluid models for the analysis of pumped slurry pipelines has been examined by Slatter (1997), who found that the Herschel-Bulkley fluid model generally provides the best representation of the flow behaviour of the slurries. In the rheogram presented in Figure 1-1, the correspondence of the Herschel-Bulkley model towards the experimental data has been illustrated.

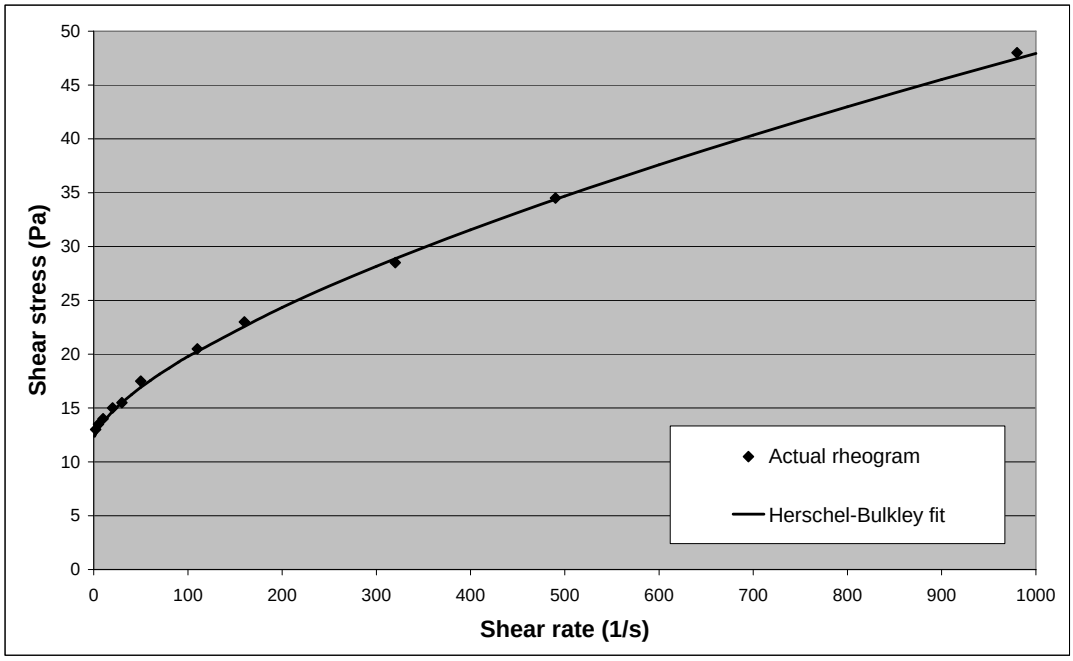

Figure 1-1: The typical rheogram of a viscoplastic material (adapted from Slatter (1997)).

In the flow problem involving the settling motion of particles in slurries and suspensions, the presence of a yield stress tends to hinder the motion of the particles that are falling in the fluid medium. This is such that if the net weight of the particle is insufficient to overcome the vertical component of the force caused by the yield stress of the fluid acting over the particle surface, the particle should theoretically stay suspended in the fluid for an indefinite length of time, and vice versa. The hindered motion of particles in slurries can thus be significantly affected by the magnitude of the yield stress.

Despite the fact that this settling problem has been studied relatively extensively in the past (prominent studies in this area include those of Ansley and Smith (1967), Atapattu et al. (1990), amongst many others), the prediction of the hindered motion of particles in viscoplastic fluids is a field that is full of uncertainties. In his extensive review of this flow problem, Chhabra (2007) has attributed these uncertainties towards the inaccuracies involved in the characterisation of the fluid flow behaviour. Particularly, the exact characterisation of the fluid flow close to the value of the yield stress has been found to be highly intricate and difficult to

measure accurately (Barnes & Walters, 1985; Nguyen & Boger, 1992). Moreover, the viscous parameters of viscoplastic materials have also been noted to be highly dependent on its shear history. This is demonstrated by the study of Atapattu et al. (1995), in which it was noted that the settling velocity of spheres falling in solutions of Carbopol tends to vary, depending on the number of preceding spheres that has been released into the fluid. Atapattu et al. (1995) observed that the settling velocity of the spheres only becomes constant after the fluid has been sheared by the movement of 4-10 spheres. These observations suggest that in the study of the steady settling behaviour of particles in viscoplastic fluids, particular attention needs to be given towards the shear history of the fluids. These factors therefore contribute towards the uncertainties associated with the analysis of the hindered motion of particles in viscoplastic fluids.

A satisfactory solution to the problem involving the effects of yield stress on the terminal (or steady-state) settling behaviour of spheres in viscoplastic fluids have recently been suggested by Wilson et al. (2004; 2003). By introducing the term 'equivalent viscosity', which can be determined directly from the rheogram of the fluid, Wilson and co-workers overcome the problems associated with the characterisation of the fluid flow behaviour that is normally calculated through idealised flow equations. Therefore, the terminal settling velocity of the particles can now be predicted relatively accurately based on the rheogram of the fluid.

Additional difficulties, however, still exist with the characterisation of the *unsteady* settling behaviour of the particles. In agreement with the observations of Atapattu et al. (1995), Gumulya et al. (2007) have determined that the falling motion of particles in viscoplastic fluids depends largely on the state of the fluid. This aspect of the fluid characteristics depends highly on the amount of time that has passed since the structure of the fluid was last disrupted by the motion of another particle. As a result, a particle that is released following the flow path of another particle tends to possess significantly higher settling velocities than the preceding one. This discrepancy in settling velocity has been attributed to the changes in the viscous parameters of the polyacrylamide solution as it undergoes a process of relaxation

and returns to its original configuration of viscous parameters, after it is sheared by the motion of the preceding sphere.

The changes in the viscous parameters of the fluid as suggested by Gumulya et al. (2007) imply that the fluid solutions used in their study possessed time-dependent rheological characteristics. This flow characteristic indicates that the fluid solutions may exhibit elasticity and/or thixotropy in addition to the viscoplastic behaviour. This is in agreement with the statement of Barnes (1999) as well as Møller et al. (2006), both of whom have indicated that most yield-stress fluids tend to possess elasticity as well as thixotropy, causing the shear response of the fluid to depend not only on the magnitude of the currently-applied shear forces, but also on the shear history of the fluid. The time frame associated with this phenomenon tends to vary widely, ranging from a few seconds to several days, depending on the relaxation characteristics of the fluid solutions after being subjected to shear forces.

Based on the discussion presented above, it can be seen that in order to fulfil the objectives of this project, a thorough examination of the flow behaviour of viscoplastic fluids, both under steady and unsteady conditions, is needed. Furthermore, numerous gaps still exist regarding the knowledge of the settling behaviour of particles in viscoplastic fluids. Particularly, aspects such as the unsteady motion of these particles, as well as the interaction of particles that are settling in close proximity to each other, are still largely unknown. In the following section, the strategy that has been adopted in tackling this flow problem, along with the framework and objectives that have been set to implement this strategy will be outlined.

1.2 Motivation

In this thesis, the focus of the study will be on the motion of *two spheres* that are settling in close proximity to each other. Through this study, it is hoped that more insights on the effects of inter-particle interaction and fluid recovery on the settling behaviour of the particles can be gained. The results of this study are hoped to

contribute towards the understanding of the hindered motion of particles in slurries commonly encountered in the mineral processing industry. The attainment of this knowledge will pave the way for large-scale simulations of the flow field in milling processes to be conducted, through which significant cost and energy saving strategies of these highly resource-demanding processes can be developed.

In performing the experiments, the flow characteristics of the slurries will be represented by dilute aqueous solutions of polyacrylamide that are commercially known as Floxit 5250L. These solutions have previously been identified to possess a significant yield-stress value as well as shear-thinning behaviour (Horsley, Horsley, & Wilson, 2004; Wilson & Horsley, 2004; Wilson et al., 2003), presenting typical flow characteristics of viscoplastic fluids. The use of these solutions in the sphere-settling experiments overcomes the problems posed by the opaque appearance of slurries, enabling the motion of the spherical particles to be observed through optical measuring devices (see Chapter 3). One of the measuring devices that have been utilised in this study include a stereo-photogrammetry system, through which the 3D movement of the particles can be measured at regular intervals during the experiment with an accuracy of ~ 1.5 mm (see Section 3.4.3 and Lichti et al. (2009)).

From the discussion presented in Section 1.1, it can be seen that the study of the settling behaviour of spheres in viscoplastic fluid needs to be preceded by a thorough examination of the fluid rheology. Furthermore, a fluid model that is able to present a closer representation of the true flow behaviour of the fluid solutions, including the time-dependent response of the fluids towards changes in the applied shear forces, needs to be implemented. The effects of these rheological characteristics on the settling behaviour of the spheres can then be examined. In doing so, the revised drag correlation suggested by Wilson et al. (2004; 2003), which enables the fall velocity of the particles to be directly predicted for a given value of shear Reynolds number, can be used as the basis of this analysis.

In examining the influence of the fluid rheological properties on the fall behaviour of the particles, two different configurations of initial sphere positions will be

considered. In the first configuration, the two spheres are vertically-aligned, i.e. one sphere is released following the flow path of another sphere, which has been released some time earlier, at the centre-line of the test column. This experimental work is a continuation of the work previously presented by Horsley et al. (2004) and Gumulya et al. (2007), where the examination has been confined to the settling of two identical spheres. In this study, spheres of varying densities and diameters will be incorporated to assess the effects of the shear history of the fluid on the particle settling behaviour. In the second configuration, the two spheres are horizontally-aligned and released simultaneously into the viscoplastic solution. Several different values of initial distance between the two spheres will be examined. This study is conducted in order to determine the effects of the fluid rheological properties on the interaction between the settling spheres.

To complement the analysis of the experimental data, a numerical study of the settling experiment will be conducted. The results of this approach are hoped to facilitate the resolution of many questions that cannot be found experimentally, such as the extent and shape of the region of moving fluid and the details of the velocity and stress fields surrounding the settling spheres.

Finally, in conducting this study, it should always be remembered that the rheological characteristics of polymeric solutions are often highly complex and intricate. As will be demonstrated later in Chapter 4, this complexity is such that the flow characteristics of the fluid solutions cannot be entirely captured by any of the fluid models available currently, regardless of their complexity and comprehensiveness in representing the rheometric results. As a result, in developing the fluid model, some degree of simplification of the actual flow behaviour has to be implemented. An example of this simplification is the use of a (non-elastic) viscoplastic fluid model to represent the flow behaviour of fluids that have been identified to possess low levels of elasticity. This is the case with the current study, as well as many other studies conducted in the field of a viscoplastic fluid. The appropriateness of this simplification for the flow problem being considered in this study, as well as the repercussions of this assumption on the

integrity of the experimental analysis, will be assessed by comparing the results of the numerical analysis with the observations of the experiments. Further comparisons will also be made with the results of other studies published in the literature.

The results of the analyses outlined above will be used towards the development of a set of correlations that are capable of relating the motion of particles settling in close proximity to each other, with the rheological characteristics of the fluid solutions. Through these correlations, predictions of the settling motion of spheres in viscoplastic fluids can be made with higher certainty than in the past.

1.3 Objectives

The primary objective of this thesis is to advance the understanding of the settling behaviour of spherical particles in viscoplastic fluids and determine the effects of fluid rheological properties on the motion of these particles. In summary, the major goals of this research project are:

1. To conduct a thorough examination of the rheological characteristics of the test fluid solutions used for this study, i.e. aqueous solutions of polyacrylamide (Floxit 5250L), and develop a suitable rheological model that can be appropriately implemented into the flow problem being considered in this research project.
2. To develop a system of experimental equipment and methodology, through which the settling motion of several particles falling from two different initial configurations (vertically-aligned and horizontally-aligned) can be examined accurately and reliably. In particular, in examining the settling behaviour of two horizontally-aligned spheres, the 3D positions of the spheres need to be determined at regular intervals during the experiment. As a result, a stereo-photogrammetry procedure, capable of measuring the positions of the spheres to within 1.5 mm level of accuracy, has to be developed and integrated into the settling-spheres experiment.

3. To experimentally investigate the settling behaviour of two vertically-aligned spheres with various configurations of densities and diameters. Several solutions of different Floxit concentrations will be tested, and the time difference, set between the releases of the spheres into the viscoplastic fluid, will also be varied.

4. To experimentally investigate the settling behaviour of two horizontally-aligned spheres with identical density and diameter. Several solutions of different Floxit concentrations will be tested, and the initial distance between the spheres will also be varied.

5. To develop a numerical formulation (CFD) for the study of the settling behaviour of spherical particles in a fluid medium. The efficiency and validity of this numerical method will be examined by considering the case of spherical particles settling in Newtonian fluids. The predicted values of terminal settling velocity will be compared with those predicted through the correlations of Clift et al. (1978).

6. To perform a numerical analysis of the settling-sphere experiments conducted in the aqueous polyacrylamide solutions. This is conducted by formulating a numerical representation of the rheological model developed in step (1) and implementing this model into the numerical strategy developed in step (5). The results of this study will be compared with those obtained experimentally.

7. To develop a set of correlations for the settling behaviour of particles in viscoplastic fluids based on the experimental observations obtained in steps (3) and (4) and the numerical results obtained from step (6).

1.4 Thesis organisation

In Chapter 1, the aim and objectives of this research project have been outlined. The challenges associated with these objectives have then been highlighted and the framework that has been set for the achievement of these objectives presented.

A comprehensive literature review and background on the terminologies commonly used in rheology and the associated mathematical equations will be presented in Chapter 2. The issues associated with the measurement of viscoplastic fluids will then be discussed, and an evaluation of the results that have been obtained and published in the literature surrounding the settling behaviour of spheres in various types of fluids will be presented.

Chapter 3 presents the apparatus and methodology used for the experiments, including the stereo-photogrammetry procedure that has been developed for this research project.

In Chapter 4, the rheological characteristics of the fluid solutions used in this research project will be discussed. The fluid model developed to represent the flow behaviour of these solutions will then be presented, followed by a discussion on the elastic properties of the fluids.

The details of the numerical study (CFD) conducted for this research will be outlined in Chapter 5, following a brief overview of the methods and techniques involved in the development of the numerical scheme. The numerical approximation of the fluid model developed in Chapter 4 will then be presented, along with the User Defined Functions (UDFs) that have been developed for the implementation of this model into the numerical scheme. The results of this study, both in Newtonian and the polyacrylamide solutions, will then be compared and validated against the experimental data.

Chapter 6 presents the results of the first category of experiments, i.e. the settling behaviour of two vertically-aligned spheres. The observations resulting from this experiment as well as the results of the numerical analysis will be used for the development of a set of correlations for the settling velocity of particles in viscoplastic fluids.

The results of the second category of experiments, i.e. the settling behaviour of two horizontally-aligned spheres, will be presented in Chapter 7. The effects of the fluid

rheological characteristics on the interaction between two spheres settling side-by-side will be examined. A set of correlations will then be developed based on these results, as well as those of the numerical analysis.

In Chapter 8, the conclusions of the work that has been conducted in this research project will be presented. This discussion will be followed with a list of recommendations of future work.

Finally, the appendices of this thesis contain the detailed description of the experimental apparatus and methodology, along with their respective error analyses. The UDFs developed for the flow behavioural representation of the experimental fluids have also been included in this section.

Chapter 2 Background and literature review

The flow behaviour of various types of fluids that are frequently encountered in industry, such as polymeric fluids, emulsions, slurries and suspensions, are often quite intricate and therefore require various specialised rheological terms and definitions for their characterisation. In this chapter, a brief introduction of the various terms commonly used in rheology, as well as their associated mathematical models will be discussed, with special emphasis on viscoplastic fluids. The discussion will then be continued with a review on the methods of rheology measurement, more commonly termed as rheometry. The issues associated with the measurement of viscoplastic fluids and the techniques and methodologies that have been used in the past to overcome these difficulties were identified.

The viscoplastic fluid used for the examination of the particle settling behaviour in this thesis is a polyacrylamide solution in water. Thus, a review on the rheological examination of similar solutions conducted in the past is required. The rheological examination of the polyacrylamide solutions, which will be presented in detail in Chapter 5, is based on the findings discussed in this section.

A review on the extensive literature on the study of the settling of particles in various types of fluid, with emphasis on the effects of the factors that may contribute to the experiments involved with this study, such as yield stress, time effects, and elasticity, is presented.

2.1 Rheology

2.1.1 Rheology definitions

The study of rheology concerns the deformation of matter while subjected to shear forces. It recognises that each matter has distinctive deformation behaviour depending on its structural composition. At the most basic level, the deformation

behaviour of various materials when subjected to simple shear forces can be described by the following equation:

$$\tau_{12} = \mu \dot{\gamma}_{12} \quad \textbf{(2-1)}$$

where τ_{12} is the shear stress, $\dot{\gamma}_{12}$ the rate of deformation (or shear), and μ the apparent viscosity. μ is usually a function of the rate of deformation:

$$\mu = f(\dot{\gamma}) \quad \textbf{(2-2)}$$

where $\dot{\gamma}$ is the magnitude of the shear tensor, $\dot{\gamma}_{12}$. In general, the rheology of fluids can be classified into two categories: Newtonian and non-Newtonian. Newtonian fluids deform at a rate that is proportional to the shear stress applied to them, i.e. they have constant viscosity

$$\mu(\dot{\gamma}) = \mu_N \quad \textbf{(2-3)}$$

Where μ_N is a constant, and is a function of temperature and pressure. This characteristic makes Newtonian fluids have easily-predicted flow behaviour.

Non-Newtonian fluids are defined as those fluids that cannot be described by Newtonian behaviour, or by a single constant viscosity. Thus, rather than using the term viscosity, rheologists prefer to use the term apparent viscosity, which is the ratio of shear stress over shear rate, to further classify various non-Newtonian fluids.

The most common behaviour of non-Newtonian fluids is shear-thinning, or pseudo-plasticity, where the apparent viscosity decreases with increasing rate of deformation. The opposite effect, i.e. increase in apparent viscosity with increasing rate of deformation, has also been encountered, although much less frequently. This behaviour is termed as shear-thickening. Both of these phenomena can normally be described sufficiently over a limited range of shear rates by a power-law model:

$$\mu = k\dot{\gamma}^{m-1} \quad \text{where if} \begin{cases} m-1>1 \Rightarrow \text{shear thickening} \\ m-1=1 \Rightarrow \text{Newtonian} \\ m-1<1 \Rightarrow \text{shear thinning} \end{cases} \tag{2-4}$$

where k and m are constants that can be easily determined from experimental data. Other models also exist and some are listed in Table 2-1.

Viscoplastic fluids are broadly defined as fluids that possess a yield point. When subjected to low shear stresses, the fluid appears to behave like a solid, i.e. ideally not experience any deformation, but once the applied shear exceeds a critical value, it behaves as a fluid with finite viscosity. The critical value of shear stress is commonly termed as the yield stress (τ_Y). The earliest model for viscoplastic fluid was suggested by Bingham (1922), who presented this ideal case of viscoplasticity:

$$\begin{aligned} \dot{\gamma} &= 0 && \text{For } \tau \le \tau_Y \\ \tau &= \tau_Y + \mu\dot{\gamma} && \text{For } \tau > \tau_Y \end{aligned} \tag{2-5}$$

The apparent viscosity in this model is presented as a constant, representing Bingham's ideal that once the fluid is sheared past its yield point, its structure breaks down completely, and thus its deformation behaviour is proportional to the shear stress that is applied to it.

In reality, this linearity is normally only encountered at high values of shear rates. This observation was also acknowledged by Bingham, who noted that there is a "curved part" that is often encountered at low values of shear rates (see Figure 1-1 for a typical plot of shear stress as a function of shear rate for viscoplastic fluids).

Thus, Bingham suggested that experimental conditions be chosen carefully so as to keep the shear rates of the experiments in the linear region of the Rheogram.

In practice, viscoplastic fluids generally exhibit a combination of yield stress behaviour with either shear thinning (more common) or dilatancy behaviours. This is because of the nature of the yield material itself, as the presence of a yield stress indicates that the material has a 'structure', which has to be overcome before it starts to behave as a fluid. As the material is sheared, its structure breaks down gradually, leading to a non-constant viscosity. Various equations have been proposed in order to accommodate to this reality (see Table 2-1).

The concept of yield stress itself has proved to be controversial, especially in the late 1980s to early 1990s. With improving instrument capabilities, it has been observed that despite the idealistic concept of yield stress presented by Bingham, even at stress values lower than the yield stress, a continual steady deformation occurs when the viscoplastic material is stressed for a long time. This contradiction with the concept of yield stress, where the material was thought to have a 'solid-like' behaviour below yield stress, caused various researchers to doubt the very existence of yield stress (Barnes & Walters, 1985).

Table 2-1: Well-known rheological equations for pseudoplastic and viscoplastic fluids

Author	Equations	Notes
Ellis et al. (1955) [Pseudoplastic]	$\mu = \frac{\mu_0}{1+(\tau/\tau_2)^{\alpha-1}}$	μ_0 = limiting zero-shear viscosity τ_2 = shear stress at which the apparent viscosity ~ 0.5 x μ_0
Sisko (1958) [Pseudoplastic]	$\tau = a\dot{\gamma} + b\dot{\gamma}^c$	n/a
Cross (1965) [Pseudoplastic]	$\frac{\mu-\mu_\infty}{\mu_0-\mu_\infty} = \frac{1}{1+k\dot{\gamma}^m}$	μ_∞ = limiting high-shear viscosity
Yasuda et al. (1981) [Pseudoplastic]	$\frac{\mu-\mu_\infty}{\mu_0-\mu_\infty} = \frac{1}{1+(k\dot{\gamma}^m)^{\frac{n-1}{m}}}$	n/a
Herschel & Bulkley (1926) [Viscoplastic]	$\tau = \tau_{HB} + k\dot{\gamma}^m$ For $\tau > \tau_{HB}$	τ_{HB} = Herschel-Bulkley yield stress k, m = constants
Casson (1959) [Viscoplastic]	$\sqrt{\tau} = \sqrt{\tau_c} + \sqrt{\mu_c\dot{\gamma}}$ For $\tau > \tau_c$	τ_c = Casson yield stress μ_c = Casson constant of viscosity
Carreau (1972) [Pseudoplastic]	$\mu = \mu_0\left[1+(k\dot{\gamma})^2\right]^{[n-1]/2}$	n/a

Nevertheless, over the past few decades, it has been proven that yield stress is a very important concept in rheology. While its existence is still highly debatable, modern rheologists have generally resolved at defining the yield phenomenon as a mathematical concept, where the yield stress is used to signify a critical value of shear stress over which a material appears to undergo a rapid and significant decrease in viscosity. Thus, it is appropriate that the term yield stress is referred to more generally as 'apparent yield stress', in order to emphasis the fact that it is more of a mathematical concept than a physical one.

A phenomenon that occurs frequently with the existence of yield stress is thixotropy. Barnes (1999) reported that the term "thixotropy" was firstly introduced by Peterfi (1927), followed by Freundlich (1935), who defined the phenomenon as the reversible change of a material from a solid-like elastic gel to a flow-able fluid through the process of shaking or stirring. This definition, although still currently widely accepted in various communities, has been expanded further, encompassing any materials that undergo reversible reduction in the magnitude of its rheological properties (this can include elastic modulus, yield stress, and viscosity) as it is subjected to shear forces under isothermal conditions (Bauer & Collins, 1967). This reduction is caused by the breakdown of the microstructure within the material (attributed by various properties, such as the alignment of fibres, the favourable spatial distribution of particles or drops, flocculated particles, entanglement of polymers, the existence of the Van der Waals forces, etc.) as it is subjected to shear forces. Upon the removal of shear, the association between particles re-forms, and thus the material regains its initial properties.

As a result of the definition above, the term thixotropy is commonly confused with shear thinning (Scott-Blair, 1943). In reality, the similarities between shear thinning and thixotropy behaviours may be much more than once assumed, due to the fact that both phenomena are caused by the destruction and reconstruction of structures upon shearing. Thus, in comparing the rheological behaviour of various fluids, special attention needs to given in distinguishing the effects of

shear-thinning and the memory of shear thinning (e.g. Joseph et al., 1994), as the latter term generally implies thixotropic behaviour.

Apart from the various types of rheological behaviour discussed above, many polymeric materials and other rheologically complex fluids also exhibit non-zero normal stresses, i.e. stresses that are at right angles to the direction of shearing. The result is a combination of an elastic response, which conserves the energy of the system (E', or storage modulus G'), with the typical, energy-dissipating viscous behaviour that have been seen so far in this discussion (E'', or loss modulus G''). The ratio between E'' and E' is termed as the loss tangent, tan δ. Fluids that possess both elastic and viscous components are termed viscoelastic.

In practice, one of the earliest signs of viscoelasticity is termed as the Weissenberg effect, which is also known as the 'rod-climbing' effect, where a liquid that is stirred with a rod begins to coil the rotor and climb it. As a viscoelastic fluid is sheared by the rod, it undergoes large elastic deformations, resulting in normal stresses, i.e. stresses in the vertical direction. As the liquid gets wrapped around the rod, the normal stresses cause the liquid to 'climb' up the rod, resulting in the Weissenberg effect.

The existence of normal stresses (denoted τ_{11}, τ_{22}, and τ_{33} in the Cartesian coordinates) in viscoelastic fluids are normally quantified as normal-stress differences, as it is virtually impossible to measure all non-zero components of the stress tensor. These differences are termed as the first and second normal-stress differences (N_1 and N_2, respectively), which are usually also presented as the first and second normal-stress coefficients (ψ_1 and ψ_2). In the Cartesian coordinates, these stress differences can be written as follows:

$$N_1 = \tau_{11} - \tau_{22} \quad \Rightarrow \quad \psi_1(\dot{\gamma}) = \frac{N_1}{\dot{\gamma}^2} = \frac{\tau_{11} - \tau_{22}}{\dot{\gamma}^2} \tag{2-6}$$

$$N_2 = \tau_{22} - \tau_{33} \quad \Rightarrow \quad \psi_2(\dot{\gamma}) = \frac{N_2}{\dot{\gamma}^2} = \frac{\tau_{22} - \tau_{33}}{\dot{\gamma}^2} \tag{2-7}$$

The first normal-stress difference can generally be measured simultaneously with the shear viscosity in commercial rheometers. The second normal stress difference, on the other hand, is more difficult to measure accurately and is commonly very small in magnitude (Chhabra, 2007); its effect on fluid flows is therefore normally ignored.

The relaxation time, φ, is an important characteristic of a viscoelastic fluid, as it represents the time required for the fluid to dissipate the energy stored due to its elasticity. The dimensionless forms of this parameter, i.e. Weissenberg and the Deborah numbers, are widely used to compare the viscous and elastic forces of various types of flows.

$$We = \frac{V\varphi}{d} \tag{2-8}$$

$$De = \frac{\varphi}{t} \tag{2-9}$$

where V, d, and t are the characteristic velocity, linear size, and time of flow, respectively. While highly similar, the Weissenberg number is generally used to characterise steady flows and Deborah number for time-dependent flows. At small values of De and We numbers (De or We << 1), the viscous behaviour pre-dominates. Conversely, high values of De or We (>> 1) indicate strong viscoelastic behaviour.

The presence of relaxation time can be demonstrated clearly by the creep experiments, where a constant stress is applied on the sample, with the time variation of strain (γ) and strain rate ($\dot{\gamma}$) being measured (Figure 2-1).

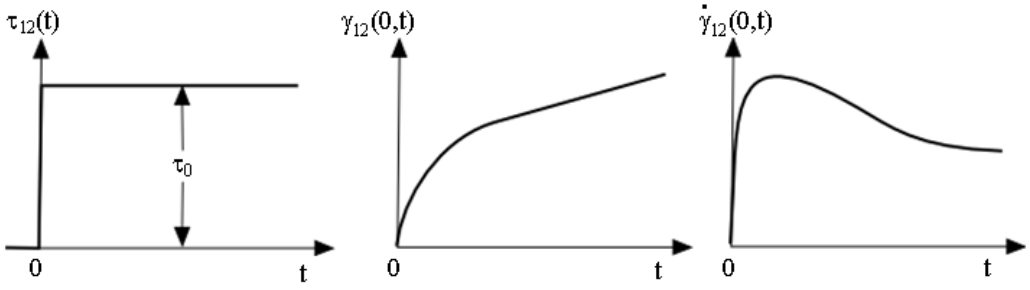

Figure 2-1: Creep experiment with the shear strain and shear rate response.

The resulting shear stress and strain response are measures of the elastic and viscous components of the system.

$$\tau = E\gamma + \mu(t)\dot{\gamma} \qquad \textbf{(2-10)}$$

where E is the elastic modulus of the fluid.

Therefore,

$$\frac{\tau}{E} = \gamma + \varphi\dot{\gamma} \qquad \textbf{(2-11)}$$

where the relaxation time, φ, is $\frac{\mu(t)}{E}$.

Another widely-accepted method of measuring viscoelasticity is the measurement of G′ and G″ (storage and loss modulus respectively) as a function of angular frequency, ω, under an oscillatory-type of movement. This experiment is known as the Small-Amplitude Oscillatory Shear (SAOS) experiment, which is conducted within the Linear Visco-Elastic (LVE) region. The LVE region can be determined through a range of oscillation amplitude (equivalent of strain) values at a constant frequency and is a range where the stress generated is linear to strain, which is normally encountered at the lower range of strain rates.

The SAOS experiment is frequently conducted by rheology researchers as a way of determining the structure of the material. Ferry (1980) has provided an extensive discussion of the shape of rheological functions in the LVE region for a wide variety of polymers. Experimental data from the SAOS experiment can provide in depth information on the dominance of the storage and loss moduli over a range of shear frequencies, as well as the characteristic relaxation time of the fluid. Furthermore, other viscoelastic material functions, such as the response of the material to step shear strain and steady uniaxial elongation, can also be determined through the fitting of these data with one of the constitutive equations (e.g. Maxwell, Kelvin-Voigt, etc.) for linear viscoelasticity.

Finally, it should be noted that most polymeric materials and solutions possess a combination of the types of rheological behaviour discussed above. As a result, they are generally classified as rheologically-complex fluids. Many polymeric liquids, for example, exhibit shear thinning behaviour as well as thixotropy and viscoelasticity. In fact, the vast progress in knowledge that has been achieved in the past few decades on the effects of elasticity on flow processes can be attributed to the discovery of Boger fluids, which have the unique quality of having significant elastic properties while maintaining Newtonian (constant) viscous properties. The interlocking of rheological behaviour poses a lot of challenges in the development of rheological models, as will be seen in section 2.1.2, because of the need for researchers to consider all of these behaviours for a realistic model to be achieved. However, it should be noted that there is generally no universal solution in rheology, and that in selecting or developing rheological models, the degree of accuracy and reality needs to be considered based on the application of the rheology model itself. Some problems may require a very complex and detailed model, while some can be sufficiently described by a simple model.

2.1.2 Modelling aspects of rheology

As can be seen from the list of mathematical models presented in Table 2-1, various equations are available to describe viscoplasticity. However, numerous difficulties

arise, such as the non-differentiability of most of these equations, as well as the general complexity of the fluids themselves, which have been discussed previously, often exhibit other types of rheological behaviour, such as shear thinning and thixotropy. As a result, more and more mathematical models have been suggested over time, with various degrees of complexity and applicability. Some of these models will be discussed in this section.

2.1.2.1 Yield Stress

The viscoplastic equations that have been discussed so far (see Table 2-1) possess discontinuity over the yield stress region, causing the equations to be non-differentiable and very difficult to solve numerically. To overcome this problem, many researchers have employed the idea of a regularisation equation, which was firstly suggested by Glowinski et al. (1981) by modifying the Bingham equation using the following apparent viscosity:

$$\mu_A = \mu + \frac{\tau_Y}{\varepsilon + \dot{\gamma}} \tag{2-12}$$

where μ_A is the apparent viscosity, to be substituted into the rheology equation as per equation 2-2, and ε is the regularisation parameter. As expected, ε is normally set to a very small number ($<< 1$) to approximate the exact Bingham behaviour. Bercovier and Engleman (1980) also suggested another (more popular) equation:

$$\mu_A = \mu + \frac{\tau_Y}{\sqrt{\varepsilon^2 + \dot{\gamma}^2}} \tag{2-13}$$

Papanastasiou (1987) also suggested another frequently-used regularisation form:

$$\mu_A = \mu + \tau_Y \frac{1 - e^{-\dot{\gamma}/\varepsilon}}{\dot{\gamma}} \tag{2-14}$$

The above models can be implemented relatively easily in standard numerical solvers, and although iteration is required due to the non-linearity of the viscosity

function, convergence is normally easily obtained. Frigaard and Nouar (2005) conducted a comparative numerical study on the three regularisation procedures and concluded that the regularisation method suggested by Papanastasiou provides a better approximation than the other two methods. However, it was also noted the large errors that can be encountered over the stable and unstable regions caused by the yield stress parameters, which depend highly on the selected value of ε.

Another method of overcoming the numerical difficulties of the yield stress phenomenon is the bi-viscosity model:

$$\mu_A = \begin{cases} \mu_0 + \dfrac{\tau_Y}{\dot{\gamma}} & \text{if } \dot{\gamma} > \dfrac{\tau_Y}{\mu_r - \mu_0} \\ \mu_r & \text{if } \dot{\gamma} \leq \dfrac{\tau_Y}{\mu_r - \mu_0} \end{cases} \qquad \textbf{(2-15)}$$

Typically μ_r is approximated to be $100\mu_0$ to represent a true Bingham fluid behaviour (Beverly & Tanner, 1992).

2.1.2.2 Thixotropy

Numerous models have been suggested in the past in order to fully describe the phenomenon of thixotropy. Over time, however, it has been found that this phenomenon is very difficult to describe mathematically, due to the fact that thixotropy is very difficult to measure (as will be discussed in Section 2.1.3) and that this phenomenon normally occurs together with other types of rheological behaviour, such as the yield stress and viscoelasticity. As a result, different approaches of modelling have been suggested.

The first approach is based on a non-constant yield stress, termed as the sliding yield stress ($\tau_{sliding}$), which is a function of shear rate and time (Slibar & Palsay, 1964):

$$\tau = \tau_{sliding}\left(\dot{\gamma}, t\right) + \mu\dot{\gamma} \quad \text{for } \tau > \tau_{rest} \qquad \textbf{(2-16)}$$

The overlap between viscoelasticity with thixotropy has also been explored by some researchers based on this approach. Elliott and Green (1972) and Elliott and Ganz (1977), for example, have suggested a modification of the Slibar and Palsay thixotropic model by incorporating a Hookean elastic behaviour before yielding. Acierno et al. (1976) have also developed a set of equations describing both viscoelasticity and thixotropy satisfactorily. Suetsugu and White (1984) introduced a transient yield stress term that is applicable both at rest and during flow, whereas Phan-Thien et al. (1997) recently recommended a model consisting of hyperelastic, viscoelastic, and purely viscous terms.

The second approach, which has been classified by Barnes (1999) as the 'direct microstructural' or 'kinetic' approach, attempts to connect thixotropy with the basic process responsible for structural changes. An important variable in this method is the number of bonds or links between the particles, n. The rate of change for n as the structure is subjected to shear is normally written as:

$$-\frac{dn}{dt} = k_1 n(\dot{\gamma})^a - k_2 (n_0 - n)(\dot{\gamma})^b \qquad \textbf{(2-17)}$$

where n_0 is the number of bonds in an undisturbed structure, k_1 and a the rate constant and exponent for the rate of structure breakdown, and k_2 and b the rate constant and exponent for the structure build-up. Examples of this type of model are: Cross (1965), who postulated the Cross model (see Table 2-1) at steady-state condition, Lapasin et al. (1996), and Chan Man Fong and De Kee (1994), who extended the thixotropic treatment to materials with yield stresses:

$$\tau_Y = \frac{n_0 - n_{crit}}{\left(k_1 / k_2\right) n_{crit}} \qquad \textbf{(2-18)}$$

where n_0 is the initial structure parameter of the fluid and n_{crit} is a critical value of structural parameter n, above which no flow can occur.

A similar approach to the direct microstructural approach is an indirect one, where a scalar parameter, λ, is used in place of n, representing the extent of structural breakdown. A value of unity for λ represents a fully built structure, whereas a completely broken structure is represented as λ = 0. A similar kinetic equation is used to express the rate of structural breakdown and build-up as that used for n in equation 2-17, except that an upper limit of unity is placed on the structure variable. Examples of this approach include: Moore (1959), Baravian et al. (1996) and De Kee et al. (1983). Recently, Mujumdar et al. (2002) proposed a model based on this approach that features a smooth transition from an elastically dominated flow to a viscous one without discontinuity. Assuming that the viscous deformation of the fluid can be modelled after the power-law equation (see equation 2-4), the following equation was obtained:

$$\tau = \lambda\left(G\gamma_e\right) + \left(1-\lambda\right)k\dot{\gamma}^{m-1} \qquad \textbf{(2-19)}$$

Where γ_e is the elastic strain associated with the flowing structure, whereas G is the elastic (Hookean) modulus of the material.

Recently, another microstructural-related thixotropy model has also been proposed by Møller et al. (2006). This method addresses yield stress and thixotropy simultaneously with the observation that the two behaviours generally occur together, caused by the destruction and reconstruction of structure in the system as it is being sheared. Møller and co-workers suggested a set of equations that combines the two phenomena, by considering the rate of change of λ, which is a scalar variable that represents the extent of structural breakdown in the fluid:

$$\frac{\partial\lambda}{\partial t} = \frac{1}{\theta} - \kappa\lambda\dot{\gamma} \qquad \textbf{(2-20)}$$

Where θ is the characteristic relaxation time of the liquid and κ is a constant. Møller and co-workers combined the above equation with two possible non-Newtonian equations for viscosity:

$$\mu = \mu_0 \, e^{m\lambda} \tag{2-21}$$

$$\mu = \mu_0 \left(1 + k\,\lambda^m\right) \tag{2-22}$$

This set of equations successfully combines the phenomena of thixotropy and yield stress and will be reviewed further in this thesis.

2.2 Rheometry

An effective rheology model requires a set of rheological data that represents the reality of the fluid behaviour, at least to within the parameters of the intended application. This is important, as the types of rheometers and methods of measurements that are available are numerous, yielding a potentially diverse range of experimental data with various levels of accuracy. Furthermore, rheologically-complex fluids such as polymeric solutions and suspensions have been shown in the previous section to have viscosities that are a function of temperature, shear rate, as well as the shear history or time. Thus, in order to obtain meaningful rheological data, the appropriate rheometers, as well as measurement method, need to be identified, and their limitations need to be addressed.

2.2.1 Rheometers

As has been mentioned previously, the measurement of rheology parameters varies widely from the type of measurement instrument to the procedures of its use. Depending on the required degree of accuracy, rheological measurements can be conducted using simple viscometers, such as flow cups, capillary, rotational, and bubble viscometers, to the more sophisticated rheometers which have added controlled environment for measurement and versatility. Due to their simplicity and user-friendliness, viscometers are frequently used in industry. However, their

measurement range is limited to several flow conditions only (sometimes only one), and as a result, they are not suitable for measuring non-Newtonian fluid properties. Rheometers, on the other hand, are generally used as research equipment, as they are generally more expensive and less user-friendly. Using rheometers, the fluid can be subjected to a large range of flow conditions and temperature, making it suitable for measuring non-Newtonian fluid properties.

While rheometers can generally be classified into two groups, shear and elongation, the shear rheometers, which applies shear forces on the sample as opposed to extensional forces for the elongational rheometers, are generally more common. These rotational rheometers are currently available with highly-advanced technology, allowing for the instruments to be robust, sensitive, and versatile, able to apply both rotational and oscillatory movements with control over the applied stress, rate, and degree of shear. Standard measurements can be done using a cone and plate, parallel plate, or concentric cylinder geometries, which are connected to a spindle which is driven via a non contact induction motor supported by a high quality porous carbon air bearing. This results in a virtually frictionless movement for the measurement process. Other geometries such as the vane and helical screw rheometers are also available, but are much less common.

The cone-and-plate viscometer consists of a rotating cone with a small angle ($0 < \alpha < 4^{o}$) and a stationary plate. The cone can either be fully extended or slightly truncated and the gap between the cone and the plate is normally set to be a very small distance (0.139 mm). Unlike the concentric cylinder and parallel-plate geometries, the cone-and-plate viscometer has the advantage in that the shear rate throughout the sample can be assumed to be uniform, provided that the cone angle is kept small and fluid inertia negligible.

Rotational rheometers differ from other more commonly-used rheology devices (such as the rotational viscometer), in that it directly measures viscosity. Traditional instruments generally measures viscosity in comparison to other standard fluids of known viscosity in a calibration process, which has to be done frequently and consistently for accurate results to be obtained. Rotational

rheometers, on the other hand, directly quantify viscosity by the measurement of shear stress and velocity gradient. Thus, in its measurement process, there are three possible sources of error: the measurement of shear stress, velocity gradient, and the temperature at which all of these measurements are taken (Marquardt & Nijman, 1993).

The quantification of shear stress is performed by the measurement (or specification, in the case of Controlled Stress measurement, see section 2.3.2) of torque, of which measurement errors can stem from inertia effects, alignment errors, and linearity errors during the determination of the motor current. In cone-and-plate rheometers, inertial effects up to Re ~ 40 have been estimated by Turian (1967), who stated that the actual torque, T_{act}, can be predicted from the rotational Reynolds number:

$$\frac{T_{act}}{T} = 1 + \frac{3\left(Re_R \sin\alpha\right)^2}{4900} \qquad \textbf{(2-23)}$$

where T is the torque due to the basic viscometric flow, α the cone angle, and Re_R the rotational Reynold's number:

$$Re_R = \frac{\rho \Omega R^2}{\mu} \qquad \textbf{(2-24)}$$

where Ω is the rotational speed of the spindle and R the radius of the cone. Therefore, care should be taken during the measurement process that the upper limit of the Reynolds number for the inertial effects estimation not be exceeded. Errors arising from misalignment have been minimised in modern rotational rheometers, due to the fact that they are mostly self-aligning. However, geometrical imperfections and linearity errors can still exist, and therefore care should be taken to characterise these imperfections. These characterisations are normally conducted during the calibration stage, which is performed by the manufacturer and as a result, built-in corrections are normally implemented once the instrument is placed online.

Errors in the measurement of the velocity gradient in modern rotational rheometers are generally quite low (< 0.5%). These are normally more prevalent at low rotational speeds because of the very small voltages involved during the measurement. Furthermore, errors caused by changes in temperature during the measurement are generally minimised by the use of a temperature-controller, which can control the temperature of the measurement to within 0.02°C.

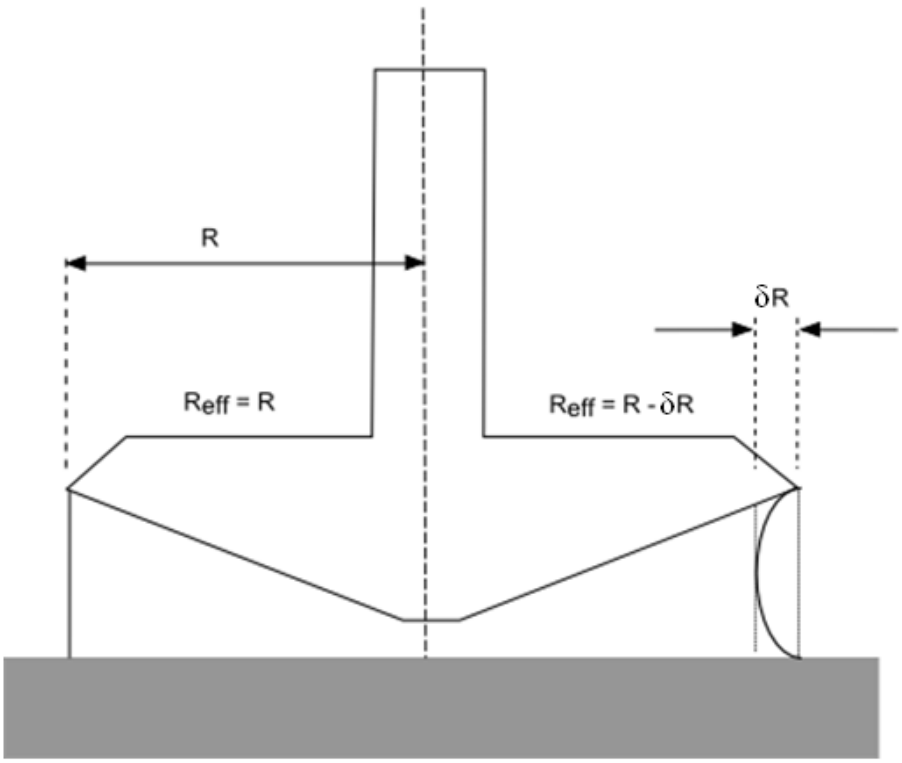

Figure 2-2: Effective radius error in cone-and-plate rheometer.

Further errors in measurement can arise from the geometry of the instrument. In cone and plate rheometers specifically, errors in the geometry characterisation of the cone, such as its radius and angle, as well as in the gap settings, can lead to detrimental effects, as explained by Marquardt and Nijman (1993). Another possible source of error from this measurement is the edge effects (see Figure 2-2), as the mathematical formulation surrounding this geometry has been developed based on the assumptions that the free surface is spherical and the velocity field is

maintained up to the edge. Errors arising from imperfections in the profile of the fluid edge can be estimated as follows:

$$\text{error} = 1 - \frac{R^3}{(R - \delta R)^3} \tag{2-25}$$

Thus, care must be taken during the loading of the sample to avoid over or under-filling.

2.2.2 Measurement technique

Aside from the various geometries available in rheometry, there are also a myriad of flow conditions that can be applied to the fluid to generate various interpretation on the flow properties of the fluid. In general, these flow conditions can be classified into two: rotational and oscillatory tests.

The rotational test is generally used to determine the viscous parameters of the fluid. In this type of experiment, the fluid is sheared at a set condition, which can be controlled either through the rate of shear (Controlled Rate), the amount of shear deviation (Controlled Strain), or the amount of stress applied (Controlled Stress). Modern rheometers are generally equipped with various modes of measurement:

- Rotation ramp (CS/CR): The preset shear stress/shear rate is continuously altered (can be increased or decreased) without waiting for the material to reach equilibrium conditions. This test is traditionally used to test for shear thinning and yield stress effects
- Rotation steps (CS/CR): A constant shear stress/shear rate is applied for a fixed amount of time. This test is used to determine the time required for the material to reach equilibrium conditions. Alternatively, a series of rotational steps at different shear stress/shear rate can also be used to determine the viscous properties of the fluid during equilibrium.

- Creep and Recovery test (CS): This measurement procedure is conducted to determine the viscoelastic properties of the fluid, as well as its characteristic relaxation time.

Contrary to the rotational tests, the oscillatory tests generally focus on the small strain properties of the fluid. The most commonly used test in this category has been discussed in section 2.1.1, i.e. the SAOS experiment. In this test, the fluid is subjected to small oscillatory strain at various oscillation frequencies. The experiment is normally conducted within the linear viscoelastic limit of the material. This range can be determined by conducting a strain amplitude-controlled sweep oscillatory test at the frequency range in which the SAOS experiment is to be conducted.

In conducting tests on the rheological behaviour of a fluid, various factors that may detract from the accuracy of the experiment need to be identified. While errors arising from instrumental and setup imperfections have been discussed in section 2.2.1, errors arising from the nature of the fluid needs to be discussed.

Without the presence of yield stress, the viscous properties of time-independent fluids are generally easy to classify, either by performing CR or CS rotational ramps. However, with the presence of yield stress, measurement procedures are generally much more complicated and various errors can result from the presence of the yield stress itself. An example of this is a case where the gap in a cone-and-plate viscometer is set by lowering the upper cone, which rests on the surface of the solid-like test fluid. As the shearing is commenced, the yield stress is exceeded and the sample starts to behave as a liquid and flow out of the gap (Wildemuth & Williams, 1985). This affects the measurement of normal stresses in yield stress fluids.

Furthermore, the interpretation of rheological measurements has so far been derived based on the assumption of negligible slip at the wall. While this assumption has been proven to be effective for most cases, it has been detrimental

for some fluid systems, especially those involving high apparent viscosity and yield stresses (Mewis & Moldenaers, 1999). Examples of these systems include particulate suspensions, emulsions and systems involving two (or more) phases, and concentrated solutions of high molecular weight polymers. Various solutions to this problem have been proposed, such as the use of a different geometry that minimises the effects of wall slip (yield vane), the use of abrasive paper attached to the surface of the geometry, and the use of optical visualisation techniques to examine the slip plane during the rheology measurement.

Furthermore, yield stress fluids are also more prone towards 'shear banding' or localisation effects, where, due to the plasticity of the fluids, uneven distribution of velocity across the gap of the rheometer is obtained. This causes the rate-of-shear to be non-homogeneous and in some cases, can adversely affect the accuracy of the rheometric analysis. The effect of shear banding is generally encountered in plastic-like materials, such as power-law fluids with very small power-law index or yield stress fluids that are sheared at approximately its yield value (Mewis & Moldenaers, 1999). In his review on the methods of measuring the flow properties of yield stress fluids, Nguyen and Boger (1992) have observed that the effects of shear banding can be minimised by keeping the cone angle and the gap between the cone and the plate as small as possible. Furthermore, some modern rheometers are also equipped with optical visualisation techniques that can characterise these effects during the rheological measurements.

Another factor that may contribute towards the accuracy of the measurement of rheologically-complex fluids is its sensitivity towards time and shear history. An extreme example of this phenomenon has been demonstrated by (Ourieva, 1999) using weakly flocculated suspensions of sterically-stabilised poly-(methyl metacrylate) (PMMA) particles. In this study, it was found that PMMA solutions that have been left to rest for 17 hours tend to possess viscosity parameters that are several orders higher than those that have not been 'rested' after its period of preparation. This suggests that rheometric properties of these solutions are highly dependent on the time that has been allowed for the solutions to rest and recover in

structure after being subjected to shear forces. Mewis and Moldenaers (1999) have thoroughly discussed various factors that may contribute towards these sensitivities. Furthermore, the problem was classified into several categories, depending on the reversibility and homogeneity of the structural and rheological changes in the fluid. Thus, in conducting rheological measurement of these rheologically complex fluids, the transient behaviour of the fluid in response to time and shear should be considered and examined.

2.3 Rheology of polyacrylamide solutions

Kulicke et al. (1982) have done a comprehensive review on the properties of polyacrylamide solutions, including the preparation method, molecular structure, methods in rheological experiments, as well as their rheology and viscoelastic properties.

Various factors can affect the viscosity of a polyacrylamide solution, such as its molecular weight, the length of the molecules, coil size, and its thermodynamic interaction with the solvent. Furthermore, it has been suggested that the energetic interactions (hydrogen bonding) between the polymer and the solvent strongly influences the rheological behaviour of the solution (see Kulicke et al. 1982; Sastry et al. 1999). Due to its dependence on these factors, the rheology of polyacrylamide solutions can seldom be accurately predicted and comparisons between solutions with different preparation methods can rarely be made.

In 1998, Ghannam and Esmail conducted a series of tests on various polyacrylamide solutions with molecular weight of $5x10^6$ (concentrations ranging from 0.25 to 1.0%). It was concluded that polyacrylamide solutions display strong yield shear-thinning behaviour, with power-law index of approximately 0.5 and yield stress values of 0.34 – 1.10 Pa. At higher values of shear rate (above 200 s^{-1}), shear thickening behaviour was detected. Ghhanam and Esmail (1998) also performed a series of dynamic (SAOS) tests on the polyacrylamide solutions and found that the solutions inhibit viscoelastic properties. The elastic behaviour of

these solutions was found to be more prominent at the lower range of test frequency ($\omega < 6$ Hz). At higher frequency values, the flow behaviour of the solutions was found to be generally dominated by viscous behaviour.

Upon conducting yield and transient tests, which were carried out by examining the stress developments as a function of time for various values of constant shear rate, it was found that the solutions display the typical responses of viscoelastic and thixotropic fluids. For example, some increase in stress (termed by the authors as rheopexy) was detected over time (~ 50 s) as a pre-sheared sample is subjected to a lower shear rate of approximately 50 s^{-1}. According to the authors, this behaviour is caused by the recovery and reformation of the molecule network structures after the disruption caused by the preshearing. The yield stress test, which was conducted by examining the change in shear rate as increasing/decreasing values of shear stress is applied (i.e. CS ramp), also reveals that the samples have lower yield stress values when subjected to the decreasing curve of applied shear stress. Again, this suggests that during this time, the full structure of the fluid has not fully recovered, thus indicated by the lower value of yield stress.

The viscoelasticity of the polyacrylamide solutions were tested by Ghannam and Esmail (1998) by conducting creep and dynamic SAOS tests. The creep tests reveal typical viscoelastic response, with time-dependent reduction in the compliance (a function of strain) of the sample upon the removal of shear stress, when the test is conducted within the linear viscoelasticity limit of the sample. Beyond this region, no reduction in strain is detected, thus suggesting a complete viscous character. It was also found that, through a series of dynamic tests, the solutions display higher complex viscosity than shear viscosity. That is, the solutions display some disparity with the Cox-Merz rule, which states that the complex dynamic viscosity should be identical to the shear viscosity at the same values of shear rate. This is in agreement with the findings of Kulicke and co-workers (1982), who have attributed the discrepancy to the energetic effect of the hydrogen bonds between the polyacrylamide and water molecules.

2.4 The settling of a particle in a fluid

2.4.1 Newtonian

The settling of a spherical particle in an incompressible fluid under isothermal condition is governed by the continuity and momentum equations:

$$\nabla \cdot V = 0 \qquad \textbf{(2-26)}$$

$$\rho \frac{DV}{Dt} = [\nabla . \tau] - \nabla p + \rho g \qquad \textbf{(2-27)}$$

where V and p are the velocity and pressure fields of the system.

In a Newtonian fluid, the viscosity term is a constant, thus simplifying the flow problem considerably. By considering the appropriate boundary conditions, typically no-slip condition with free velocity stream at regions far away from the sphere, the velocity and pressure fields can theoretically be determined directly from equations 2-26 and 2-27. Problems, however, arise from the non-linear inertial terms present in the momentum equation, which makes even the simpler Newtonian flow problems difficult to solve.

In 1851, Stokes proposed a solution for the flow problems as presented in equations 2.26 and 2.27 by assuming negligible inertial forces. This condition is encountered at extremely low values of Reynolds numbers (Re << 1), typically where the fluid velocities are very low and the viscosities very high. Equation 2-27 thus simplifies to:

$$\nabla p = \mu \nabla^2 V \qquad \textbf{(2-28)}$$

By solving for the velocity and pressure fields, Stokes hypothesised that the drag force (F_D), which is the summation of the form drag experienced by the particle caused by pressure downstream of the sphere and the viscous drag, can be written as:

$$F_D = 6\pi\mu RV \tag{2-29}$$

The dimensionless form of the drag force is known as the drag coefficient (C_D):

$$c_D = \frac{2F_D}{A_P.(\rho.V^2)} \tag{2-30}$$

where A_P is the projected area. In the case of a spherical particle of diameter D, this parameter is customarily equated to $\pi D^2/4$. Thus, for cases where the inertia effects are negligible in comparison to the viscous effects, the drag coefficient is:

$$C_D = \frac{24}{Re} \tag{2-31}$$

The hypothesis of Stokes, although highly limited, has been the basis of many numerical analyses in the prediction of the settling behaviour of spheres in both Newtonian and non-Newtonian fluids. This is reflected by the numerous numerical solutions and correlations available today, most of which attempt to correlate the drag forces experienced by the particle with the Reynolds number of the flow. Notable solutions for this flow problem include those suggested by Oseen (1927) as well as Ockendon and Evans (1972) for creeping flows, Jenson (1959), LeClair et al. (1970), Fornberg (1988), Heider and Levenspiel (1989) for flows well outside the creeping region. Clift et al. (1978) and Khan and Richardson (1987) have done a comprehensive review on these solutions.

2.4.2 Non-yield stress fluids

Similar to the case with the Newtonian fluids, the theoretical analysis in the creeping flow regime is centred on the solution of momentum equation with the

inertial terms neglected. Additional difficulties were encountered, simply due to the fact that the viscosity in this case is a variable.

The power law fluid model is used widely in the early studies of this field, mainly due to the fact that it is relatively simple compared to the other models. The power law index, m, is normally viewed as a gauge in the importance of shear thinning effects in flow problems (Chhabra, 2007). The theoretical analysis of studies using this model usually uses the following expression for the drag on the sphere:

$$Y = \frac{C_D Re_{PL}}{24} \tag{2-32}$$

Where Y is a drag correction factor and the Reynolds number is defined as follows:

$$Re_{PL} = \frac{\rho V^{2-m} D^m}{k} \tag{2-33}$$

Various researchers have conducted dimensional analysis on Y, and concluded that this variable can be related directly to m. Notable correlations include that of Acharya et al. (1976), who evaluated the viscosity term by assuming the Newtonian flow field, as well as Kawase and Moo-Young (1986), who used the standard perturbation method to solve the momentum equation.

In the past few years, some efforts have been put forward in expanding the available correlations to the non-creeping flow region. The standard approach is to use a C_D-Re relationship that has already been well-established for Newtonian fluids (e.g. Heider & Levenspiel, 1989) and introduce various modified forms of the Reynolds equation, such as that in equation 2-33. An example of this approach is presented by Kelessidis and Mpandelis (2004). In another publication, Kelessidis (2004) has also proposed a more implicit form of the prediction of the settling velocity in this type of fluid based on the approach proposed by Turton and Clark (1987) for Newtonian fluids. Ceylan et al. (1999), on the other hand, presented a more theoretical approach, where the Y-m correlations used in calculating the drag coefficient are derived by using a stream function and by solving the energy

dissipation equation. It is claimed that the proposed correlation is valid for power law values of $0.5 < m < 1$ and Reynolds number of $10^{-3} < Re_{PL} < 10^{3}$. Alternatively, several modifications of the C_D-Re relationship itself have also been proposed. An example of this method is Shah et al. (2007) whose suggested correlation is reportedly valid for a wide range of power law flow behaviour index m (0.281-1) and particle Reynolds number (0.001-1000).

Despite the wide-range of work surrounding the power-law model, it has been criticised due to the fact that it does not predict the viscosity of the fluid at conditions of very low shear rates ($\dot{\gamma} \to 0$). The flow field generated by a moving sphere is characterised by a shear rate which varies from zero to a maximum value on the sphere surface, and thus this aspect of the model is relatively important. Chhabra (2007) also noted that conflicting results and poor reproducibility displayed by the large number of experimental data surrounding the analysis of the creeping motion of spheres in pseudoplastic fluids has been caused by the use of inadequate power-law models and the fact that the fluid model does not provide a good estimation of the fluid viscosity at shear rates of nearing zero (termed as zero-shear viscosity). Several notable studies featuring the analysis of the creeping motion of spheres in pseudoplastic fluid models with zero-shear viscosity include Hopke and Slattery (1970), who used the Ellis fluid model, and Chhabra and Uhlherr (1980), Bush and Phan-Thien (1984), and Machac et al. (2000), who used the Carreau model (see Table 2-1).

The theoretical analysis of the motion of a sphere in a power-law fluid has also been enhanced by the use of computational fluid dynamics (CFD) methods. Crochet et al. (1984) have solved the continuity and momentum equations for the creeping motion of a spherical particle in power law fluids, and were able to present some details about the velocity field around the sphere. Their conclusion upon conducting this analysis was that as the value of the power law index decreases, the disturbance in the flow field caused by the presence of a sphere is felt over shorter distances. This theory was found to be consistent with the experimental observations of Sigli and Coutanceau (1977). More recently, Missirlis et al. (2001) conducted both finite-

element (FE) and finite-volume (FV) analysis on the wall effects on the creeping motion of a sphere in a power-law fluid. The wall effects established through this series of simulation was found to agree relatively well with the experimental data, and the influence of tube/sphere diameter ratio as a function of the shear-thinning character of the fluid can be established. Through this study, it was found that in fluids with strong shear-thinning character (m ~ 0 for equation 2-4), the effects of the sphere-to-tube diameter on the terminal settling velocity of the sphere is less pronounced than in cases where Newtonian fluids are used. This finding suggests that particles that are settling through highly shear thinning fluids would experience less significant wall effects than those settling through fluids of weaker shear thinning characteristics.

Chhabra (2007) also noted that some of the experimental data that has been published in the past (Chhabra and Uhlherr 1980; and Dunand et al. 1984) have used liquids with significant viscoelastic properties. The experimental data from these studies show considerable agreement with the theoretical results based on purely viscous models (e.g. Carreau and Ellis fluid models, see Table 2-1). Based on this finding, it was concluded that the dynamics of the settling particle is largely dependent on the viscous properties of the fluids and that their elastic properties do not contribute significantly towards the settling velocity of the particles.

2.4.3 Yield-stress fluids

While there have been many studies done on the motion of spheres in fluids without yield stresses, not as many have been done for viscous fluids with a yield stress. Theoretically, it is clear that yield stress is one of the most influential factors that determine the settling behaviour of particles. A particle that is suspended in a yield stress fluid would theoretically have to have a gravitational stress that exceeds the stresses that are caused by the buoyant effects and the yield stress of the fluid for it to settle.

Yield stress also plays an important role in the flow field surrounding a settling particle. While it has been established that the flow field surrounding a sphere

settling in fluids without any yield stress extends several radii (theoretically extending to infinity), earlier analytical studies in viscoplastic fluids have identified a zone with flow restrictions around the sphere, outside of which shear is not transmitted and only elastic deformation exists (Volarovich & Gutkin, 1953; Tyabin, 1953). Furthermore, an "envelope" region adhering to certain parts of the sphere was also identified by Rae (1962) and later supported by Whitemore and Boardman (1962). This phenomenon is mainly attributed to the presence of the yield stress.

The shape and size of the "envelope" region have been studied and debated in several studies, with notable works including Ansley and Smith (1967), Yoshioka et al. (1971), and Beris et al. (1985) (see Figure 2-3). In 1989, Atapattu (1989)calculated the radial and angular velocities for a sphere moving at constant speed on the axis of a cylindrical tube, thereby obtaining velocity profiles at different angular positions for various sphere-to-tube diameter ratios. The results of this calculation were then confirmed by optical experimental techniques. The shape of the sheared zone obtained by this method resembled that of Ansley and Smith (1967) and Beris et al. (1985). However, Atapattu also stated that a different sheared zone may be obtained with differing Bingham numbers and yield stresses. The results of this study were further confirmed, at least qualitatively, in subsequent numerical studies by Beaulne and Mitsoulis (1997), Blackery and Mitsoulis (1997), and Liu et al. (2002).

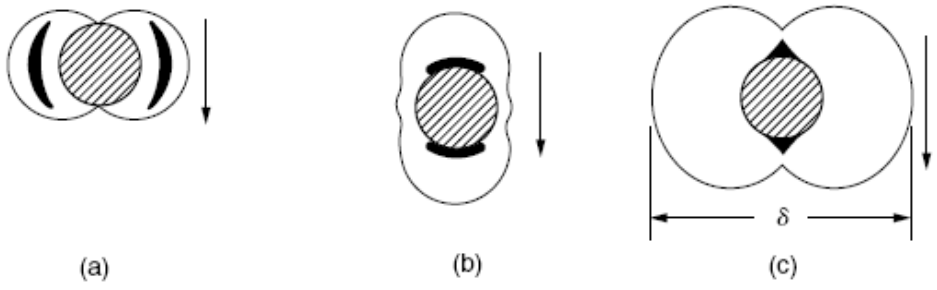

Figure 2-3: Flow field of a viscoplastic fluid around a spherical particle (Chhabra, 2007): (a) Ansley and Smith (1967); (b) Yoshioka et al. (1971); (c) Beris et al. (1985).

Over the years, researchers have used a dimensionless parameter, Y_G, in order to quantify the critical buoyant weight that a particle has to have for it to settle in a yield stress fluid:

$$Y_G = \frac{\tau_y}{gd(\rho_s - \rho_f)} \tag{2-34}$$

Theoretically, by equating the two forces involved in the movement of the particle, a critical Y_G can be calculated. In 1960, Andres postulated that this critical value is 0.212. This theory is known as the criterion for the initiation of motion.

Many researchers have since studied the critical value of Y_G for various types of viscoplastic fluids. Chhabra (2007) has presented a comprehensive comparison between the various values of critical Y_G that have been suggested in the past, highlighting the fact that there has been a wide range of suggested values, ranging from 0.04 to 0.2. Furthermore, Broadman and Whitmore (1961) have also pointed out the flaws of the Y_G theory, commenting that at a "no-motion" condition, neither the shear stress nor the normal stress distributions are known over the sphere surface. Furthermore, it has also been suggested that the distribution of pressure and shear stress in the fluid medium surrounding the sphere has not been characterised thoroughly. This causes some uncertainties in the analysis of the buoyant forces experienced by the settling sphere (Chhabra, 2007). Nevertheless, the dimensionless parameter Y_G has been used by various researchers to compare various experimental results and theoretical analyses (Atapattu, Chhabra, Tiu, & Uhlherr, 1986; Uhlherr, 1986) although its wide-ranging value indicates that there is still a fundamental mechanism that is largely unaccounted for.

The differences in the critical values of Y_G can be attributed to the uncertainties involved with the value of the yield stress itself, as well as its method of determination, which is still not yet well-established. Furthermore, other factors such as the elasticity of the fluid and the dependency of the fluid viscous parameters on its shear history (these factors will be discussed further in Section 2.4.4) are also possibly unaccounted for during those earlier experiments.

Theoretical work in the solution of the field equations describing the motion of particles in a viscoplastic fluid has been relatively limited so far. Beris et al. (1985) presented a comprehensive solution for the creeping flow region, albeit treating the yield surfaces as unknown boundaries. Blackery and Mitsoulis (1997) followed the work of Beris et al., this time using the regularisation technique of Papanastasiou (1987)(see equation 2-14). This technique allowed the equations of both solid- and fluid-like regions to be solved, and hence the location of the yield surfaces can be determined as part of the solution. As a result of this approach, the location of the fluid and solid-like domain suggested by Blackery and Mitsoulis (1997) differ significantly to that of Beris et al. (1985), although the resulting prediction of drag differ only slightly. Liu et al. (2002) revised the fluid problem devised by Blackery and Mitsoulis, this time using the regularisation formulation suggested by Bercovier and Engleman (1980) (see equation 2-13), and examined the effects of the regularisation parameter on the numerical solution. It was found that the position and shape of the yield region depend highly on the value of the regularisation parameter P_B, which is the inverse of ε in equation 2-13, and that the use of very high regularisation parameter would eventually lead to numerical error. It has since been suggested that the use of $P_B > 1000$ is satisfactory for this flow problem (Chhabra, 2007). Other similar studies in this area include Beaulne and Mitsoulis (1997), who used the regularised Herschel-Bulkley equation and de Besses et al. (2004), who examined the effect of slip on the drag coefficient. Under no-slip conditions, de Besses et al. (2004) found their results highly comparable to those of Liu et al. (2002) and Blackery & Mitsoulis (1997). Under slip conditions, de Besses et al. (2004) noted that the drag coefficient is reduced by about 30%.

While theoretical studies in this area have been relatively limited, plenty of empirical correlations have been suggested in the past in order to correlate the drag coefficient with the Reynolds number. Notable studies of this class include those by Pazwash and Robertson (1971), duPlessis and Ansley (1967), and Ansley and Smith (1967).

Furthermore, there has also been a drive towards the construction of a single drag curve, which would not only imitate the correlations for Newtonian fluids, but also incorporate Newtonian limits into a single, generalised correlation. Unfortunately, as can be seen later, this has been found to be extremely hard to achieve. This is due to the fact that the drag coefficient is extremely sensitive to small values of the dimensionless yield parameter (Y_G, see equation 2-34), which makes it difficult to accurately include results for fluids without a yield stress as a limit in the correlations for viscoplastic media. Furthermore, the dimensional groups that are to be correlated to the drag coefficient are also fluid model-dependent, making it difficult to compare one model to the other. An example of this approach is the correlation suggested by Atapattu et al. (1995), who based their analysis on the Herschel-Bulkley model:

$$C_D = \frac{24}{Q_A} \tag{2-35}$$

where Q_A is the modified dynamic parameter:

$$Q_A = \frac{Re_{PL}}{1 + kBi_{HB}} \tag{2-36}$$

where Re_{PL} is the particle Reynolds number as defined in equation 2-33 and Bi_{HB} is the Herschel-Bulkley Bingham number:

$$Bi_{HB} = \frac{\tau_Y}{k(V/D)^m} \tag{2-37}$$

This correlation is reportedly valid for $9.6x10\text{-}5 \leq Re_{PL} \leq 0.36$; $0.25 \leq Bi_{HB} \leq 280$ and $0.43 \leq m \leq 0.84$.

All of the aforementioned empirical correlations have focused on the attainment of accurate predictions of the drag coefficient C_D. Unfortunately, these correlations have been found to be very difficult to apply in the calculation of particle terminal settling velocity, mainly due to the fact that this variable affects both C_D and Re,

thus requiring an extensive number of iterations. Furthermore, the iterations are generally further complicated by the fact that the apparent viscosity of the fluid is dependent on the shear rate applied to it. This dramatically lowers the chance for the iteration to converge.

To ease the calculation for terminal velocity of a settling particle, another pair of dimensionless variables was suggested by Wilson et al. (2004; 2003) These authors adapted the pipe-flow analysis of Prandtl (1933) and Colebrook (1938-1939) to the system of falling particles. The first adaptation that was made was the concept of shear velocity, which in the pipe-flow analysis is defined as the square-root of the shear stress at the inner surface of the pipe divided by the fluid density. Thus, for the case of falling spheres, this can be written as:

$$V^* = \sqrt{\frac{(\rho_s - \rho_f)gD}{6\rho_f}} \tag{2-38}$$

Furthermore, one of the variables used in the pipe flow method is the dimensionless form of the fluid velocity in the pipe, which is the ratio between the mean velocity and the shear velocity V*. A similar approach is taken for the analysis of a falling ball in viscoplastic fluids, in which one of the dimensionless variables is defined as the ratio between the terminal velocity of the particle (V_t) with the shear velocity (V*).

The other dimensionless variable that was suggested by Wilson et al. is the shear Reynolds number:

$$Re^* = \frac{\rho_f V^* D}{\mu_{eq}} \tag{2-39}$$

where D is the particle diameter and μ_{eq} is the equivalent Newtonian viscosity.

μ_{eq} is defined as the calculated viscosity of a Newtonian fluid (with the same density as the medium) that would produce the same terminal fall velocity for a particle of

this type (Horsley et al., 2004). This variable can be obtained directly from the rheogram of the material. Furthermore, on the basis of experimental data, it was recommended that the equivalent viscosity be obtained at the following point of reference (Wilson et al., 2003):

$$\tau = 0.3\bar{\tau} \qquad \textbf{(2-40)}$$

Where τ is the shear stress caused by the submerged weight of the particle, and $\bar{\tau}$ is the mean surficial shear stress:

$$\bar{\tau} = \frac{(\rho_s - \rho_f)gD}{6} \qquad \textbf{(2-41)}$$

In relating the two dimensionless variables, Wilson et al. (2003) have based their analysis on the customary C_D-Re graph, by transforming numerous C_D and Re values into Vt/V* and Re* values. From these calculations, a new curve with Vt/V* versus Re* co-ordinates was plotted (see Figure 2-4). In practice, this plot can be used in a similar manner to the C_D-Re curve. Furthermore, unlike the C_D-Re curve, it allows the terminal velocity of particles to be determined directly without requiring iterations.

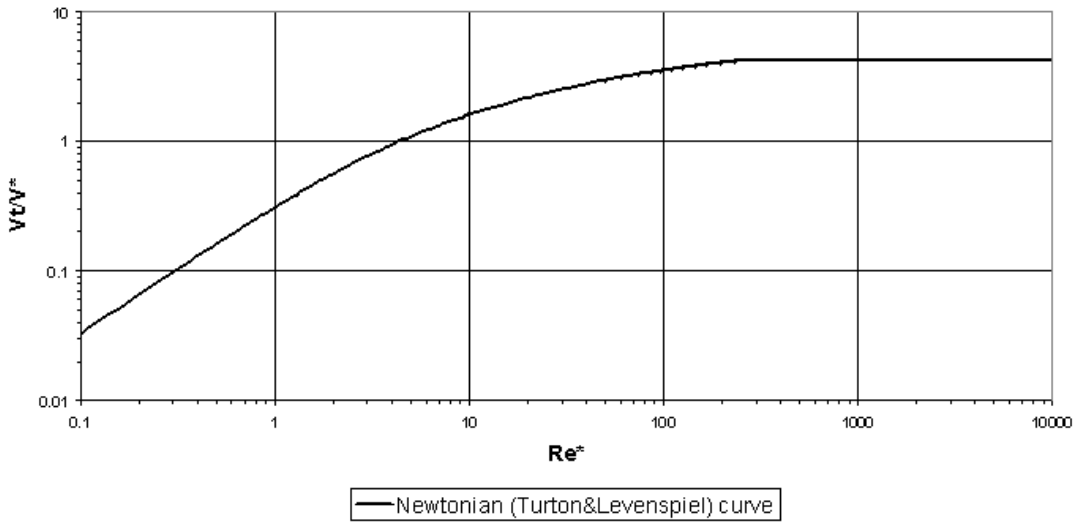

Figure 2-4: Plot of Vt/V* as a function of shear Reynolds number (Wilson et al., 2003).

The correlation suggested by Wilson et al. (2003) has been tested against various types of non-Newtonian fluids, as well as various densities and diameters of spherical particles. It also can be applied for both Newtonian and non-Newtonian medium (Wilson et al., 2003), and therefore is very versatile in determining the terminal velocity of the gravitational flow of particles in fluids.

2.4.4 Effects of fluid elasticity

The effects of elasticity on the settling behaviour of particles in a fluid have been briefly discussed in Sections 2.4.2 and 2.4.3. This field of rheology has garnered a lot of interest in the past few decades, especially due to the recent improvements in rheometry, which greatly facilitate the identification and quantification of viscoelasticity. Furthermore, this flow problem or more specifically the study of fluid flow over a spherical particle has been used as a benchmark problem for the testing of new solution procedures for the computation of viscoelastic flows. Notable studies in this area include Keunings (2000), Reddy and Gartling (2001), McKinley (2002), Owens and Phillips (2002), and Petera (2002), who all have successfully developed numerical algorithms for computing viscoelastic flows.

The study of the effects of elasticity on the flow behaviour of a fluid over an obstructive object (either a sphere or cylinder) has earlier been dominated by theoretical analysis. Several limiting conditions would generally be assumed, mainly due to the fact that it is impossible to consider all factors in the flow problem, i.e.

$$\frac{\varphi V}{D} = f\left(\frac{\rho_s}{\rho_f}, \frac{\mu(\dot{\gamma})}{\mu_0}, \frac{\mu_{solvent}}{\mu_0}, \frac{D}{d}, Re, El\right) \qquad \textbf{(2-42)}$$

Where φ is the characteristic relaxation time of the fluid, $\mu_{solvent}$ is the viscosity of the solvent that is used to prepare the polymer solution, D is the diameter of the sphere, d is the diameter of the column, and El (~ De/Re) is the elasticity number.

Similar to the theoretical analyses conducted in Newtonian, shear thinning, and yield stress fluids, a limiting condition of creeping flow (Re ~ 0) is generally assumed. Various studies with a number of fluid models in this region have established that very slight drag reduction exists at low to moderate values of Weissenberg number (We < 1.5) when compared to Newtonian flows with the same value of Reynolds number (Crochet et al. 1984; Chilcott and Rallison 1988; Gervang et al. 1992 for unbounded flows; Luo 1998; Jin et al. 1991; Warichet and Legat 1997; Baaijens 1998; Sun et al. 1999 for D/d = 0.5). At higher values of Weissenberg number, some disagreement still exists, with some studies suggesting that the pattern of drag reduction continues (Luo, 1998). The majority of the findings, however, suggested that a slight drag increase occurs, at least up to Weissenberg value of 2.5-3.5 (Gervang et al., 1992; Debbaut and Crochet, 1988; Harlen et al., 1990). It has been suggested that this increase in drag is caused by the increasing significance of elongation in the viscoelastic fluid, resulting in the existence of a thin region of highly extended molecules on the downstream side of the sphere. It is also because of this elongation that the velocity in the wake region decays much more slowly in viscoelastic fluids than in Newtonian fluid.

At even higher values of Weissenberg numbers, convergence has been found to be difficult to achieve. This is again caused by the increasing effect of elongation in the molecules of the fluid material, resulting in sharp stress gradients in the fluid medium. As a result, the effects of elasticity in this flow region are still largely unknown.

A very limited number of studies have been conducted on the effects of fluid inertia on the motion of the spherical particle moving in a viscoelastic fluid. The studies of El Kayloubi et al. (1987) and Sigli and Kaddioui (1988) concluded that there are significant discrepancies on the rate of deformation and stress fields caused by the effects of fluid inertia, although no shifts in streamlines were detected. It has also been suggested that different rheological models be used for different values of D/d (Yang & Khomami, 1999).

Experimentally, the effects of elasticity on the settling behaviour of a sphere in a viscoelastic fluid have been harder to determine. Up to the recent development of Boger fluids, which possesses shear rate independent viscosity properties (at least over an extended range of shear rates); it has been difficult for researchers to separate the effects of elasticity from shear thinning. In fact, several researchers (Kato et al. 1972; Chhabra and Uhlherr 1980, Bush and Phan-Thien 1984) have observed that there is a high agreement between the values of drag coefficients in viscoelastic and purely viscous media (in the creeping region), prompting the conclusion that shear-thinning effects are much more dominant and determining in the particle's settling behaviour than viscoelastic effects. Beyond the creeping region, Acharya et al. (1976) have suggested a correlation featuring a drag reduction with increasing values in Weissenberg number. Through flow visualisation studies, Acharya et al. (1976) also observed that different size and shape of wakes were encountered with different magnitudes of viscous, inertial, and elastic forces. By performing drag measurements for shear-thinning viscoelastic medium, Mena et al. (1987) concluded that at low shear-rate region elastic effects are the dominant factor in drag reduction. At higher shear-rate region, however, shear-thinning effects become more dominant and are the primary cause for further drag reduction.

Experiments in Boger fluids have been numerous, with various results and conclusions. Chhabra (2007) have compiled the various correlations of drag correction factor (Y) as a function of the Weissenberg number that have been suggested in the past by Jones et al. (1994), Chmielewski et al. (1990), and Tirtaatmadja et al. (1990). From this compilation, it was concluded that there is little agreement between the correlations. Furthermore, the experimental results do not match the theoretical predictions of a decrease in drag force with increasing value of Weissenberg number. Instead, the experimental results, although with very little quantitative agreement, generally indicate a plateau region of drag over the low range of Weissenberg number. This is followed by a negative slope and a second plateau, before increasing significantly with increasing Weissenberg number. This disagreement led to the conclusion that the drag on a sphere in a

purely elastic fluid is determined by various factors, including the interplay between shear and extensional rheological characteristics, which in turn are strongly influenced by the molecular architecture, the quality of the solvent, polymer conformation, and hysterisis of the fluid (McKinley, 2002). Thus, the numerical simulation of a purely elastic fluid needs to completely incorporate its shear and elongational properties for the accurate prediction of the settling behaviour of spheres in this type of fluid.

An interesting observation that has been made in experiments on the settling behaviour of a sphere in an elastic fluid is the existence of a velocity overshoot, and in some cases, negative velocity or "sphere bouncing" (Walters & Tanner, 1992). It was observed that a distance of approximately 20D is required for the sphere to reach a terminal velocity, unlike other experiments featuring non-elastic fluids. Furthermore, Walters and Tanner (1992) also reported on a velocity overshoot that is nearly three times higher than the terminal velocity. Similar and more detailed observations were outlined by Jones et al. (1994) and Becker et al. (1994) in a Boger fluid, as well as Arigo and McKinley (1998) in a shear thinning elastic fluid. King and Waters (1972) have outlined a scheme for evaluating viscoelastic material parameters from these transient properties.

Another interesting aspect that is associated with the effects of fluid elasticity on the settling behaviour of a sphere in a viscoelastic fluid is a phenomenon termed as the negative wake, where a flow reversal is observed, sometimes up to 30 radii downstream (Chhabra, 2007). This phenomenon was firstly recorded by Hassager (1979), who studied the rising of bubbles in shear-thinning viecoelastic fluids. Since then, similar observations have been reported by Bisgaard (1983), Maalouf and Sigli (1984), and Putz et al. (2008). Interestingly, several researchers reported the absence of negative wake in Boger fluids (Arigo, Rajagopalan, & McKinley, 1995; Bush, 1993). Based on these observations, Owens and Phillips (2002) concluded that the phenomenon of negative wake is the result of the interaction of shear and extensional flow in the wake of the sphere. This is a conclusion that supports the observation of Maalouf and Sigli (1984), who stated that the

phenomenon of negative wake was only observed in the case of shear-thinning viscoelastic fluids and only when the elasticity number exceeds a critical value. This critical value was found to be highly dependent on the dimensions of the experiment, i.e. the sphere and the column, in addition to the elastic and shear-thinning properties of the fluid.

2.4.5 Inter-particle interaction

2.4.5.1 Tandem formation

The settling behaviour of a number of spheres in a fluid medium has been extensively investigated, especially in the area of viscous Newtonian flow. In 1960, Happel and Pfeffer's assessment on the settling of two spherical particles arranged in a tandem formation in a viscous fluid found that the terminal velocity of the two spheres is greater than that of an isolated sphere. It should be noted at this point that the exact rheological nature of the fluid is not clear, as it is only described as 'viscous'. Nevertheless, the reduction in drag force leads to the conclusion that inter-particle interaction is significant in this type of flow problem.

The study of Lee et al. (2003), which uses Particle Image Velocimetry (PIV) to visualise the flow field formed as the fluid flow over a tandem arrangement of spherical particles, revealed that fluid inertia is a highly determining factor in the particle-particle interaction. As a result, the motion of particles in suspension is not reversible even in Newtonian fluids. This conclusion is in line with the experimental study of Tsuji et al. (1982), who observed that with two tandem spheres, the vortex behind the upstream sphere undergoes some changes, whereas the vortex behind the downstream sphere is similar to that of a single sphere. Furthermore, this conclusion is also supported by the recent numerical study of Prahl et al. (2007) using a Newtonian fluid at relatively high Reynolds numbers (50, 100, and 200), which reveals that the drag reduction for a secondary particle in tandem arrangement can be as high as 60-80%.

The extent of inter-particle interaction in a viscous Newtonian fluid was studied by Chen and Wu (2000), who measured the drag force experienced by two spheres with varying distance apart (here represented by the variable ℓ). Similar to the case with Prahl et al. (2007), Chen and Wu discovered that a reduction of up to 80% in drag, in comparison to that experienced by a singular sphere, is possible, especially at small distances. The interaction effect reduces significantly as the distance between the two spheres increases (C_D/C_{D0} increases from 0.2 to 0.6 as the ℓ/D value varies from 1/3 to 3 for flow with Re = 54). This result is similar to the results of Tsuji et al. (1982), who observed that the drag reduction effect from the sphere interaction disappears at $\ell/D > 5$ to 10.

The effects of shear thinning on inter-particle interaction were studied by Zhu et al. (2003), who conducted their experiment in a power-law fluid. At moderate values of Reynolds number ($0.7 < Re < 23$), Zhu et al. reported a decrease of up to 40% in the drag coefficient, which was obtained when the two spheres are touching, i.e. $\ell/D = 0$. An exponential correlation, where the drag reduction is shown to increase with increasing particle Reynolds number and decreasing separation distance ($0 < \ell/D < 3.5$), was then proposed. Furthermore, the results of Zhu et al. shows that the reduction in drag forces becomes relatively negligible ($C_D/C_{D0} \sim 1$) at ℓ/D value of 3.5, especially at the lower range of particle Reynolds number ($Re < 3.2$). Zhu et al. also demonstrated that the dependency of inter-particle interaction on the shear-thinning nature of the fluid is relatively weak compared to the particle Reynolds number and the distance between the particles.

In their study of two tandem spheres in a viscoplastic fluid, Gumulya et al. (2007) suggested a correlation for the settling velocity of two interacting spheres that have collided with each other, as the result of the second sphere settling faster than the first one (due to time effects, as will be discussed in Section 2.4.6). To take into account the interaction between the two spheres, Gumulya et al. introduced a new variable, β, which takes into account the different surficial stress of the combined spheres. This variable was used in conjunction with the correlation for the terminal settling velocity of a sphere in a viscoplastic fluid suggested by Wilson et al. (2003):

$$\bar{\tau}_{12} = \frac{2\bar{\tau}_1}{1+\beta} \qquad \textbf{(2-43)}$$

where $\bar{\tau}_{12}$ is the mean surficial stress and $\bar{\tau}_1$ is the individual surficial stress calculated as per equation 2-41. β was found to be a function of the particle Reynolds number, Re* (see equation 2-39), as well as the rheogram shape factor, α:

$$\beta = -56.04\Omega^2 + 214.32\Omega - 203.92 \qquad \textbf{(2-44)}$$

where

$$\Omega = \alpha\, \mathrm{Re}^{*0.065} \qquad \textbf{(2-45)}$$

The shape factor of the rheogram, α, is a measure of the viscoplasticity of the fluid. It is calculated as the ratio of the total area beneath the rheogram (to the left of the representative value of shear rate produced due to the motion of the sphere) to the triangle beneath the same rheogram section. A value of 1.0 represents a fully Newtonian fluid, whereas a value of 2.0 represents a pure plastic material.

Lee et al. (2003) also studied the effect of elasticity on inter-particle interaction, by comparing the flow fields formed by a Newtonian fluid with that of a Boger fluid. Through this study, it was concluded that in addition to fluid inertia, normal stress differences and elongation also have important effects on the inter-particle interaction. This is reflected by the conflicting inter-particle interaction effects

(both drag reduction and enhancement have been reported with increasing We number) that have been suggested in past literature, as highlighted by Solomon and Muller (1996). It was thus suggested that the conflicting results is caused by the different extensional characteristics of the fluid.

2.4.5.2 Parallel (horizontally-aligned) formation

The interaction of two parallel spheres in a Newtonian fluid has been studied by Wu and Manasseh (1998). Through experiments at various Reynolds numbers, it was concluded that the separation distance between the two spheres is highly dependent on the value of the Reynolds number. At low values of Re (Re < 0.1), no separation occurs, whereas at higher values, the particles tend to repel each other. Furthermore, Wu and Manaseh also observed that the two particles experience counter-rotating spinning in the range of 0 < Re < 10 and that the settling velocity of the two spheres is approximately 30% higher than a single particle for cases where the Reynolds number is low (< 2). At higher Reynolds number, due to the separation of the two particles, no drag reduction was observed.

Chen and Wu (2000) also conducted their study in a Newtonian fluid (30 < Re < 200) and observed that there is a drag increase for two parallel spheres. This result is in agreement with the observations of Tsuji et al. (1982), who reported a drag increase at distances of ℓ/D < 2 3 at Re ~ 400. This increase in drag forces was found to be caused by the nozzle effect that occurs between the two spheres at small distances as well as the increasing effect of form drag as the distance increases. The inter-particle interaction of spheres arranged at various other orientation angles was also examined by Chen and Wu (2000), who found that the trend for the drag to increase occurs with all the arrangements. This increase in drag was found to reach a maximum when the spheres are located at an angle of 45^{o} to each other, with the sphere that is placed upstream experiencing the maximum drag effects. The downstream sphere, on the other hand, has been shown to experience a slight drag reduction due to the wake of the other sphere.

In 1994, Joseph and co-workers (1994) observed that in viscoelastic fluids, spheres that are horizontally-aligned tend to attract when the initial separation distance between them is small. Upon converging, the two spheres tend to undergo a re-orientation motion, where one of the spheres slightly decelerates and move towards the flow path of the other sphere. This continues to occur until the two spheres touch and aggregate, with their line of centres oriented vertical. The attraction between closely-distanced spheres in viscoelastic fluid was found to be contrary to the effects found in Newtonian fluids, where closely-distanced spheres experience repulsion effects rather than attraction.

2.4.6 Transient effects in the experiment of vertically-aligned spheres

The effects of a surrounding particle on the settling behaviour of a downstream particle have been discussed in the previous section. However, in yield-stress fluids, the experiment of vertically-aligned spheres is further complicated as the effects of inter-particle interaction is compounded with transient effects. This difficulty is highlighted due to the low reproducibility of the seemingly simple sphere-drop experiment in yield stress fluids, as noted by Chhabra (2007) and Atapattu et al. (1995). Atapattu et al. (1995), who conducted their experiments in viscoplastic solutions of Carbopol, mentioned that a good reproducibility of the result is only obtained after 4-10 releases of spheres, and that the first release generally has a much slower settling velocity. As more spheres are released, the settling velocity increases, until an asymptotic value is reached. This conclusion is in agreement with the findings of Hariharaputhiran et al. (1998), who suggested that the changes in the terminal velocity of particles settling in viscoplastic fluids can be explained by the hypothesis of network damage caused by shear and subsequent healing, similar to the hypotheses of Cho et al. (1984) and Ambeskar and Mashelkar (1990) for viscoelastic fluids. Thus, it is clear that whereas inter-particle interaction effects are significant in all types of fluid rheology, in yield stress fluids the extent of interaction effects appear to last over a longer time frame and over much larger distances.

The transient effects in the experiment of vertically-aligned spheres have been studied further by Horsley et al. (2004) using a polymeric solution. It was shown that the difference in the velocity of the two spheres diminishes as the time interval between releases is increased, and that the reduction in the velocity difference generally follows asymptotic behaviour.

In 2007, Gumulya and co-workers (2007) presented a correlation between the settling velocity of a sphere that follows the flow-path of another sphere in a viscoplastic fluid with the dimensionless form of the time interval between releases and the shape factor of the rheogram of the fluid. The dimensionless form of the time interval was assigned as:

$$t^* = \dot{\gamma} t \qquad \textbf{(2-46)}$$

where t is the time interval between the releases of the spheres and $\dot{\gamma}$ is the shear rate produced by the flow of the sphere if it was travelling in an undisturbed fluid medium. The suggested correlation was as follows:

$$V_2 = V_{t1}\left[1.0 + 4.94 t^{*-0.30}(\alpha - 1)^{1.89}\right] \qquad \textbf{(2-47)}$$

where α is a measure of the fluid viscoplasticity (see Section 2.4.5.1). The correlation was found to have good agreement with the experimental data involving two spheres with identical diameter and density.

Transient effects are also commonly encountered in viscoelastic fluids, despite the existence of some studies that did not recognise its effects at all (Tirtaatmadja et al., 1990). Bisgaard (1983) showed that a sphere that is released in a Boger fluid (with a characteristic time of 12s) 10 minutes after the first release can have a velocity that is 30% higher than the first sphere. Cho et al. (1984) studied this phenomenon in viscoelastic fluids, and observed that the time interval effect is reduced with a reduction in the viscoelasticity of the solution.

Based on these observations, Cho et al. (1984) concluded that the dependence of the steady settling velocity on the time interval between successive releases of spheres is due to the local rupture of the polymer network, thus leading to the formation of a "cavity", as the spheres move through the solution. The rupture of the polymer network leads to reduced viscosity parameters, thus resulting in the sphere that is released some time after the first one to have a higher settling velocity. This view, however, was contradicted by the experiments of Ambeshkar and Mashelkar (1990) who measured the concentration of the polymer molecules behind the settling spheres, and did not observe any changes in the fluid concentration. This phenomenon was later examined by Gheissary and van den Brule (1996), who noted that a sphere that is released in a Carbopol solution two hours after the first one has a much larger velocity than the previous sphere, indicating that the solutions that were used in this study tend to require very long periods of relaxation (after being sheared) for the original viscous parameters to be recovered. The slow rates of relaxation found in this study seem to contradict the theory of cavity formation suggested by Cho et al. (1984). Based on this finding, Gheissary and van den Brule (1996) suggested that other factors, such as shear-thinning and elasticity, may be responsible for the differences in the settling velocity of the two spheres.

The effects of fluid elasticity on the settling behaviour of two vertically-aligned spheres was examined by Bot et al. (1998), who found that the two spheres tend to form a ‘stable distance’ between them. That is, although the velocity of a sphere following another along the same line-of-centre would be higher than the first one, when the distance between the two spheres diminishes, the velocity of the first sphere increases, thus forming a stable distance between the two. Furthermore, Bot et al. also found that the stable distance between the two spheres increases with increasing Deborah number. This finding was therefore in agreement with the findings of Gheissary and van den Brule (1996). Through comparing the effects of shear-thinning with elasticity on the stable distance between the two spheres, it was concluded that particle aggregation always occurs in shear-thinning fluids. The stable distance that has been observed for Boger fluids has therefore been

attributed to the extent of particle-particle interaction that is highly dependent on inertia and elongation.

Thus, from the discussion in this section, it is clear that the experiment of vertically-aligned spheres settling in a rheological solution is still full of uncertainties and that the behaviour of the downstream particle is dependent on various factors, such as the transient behaviour of the fluid itself, as well as inertia and elasticity as effected by the surrounding particle.

2.5 Conclusion

A comprehensive review has been conducted on the study of the settling behaviour of particles in various types of fluids. Through this review, it is apparent that a problem that seems simple at first is actually quite intricate, due to the interweaving effects of the various rheological attributes of the fluid solutions. Based on this knowledge, it is apparent that the study of the settling of particles in fluids requires thorough characterisation of their flow behaviour.

In the past few decades, a large body of work has been dedicated towards the prediction of the steady settling behaviour of particles, or similarly, the flow of various fluids through obstructive objects. Numerous correlations and numerical solutions have been suggested, with varying degree of success. The effects of yield stress on the terminal settling behaviour of spheres in viscoplastic fluids have been effectively captured by Wilson et al. (2004; 2003). Furthermore, the author and co-workers (Gumulya et al., 2007) have also attempted, with a degree of success, to determine the transient nature of the yield stress fluids through the study of the settling behaviours of two identical spheres settling co-linearly. In this study, it was found that a sphere that follows the flow path of another sphere settles at a much higher velocity, often causing the subsequent sphere to catch-up and collides with the previous one. The effects of yield stress on the interaction of particles while settling in a non-co-linear configuration, however, are still largely unknown. This

thesis, therefore, aims to resolve this problem through the use of experimental and numerical techniques.

Through conducting this literature review, it was also revealed that the solution of polyacrylamide, which is the fluid medium selected for this study, may exhibit elasticity, thixotropy, as well as viscoplasticity.

It is therefore important to start this study with a careful and precise characterisation of the rheological behaviour of the fluid solutions. In doing so, however, it should be kept in mind that the complexity of the rheological behaviour of the fluid solutions can present numerous errors during the measurement. Factors such as wall slip, fluid inertia, and secondary flow, which can cause uneven stress distribution, are commonly found in the rheometry of viscoplastic and viscoelastic fluids, and can affect the accuracy of measurement considerably. In such cases, a study of CFD has been found to be effective in identifying such errors and anomalies.

Chapter 3 Experimental apparatus and methodology

3.1 Introduction

The literature review presented in Chapter 2 reveals that the rheological nature of polymeric fluids, such as one that is used in this study, can be very complex. As a result, the study of the settling behaviour of spheres in this type of fluid, while may have seemed relatively simple at first, can become highly intricate, involving a large number of factors and variables.

Firstly, the most obvious factors are the viscosity of the fluid and the drag force of the particles on the fluid material. These are influenced by the densities of both the fluid and the solid materials, as well as the diameter of the particles. Thus, to examine the effects of these factors, several fluid solutions of slightly different rheology will be used. The details of the sphere and the fluid solutions are presented in sections 3.2.2 and 3.2.3, respectively.

Secondly, two types of experiment are planned for this study:

- Category I: Experiment involving two vertically-aligned spheres, where one sphere is released into the fluid following the flow path of another sphere
- Category II: Experiment involving two horizontally-aligned spheres, where two spheres of known initial distance are released simultaneously into the fluid.

Through the first category of experiments, it is expected that the dependence of the particle settling behaviour on the shear history of the fluid can be examined. This is an extension of the study conducted by Horsley et al. (2004) and Gumulya et al. (2007), in which the examination has been confined to the settling of two identical spheres. In this study, spheres of varying densities and diameters will be incorporated to assess the effects of the shear history of the fluid on the particle settling behaviour.

In the second category of experiments, an aspect of the viscoplastic fluid that is still largely unknown, which is the influence of the yield stress on the interaction between two particles settling in close proximity to each other, will be examined. It is expected that this study can give an understanding on the flow field surrounding the settling particles.

The two experiments described above require a slightly different experimental procedure. In the first category of experiments, the design of the particle-release mechanism ensures that the two spheres are consistently dropped at the centre of the column. As a result, a relatively simple set of optical sensors can be used to determine the position of the spheres down the column. The second category of experiments involved the study of two spheres that are horizontally-aligned. This required the 3D position of the spheres to be determined at various times during the experiment. A more complex sensor system is needed and a stereo-photogrammetry procedure was incorporated. The details of the particle-release mechanisms and the respective sensor systems are presented in this chapter.

Throughout the experiments, a standardised 'resting' time of 15 minutes between each experiment was established. This was to allow the fluid solution to reconstitute itself and to regain its original viscous properties. By employing such a procedure, repeatable values of a steady-settling velocity can be obtained (Gumulya et al., 2007).

3.2 Main apparatus: design and preparation

3.2.1 Column

The main experimental apparatus consists of a straight-walled column with square cross section and closed bottom. The dimensions of the column are 0.2m x 0.2m x 1.2m. These dimensions have been selected based on the rheology of the fluid solutions, such that particles having diameter of less than 10 mm can fall through

the fluid solutions without experiencing significant wall effects (Atapattu et al., 1990). The walls of the column are made of clear Perspex, allowing measurements to be carried out by optical sensing devices.

The ball dropper is located at the centre of the upper enclosing cover. This can be removed to charge a fresh solution and can be relocated to its original position by using locating pins (see Figure 3-2 and Figure 3-5).

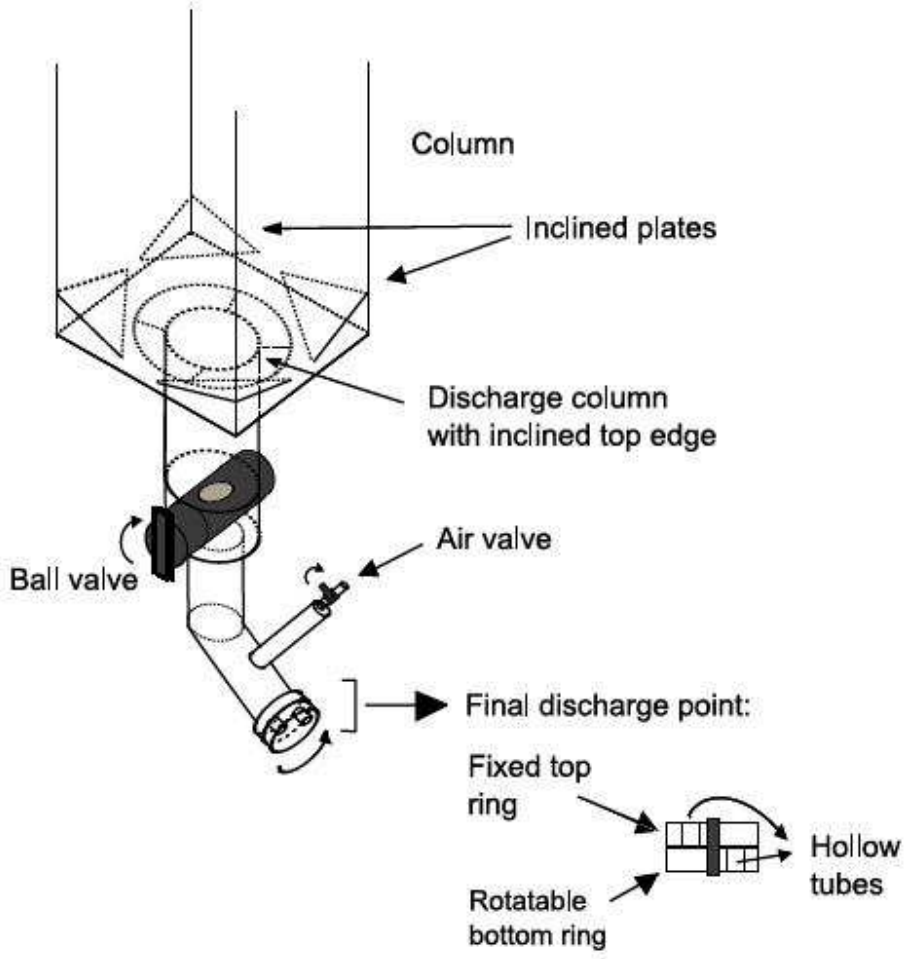

Figure 3-1: Schematic diagram of the discharge mechanism installed at the bottom of the column.

The lowest section of the column is inclined towards a central discharge point. The retrieval mechanism consists of two valves, which ensure that any air bubbles are caught in the lower section and never enter the column (see Figure 3-1).

3.2.2 Spheres

Three different ball materials (bronze, chrome-plated steel and stainless steel) with different diameters (6.35, 7.95, and 9.95 mm) are used during all the experiments. The densities of these spheres are 8876.0, 7792.2, and 7638.0 kg/m^3, respectively.

3.2.3 Fluid solutions

The viscoplastic fluid used in the experiments are aqueous solutions of Floxit 5250L (supplied by Ciba Specialty Chemicals, Perth, WA), which is an acrylamide/acrylic copolymer used widely in various industries as a viscosity modifying additive.

The solutions were prepared using a standardised procedure as recommended by the manufacturer. Based on the required final concentration, a known mass of Floxit 5250L powder was added gradually to 60.0 L of tap water, which was stirred continuously. The Floxit 5250L powder is then added slowly to ensure even dispersion, while the stirring speed of the agitator is adjusted such that a stable vortex is created in the solution. Once all of the solids have been added, the solution is allowed to stabilise (3 days), whilst the agitation is continued to ensure a homogeneous mixture.

The solution is then transferred to the column and is left for 1 week to allow for all of the air bubbles to escape. Samples from various parts of the column were then taken periodically throughout the experiments to ensure that the rheology of the fluid is consistent.

The solutions used in this experiment were 0.9%, 1.0%, and 1.1% (w/w) Floxit 5250L concentrations. These solutions have been found to be stable (Horsley et al., 2004). Therefore, they were seldom replaced due to a change in rheometry. The

resulting solution is also clear and highly transparent, thus allowing for optical sensors to be used for the monitoring of settling velocities of particles falling through the fluid.

3.2.4 Rheometer

The rheology of the fluid solutions is periodically tested using a rheometer from HAAKE (Thermo Electron Corporation, Karlsruhe, Germany) (HAAKE MARS II) that features the use of a set of air bearings for the minimisation of motor inertia and the maintenance of axial stiffness of the rotor during measurement. Numerous modes of measurements are available, including controlled stress (CS), controlled shear rate (CR), and controlled deformation (CD), as well as rotational and oscillation testings. The rheometer is connected to a temperature control unit, which is automatically driven by the computer through HAAKE's RheoWin software. This software also controls the rheometry process.

The cone-and-plate geometry (C35/4Ti from Thermo Electron Corporation, Karlsruhe, Germany) is used for all rheological testings at a standardised temperature of 23.5^{o}C. The diameter of the cone is 35.007 mm with an angle of 3.99^{o}. The tip of the cone is truncated and a gap of 0.139 mm with the metal plate is set before each measurement.

3.3 Category I: the settling of two vertically-aligned spheres

This experiment studies the settling behaviour of two spheres falling one after the other in the Floxit solutions at three concentrations (0.9, 1.0, and 1.1%). This is a continuation of the work conducted by Horsley et al. (2004) and Gumulya et al. (2007), where the study was limited to the case of two identical spheres falling one behind the other with the second sphere falling at variable time gaps after the first sphere. The experimental work being considered for this study involved several different sphere parameters:

- Case A: two spheres with identical density and diameter
- Case B: two spheres with identical diameter, with the second sphere having greater density than the first one ($\rho_{s1} < \rho_{s2}$)
- Case C: opposite of case B ($\rho_{s1} > \rho_{s2}$)
- Case D: two spheres with identical density, with the second sphere having greater diameter than the first one ($D_1 < D_2$)
- Case E: opposite of case D ($D_1 > D_2$)
- Case F: two spheres of different densities and diameters

The resulting flow and velocity profiles obtained from each type of these experiments will be discussed briefly in Section 3.3.2 and with more detail in Chapter 6.

3.3.1 Apparatus

3.3.1.1 Initial ball dropping mechanism

The ball dropper was designed based on a two-gate system, which makes it able to drop two balls, one behind the other, at specific time intervals. The design of the gates was such that no rotational movement or initial velocity is induced during the

release of the spheres into the solutions. A ball is positioned above each gate and as the motor is started, both gates open. The lower gate releases the first ball into the solution, whereas the upper gate releases the second ball to the lower one. After a specified time delay, the motor would then be activated again, and the second ball is then released into the solution. The schematic diagram for the ball dropper is presented in Figure 3-2.

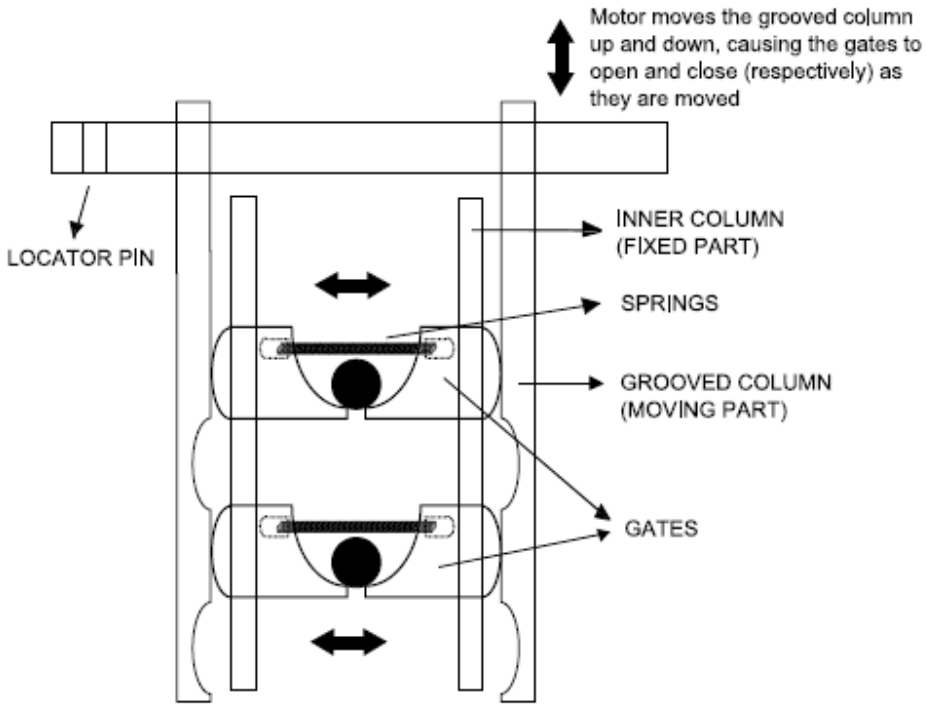

Figure 3-2: Schematic diagram of the ball dropper mechanism for the experiment of vertically-aligned spheres (Category I)

To accurately drop each ball at the specified time difference, the activation time of the gates is controlled by developed software (Devenish, 1998). To minimise splashing and externally induced rotation, the lower gate needs to be adjusted such that it is immersed in the fluid. The upper gate, however, should not be immersed, as the buoyancy of the fluid may impede the gravitational acceleration of the upper sphere, causing a delay in its movement to the lower gate. In some extreme cases,

the movement of the upper sphere may become very slow, such that it gets 'caught' while settling through the upper gate, causing the ball dropper to be congested.

3.3.1.2 First optical system

The fall velocity of the spheres is recorded by taking advantage of the transparency of the fluid and the Perspex column walls. The column is equipped with a number of optical sensors, which are distributed evenly along the length of the column. Each sensor consists of an infra-red light source and a detector, which detects the infrared beam that is located on the other side of the column. Figure 3-3 shows the setup of the optical sensor system fitter to the Perspex column.

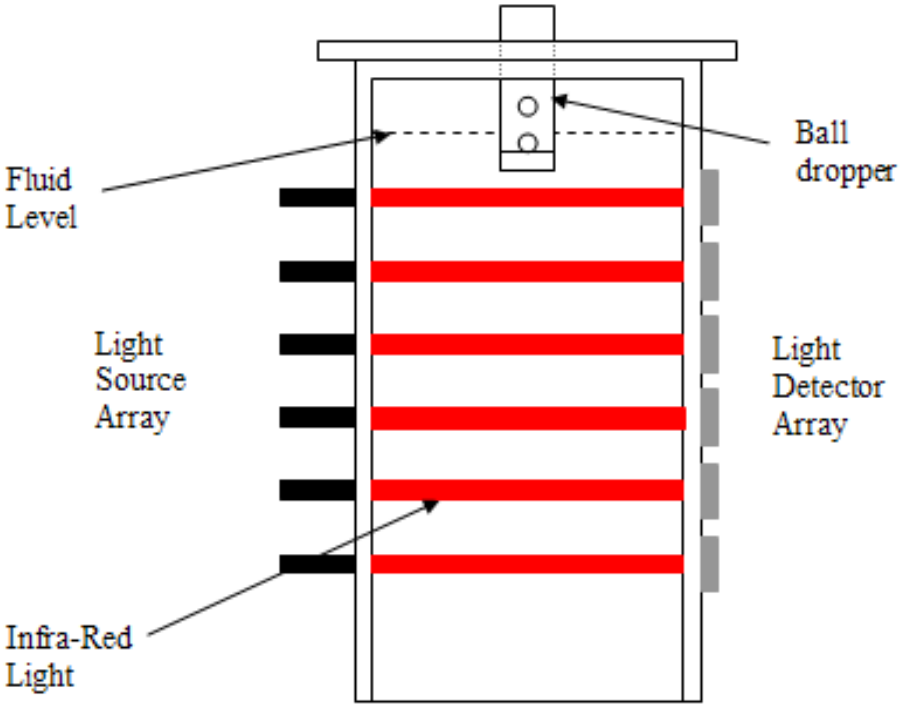

Figure 3-3: Schematic diagram of the optical sensor system employed for the experiment of vertically-aligned spheres (Category I).

As each sphere was released from the ball-dropping mechanism located at the top of the column and falls down the centre-line, it interrupted each of the light beams

generated by the light source. The interruption of these light beams was detected by the sensors and thus, the position of the sphere, as well as the time of this interruption, was recorded. The location and time data obtained was transmitted to a computer using custom written data-collection software.

3.3.2 Methodology

The experiments were conducted in a laboratory with a controlled temperature of 23.5°C (± 1°).

The settling velocities of the spheres are approximated by considering the amount of time required for the spheres to travel from one sensor to the other. The typical result for this analysis for a case of two identical spheres falling one behind the other (case A) is presented in Figure 3-4. The first sphere, which travels through the undisturbed fluid, reaches a constant velocity shortly after it enters the column. On the other hand, the second sphere, which travels in-line with the first sphere a few seconds later, travels at a much higher velocity. Furthermore, the velocity of the second sphere also increases as the gap between the first and the second sphere decreases. The second sphere eventually catches up with the first one, and the two spheres collide. After the collision, the two spheres attach and travel at the same velocity.

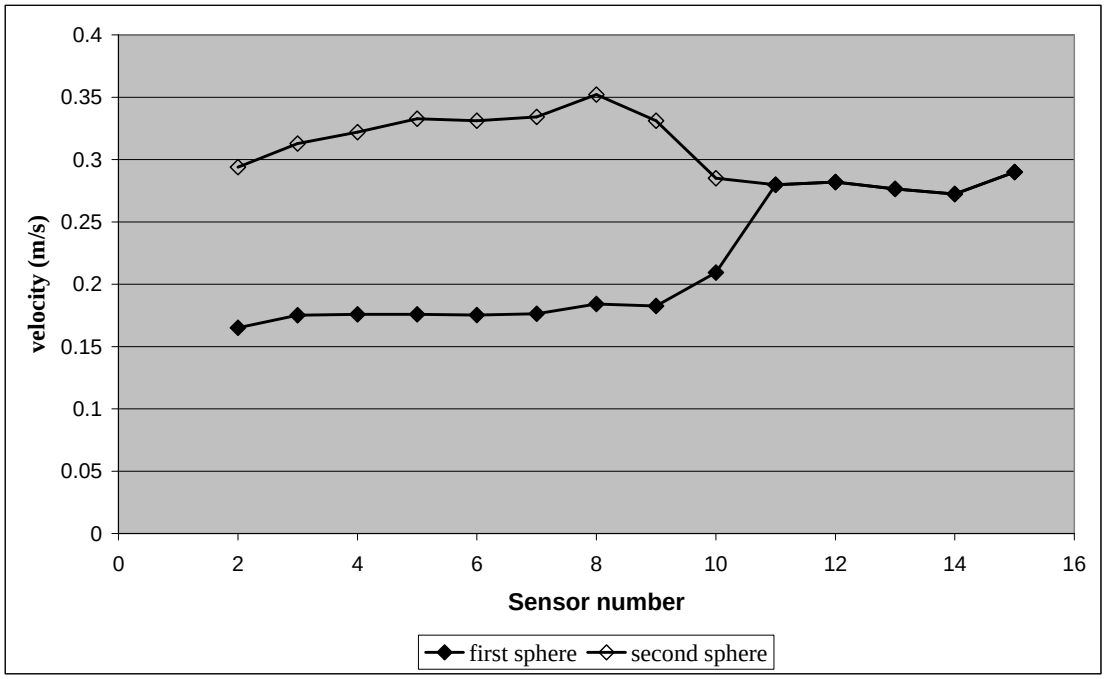

Figure 3-4: Velocity trace of 6.35 mm bronze spheres travelling in a 0.9% Floxit 5250L solution, with 2.5 s time difference.

The constant velocity attained by the first sphere shortly after it enters the solution and prior to its collision with the second sphere is considered to be a terminal settling velocity (V_t). The same consideration can be applied to the settling condition after the two spheres collide, where the combined spheres, as can be seen in Figure 3-4, tend to maintain a steady settling velocity. The second sphere, on the other hand, tends to continually accelerate towards the first sphere, and therefore is not considered to have reached a terminal settling condition.

3.3.3 Error estimation

The error involved with this experiment is caused mainly from the approach of taking the average ball settling velocity between the sensors. The level of percentage error, therefore, is a strong function of the settling velocity of the particles themselves (~ 0.05 – 0.6 m/s), as well as the distance between the sensors.

The average distance between the sensors is 90.6 mm (± 5%). The measurements have been conducted up to an accuracy level of 1 mm. The sensors are capable of measuring time fractions with up to 0.01 s degree of accuracy.

For this experiment, the percentage error involved with the measurement of terminal settling velocity is considerably lower than that for cases where the terminal velocity is not reached. For the case presented in Figure 3-4, for instance, the terminal settling velocity of the first sphere is calculated by taking the average value of the settling velocities over sensors 2 to 9. Similarly, the terminal settling velocity of the combined spheres is calculated by taking into account data from sensors 11 to 15. As the second sphere does not reach a terminal velocity and undergoes continual acceleration towards the first sphere, such calculation procedures cannot be applied. The instantaneous settling velocity of the second sphere, therefore, utilises data acquired from two adjacent sensors only.

Based on the considerations stated above, it is estimated that the maximum percentage errors, estimated at a maximum settling velocity of 0.6 m/s, are 1.8% and 6.7% for V_t and the transient velocity of the second sphere, respectively. The details of this calculation are presented in Appendix A.1.

Shortly before the two spheres collide, there is a significant decrease in the velocity of the second sphere, as well as an increase in the velocity of the first sphere (see the settling velocities over sensors 9 and 11 in Figure 3-4). This stage of the experiment is referred to as the 'critical condition', where the interaction between the two spheres causes some changes in the velocity pattern. With the current experimental configuration, it is very difficult to obtain an accurate depiction of the fluctuations in the settling velocities during this critical condition, as these fluctuations normally occur over a very short distance and time frame. The effects of inter-sphere interaction in this experiment, therefore, are very difficult to determine. The implications of the high uncertainties involved with this stage of the experiment will be discussed in more detail in Chapter 6.

3.4 Category II: the settling of two horizontally-aligned spheres

To determine the effects of sphere interaction on the settling behaviour of particles in viscoplastic fluids, two spheres having the same terminal velocities (i.e. identical) are released side-by-side, with a horizontal gap between them, into the fluid. The trajectories of the spheres along the length of the column, as well as their settling velocities, are monitored using a stereo photogrammetry sensor system. The initial distance (d_0) between the spheres is varied (25, 37.5 and 50 mm), giving an initial-distance-to-diameter ratio (d_0/D) range of 2.5 to 7.9.

3.4.1 Apparatus

3.4.1.1 Second ball dropping mechanism

Similar to the ball dropper used for the experiment of vertically aligned spheres, the ball dropper in this configuration uses a system of gates that are opened and closed through the activation of a motor. The design of the gates was such that no rotational movement or initial velocity is induced during the release of the spheres into the solutions. A set of four gates is used to release up to four balls simultaneously. These gates are opened and closed through the vertical movement of a set of inverted cones (see Figure 3-5), which are evenly distributed and attached on a steel plate with uniform thickness. To ensure that the gates are opened and closed at the same time, the movement of the plate is controlled at its centre by a spring-supported cylinder, which in turn is connected to the motor.

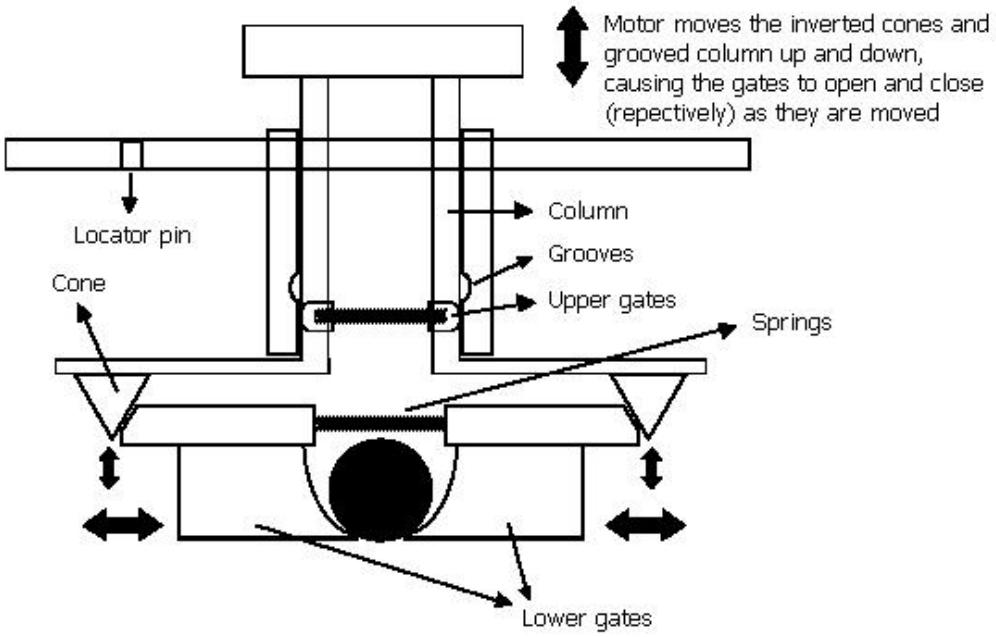

Figure 3-5: Schematic diagram of the ball dropper mechanism for the experiment of horizontally-aligned spheres (Category II).

The position of the gates along their axes can be adjusted such that the distance between the spheres can be varied (0.025 – 0.050 m). The gate system is schematically described in Figure 3-5.

3.4.1.2 Second optical system

The 3D position of the spheres as they settle in the column is measured with a stereo-photogrammetry system. The components involved with this measurement system have been listed in Appendix A.2.2, whereas the schematic setup of this equipment can be seen in Figure 3-6. Two progressive scan video cameras having 1300 × 1030 effective pixels and a pixel size of 6·7 µm in both dimensions were used, allowing the capture of high quality images of fast moving objects. The two cameras were synchronised and set to capture images at a rate of 10 Hz. This frame rate has been found to allow for sufficient number of samples along each sphere's trajectory to be captured.

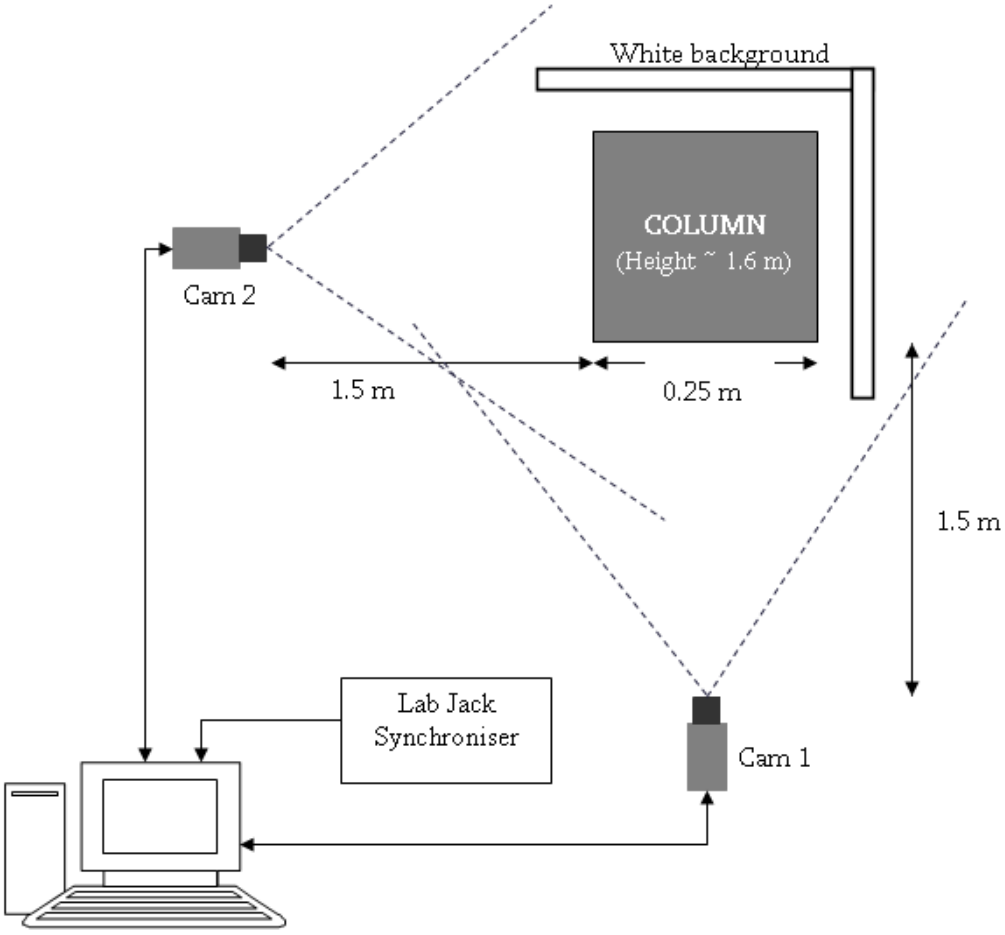

Figure 3-6: Setup of stereo-photogrammetry Sensor system

The cameras were oriented towards different sides of the column with a convergence angle of ~ 90°. The optical axes of the cameras were orthogonal to the side of the wall column that they are facing, thus allowing the column walls to be considered as plane-parallel interfaces for the refraction modelling, which will be discussed later in Section 3.4.2.2. Because of dimensional limitations, the cameras had to be rotated by ~ 90° to allow for the largest dimension of the image format to be parallel to the column.

3.4.2 Methodology

3.4.2.1 Calibration of cameras

Prior to the implementation of each camera, a calibration process needed to be conducted to determine its focal length as well as the distortion effects caused by the imperfections of the lenses.

The calibration method used for this study was the Self-Calibration Bundle Adjustment method, where multiple images of a 3D target field were taken from a variety of perspectives and rotational angle. The 3D target field used for this study was made up of 70 target points, which were essentially flat circles of highly reflective material with precise dimensions and reflectivity, as well as adhesive-tape backing (RTR – 0.25 Dot Diameter x 1.00 Spacing supplied by Hubbs Machine & Manufacturing Inc. ®). These target points were attached to various objects with flat surfaces within the field-of-view of the cameras. The target field was captured at various viewing and camera rolling angles, as well as distances, resulting in a total of 10 images for each camera.

These frames were then evaluated using close-range photogrammetry software, Australis (Photometrix, 2004), which has the capability of identifying and measuring the centroid of the target points in each image and performing a Bundle Adjustment calculation for the calibration process. In the Bundle Adjustment calculation, a Least Squares Estimation (LSE) method is employed to analyse the target points based on the collinearity equations:

$$X = X_P - c\frac{R_{11}(x-x_0)+R_{12}(y-y_0)+R_{13}(z-z_0)}{R_{21}(x-x_0)+R_{22}(y-y_0)+R_{23}(z-z_0)}$$

$$Y = Y_P - c\frac{R_{21}(x-x_0)+R_{22}(y-y_0)+R_{23}(z-z_0)}{R_{31}(x-x_0)+R_{32}(y-y_0)+R_{33}(z-z_0)} \quad \textbf{(3-1)}$$

where X, Y are the photo-coordinates in the image frame, x, y, z the 3D coordinates of the object, c the focal length of the camera, x_0, y_0, z_0 the 3D coordinates of the

camera's perspective centre in the image frame, and X_P, Y_P the photo-coordinates of the projection of the perspective centre to the image plane. R_{ij} represents element ij of the rotation matrix R:

$$R_{ij} = f_{ij}(\omega, \varphi, \kappa) \quad \textbf{(3-2)}$$

where ω, φ, and κ are the rotational angles of the perspective centre around the x, y, and z axes, respectively. Using this calculation procedure, the positions of each target point, the location and orientation of the camera for each exposure, as well as the calibration parameters of the camera were determined. Furthermore, the distortion characteristics of the cameras due to imperfections in the lenses, characterised by radial and decentring constants, k_1, k_2, k_3, P_1, and P_2, were also determined. More details of this aspect of the calculation are presented in Appendix A.2.1. As this procedure does not require prior knowledge of the target points, the self-calibration method is used extensively in the field of close-range photogrammetry (Fraser, 1997).

The results of the calibration are described in Appendix A.2.2. The accuracy and reliability of this process was reviewed by the root-mean-square values of the resolved target field, which were found to be ±0.034 and ±0.045 pixels for cameras 1 and 2, respectively (Lichti et al., 2009), indicating that the quality of the self-calibration process is satisfactory for both cameras.

3.4.2.2 Correction for refraction effects

From the perspective of photogrammetry, the settling-sphere experiment is multi-media in nature, due to the difference in the refractive indices for air, Perspex, and the Floxit solution. Some adjustment in the calculation procedure, therefore, needs to be incorporated to include the effects of refraction.

The refraction correction equation used in this study was a modified version of that suggested by Li et al. (1997):

$$\delta r = \frac{c}{(L + t_C + H)}\left(\frac{r}{c}(t_C + H) - d\tan\theta_2 - H\tan\theta_3\right) \quad \textbf{(3-3)}$$

where L is the distance from the camera perspective centre to the outside of the column, t_C the column wall thickness, and H the distance from the inside face of the column to the object point, as shown in Figure 3-7. r is the 2D radial position of the point of interest from the principal point:

$$r^2 = (X - X_p)^2 + (Y - Y_p)^2 \quad \textbf{(3-4)}$$

The parameters θ_2 and θ_3 in equation 3-3 represent the angles between the object point ray and the surface normal at the interface between the Perspex with the Floxit solution, as shown Figure 3-7. These angles are related through Snell's law of refraction:

$$n_1\sin\theta_1 = n_2\sin\theta_2 = n_3\sin\theta_3 \quad \textbf{(3-5)}$$

where θ_1 is the angle between the object point ray and the surface normal at the interface between the Perspex and air. A value of 1.0003 was used for the index of refraction for air. Indices of 1.333 and 1.583 were determined for the Floxit and the Perspex, respectively, using a Carl Zeiss Jena Abbe refractometer (Carl Zeiss, Oberkoschen, Germany).

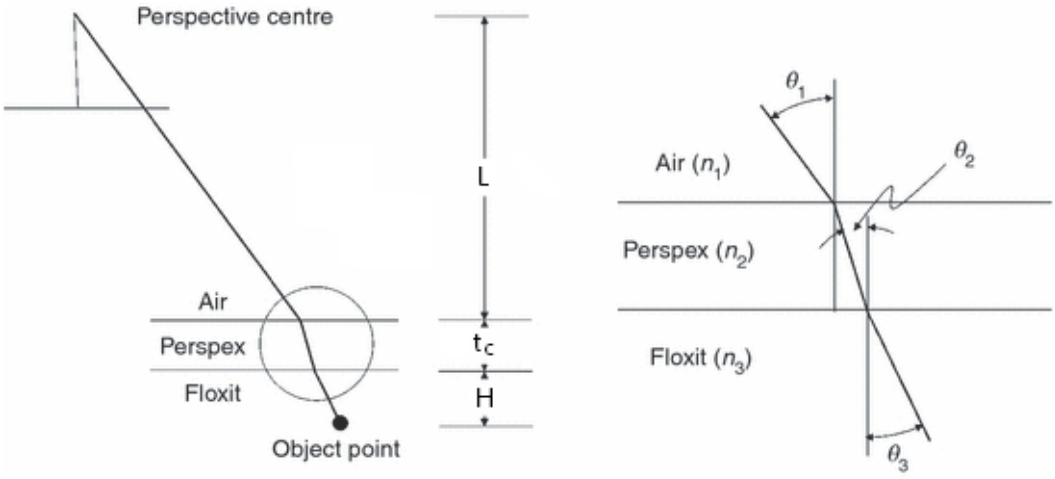

Figure 3-7: Media interface geometry (Left) and refraction angles at the media interfaces (Right). Adapted from Lichti et al. (2009)

Purpose-built software, incorporating the triangulation of points observed in the calibrated and oriented images from the two cameras, as well as the corrections for the refraction effects resulting from the multi-media nature of the experiment, have been written by Lichti (Lichti et al., 2009).

The validity of the calculation algorithm was tested and verified using a trial involving a smaller column (0.22 x 0.22 x 0.22 m) of the same Perspex material as that used for the falling-ball experiment. In this trial, a rigid plastic board with a set of 33 retro-reflective targets was suspended inside the column. The position of these targets was determined by conducting the spatial intersection (also known as triangulation) calculation procedure, where the collinearity equations using data taken from the perspectives of the two cameras were solved simultaneously. The procedure was repeated with the column filled with the test solution. The intersection calculation was then reiterated, this time with the incorporation of the refraction correction model. A comparison of the calculated target coordinates obtained from the empty-column data set with those obtained from the column-filled data, both corrected and uncorrected by the refraction model, reveals that the refraction model significantly improves the accuracy of the measurement. Thus, the refraction model was deemed as highly effective for the purpose of this

experiment. Through this study as well as some primary testings on the full-scale column, it was found that the accuracy of this measuring system is better than ± 1 mm. More details of the verification of this experimental procedure have been reported by Lichti et al. (2009).

3.4.2.3 Orientation of cameras

Once calibrated, the cameras were fitted on tripods and fixed to stable positions as outlined in Figure 3-6. A network of retro-reflective targets, consisting of 30 target points, was attached to the column and surrounding walls. This target field, once co-ordinated, was then used to assist with the determination of the positioning and orientation angles of the cameras throughout the process of falling-ball experiment. Through this method, any slight changes in the positions and orientation angles in the cameras could be detected.

The co-ordinates of the target field surrounding the column were determined by a similar process to the Self-Calibration procedure, i.e. by capturing images of the target field at various different angles and distances using the calibrated cameras. The resulting Bundle Adjustment calculation yielded a set of target field co-ordinates with a confidence factor of ± 1.59 μm (± 0.24 pixels).

With the cameras calibrated and their positions and orientation angles readily available, the 3D positioning of the spheres throughout the sphere-settling experiment could then be determined.

3.4.2.4 Experiment and data analysis

Similar to the experiments of category I, the experiments of this category were conducted in a laboratory with a controlled temperature of 23.5°C (± 1°).

The cameras and all other equipment included in the stereo-photogrammetry system are initiated 15 minutes prior to the commencement of the experiments, to ensure that all components are warmed up during the measurement process. The

target fields relevant to the field-of-view of each camera are then illuminated and a series of 20 images are captured for each camera. This procedure is repeated several times throughout the experimental session, to be used for the orientation of the cameras. Any changes in the positioning and orientation of the cameras during the experiment can therefore be detected and incorporated into the calculation process.

The 2D positions of the spheres with respect to each camera are determined using commercial image processing software, OPTIMAS 6.51 (Media Cybernetics, 1999). The combination of the data sets resulting from the two cameras is then used to calculate the 3D positioning of the spheres at each time frame by considering the orientation of both cameras as well as the refraction effects using the purpose-built software written by Lichti (2009).

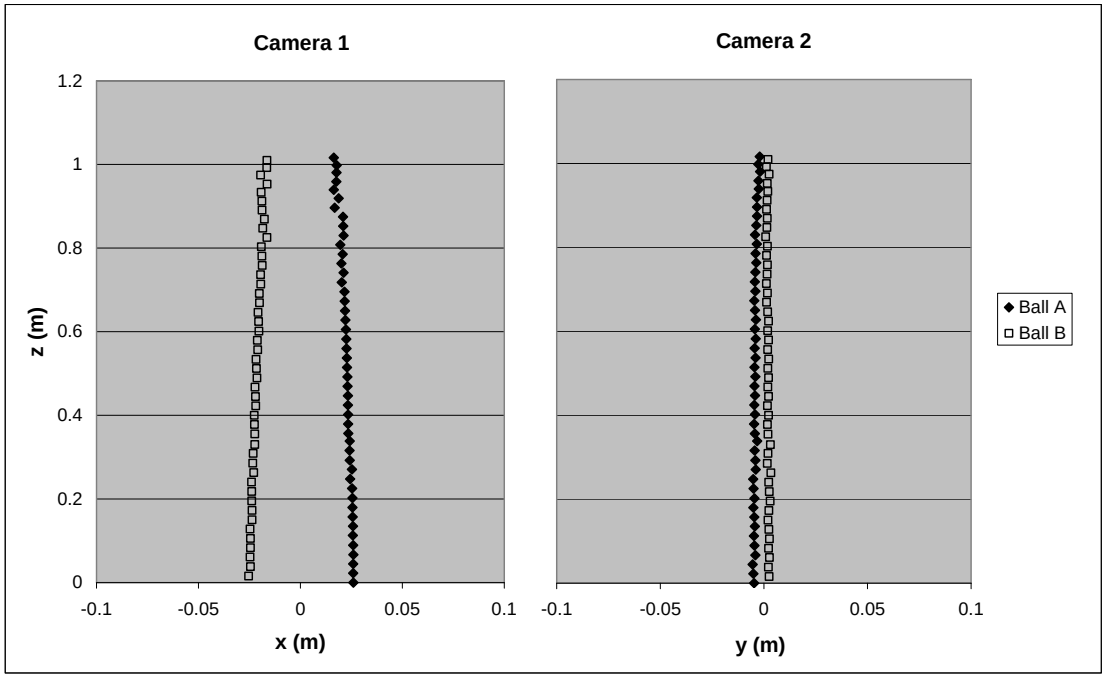

Figure 3-8: Results of the stereo-photogrammetry calculation with refraction correction for two chrome steel spheres (7.95 mm) in a 0.9% Floxit solution with initial separation distance of 37.5 mm.

The results of this calculation can be seen in Figure 3-8, where the refraction corrected trajectory of the spheres from the point-of-view of the two cameras is displayed. The case presented here clearly shows two spheres that slightly repel each other as they settle through the column. Throughout the experiments, several different types of particle trajectory were obtained, some of which shows strong inter-particle interaction to the extent that inter-sphere collision occurs. These trajectories will be discussed in further detail in Chapter 7.

Based on the values obtained from the photogrammetry calculation, the horizontal distance between the spheres at each time step was evaluated as follows:

$$d_H = \sqrt{(x_A - x_B)^2 + (y_A - y_B)^2} \tag{3-6}$$

where (x_A, x_B) and (y_A, y_B) are the co-ordinates of spheres A and B from the perspective of cameras 1 and 2, respectively.

The settling velocity of the spheres is calculated by numerically differentiating the vertical component of the sphere co-ordinate data (z) with respect to time (t). A five-point-stencil calculation procedure is employed to minimise the noise resulting mainly from the 2D photo frame analysis:

$$V(t) = \frac{-z_{t-2} + 8z_{t-1} - 8z_{t+1} + z_{t+2}}{12\Delta t} \tag{3-7}$$

3.4.3 Error estimation

Errors arising from the measurement system associated with this experiment can be sourced from several elements: the manual 2D determination of the sphere positions with respect to each camera using OPTIMAS, the triangulation and refraction correction calculations, and the timing error associated with the trigger for the cameras. The level of uncertainty associated with the stereo-photogrammetry calculation system has been estimated by Lichti et al. (2009) to be less than 1 mm. On the other hand, the maximum error in the

synchronisation between the computer and the two cameras is estimated to be relatively small, in the order of 0.001 s. Of the three error-contributing elements, therefore, only the level of uncertainty associated with the point-by-point determination using OPTIMAS is still unknown. The errors associated with this stage of the analysis are discussed below.

Considering a settling experiment involving spheres of the smallest available diameter (6.35 mm), the error associated with the point-by-point measurement using OPTIMAS in this experiment is estimated to be a quarter of the sphere diameter, i.e. ± 1.5875 mm. An assessment on the effects of this uncertainty on the results of the triangulation and refraction correction calculation indicates that this uncertainty translates to ± 0.8 mm and 0.6 mm in the vertical and radial directions of the resolved 3D co-ordinates, respectively (see details in Appendix A.2.3).

Based on the considerations outlined above, it was concluded that the uncertainties associated with the stereo-photogrammetry measurement system is ± 1.5 mm. This level of accuracy was deemed to be acceptable for the objectives of the current experiment. The implications of this uncertainty on the analysis of the settling behaviour of side-by-side spheres will be discussed further in Section 7.4.1.

3.5 Conclusions

The details of two experiments to be conducted for this study, i.e. the settling of two spheres along their line-of-centres (vertically-aligned, category I) and two spheres placed side-by-side (horizontally-aligned, category II), have been discussed thoroughly. In considering the requirements for these experiments, new designs, specifically for the experiment of horizontally-aligned spheres, were developed and incorporated. Through careful examination of the methodology and equipment design, it was determined that the error associated with the measurement of settling velocities is 6.7% for experiments of category I. In the second category of experiments, the main sources of error have been identified to be the 2D frame-by-frame analysis conducted using OPTIMAS (Media Cybernetics, Inc.) as

well as the set of triangulation calculations that were required to interpret this set of two-dimensional data. The errors associated with this measurement have then been estimated to be ± 1.5 mm. Based on this figure, it was concluded that the measurement system developed for this analysis is able to yield three-dimensional data of the positions of the spheres with sufficient accuracy for the objectives of the current research.

Chapter 4 Rheology of fluid

4.1 Introduction

Most of the slurries and suspensions that are utilised in the mineral processing industry exhibit viscoplastic fluid behaviour. This rheological term identifies the presence of yield stress in the fluid flow behaviour. Viscoplastic fluids that are subjected to shear stresses lower than their yield stress would ideally behave as solids and do not undergo any significant deformation. Above the critical yield stress value, deformation starts to occur and the viscoplastic material would start to behave as a fluid. A number of fluid models can be used for the description their flow characteristics, such as the Bingham, Herschel-Bulkley, and Casson models, all of which include constant values for the incorporation of yield stress. The use of these models for the analysis of the flow behaviour of slurries and suspensions at conditions of high shear rates, e.g. in pumped pipeline, has been proven to be highly effective (Slatter, 1997; Wilson, Addie, Sellgren, & Clift, 2006).

The flow problem presented in this thesis involves the settling behaviour of particles falling through quiescent viscoplastic fluids. In contrast to the example given above (i.e. the pumped slurry pipelines), where the level of deformation in the fluid is relatively uniform throughout the control volume, the present flow problem involves a fluid medium that undergoes deformation of various degrees of severity. In regions close to the surface of the settling particle, the level of the fluid deformation is relatively severe in comparison to regions several radii away from the sphere. In conducting this analysis, therefore, the fluid flow behaviour while being subjected to various levels of shear forces needs to be thoroughly examined. In addition, a fluid model that is suitable for the description of this flow behaviour needs to be incorporated.

Frequently, the flow behaviour of many viscoplastic fluids has also been associated with other rheological phenomena, such as thixotropy and elasticity. The effects of these rheological aspects on the settling behaviour of particles have been

thoroughly discussed in Chapter 2. In conducting this study, therefore, the contribution of these rheological phenomena on the flow behaviour of the experimental fluids needs to be thoroughly assessed. The fluid model that is adopted for the analysis of the flow problem should therefore accommodate these rheological properties.

In this thesis, to overcome the problems associated with the opaque appearance of slurries, the flow behaviour of these materials has been represented by aqueous solutions of polyacrylamide (commercially known as Floxit 5250L). The incorporation of these solutions into the sphere-settling experiment enables the motion of spherical particles to be observed through optical measuring devices (see Chapter 3). Furthermore, these solutions have previously been identified to possess a significant yield-stress value as well as shear-thinning behaviour (Horsley et al., 2004; Wilson & Horsley, 2004; Wilson et al., 2003), thus presenting typical flow characteristics of viscoplastic fluids.

The rheometric assessments of the experimental fluids were conducted using the HAAKE MARS II rheometer (Thermo Electron Corporation, Karlsruhe, Germany), under a standardised temperature of 23.5^{o}C. Furthermore, the cone-and-plate geometry has been selected for these measurements, due to its versatility and suitability towards various modes of rheology testing for a wide variety of fluids.

In this Chapter, the flow behaviour of the experimental fluids will be firstly examined using the standard method of rheometry, in which the fluids are subjected to varying degrees of deformation using the controlled-rate (CR) ramp testing. The results of this assessment will then be compared with the outcomes of other tests, through which the deformations of the fluids around the value of the yield stress, as well as the time dependency of their viscous parameters, can be determined. The limitations of the standard viscoplastic models will then be established through this analysis. An alternative testing regime and fluid model will then be formulated and performed. Finally, an analysis on the elastic properties of the fluid solutions will be presented and the transient properties of the fluids discussed.

4.2 The standard approach – Controlled Rate (CR) ramp experiment

4.2.1 Herschel-Bulkley fluid model

A standard approach to the rheology measurement of liquids is to subject the liquid sample to shear stresses at various rates of deformation. This is commonly done by the ramp-up and ramp-down experiments, in which the fluid is subjected to shear rates that are continually increased or decreased over a specified range and timeline. The response of the fluid solutions used for this study towards this testing regime is presented in Figure 4-1.

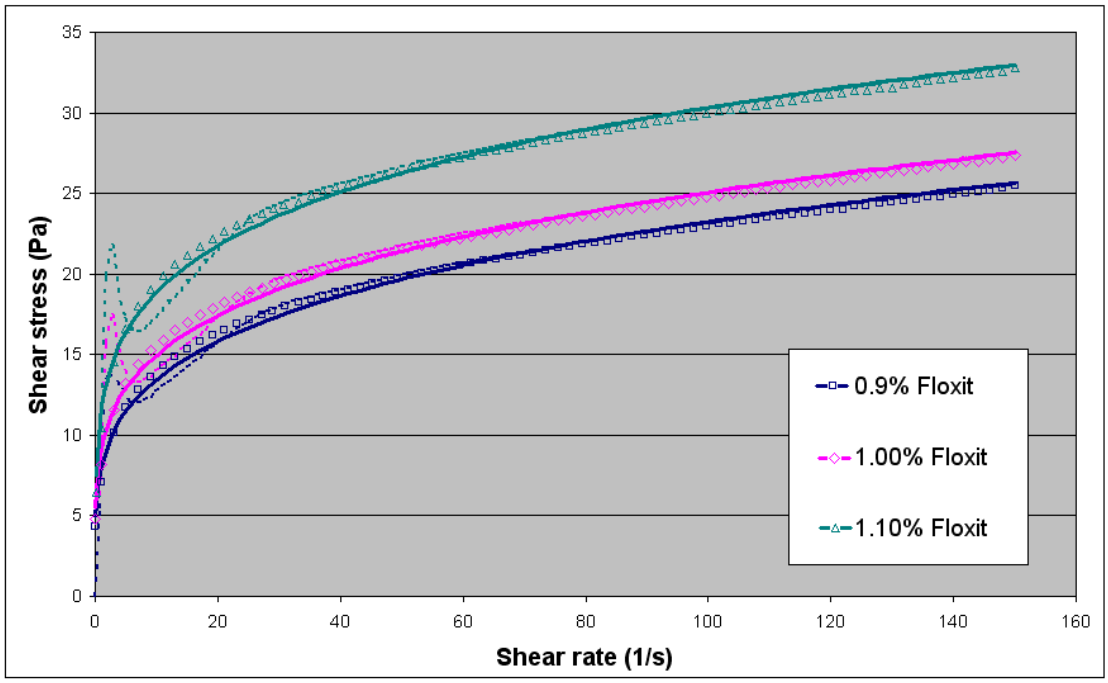

Figure 4-1: The stress response of the FLOXIT solutions while being subjected to CR ramp testings. The acceleration in shear ($d\dot{\gamma}/dt$) is 0.833 s^{-2}. The continuous lines show the fitted Herschel-Bulkley model (see Table 2-1). The discontinuous lines indicate the response of the fluid at the start of the rheometric testing.

Figure 4-1 shows that the Floxit solutions tend to display typical viscoplastic characteristics, as indicated by the very high slopes (i.e. absolute viscosity) at the low-shear-rate regions, followed by a significant decrease in viscosity once a critical value has been exceeded. This critical value is often used to indicate the presence of a yield point. As the shear rate is further increased, more decrease in viscosity is observed. Based on this observation, it was concluded that the Floxit solutions exhibit significant yield stress and shear thinning behaviour.

The effects of increasing concentrations of Floxit in the solutions can also be seen in Figure 4-1. In this graph, it is shown that solutions with higher concentration values require more shear stress to yield the equivalent rate-of-shear to those with lower concentration of Floxit. Thus, it can be concluded that Floxit concentrations result in higher yield stress values as well as viscosity in general. It can also been seen in Figure 4-1 that the rheograms can be satisfactorily fitted with a Herschel-Bulkley equation over a wide range of shear rate values. These parameters are presented in Table 4-1.

Table 4-1: Herschel-Bulkley fit parameters for the Floxit solutions (see Table 2-1) under shear-rate range of 2.5 to 150 s^{-1}.

% Floxit	τ_{HB} (Pa)	m (-)	k (Pa.s^m)	R^2
0.90%	1.289	0.257	6.718	0.99
1.00%	1.685	0.246	7.536	0.99
1.10%	0.264	0.209	11.486	0.99

4.2.2 Stress overshoot

Figure 4-1 shows that some discrepancies exist in the up- and down- curves of the rheogram. Stress overshoots can be seen in the up-curves, whereas in the down-curves, more steady stress development is obtained. Over time, it has also been observed that in cases where the fluid sample has previously been subjected to shear forces or deformation, no overshoot in the ramp-up curve would be obtained and that the rheogram obtained through this mode of testing closely resembles that obtained from the down-curve of the Controlled Rate (CR) ramp experiment.

The discrepancy in the up- and down- curves in the rheogram is traditionally attributed towards the inertia caused by the start-up motion of the rheometers. In the flow behavioural analysis of the fluid samples, therefore, the stress overshoot observed in the start-up curve is generally neglected, as has been the case with the analysis presented in Section 4.2.1. Within the context of the current experiment, however, the validity of this assumption has to be re-examined, mainly due to the fact that the measurement was conducted using a rheometer with very low levels of motor inertia (~ 10 μNms^{-2}, Thermo Fisher Scientific (2009)). The stress overshoot observed in Figure 4-1 may therefore have been caused by factors other than inertial effects during start-up, such as flow instabilities caused by the collapse of particle network structure, as suggested by Heymann and Aksel (2007) in their study of suspensions with yield stress characteristics.

The absence of stress overshoots in the down-curve of the rheogram, as well as in cases where the fluid sample has previously been sheared or deformed, suggests that this phenomenon only occurs in cases where the structure of the fluid is intact or undeformed. Furthermore, the presence of a yield stress, as has been discussed previously in Section 2.1.1, signifies a critical condition in which the material possesses both solid-like and liquid-like behaviour. The occurrence of a stress overshoot that is close to the starting point of the up-curve therefore represents solid-like behaviour, which is then followed by fluid-like behaviour once the fluid is sheared beyond its critical point. The absence of this overshoot in cases where the fluid has previously been subjected to shear forces (and consequently has undergone some deformation), suggests that the fluid requires some time to recover its original viscous parameters as well as its yield stress characteristics after being subjected to shear. Based on the considerations stated above, it was concluded that the stress overshoots observed in the rheograms of the fluids are caused by the yield stress of the fluids. More specifically, they represent the transition of the materials from being 'solid-like' to 'liquid-like' during the application of shear. This is in agreement with the hypothesis of Heymann and Aksel (2007) in their study of the rheological characteristics of viscoplastic suspensions.

The occurrence of stress overshoot is examined further in Figure 4-2, where a comparison of the rheometric response of the fluid when subjected to different values of acceleration in shear ($d\dot{\gamma}/dt$) is presented. In this figure, it can be seen that the presence of the stress overshoot depends highly on the rate of acceleration. As the value of $d\dot{\gamma}/dt$ is decreased, a noticeable shift in the stress overshoot is obtained, with the overshoot occurring at lower values of shear rates and with considerable decrease in severity.

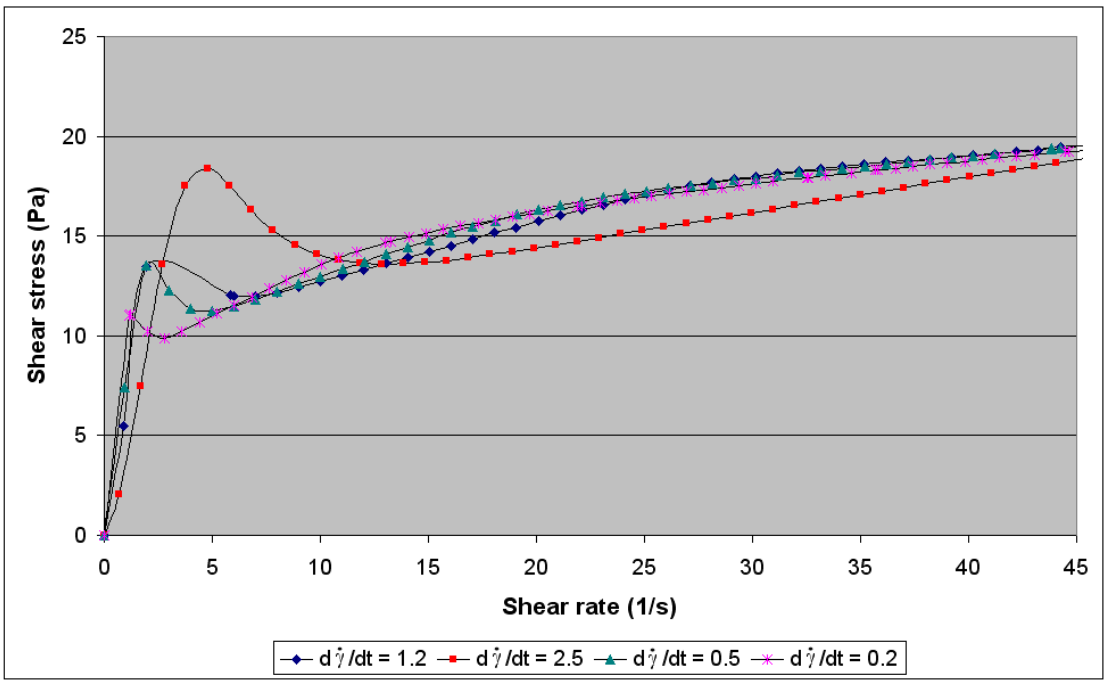

Figure 4-2: Shear stress response of the 0.9% Floxit solution as it is subjected to CR ramp with different $d\dot{\gamma}/dt$ values.

The shift of the stress overshoot as seen in Figure 4-2 suggests that the fluids used for the experimental study in this project possess a certain level of time dependency. The nature of this dependency, i.e. whether it is due to elasticity or thixotropy, as well as the significance of this dependency on the flow behaviour of the fluids with respect to the settling-sphere experiment, cannot be determined with the current mode of testing. In Section 4.3, several other modes of rheometric testings will be conducted to further identify these aspects of the fluid rheology.

4.3 Further experiments – a more detailed study of the fluid rheology

4.3.1 Controlled-stress (CS) ramp experiment

The shift of the position and magnitude of stress overshoots as seen in Figure 4-2 suggests that a detailed study of the flow behaviour of viscoplastic fluids close to the value of the yield stress cannot be based solely on the results of the rheometric test procedure presented in Section 4.2 (i.e. the CR ramp test method). A different testing procedure has been suggested by Kutschmann (1997), in which the fluid sample is subjected to gradually increasing value of shear stress (Controlled Stress, or CS, test). The resulting strain from the applied shearing motion is measured, and the log-log plot of the applied stress and deformation should ideally, for viscoplastic fluids, reveal two regions of linearity with considerably different slopes. Figure 4-3 depicts the deformation response for a 0.9% Floxit solution under this mode of testing.

In Figure 4-3, it can be seen that the yield stress of the fluid lies at shear stress value of 9.0 ± 0.1 Pa. This is in close agreement with the shear rate-stress curves of 0.9% Floxit solution presented in Figure 4-2, in which it is shown that the stress overshoot occurs at shear stress value of ~ 11 Pa when a deformation acceleration rate of $d\dot{\gamma}/dt \sim 0.2\ s^{-2}$ is applied. This supports the suggestion presented above that the stress overshoot observed in Figure 4-1 and Figure 4-2 are caused by the yield stress of the fluids, which marks the transition of the materials from being 'solid-like' to 'liquid-like' during the application of shear.

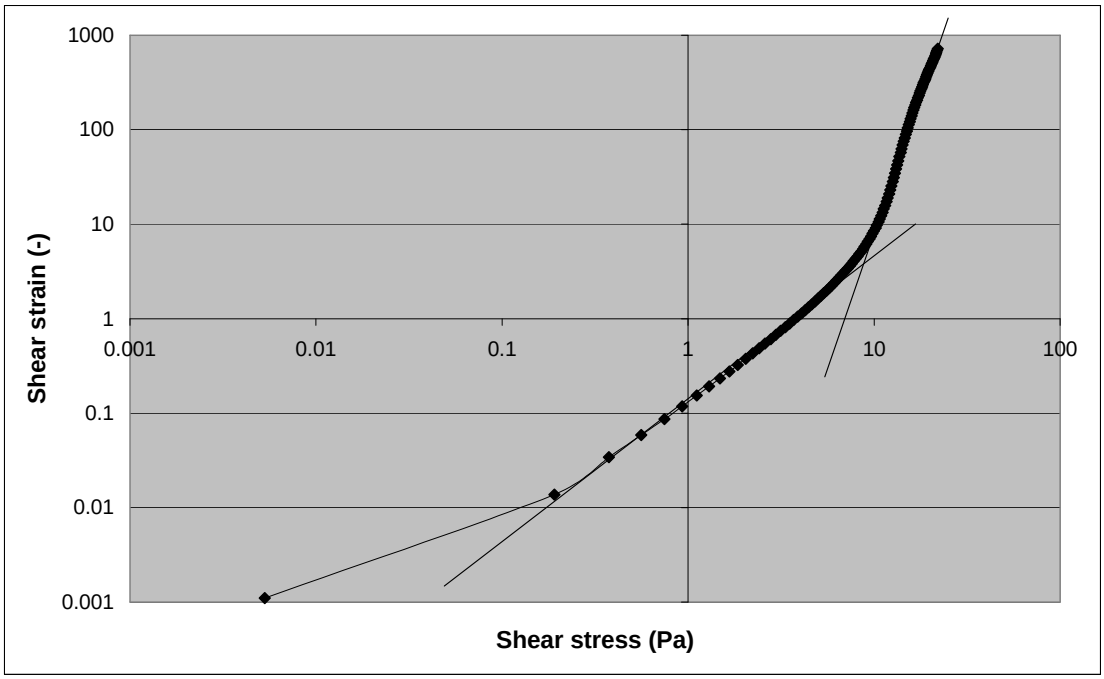

Figure 4-3: The deformation of 0.9% Floxit solution while being subjected to CS ramp testing

4.3.2 CR step experiment

Besides indicating the presence of yield behaviour, the different curves and stress overshoots obtained in the ramp-up and ramp-down experiment featured in Figure 4-1 and Figure 4-2 can also indicate the presence of thixotropic behaviour. In fact, this type of measurement has previously been used to indicate the level of thixotropy (or transient response) on various fluid solutions, based on the hysteresis-loop technique introduced by Green and Weltmann (1943). This test, however, has been criticised due to its dependency on the shear history prior to the start of the experiment, the maximum value of shear rate, and the rate of acceleration (Mewis & Wagner, 2009), and therefore cannot be used exclusively to indicate the thixotropic nature of the fluid solution. The dependency of the hysteresis loop on the acceleration rate of shear can be seen in Figure 4-2, where different 'positions' and severity of stress overshoot is obtained when different values of shear acceleration is applied on the fluid samples.

The transient response of the fluid towards changes in the applied shear forces can be examined further in Figure 4-4. In this Figure, the fluid sample is subjected to a sudden decrease, or step-down, in shear rate. Upon the application of this change, a nearly instantaneous drop in stress is obtained, followed by a gradual relaxation towards a steady-state stress value. This response indicates that the fluid solution exhibits both thixotropic and viscoelastic tendencies (cf. the various types of response towards a sudden reduction in shear rate listed by Mewis and Wagner (2009)).

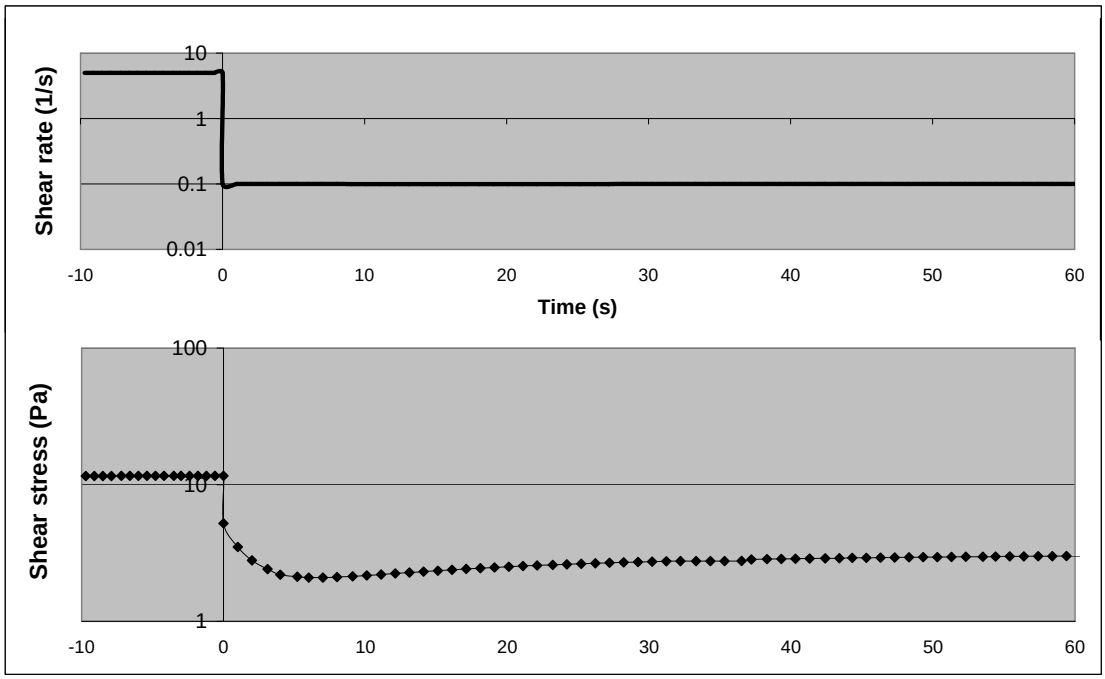

Figure 4-4: Stress response of the 0.9% Floxit solution towards CR step-down experiment. The shear rate is decreased instantaneously from $5s^{-1}$ to $0.1s^{-1}$.

The results presented above were as expected, as it has been established that many viscoplastic fluids also exhibit transient effects resulting from thixotropy and elasticity (Barnes, 1999; Mewis & Wagner, 2009; Møller et al., 2006). In this study, the prominence of these transient effects is demonstrated in the experiment of vertically-aligned spheres, where a sphere that is released following the flow path of another sphere is shown to have a much higher settling velocity than the preceding one. Gumulya et al. (2007) has attributed the discrepancy in the settling

velocity to the change in the viscous parameters of the fluid as a particle flows through and shears its structure. It is due to this structure that the fluid attains its yield stress properties. After being sheared by the settling movement of a sphere, the Floxit solution takes some time to regain its original structure, and hence, when another particle flows through the same path way, the partially-recovered fluid displays different apparent viscosity.

Based on the considerations presented above, it is clear that the rheological behaviour of the Floxit solutions depends highly on the integrity of its 'structure', as well as the tendency of this structure to breakdown and recover over time and under various shear conditions. The standard approach in rheometry and its associated viscoplastic fluid models, therefore, cannot capture the true yield stress and transient aspects of the test fluid solutions used for this study. Based on these considerations, another fluid model, which takes into account the structural nature of the fluid, as well as the time and force required to destroy or recover this structure, has been developed. The processes of analysis involved with the development of this fluid model, as well as the details of its characteristics, have been outlined in Section 4.4.

4.4 A new approach – the 'semi-viscoplastic' fluid model

The association between the 'structure' of a fluid with its rheological behaviour has been established relatively well in various models of thixotropy, some of which have been discussed in section 2.1.2.2. Of the various models that attempt to correlate the rheological behaviour of fluids to their 'structure', two different approaches have been encountered: microstructural and structural kinetics models. Microstructural-based models attempt to correlate rheological behaviour from accurate descriptions of processes that are responsible for structural changes. This approach can potentially give a highly accurate representation of the rheological behaviour of various rheologically-complex system (Barnes, 1997). However, it requires prior knowledge of the underlying mechanism behind these structural changes, which is very difficult to identify in most practical cases (Dullaert &

Mewis, 2006). Structural kinetics models, on the other hand, generally rely on structural parameters that are more abstract. Most models of this class use a scalar structural parameter, λ. A fluid medium with a fully intact structure can be represented by a λ value of 1.0. On the other hand, a λ value of 0.0 represents of a fluid medium where its internal structure has been completely destroyed.

An example of the structural kinetics model is one that has been suggested by Møller et al. (2006), which has been reviewed in Section 2.1.2.2 (see equations 2-20 to 2-22). The development of this model was based on the flow behaviour of clay suspensions, featuring the description of a thixotropic behaviour based on a structural rate equation. The yield stress characteristics of the suspensions are implicitly included within the model and is classified as the stress below which no permanent flow occurs (Møller et al., 2006):

$$\frac{\partial \tau_{ss}}{\partial \dot{\gamma}} < 0 \qquad \textbf{(4-1)}$$

where τ_{ss} is the steady-state value of shear stress for a given shear rate. This variable can be evaluated by solving the structural-rate equation (see equation 2-20), such that:

$$\frac{\partial \lambda}{\partial t} = 0 \qquad \textbf{(4-2)}$$

In this thesis, this definition of yield stress will be used to evaluate the fluid model that has been developed to describe the flow behaviour of the experimental fluids (see Section 4.4.4).

4.4.1 Rate equation

The rheological properties of polyacrylamide solutions in water has long been identified to be highly dependent on the level of entanglement of the polymer chain, as well as the inter- and intra- molecular interactions resulting from the hydrogen bonding between the polyacrylamide and water molecules (Kulicke et al., 1982).

The structural parameter, λ, therefore, is expected to reflect these parameters, which in turn affects the viscosity of the solutions.

For this study, the rate equation suggested by Møller et al. (2006) has been modified to a more bounded form, similar to that suggested by Mujumdar et al. (2002), where the value of λ is limited to vary between 0 and 1:

$$\frac{\partial \lambda}{\partial t} = \frac{1-\lambda}{\theta} - \kappa \dot{\gamma} \lambda \qquad \textbf{(4-3)}$$

The definitions of the parameters θ and κ have been retained from the rate model suggested by Møller et al. (2006), with θ representing the characteristic relaxation time of the liquid and κ the rate of structural destruction.

At steady state conditions, equation 4-3 can be written as follows:

$$\frac{\partial \lambda_{ss}}{\partial t} = 0 \;\Rightarrow\; \lambda_{ss} = \frac{1}{1+\kappa\theta\dot{\gamma}} \qquad \textbf{(4-4)}$$

The zero-shear value of λ at steady state condition is thus 1.0.

The bounded equation for λ is coupled with an equally bounded form of viscosity equation:

$$\mu = \mu_{\infty} + (\mu_0 - \mu_{\infty})\lambda^m \qquad \textbf{(4-5)}$$

where μ_0 is the theoretical maximum viscosity of the fluid and μ_∞ is the minimum viscosity to be fitted by the experimental data. Under steady-state conditions, the above viscosity equation can be rewritten as follows:

$$\mu_{ss} = \mu_{\infty} + (\mu_0 - \mu_{\infty})(1+\kappa\theta\dot{\gamma})^{-m} \qquad \textbf{(4-6)}$$

The evaluation of the parameters contained in the rheological equations discussed above requires several steps, comprising the examination of the flow behaviour of

the fluid at both steady and transient states. These steps will be discussed in the next two sections.

4.4.2 Steady-state conditions

A primary assessment on the parameters for the rate equation, namely the viscosity parameters (μ_0 and μ_∞), the lumped version of κ and θ, $\kappa\theta$, as well as the power constant, m, can be conducted based on the steady-state viscosity equation (see equation 4-6). This assessment, however, requires prior knowledge of the rheological properties of the fluid at steady-state condition. Due to this requirement, the standard approach of measuring rheological properties, such as the testing procedure outlined in Section 4.2, where the fluid is subjected to continual increase/decrease in shear rate, cannot be applied, as it does not allow the fluid to reach steady-state during the testing period.

The steady-state conditions required for the assessment of μ_0, μ_∞, m and $\kappa\theta$ can be examined experimentally using the 'step-ramp' test settings on the HAAKE rheometer. This test setting basically contains a series of step tests, where a sequence of set values for shear stress or shear rate is applied on the fluid sample. Each shear step is held for a length of time, which can either be directly specified or set according to the results of the measurement. In the second option, the applied shear rate or shear stress is held constant until a steady value of measured viscosity (± a specified uncertainty factor) is reached. Through this testing regime, the steady-state viscosity of the fluid at various rates of shear can be determined.

In this work, the controlled-stress step-ramp setting was used, where the set values for step-ramp are in the form of shear stress. An uncertainty factor of 5% of the measured shear rate, which is to be held for a minimum of 10 s before the next stress-step is applied, was imposed. The total measurement time was limited to 5 minutes to avoid the effects of solvent evaporation from affecting the accuracy of the measurement. The resulting rheogram, shown in Figure 4-5, is considerably

smoother than that shown in Figure 4-1. No noticeable difference was obtained with the up and down curves resulting from this test.

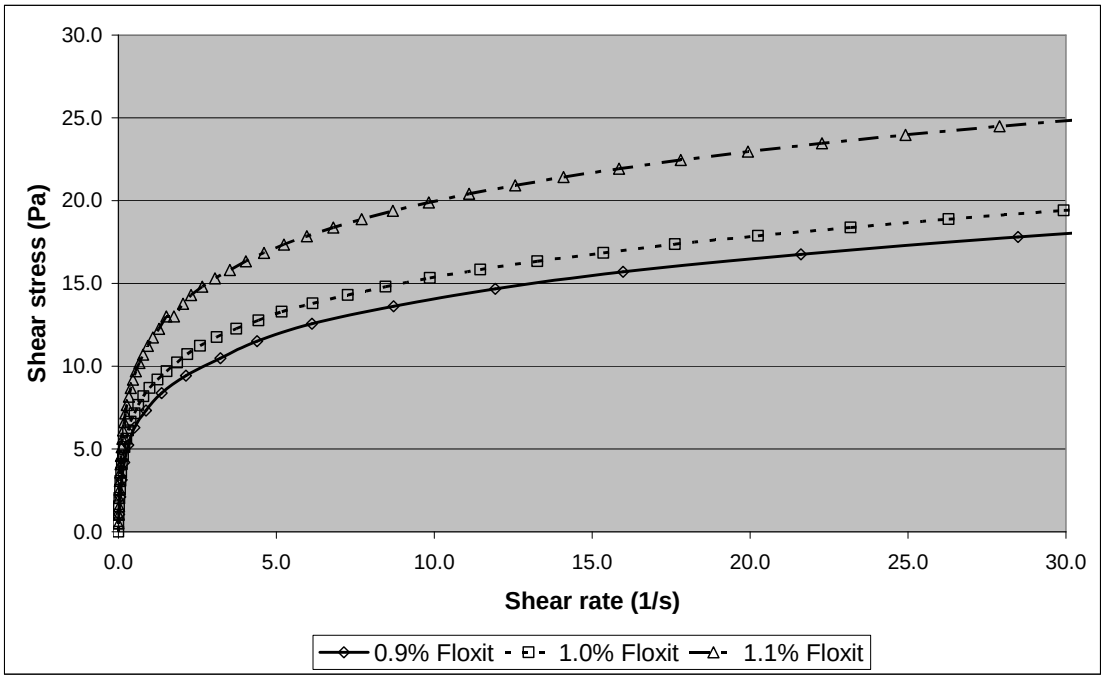

Figure 4-5: Rheogram of Floxit solutions, measured under steady-state conditions (CS step-ramp testing, conducted under the condition that the resulting shear rate should be constant (±5%) for at least 10 s before a new value of shear stress is applied).

The best fit settings for equation 4-6 can be determined by examining plots of the ratio of the viscosity parameters, $\log\left(\frac{\mu-\mu_\infty}{\mu_0-\mu_\infty}\right)$, as a function of $\log(1+\kappa\theta\dot{\gamma})$ resulting from the step-ramp testing. The power constant, m, can be obtained by directly measuring the slope of the graph, provided that a constraint of zero at the x-axis is imposed on the line-of-best-fit. To conduct this analysis, the degree of freedom of the fit equation was firstly minimised by assigning a value of 1×10^{-4} Pa.s for the parameter μ_∞. Through a series of trial-and-error, it was found that this level of μ_∞ yields good regression between the logarithmic values of the viscosity ratio and the rate-of-shear. This level of μ_∞ was also found to generate good correspondence between the calculated and observed viscosity values, as will

be seen in Table 4-2. The resulting logarithmic plots of the viscosity ratio as a function of the rate-of-shear are presented in Appendix B.1.

The corresponding values of μ_0 and $\kappa\theta$ were then obtained by minimising the sum-of-squared-error (SSE) between the calculated and observed values of steady-state viscosity, $\mu_{ss,\,calc}$ and μ_{ss}, respectively:

$$SSE = \sum_{i=1}^{N} \left(\mu_{ss} - \mu_{ss,\,calc}\right)^2 \qquad \textbf{(4-7)}$$

where N is the number of assigned steps in the step-ramp testing.

The resulting fit parameters obtained through the calculation method discussed above can be seen in Table 4-2. The high values of root-mean-square obtained using the optimised fit parameters support the validity of this analysis.

Table 4-2: Fit parameters for the semi-viscoplastic fluid model under steady-state conditions (see equation 4-6).

% Floxit	μ_∞ (Pa.s)	μ_0 (Pa.s)	$\kappa\theta$ (-)	m (-)	RSQ	SSE
0.9	0.0001	54.92	11.36	0.7749	0.999	1.28
1.0	0.0001	70.18	12.74	0.7888	0.996	2.91
1.1	0.0001	101.8	14.55	0.788	0.997	3.55

4.4.3 Transient conditions

The discussion on the rheological behaviour of the Floxit solution so far has only covered the steady state behaviour of the solutions and the distinction between the parameters of κ and θ is yet to be made. To determine these parameters, the transient response of the solutions towards step testing in either shear stress or shear rate has to be examined.

It should be noted at this stage that within the scope of this study, the parameter representing the shear relaxation time of the fluid (θ) has been assumed to be

constant. While there is a possibility that θ is not a constant and is a function of the rate of shear, the major utilisation of θ in this work is as the accounting parameter for the fluid structure recovery behind a settling sphere. In the development of this work, which will be explained in more detail in Chapter 6, it is assumed that the region above a settling sphere does not experience any further disturbance ($\dot{\gamma} \sim 0$), unless it is sheared again by the motion of another settling sphere. Thus, the assumption of a constant θ, which is measured at low rates of shear is considered to be appropriate. The implications of this assumption will be examined later through more step experiments (Section 4.4.5) and CFD simulations (Chapter 5).

When subjected to a constant shear rate, the structural-rate equation presented in equation 4-3 can be solved as follows:

$$\lambda(t) = \frac{1}{1+\kappa\theta\dot{\gamma}} + \exp\left(-\frac{t\left(1+\kappa\theta\dot{\gamma}\right)}{\theta}\right)\cdot\left(\lambda_{t_0} - \frac{1}{1+\kappa\theta\dot{\gamma}}\right) \qquad \textbf{(4-8)}$$

where λ_{t_0} is the value of the structural parameter at the time the change in shear rate is applied. Under ideal circumstances, a Floxit solution that is subjected to a step testing in shear rate should then give an exponential response that is similar to that described by equation 4-8.

Figure 4-6 presents the typical changes in the viscosity of a Floxit solution towards sudden changes in shear rate. As can be seen from this figure, an abrupt change in viscosity is obtained when the rate of applied shear is suddenly changed from 0.1 to 5.0 s^{-1}. On the other hand, the response of the Floxit solution as the rate of shear is reversed back to 0.1 s^{-1} approximately follows an exponential pattern, with apparent compatibility to the response predicted by equation 4-8. The response time to the first change in shear rate is only a few seconds, as compared to the 60 - 70 s of response time obtained from second change of shear rate.

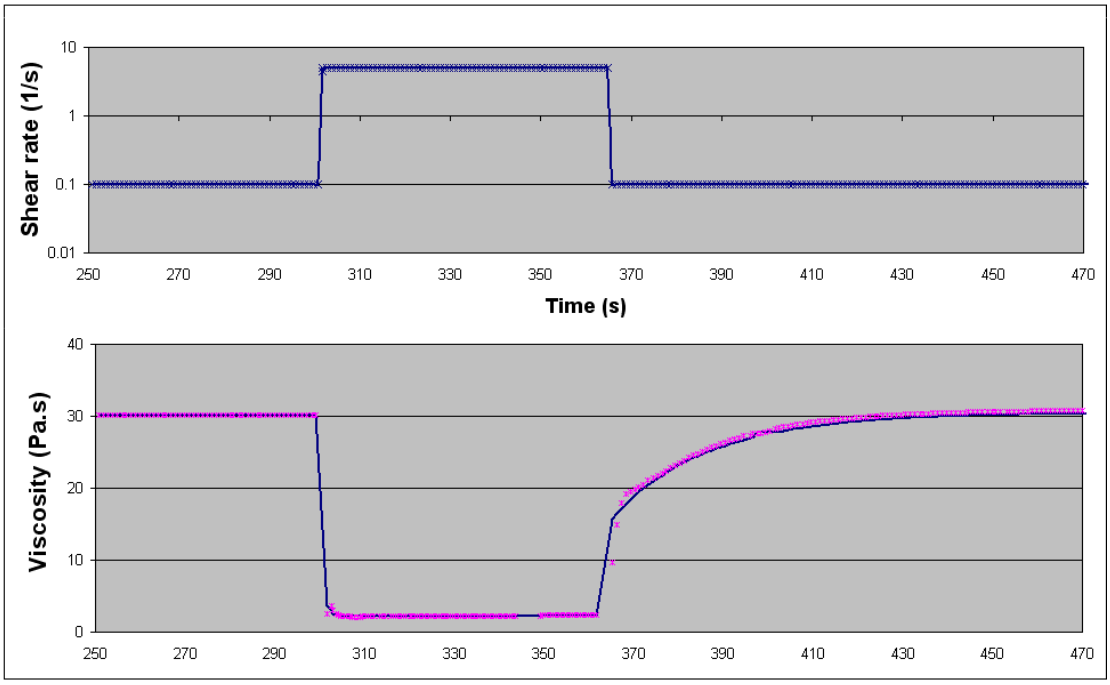

Figure 4-6: The response of 0.9% Floxit solution when subjected to a series of CR step experiments. The sample was subjected to a shear rate of 0.1 s^{-1} for 300s, followed by 5 s^{-1} for 60 s, and 0.1 s^{-1} for 150 s. The continuous line at the bottom graph indicates the predicted fluid response, calculated based on the semi-viscoplastic fluid model.

Through comparisons of various experimental data resulting from step testings conducted at several rates of shear, it was found that the value of θ can be consistently estimated by considering the transient response of the fluid as it is subjected to step-down experiments from relatively-high to low rates of shear (e.g. 5 – 10 s^{-1} to 0.1 s^{-1}), as well as step-up experiments from very-low to moderate values of shear rate (e.g. 0.01 s^{-1} to 1 s^{-1}). The considerable amount of time required for the sample to reach equilibrium or steady-state conditions at these low to moderate values of shear rates enables the collection of sufficient experimental data at transient conditions.

According to equation 4-8, the estimation of θ based on the transient change in viscosity (and hence the structural parameter, λ) in a controlled-rate step experiment can be calculated as follows:

$$\theta = \frac{(t - t_0)(1 + \kappa\theta\dot{\gamma})}{-\ln\left(\frac{\lambda_t - \frac{1}{1+\kappa\theta\dot{\gamma}}}{\lambda_{t_0} - \frac{1}{1+\kappa\theta\dot{\gamma}}}\right)} \quad \textbf{(4-9)}$$

where t_0 is the time where the change in shear rate is applied. An initial deduction of the value of θ can then be obtained by considering the time taken for the fluid to reach 25, 50, 75, 90, and 95% of the steady-state viscosity at shear rates of 0.1 and 1.0 s^{-1}. This value is then fine-tuned and optimised by the minimisation of the sum-of-square error (SSE) between the calculated and observed values of the structural parameter, λ:

$$SSE = \sum_{i=1}^{N} (\lambda_i - \lambda_{i,calc})^2 \quad \textbf{(4-10)}$$

where N is the number of measurements taken during the controlled-rate step testing.

The calculated values of θ based on measurements conducted at 0.1 and 1 s^{-1} are then compared and averaged. The results of this calculation can be seen in Table 4-3 and the correspondence of the resulting rate models with the experimental data can be seen in Figure 4-7 and Figure 4-8. The similarities between the calculated values of θ obtained from the measurements conducted at 0.1 and 1 s^{-1} and the good correspondence between the experimental and calculated rheological responses displayed by all three Floxit solutions (see Figure 4-7 and Figure 4-8), substantiate the assumption discussed above that the value of θ can be assumed to be constant at low rates of shear, along with the suggested calculation method.

Table 4-3: Fit parameters for the semi-viscoplastic model under unsteady-state conditions (see equations 4-3, 4-5, and 4-9).

% Floxit	Relaxation parameter, θ (s)		
	0.1 s^{-1}	1s^{-1}	Average
0.9	47.26	49.36	48.31
1	52.81	52.16	52.48
1.1	43.59	45.48	44.53

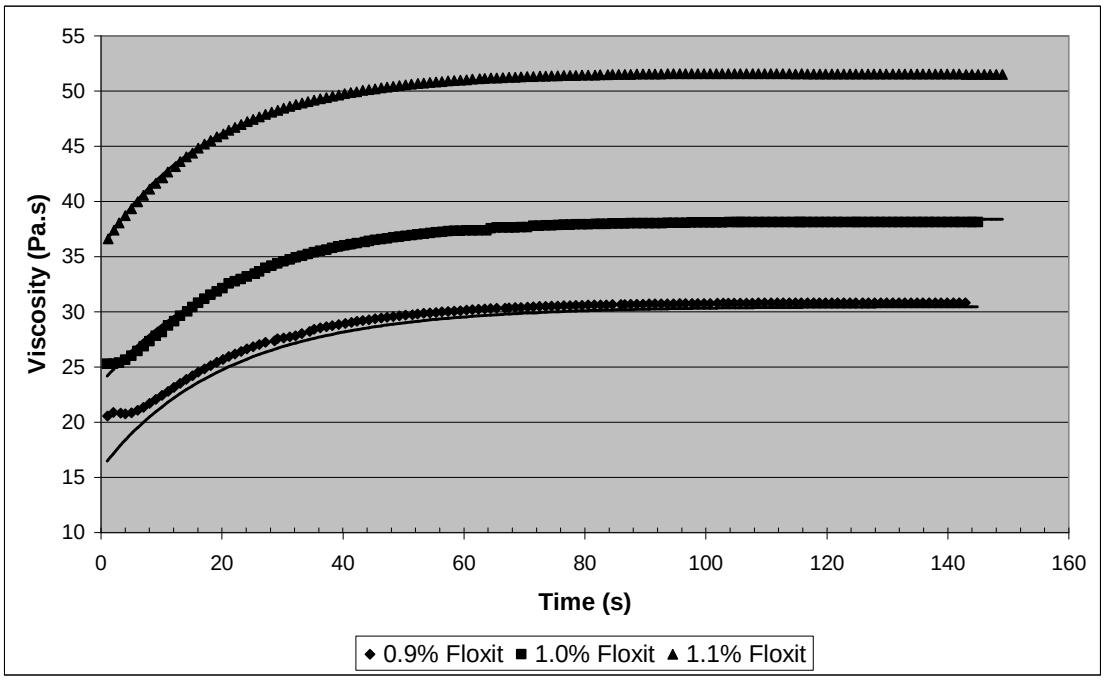

Figure 4-7: The response of 0.9% Floxit solution when subjected to CR step-down experiment (from 5s^{-1} to 0.1s^{-1}). The continuous line indicates the predicted fluid response, calculated based on the proposed fluid model.

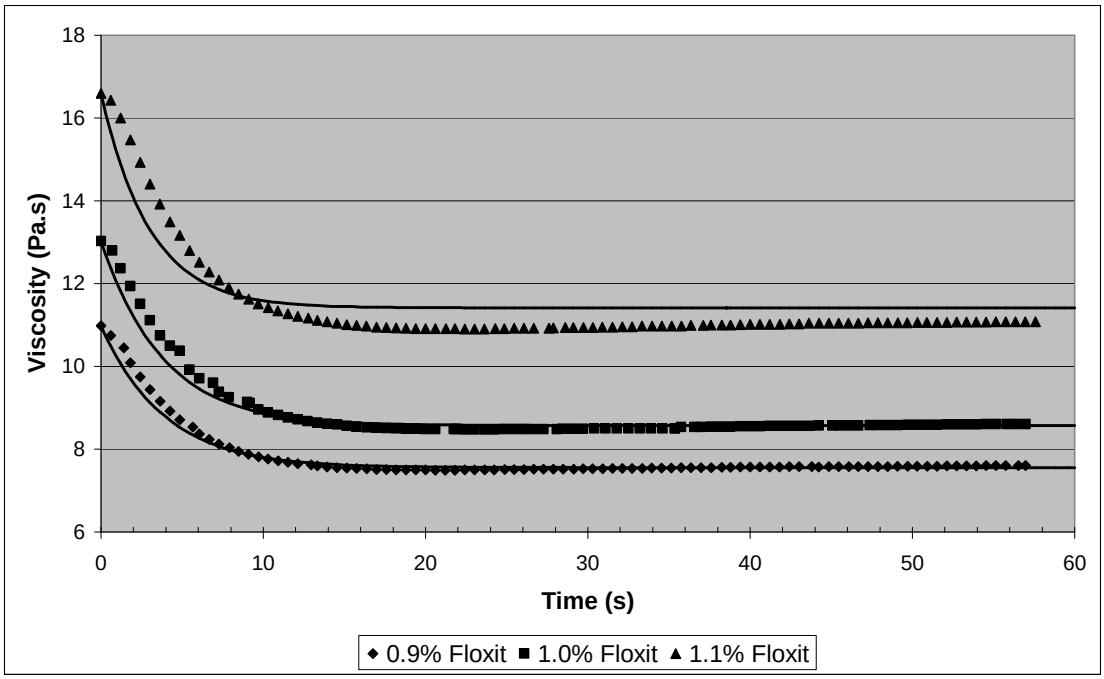

Figure 4-8: The response of 0.9% Floxit solution when subjected to CR step-down experiment (from $0.1s^{-1}$ to $1.0s^{-1}$). The continuous line indicates the predicted fluid response, calculated based on the proposed fluid model.

4.4.4 Yield stress

Under steady-state conditions, the derivative of the shear stress with respect to the shear rate can be written as follows:

$$\frac{\partial \tau_{ss}}{\partial \dot{\gamma}} = \mu_{\infty} + \frac{(\mu_0 - \mu_{\infty})}{(1+\kappa\theta\dot{\gamma})^{m}} - \frac{(\mu_0 - \mu_{\infty})\kappa\theta\dot{\gamma}m}{(1+\kappa\theta\dot{\gamma})^{m+1}} \qquad \textbf{(4-11)}$$

An examination of the parameters determined by the procedures outlined above reveals no region of shear rates at which $\partial\tau_{ss}/\partial\dot{\gamma} < 0$. Thus, it can be concluded that there is no region where a permanent unstable flow occurs, which according to Møller et al. (2006), is the definition of yield stress.

However, upon conducting a simple numerical study using MATLAB under conditions of continually-increasing shear rate similar to the shear ramp testing of

Figure 4-1, it was found that a region of temporary negative slope (indicating absolute viscosity) does exist, following an overshoot, as can be seen in the numerical results presented in Figure 4-9. Furthermore, the magnitude of the overshoot decreases with decreasing acceleration in shear. This result is interpreted to be analogous to the stress overshoot observed in the Ramp-up curve in the standard Rheometry approach displayed in Figure 4-1 and Figure 4-2. Similar to the results of the ramp-down experiment, no such overshoot was obtained with the calculated Ramp-down curve.

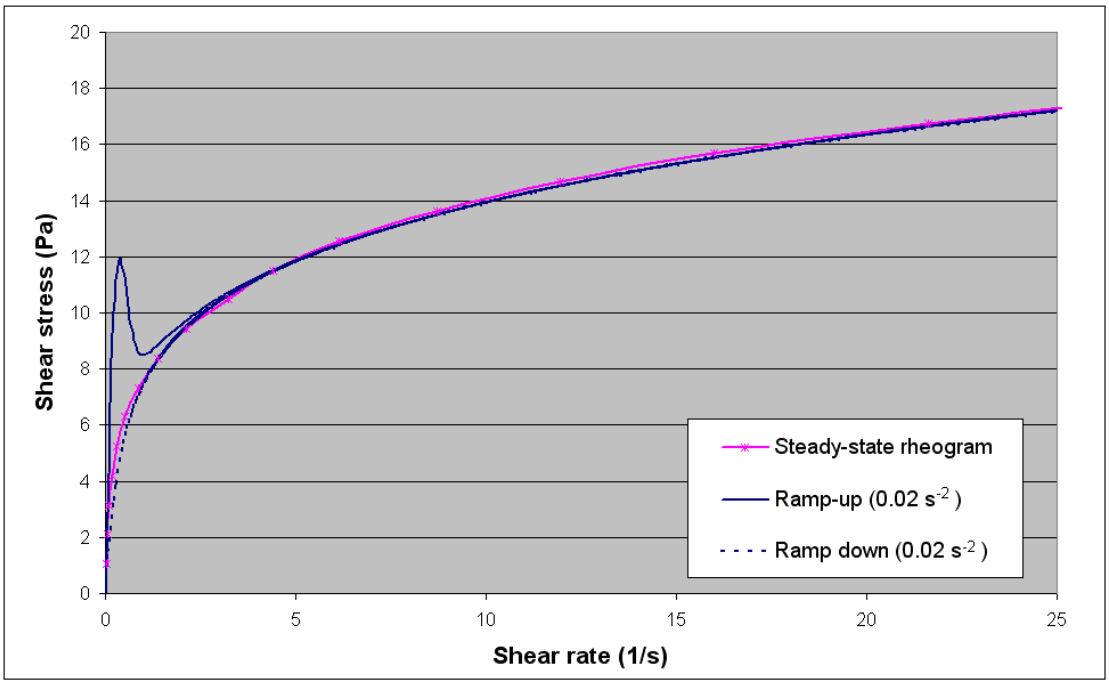

Figure 4-9: An estimate of the response of the 0.9% Floxit solution towards CR ramp experiment ($d\dot{\gamma}/dt$ = 0.02 s^{-2}), calculated using the ODE45 method in MATLAB. For comparison, the experimental data for the steady-state rheogram was included.

Figure 4-10 presents the results of another numerical study, where the fluid is subjected to a controlled-stress ramp testing, parallel to that suggested by Kutschmann (1997) for the testing of yield point. As can be seen in this graph, the numerical results indicate two regions of linearity with different slopes in the

log-log plot of shear stress and deformation, comparable to the experimental result for 0.9% Floxit solution presented in Figure 4-3.

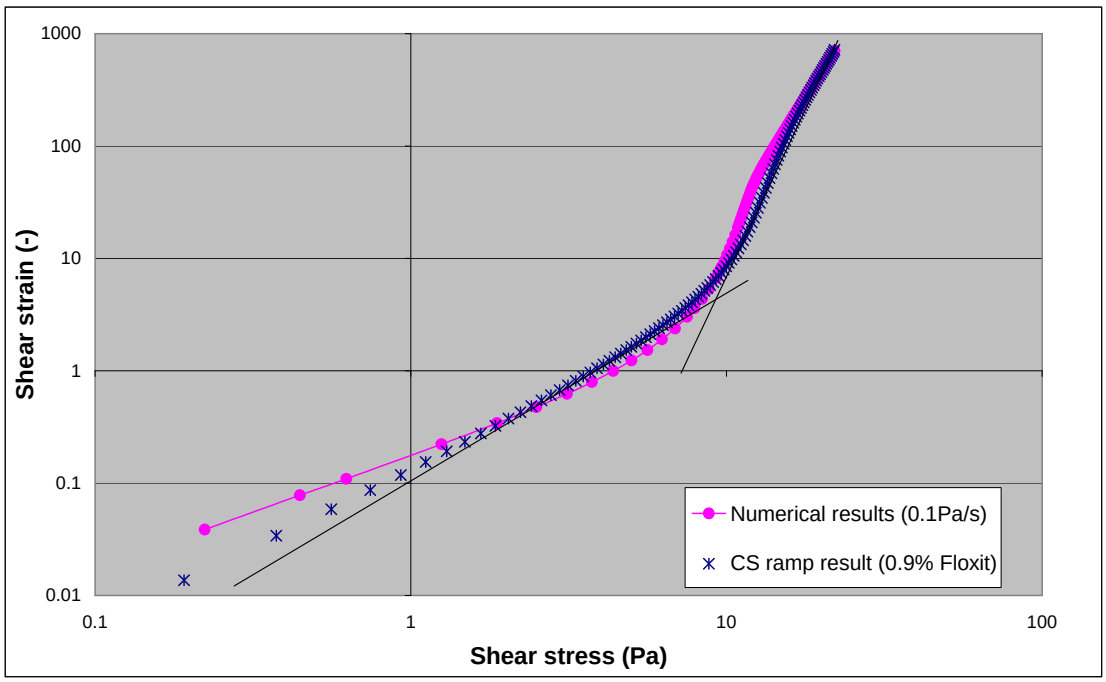

Figure 4-10: An estimate of the response of the 0.9% Floxit solution towards CS ramp experiment ($d\tau/dt$ = 0.1 Pa/s), calculated using the ODE45 method in MATLAB. For comparison, the corresponding experimental data has been included (cf. Figure 4-3).

The numerical results presented above suggest that the proposed rheological model presents a temporary yield-stress behaviour that dissipates once the structure of the fluid has been destroyed due to the application of shear forces. This characteristic was found to be similar to the characteristics of the viscoplastic solutions used for this study. Due to the temporary nature of the yield stress behaviour posed by this fluid model, it is referred to as 'semi-viscoplastic' model from this point onwards. The details of the MATLAB codes for the numerical testings presented in this section are available in Appendix B.2.

4.4.5 Characteristics of the semi-viscoplastic model at higher rates of shear

Having evaluated the values of θ for each solution, the applicability of these fitted rate equations on other rates-of-shear was then tested. In Figure 4-11, the response of the 0.9% Floxit solution to changes from a shear value of 0.1 s^{-1} to several different rates-of-shear is compared to that calculated by the semi-viscoplastic fluid model. From this Figure, it can be seen that there is a good correspondence between the observed and calculated values of viscosity when shear values of 5 and 10 s^{-1} are used. However, experiments using higher rates-of-shear, such as the step-up experiment from 0.1 to 20 s^{-1}, shows significant levels of undershoot, where the fluid temporarily exhibits lower viscosities from the steady-state value (usually for several seconds) before reaching its steady-state viscosity. The graph presented in Figure 4-11 shows that the proposed rate equation cannot predict such unusual behaviour.

Figure 4-12 and Figure 4-13 also present comparisons of the fluid responses for 1.0% and 1.1% Floxit solutions, respectively, towards several different step-up experiments from a shear rate value of 0.1 s^{-1}. As can be seen from these figures, the undershoot behaviour occurs at even lower values of shear rate and is featured prominently in both fluids. This behaviour is also overlooked by the numerical results of the proposed rate equation.

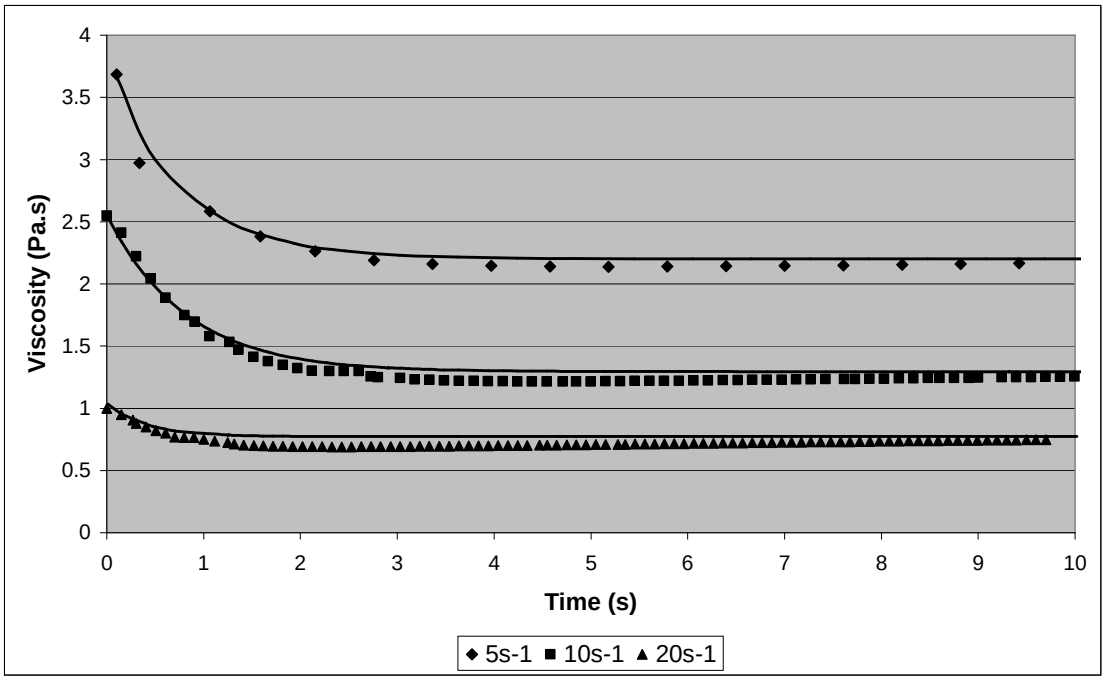

Figure 4-11: The response of the 0.9% Floxit solution when subjected to a series of CR step experiment, with an initial shear rate of $0.1s^{-1}$. The calculated response based on the semi-viscoplastic fluid model is indicated by the continuous lines.

The existence of such undershoot in step-up experiments could be caused by the abrupt nature of the step-test itself. Such sudden change in shear rate may have induced wall slip effects as well as non-uniform shear gradients, where fluid near the surface of the rotating cone may have experienced higher shear rates than fluid near the stationary plate. In the case of yield-stress fluids, the extent of such non-uniformity can be expected to be much more significant than in Newtonian fluids, due to the large differences in viscosity obtained at different shear conditions. That is, fluid near the rotating cone would have much lower viscosity than that near the stationary plate. Furthermore, such sudden change in shear rate may also induce an abrupt change in the fluid structure, causing some of the yield-stress fluid to be ejected from the cone-and-plate geometry. All of the factors mentioned above contribute towards the stress-undershoot observed in the step-up experiments. Some time after the imposed change in shear rate, the fluid stabilises, and a gradual relaxation towards the steady-state value of viscosity is effected.

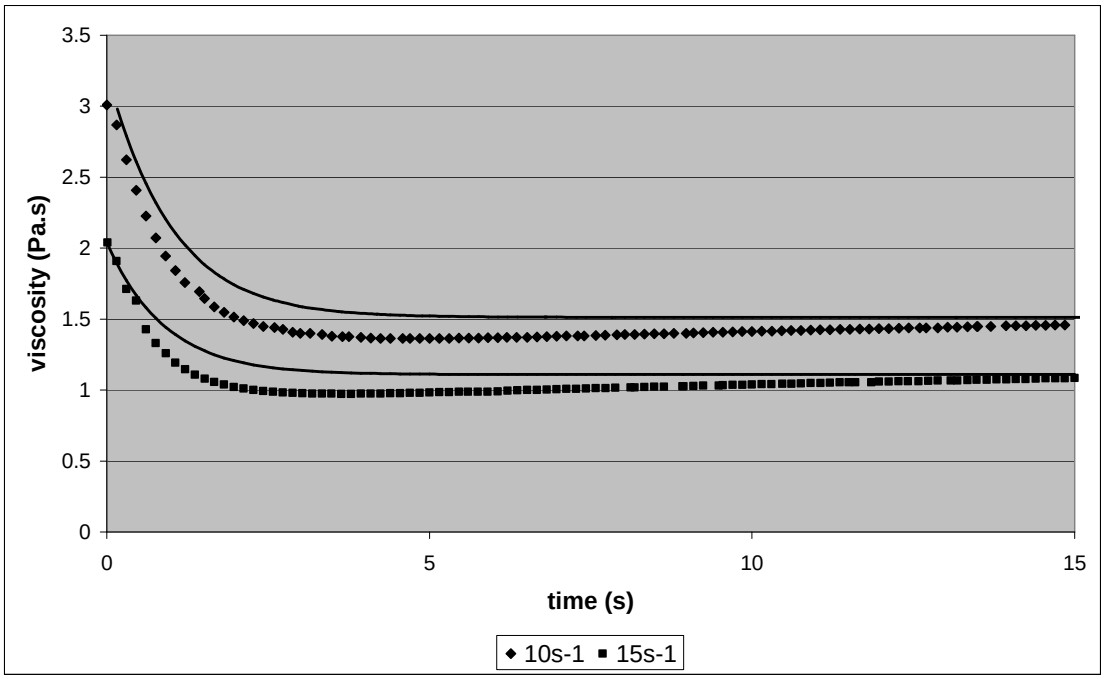

Figure 4-12: The response of the 1.0% Floxit solution when subjected to a series of CR step experiment, with an initial shear rate of 0.1s^{-1}. The calculated response based on the semi-viscoplastic fluid model is indicated by the continuous lines.

Despite the errors indicated above, Figures 4-11 to 4-13 indicate that the semi-viscoplastic fluid model is able to predict relatively closely the time required for the Floxit solution to respond to changes in shear rates and reach its steady-state viscosity. As a result, it can be concluded that the model is able to provide adequate description of the data of fluid structural breakdown resulting from step-up experiments conducted at various shear rates. This substantiates the assumption stated earlier in Section 4.4.3, where the relaxation parameter, θ, is assumed to be constant for all values of shear rate.

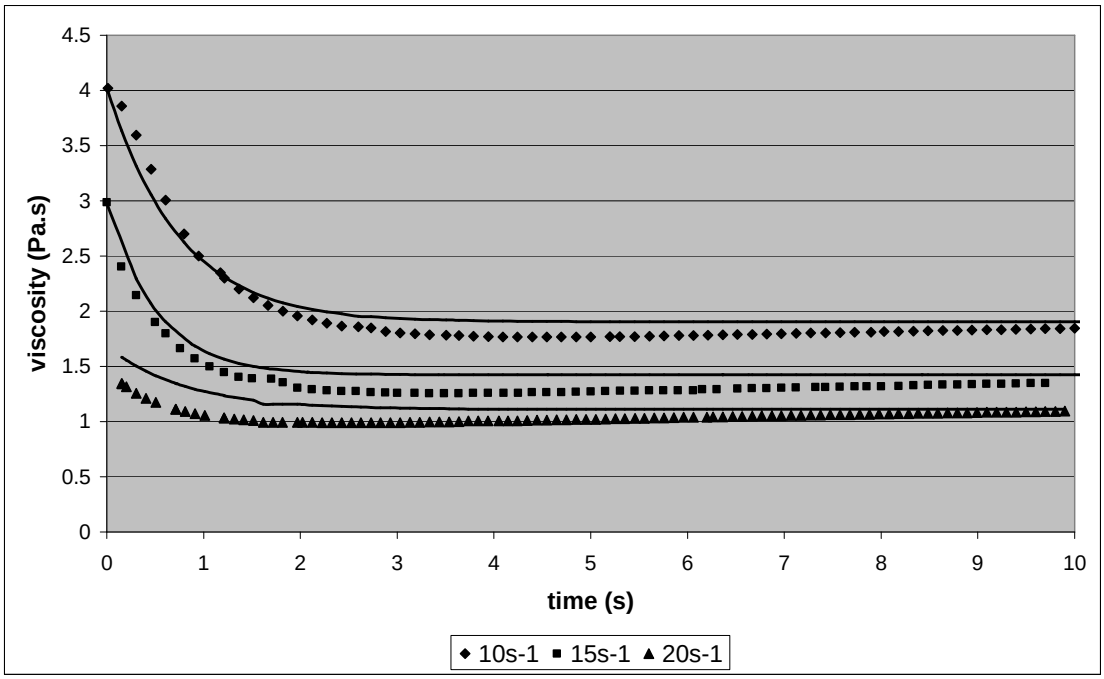

Figure 4-13: The response of the 1.1% Floxit solution when subjected to a series of CR step experiment, with an initial shear rate of $0.1s^{-1}$. The calculated response based on the semi-viscoplastic fluid model is indicated by the continuous lines.

4.5 Fluid viscoplasticity

The rheogram shape factor, α, which has been discussed previously in Section 2.2.5.1, is a measure of the level of viscoplasticity of a fluid. This parameter is defined as the ratio of the total area beneath the rheogram to the triangular area beneath the same rheogram sections (see Figure 4-14). A α value of 1.0 represents a fully Newtonian fluid, whereas a value of 2.0 represents a pure plastic material.

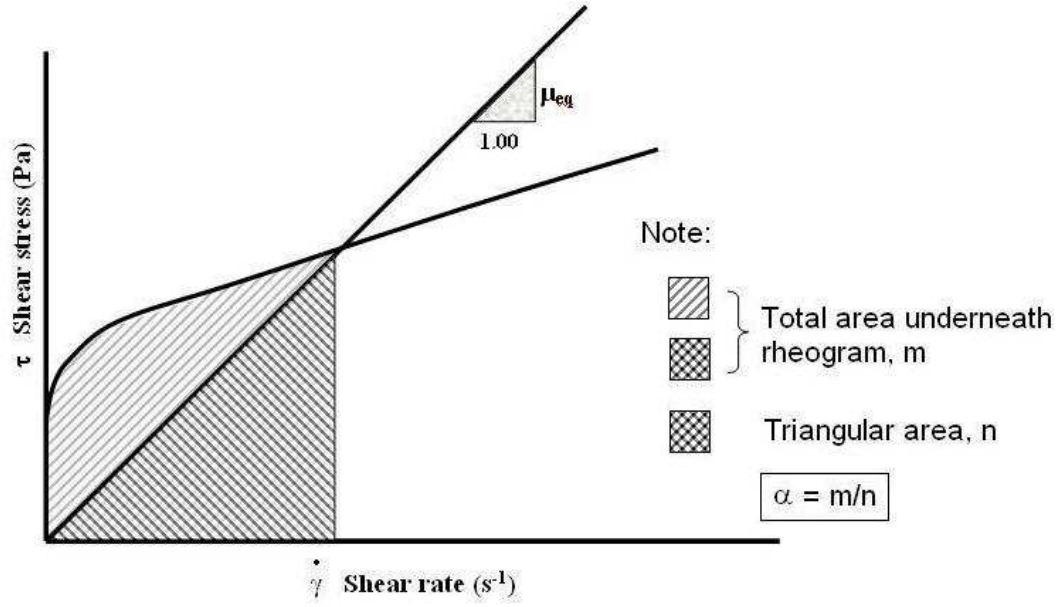

Figure 4-14: Calculation of α.

Another parameter, P, has also been used to describe the level of plasticity of a material (Horsley et al., 2004):

$$P = \frac{\alpha - 1}{2 - \alpha} \qquad \textbf{(4-12)}$$

P corresponds to a value of 0 for a Newtonian fluid. On the other extreme, which is a fully plastic material, the value of α increases to 2.0 and P becomes an indefinitely large number.

For a rheological model based on a structural rate equation, the values of α and P are calculated based on the steady-state condition. The calculated shear stress based on equation 4-6 is integrated numerically as a function of the shear rate, using the trapezoidal method of integration. The results of this calculation are presented in Table 4-4.

Table 4-4: Viscoplasticity of the Floxit solutions

% Floxit	α	P
0.9	1.627	1.681
1	1.6475	1.837
1.1	1.62	1.632

4.6 Fluid elasticity

The elasticity of the fluids in comparison to their viscous characteristics was examined using a series of dynamic SAOS test, which has been discussed in Chapter 2. A region of linear viscoelasticity was firstly established, by subjecting the samples to an oscillatory motion of a range of amplitudes at a fixed frequency of 1.0 Hz. This region is defined as that in which the stress generated is linear to the degree of strain. For the fluids being used in this study, it was found that the upper limit of the region of linear viscoelasticity is ~ 1.8 to 5.4 Pa (see Figure 4-15). As expected, higher upper limits were found with the solutions containing higher concentrations of Floxit.

Based on the findings of the amplitude sweep, a frequency sweep within the limits of the LVE was conducted. The results of this test can be seen in Figure 4-16. As can be seen from this graph, both the 0.9 and 1.1% Floxit solutions seem to have a storage modulus (G′) that is approximately 2-3 times higher than their loss modulus (G″), indicating a definite viscoelastic behaviour.

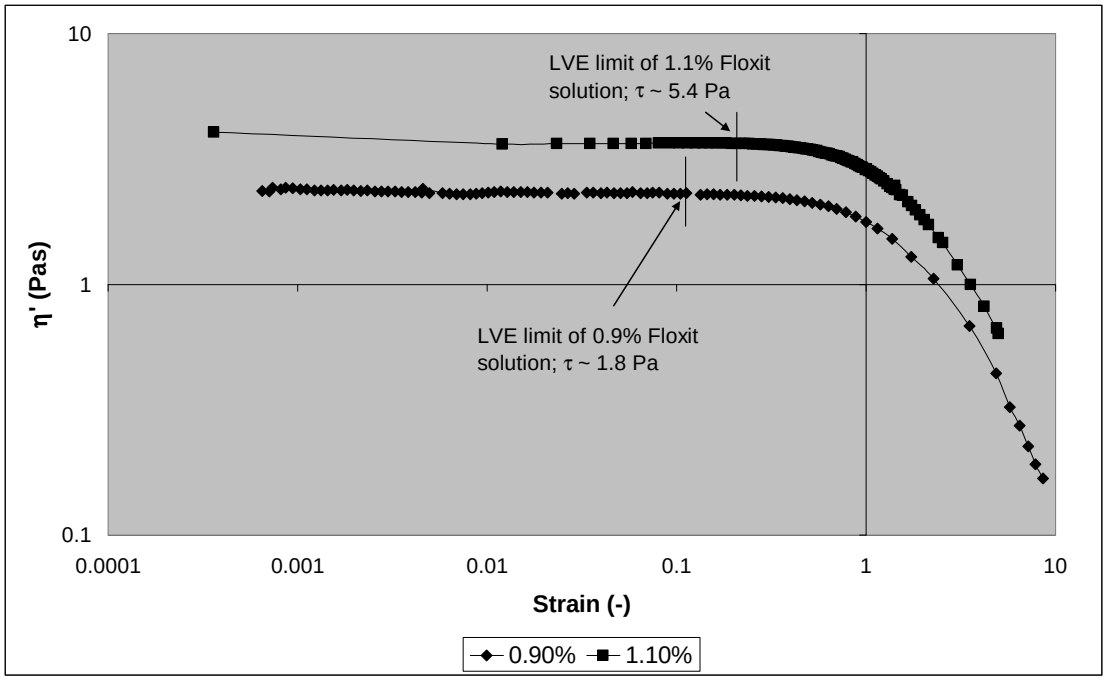

Figure 4-15: SAOS amplitude sweep test, conducted at a frequency of 1.0 Hz, of the 0.9 and 1.1% Floxit solutions.

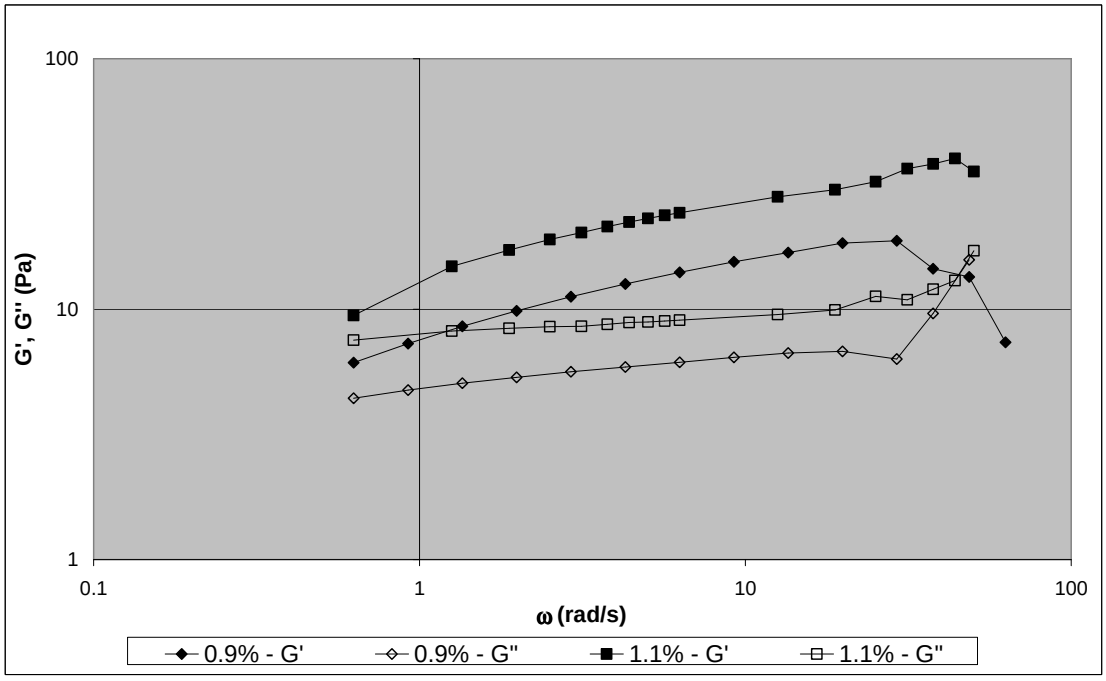

Figure 4-16: SAOS frequency test at a shear rate of 1.0 Pa of the 0.9 and 1.1% Floxit solutions.

The quantification of elasticity with respect to the inertial forces of viscoelastic fluids is commonly done through the calculation of relaxation time. This is done by considering the viscosity of the solution in comparison to its recoverable element (Marin, 1998):

$$\varphi = \eta_0 J_0 \tag{4-13}$$

where η_0 is the zero-shear viscosity:

$$\eta_0 = \lim_{\omega \to 0} \frac{G''(\omega)}{\omega} \tag{4-14}$$

and J_0 is the recoverable compliance:

$$J_0 = \frac{1}{\eta_0^{\,2}} \lim_{\omega \to 0} \frac{G'(\omega)}{\omega^2} \tag{4-15}$$

The limiting values were estimated by interpolating their corresponding logarithmic value to the zero axis of $\log(\omega + 1)$. The resulting relaxation times for all the fluids are 1.63, 2.15, and 2.99 s, for the 0.9, 1.0, and 1.1% Floxit solutions, respectively.

The values of the fluid relaxation times listed above were compared to the values of θ, which is the characteristic relaxation time that was obtained from the shear viscosity data. In Table 4-3, it can be seen that the values of θ for all of the Floxit solution generally range around 11 – 27 s, indicating that the time required for the fluid to regain its original structure due to the application of shear is considerably longer than the time required for the fluid to dissipate the energy stored due to its elasticity. This is consistent with the assessment of Gheissary et al. (1996), who upon studying the settling behaviour of two vertically-aligned spheres in a viscoelastic shear-thinning polyacrylamide solution, concluded that the memory effects of the fluid (termed as a 'hole') are enough to overcome the effects of elongation resulting from the elasticity of the fluid.

The Weissenberg number, commonly formulated for the settling-sphere experiment as a function of the sphere settling velocity and its diameter (see equation 2-8), is also widely used to compare the characteristic relaxation time-scale of the fluid with the time-scale of the experiment. Interestingly, as the settling velocity of the spheres is very large (~ 0.05 – 0.5 m/s) in comparison to the diameters of the spheres (~ 0.00635 – 0.01 m), very large Weissenberg numbers were obtained (in the order of 70-100), suggesting that the elasticity of the fluid solutions is highly prominent and cannot be neglected in the fluid models (Winter, Mours, & Baumgartel, 1998). Based on the comparison of the relaxation time to the shear relaxation of the fluid (θ), however, the comparative method based on the Weissenberg number is perceived as non-representative of the level of fluid elasticity. In later chapters, it will be demonstrated that this view is supported by the observed velocity profiles of the settling spheres through the fluid solutions (see chapters 5 and 6).

An alternative presentation of the Weissenberg number has been suggested by Arigo and McKinley (1997) based on the shear-rate-dependent parameters of the fluid rheology:

$$We(\dot{\gamma}) = \frac{\psi_1(\dot{\gamma})}{2\,\mu(\dot{\gamma})}\,\dot{\gamma} \qquad \textbf{(4-16)}$$

where $\psi_1(\dot{\gamma})$ is the first normal stress coefficient at shear rate of $\dot{\gamma}$:

$$\psi_1(\dot{\gamma}) = \frac{N_1(\dot{\gamma})}{\dot{\gamma}^2} \qquad \textbf{(4-17)}$$

and $N_1(\dot{\gamma})$ the first normal stress difference of the fluid at shear rate of $\dot{\gamma}$.

The first normal stress difference of the fluid solutions can be directly measured using the HAAKE rheometer. Its variation with the shear rate, in comparison to the shear viscosity, in the 0.9% Floxit solution, can be seen in Figure 4-17. From

this figure, it can be seen that the first normal stress can be correlated satisfactorily according to the power-law fit equation:

$$\psi_1(\dot{\gamma}) = k_N \, \dot{\gamma}^{m_N - 2} \qquad \textbf{(4-18)}$$

where k_N and m_N are the fit parameters determined through the rheological data. The corresponding values of these parameters for all the test fluid solutions are presented in Table 4-5.

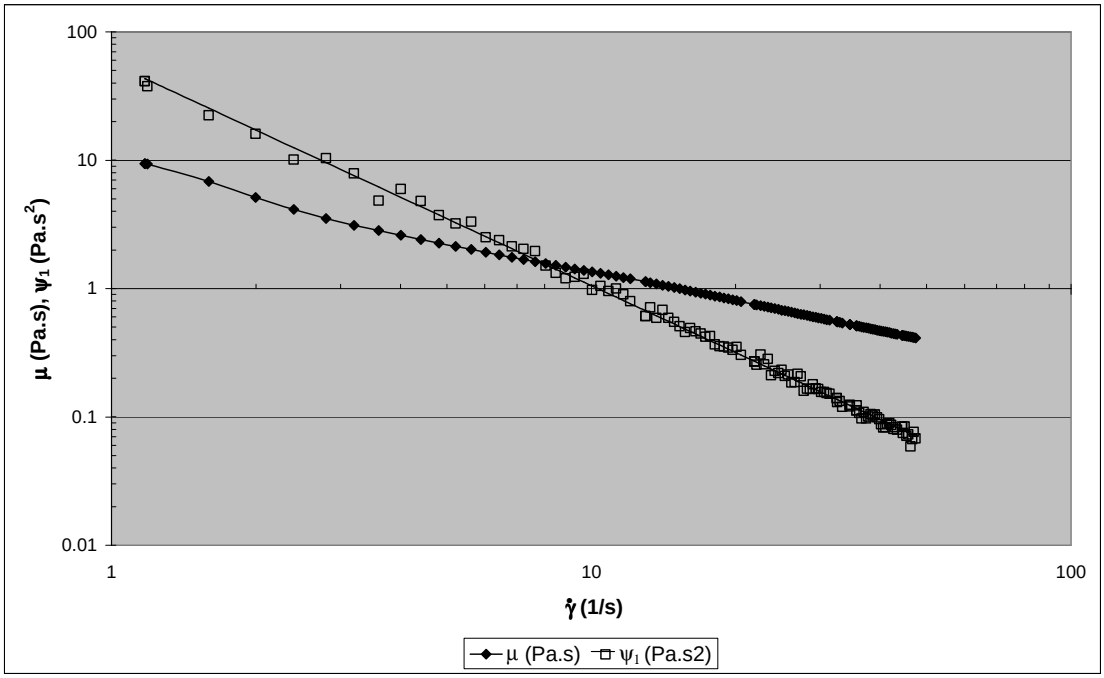

Figure 4-17: Viscosity and first normal-stress coefficient (ψ_1) of the 0.9% Floxit solution.

Table 4-5: Fit parameters of the first normal stress coefficient, ψ_1 (see equation 4-18).

% Floxit	k_N	m_N	R^2
0.9	57.073	0.2669	0.9974
1	46.511	0.7191	0.9894
1.1	62.645	0.8327	0.9967

4.7 Conclusion

Upon conducting a study on the rheological characteristics of the fluids used for this work, it was found that the standard assessment of viscoplastic fluids cannot adequately describe their flow behaviour. Through a series of tests, the fluids were identified to possess thixotropic (or time-dependent) characteristics in combination with their viscoplasticity. This combination of rheological behaviour has been attributed to the strong inter- and intra- molecular interactions resulting from the hydrogen bonding between the polyacrylamide and water molecules. This strong interaction imparts a structural network configuration in the fluid solutions, requiring the application of stress for its breakdown. Upon the removal of stress, the molecules gradually relax back to their original configuration and the fluid regains its original rheological behaviour.

A new viscoplastic fluid model based on the structural kinetics equation proposed by Møller et al. (2006) for thixotropic fluids was thus developed. This model features the inclusion of a scalar structural parameter (λ), of which the rate of change is dependent on the amount of shear applied on the fluid. As the apparent viscosity of the fluid is a direct function of λ, this enables the mathematical modelling of a fluid whose yield stress is highly dependent on its shear history. The rheological parameters of the proposed structural-rate equation were determined based on the behaviour of the fluid solutions at steady and transient states.

Although the proposed fluid model does not feature a constant yield-stress value, a simple numerical study on its transient response towards a variety of changes in shear conditions, namely the controlled-rate (CR) step and controlled-stress (CS) ramp testings, suggests that the fluid model is able to reflect the actual transient response of the fluids under similar testing conditions. In particular, the fluid model is able to reflect the instability of the fluids when subjected to CR ramp testings. In these tests, it was found that fluids that initially possess fully-intact structures tend to exhibit stress overshoot at the beginning of the ramp-testing, followed by a temporary region of negative slope, indicating the temporary

existence of unstable flow. This flow instability was not encountered in cases where the structure of the fluid has previously been destroyed due to the application of shear.

The flow instability discussed above was compared to the definition of yield stress suggested by Møller et al. (2006), who proposed that this parameter be defined as the critical stress value below which no permanent (stable) flow occurs. The presence of a temporary negative slope in the numerical response of the fluid when subjected to CR ramp testings indicates that the fluid model features temporary yield-stress characteristics that dissipate once the structural network of the fluid is destroyed due to the application of shear. Once the structure is destroyed, the fluid model features very prominent shear-thinning flow behaviour. Due to these characteristics, the term 'semi-viscoplastic' has been adopted to describe this fluid model.

The level of elasticity of the fluid solutions are examined through a series of small amplitude oscillation (SAOS) tests. The resulting profiles on the storage and loss moduli are then analysed to yield the characteristic relaxation time of the fluid solutions, which are then compared to the characteristic parameters of the experiment. Through this analysis, it was found that the elastic response of the fluid is relatively short in comparison to the measurement time of the experiment, as well as the shear relaxation parameter (θ) of the fluid solutions. This indicates that the elastic properties of the fluids should not significantly affect the dynamics of the sphere-settling experiment. The resulting normal-stresses due to the elasticity of the fluids were characterised through the measurement of first normal-stress difference (N_1), which was then correlated with the rate-of-shear through a power-law equation.

Chapter 5 Computational Fluid Dynamics

5.1 Introduction

In an effort of developing a greater understanding of the movement of mineral particles in tertiary grinding circuits, a series of experiments have been performed for the analysis of the settling behaviour of spheres in fluids of similar flow behaviour to those normally found in these unit processes, i.e. viscoplastic slurries and suspensions. In this thesis, the flow behaviour of the slurries has been represented by aqueous solutions of polyacrylamide (commercially known as FLOXIT 5250L), which have previously been identified to possess significant yield stress and shear-thinning characteristics (Horsley et al., 2004; Wilson & Horsley, 2004; Wilson et al., 2003). In conjunction with these experiments, the settling motion of the spheres in these types of fluids is also analysed using numerical (CFD) methods. Through this analysis, the flow fields surrounding the sphere can be further characterised, and the factors affecting the settling behaviour of these spheres can be identified.

In Chapter 4, a thorough examination of the rheological characteristics of the fluid solutions used for the experimental study has been presented. Through a series of rheological tests, it was discovered that in addition to the flow characteristics mentioned above, the solutions also possess a degree of time-dependency, resulting from thixotropy as well as elasticity. To describe the viscous characteristics of the fluid solutions, a new fluid model termed 'semi-viscoplastic', based on the scalar representation of the 'structure' of the fluid (λ), was developed. The term 'structure' in this case loosely refers to the network of structure in the fluid resulting from the existence of hydrogen bonding between polyacrylamide and water molecules in the aqueous solutions (Kulicke et al., 1982). This fluid model, which was developed based on the structural kinetics approach commonly used to describe the flow behaviour of thixotropic fluids, directly relates the viscosity of the fluid with λ. In turn, the rate-of-change in λ is dependent on the magnitude of shear that the fluid experienced. Upon examining the dynamic properties of the fluid model, it was

found that a fluid medium that is fully intact in structure requires the application of stresses that are significantly larger in magnitude for the initiation of its deformation than in cases where the structure of the fluid is already partially-deformed. Due to this dynamic characteristic, in which the fluid model seems to exhibit a yield stress-like quality that dissipates once the 'structure' of the fluid has been deformed due to the application of shear, the term 'semi-viscoplastic' has been adopted to describe this fluid model.

In this chapter, Computational Fluid Dynamics (CFD) methods will be used to examine the flow field surrounding spheres settling in a fluid medium modelled with the proposed semi-viscoplastic equation. Through this study, it is hoped that the effects of the transient viscoplastic characteristics and fluid 'structure' on the settling sphere can be determined. The results of this study will be compared with experimental data, as well as the results of several numerical and visualisation studies available in the literature. The outcomes of this analysis are hoped to aid the development of correlations for the prediction of particle settling velocity, as will be discussed later in chapter 6.

Aside from the viscous characteristics discussed above, the results of the rheometric analysis also reveal that the fluid solutions possess low to moderate levels of elasticity, with Deborah numbers of 0.2 – 0.75. As can be seen from the discussion presented in Chapter 4, the development of the semi-viscoplastic fluid model was based on the sole consideration of shear viscosity measurements, i.e. the normal stresses arising from the inherent elasticity of the fluids have been assumed to be negligible. Through the implementation of the semi-viscoplastic fluid model to the CFD analysis and comparisons of the predicted settling velocities with the experimental data, it is hoped that the implications of the assumptions stated above can be examined.

To conduct this study, a numerical formulation that is relatively simple to use and accessible through a well-established CFD code needs to be developed. In Section 5.2, a brief overview of CFD methods will be discussed, followed by a discussion on the numerical approaches that have been used in the past for the study of the

settling behaviour of particles in various types of fluid media (Section 5.3). The selection of the numerical approach used in this study was based on the considerations outlined in Section 5.3. The details of the numerical formulation, as well as the methods of approximations and solutions used to solve the problem will then be discussed in Sections 5.4 and 5.5. The resulting numerical method was then tested against cases of a sphere settling in Newtonian fluids (Section 5.6). Potential problems and pitfalls of such numerical formulation were then identified, and a set of numerical strategies developed to avoid these problems. The final formulation for the numerical analysis was then used to obtain a description of the flow field surrounding spheres settling in semi-viscoplastic fluid solutions. The results of this analysis will be discussed in Section 5.7.

5.2 Computational Fluid Dynamics: an overview

In this section, a brief overview of CFD will be presented. A more thorough overview, particularly of the capabilities and characteristics of FLUENT 6.3, which is the computational code used for the CFD analysis in this research, can be seen in the FLUENT 6.3 User's Guide (2006).

The concept of CFD revolves around the Navier-Stokes equation as outlined in equations 2-26 and 2-27. These equations involve several partial differentials components, making them very difficult to solve analytically. CFD employs approximation methods to solve these equations. These approximations are applied over small domains in space and/or time, resulting in numerical solutions at discrete locations within the specified space and time.

The process of CFD analysis comprises several steps (see Figure 5-1). Initially, a mathematical model needs to be formulated with an appropriate set of initial and boundary conditions. This is a crucial phase, as often a solution method needs to be selected based on the mathematical problem itself. The computational domain is then defined and assigned with a series of discrete points (numerical grid or elements for finite element analysis), in each of which numerical calculations and

approximations of the formulated mathematical model are to be performed. As can be seen in Figure 5-1, this process is commonly known as discretisation. The resulting set of algebraic equations is then solved through numerical methods, often requiring a number of iterations, and analysed through flow visualisation techniques. Some of these methods will be discussed in Section 5.5.

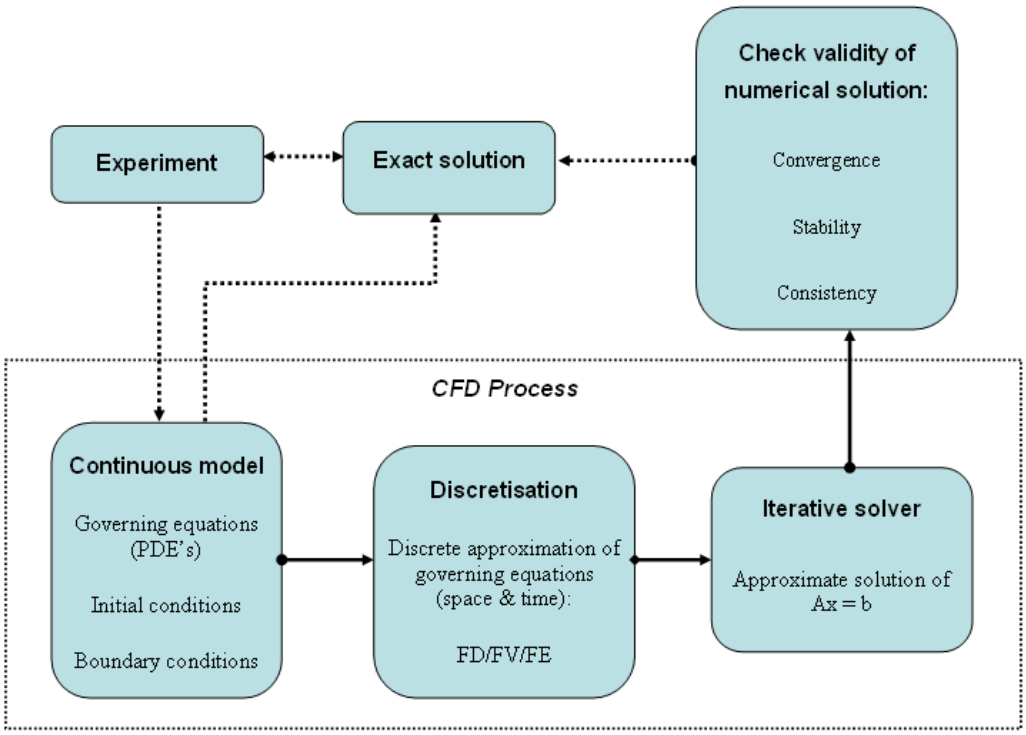

Figure 5-1: Development process of CFD analysis.

Based on the above description, it can be seen that discretisation, which is essentially a process of replacing the governing equations with a series of approximations over discrete points over the whole computational domain, is crucial for the accuracy of the CFD analysis. Not surprisingly, many methods of discretisation are available. The most common methods being used currently are:

- Finite Difference (FD): based on the approximation of differential equations using the Taylor series expansion or polynomial fitting methods. It is highly simple and effective, although its use is generally limited for structured grids.

This method, therefore, is normally reserved for problems involving very simple geometries (Ferziger & Perić, 1999).

- Finite Element (FE): revolves around the method of weighted residuals, which is used to reduce the second order partial derivatives to first order terms. The solution is approximated by a function, the simplest of which is a linear-shape function, in such a way that continuity is assured across the element boundaries. The approximated solution is then substituted into the weighted integral of the problem equation and the solution is obtained by requiring the derivative of the integral to be zero. This method is highly suitable for complex geometries and is slowly gaining popularity in the CFD community.

- Finite Volume (FV): based on the integral form of the conservation equations, which are then applied into smaller control volumes (CVs). Approximation methods, such as first-order upwinding and central differencing, are used to approximate the variable values involved with the integrals. Similar to the FE method, quadrature formulae (e.g. Gauss) is applied to approximate the surface and volume integrals.

Due to its numerical formulation of the conservation equation, the FV method inherently ensures the conservation of various properties in a control volume. It is therefore very versatile and is applicable to many different types of numerical grids and mathematical models. As a result, it is the most commonly used numerical technique for the solution of partial differential equations and is the basis of many numerical codes (FLUENT, OPENFOAM, etc.).

Once discretisation is applied, a large system of non-linear algebraic equations is produced. Numerous solution schemes are available for solving these equations, including those involving direct methods, such as the Gauss elimination and cyclic reduction. The iterative methods, however, are used much more often in the CFD community, as they are less sparse, i.e. require less memory space in storing the matrix problem, and can be used to solve non-linear equations. A set of convergence criteria is normally enforced during the calculation process to optimise the balance between accuracy and efficiency of the numerical analysis.

As can be seen from the discussion above, there are many choices of calculation methodology in CFD. Some of these methods, with an emphasis to those used in this thesis, are outlined in Section 5.5. Depending on the fluid model, discretisation methods, solution strategy, and the numerical capabilities of the computing system, different levels of accuracy, convergence, and stability can be obtained from a common mathematical model. A CFD practitioner, therefore, needs to study the characteristics of the mathematical problem at hand and be aware of the errors stemming from each aspect of the CFD process, such as the assumptions made during the model development, the inaccuracies initiated during the discretisation process, as well as the errors involved due to the limitation of the calculation procedure itself (e.g. round-off errors). Through this knowledge, methods that minimise these errors can be implemented.

A crucial part of the CFD analysis is therefore the determination and verification of its validity. This step is shown in Figure 5-1, where various aspects of the numerical analysis are examined. More specifically, these aspects can be listed as follows:

- The conservation of mass, momentum, and energy across the whole computational domain.
- The consistency of the discretisation method: the discretised equations should theoretically approach the exact solution of the governing partial differential equations when the mesh spacing and step size verge towards zero.
- Stability considerations: the tendency of the system of numerical equations to converge/diverge due to the magnification of errors over the calculation process.
- Solution convergence: the results of the CFD analysis should tend towards the exact solutions of the governing partial differential equations when the mesh spacing and step size verge towards zero. This is normally examined by successively refining the numerical grid and the time step size.

While all of the criteria stated above can theoretically be achieved through careful formulation and robust solution procedure, it should be noted that currently most CFD analyses are still not able to provide quantitative agreement with experimental data. Most commonly, this is caused by difficulties in the replication of exact experimental boundary conditions, which may require very complex models that can render the mathematical problem to be very computationally expensive. Nevertheless, many CFD analyses have been shown to be able to produce numerical results that qualitatively agree with experimental data, and the results of these analyses have in turn been crucial in advancing the understanding of various flow developments in many experiments where these flow structures may be undetectable. In many studies, therefore, numerical approaches can be highly complementary towards obtaining a comprehensive analysis of experimental observations and results (Reizes & Leonardi, 2005). In this thesis, similar benefits can be obtained from the numerical analysis of the sphere-settling experiment.

5.3 CFD modelling approaches for fluid-particle dynamics problem

Several different approaches have been used to study the motion of solids in a fluid medium. In this section, an overview of these approaches will be presented, along with a discussion of their advantages and disadvantages. The suitability of these methods towards the problem presented in this thesis has been considered and the selection of the numerical method used for the current CFD analysis has been selected based on these considerations.

The most common approach for the analysis of the flow field surrounding a settling object involves the representation of the settling object as a stationary solid body that acts as an obstruction to flow. The resulting flow field and drag force experienced by the fluid should mirror that of a settling particle in the same fluid. The discretisation of this flow problem is normally conducted using the finite element (FE) method, mainly due to the suitability of this numerical scheme towards flow problems with complex geometries, as well as flow problems that lack

'smoothness', i.e. involving large or abrupt changes in flow parameters, such as those involved in the interface between the sphere surface and the fluid.

The applicability of this technique with respect to various rheological fluid models has been varied. Successful simulations of this type in viscoplastic and shear-thinning fluids include Blackery and Mitsoulis (1997), Beaulne and Mitsoulis (1997), deBesses et al. (2004), and Hsu et al. (2005). Missirlis et al. (2001) have conducted a comparative study on the efficiency of the FE and FV discretisation methods for such mathematical problem, and found that while the two methods yielded similar results, the FE method requires more space for its computation. The application of this numerical technique for the simulation of viscoelastic fluid flows, however, has been found to be challenging. Simulations involving high values of Deborah numbers (De > 1.0) have generally encountered convergence problems, with some early numerical works demonstrating such difficulties (Delvaux & Crochet, 1990; Pilate & Crochet, 1981; Townsend, 1980). In 1987, Marchal and Crochet have developed an effective model based on the streamline-upwind Petrov-Galerkin (SUPG) FE method to overcome this problem. The resulting numerical scheme, however, requires high computational costs. Mendelson et al. (1982) also suggested another technique, termed the elastic viscous split stress (EVSS) finite element method, which is more computationally economic, by splitting the extra-stress into viscous and elastic terms, yielding an extra elastic-stress term. Debae et al. (1994) suggested a combination of the two methods, termed as EVSS/SUPG finite element, which has been successfully applied to the sphere-flow problem by Wu et al. (2003).

While it has been found that the method outlined above is useful for illustrating the flow fields around a sphere settling at a constant terminal velocity, the disadvantage of this setup is that no transient effects can be considered. It is therefore unsuitable for the purpose of this thesis.

Another approach has been suggested by Liu et al. (2002; 2003), who applied a fixed velocity on a spherical particle and calculated the velocity field of the viscoplastic fluid around the sphere using the biquadratic penalty FE method.

Their findings were in agreement with the numerical analyses of Beris et al. (1985) and Blackery and Mitsoulis (1997). This simulation procedure, however, requires prior knowledge of the particle settling velocity and is therefore unsuitable for the study of the dynamic behaviour of spheres settling in a fluid medium.

Bodart and Crochet (1994) presented a numerical analysis based on the moving-mesh technique, in which the mesh surrounding the sphere 'moves' along with the motion of the sphere. The surrounding mesh regions are re-adapted each time, either by stretching or compressing in an accordion-like movement. While it is likely that this method can yield relatively accurate results, it is computationally expensive. The re-meshing process can also be another source of error, where the new mesh does not necessarily yield accurate results. Therefore, it requires considerable experience by the researcher to continually check the quality of mesh. Furthermore, in numerical simulations involving two or more particles, as will be the case with some of the simulations conducted for this study (see the numerical study presented in section 5.7.3), the re-meshing process could potentially be much more complicated. In such cases, to maintain the accuracy of the calculation procedure, the re-meshing process has to be done over much shorter time step, potentially escalating the costs of the computation process. Small gaps between the particles may also lead to extreme skewness in meshing, causing divergence in the iteration process.

A new finite volume-based method has recently been suggested by Agrawal et al. (2004), termed as the Macroscopic Particle Model (MPM). This method has specifically been designed for the modelling of particles in fluids where factors such as the hydrodynamic effects and inter-particle interaction are important. In this method, the particle is treated in a Lagrangian frame-of-reference and is assumed to span over several computational cells. Furthermore, every cell that contains at least one node within the region occupied by the particle is considered to be in contact with the particle. The flow field of the cells surrounding the sphere is then calculated by considering the volumetric average of the velocity field:

$$V_{f,\text{after fixing}}(t) = \alpha_p(t) V_p(t) + \left(1 - \alpha_p(t)\right) V_{f,\text{beofre fixing}}(t) \qquad \textbf{(5-1)}$$

Where α_p is the particle volume fraction, V_f the velocity of touched fluid cell, and V_P the average velocity of the phase representing the particle. The resulting momentum, hydrodynamic force, and the fluid flow around the particle, are then calculated based on the calculated velocity before and after the 'fixing' ($V_{f,\ after\ fixing}$ and $V_{f,\ before\ fixing}$). Upon conducting a study on the settling behaviour of a spherical particle in a Newtonian fluid using this method, Ookawara et al. (2005) found that this method tends to over-estimate the settling velocity of the sphere. Another disadvantage of using this method is that the flow field surrounding the sphere as affected by the assumptions stated in equation 5-1 is still largely unknown.

In 1998, Chen et al. presented the study of the settling of a spherical object in a viscoplastic fluid using the Volume-of-Fluid (VOF) method. This method was initially developed to study the flow between two (or more) immiscible fluids and has since been extensively used for the simulation of the upwards flow of bubbles through a fluid (L. Chen et al., 1998; Gaston, Reizes, & Evans, 2002). The VOF method revolves around an indicator scalar function α, which represents the volumetric fraction of one of the fluids. The VOF method incorporates an additional conservation equation for α, as well as modified conservation equations for mass, momentum and energy balances. As a result, the whole velocity field can be evaluated based on the changing values of α and the interface between the two liquids can be determined with reasonable accuracy. In their study of solid-fluid interaction in 1998, Chen et al. have represented the solid material with an extremely viscous fluid ($\sim 10^3 \times \mu_f$) and "reconstructed" the shape of the solid body at the end of each time step. It was found that this method is appropriate for the simulation of such flow problems, requiring much less computational time in comparison to the moving mesh simulations, and that it gives reasonable predictions of the settling behaviour of the sphere in a viscoplastic fluid.

A modification of the VOF method has recently been developed, termed as the Volume of Solid (VOS) method (Lörstad & Fuchs, 2001). As the name suggests, this method has specifically been developed for the simulation of solids in a fluid medium. The "second fluid", which is the solid body, is assumed to have an infinite

viscosity. By considering that viscous forces are dominating close to the solid surface, the shear stresses can be assumed to be constant. Thus, the averaged viscosity is:

$$\mu = \frac{\mu_f}{\alpha_{fluid}} \tag{5-2}$$

where μ_f is the dynamic viscosity of the liquid phase. Since there is no flow in the solid body, cells containing the solid phase are blocked and no computations are carried out for these cells. Prahl et al. (2007) has conducted a study using this method, examining the interaction between two fixed particles in a fluid. Through this study, it was found that this method can satisfactorily resolve the flow field around the particles and calculate the drag forces experienced by the particles.

The applicability of VOS on the sphere-settling problem in this thesis is still relatively unknown. As has been mentioned above, the study of Prahl et al. (2007) involve the simulation of two particles in fixed locations. Thus, the interface between the primary and secondary phases does not need to be reconstructed at each time step. The flow problem presented in this thesis requires that dynamic simulation be conducted, and as a result, it is likely that the VOS method is still inapplicable, at least until a suitable algorithm for the accounting of partially filled cells is developed.

Based on the above considerations, the VOF method was selected for the numerical study of the settling-sphere problem in this thesis.

5.4 Mathematical formulation

Consider an initially stationary metal sphere in a rectangular column filled with a fluid medium (see Figure 5-2). The metal sphere exerts a downward shear force on the fluid medium due gravitational effects. Part of the fluid medium, which is modelled with the semi-viscoplastic equation (see equations 4-3 and 4-5), undergoes

changes in viscosity and flows as the shear forces induced by the weight of the sphere overcomes the yield stress of the fluid.

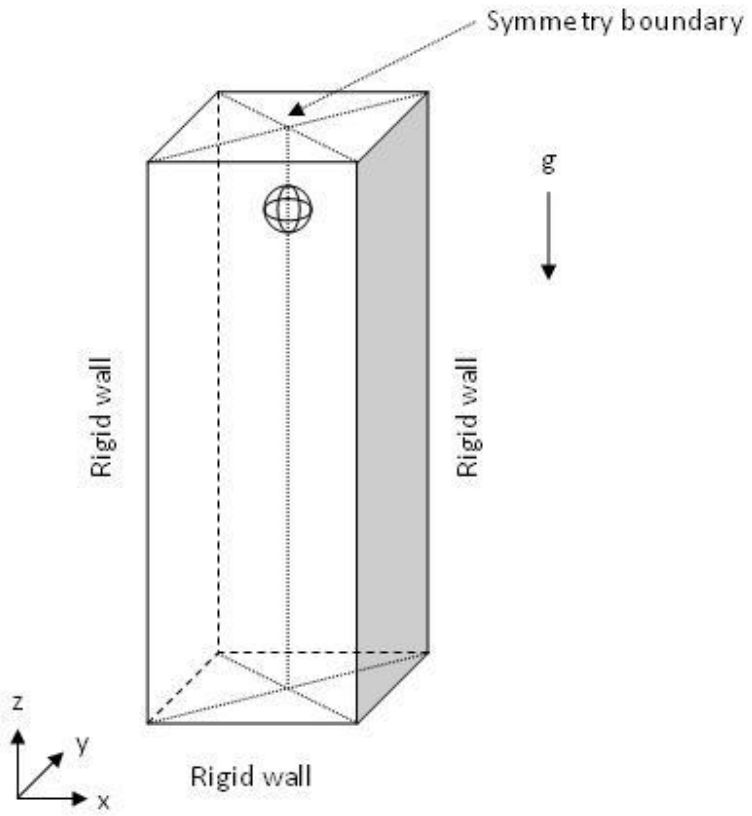

Figure 5-2: A schematic description of the problem

To develop a mathematical representation of the problem stated above, the metal sphere is firstly likened to a fluid with very high viscosity (200 – 1000 Pa.s). The sphere-settling problem thus reduces down to a dual-phase flow problem, with the two phases possessing vastly different values of density and viscosity.

The momentum equation as outlined in equation 2-33, can be re-written as follows:

$$\frac{\partial}{\partial t}\left(\rho\vec{V}\right)+\nabla\cdot\left(\rho\vec{V}\vec{V}\right)=-\nabla p+\nabla\cdot\left[\mu\left(\nabla\vec{V}+\nabla\vec{V}^{T}\right)\right]+\rho\vec{g}+\vec{F} \qquad \textbf{(5-3)}$$

where $\vec{V}$ is the velocity vector, p the pressure, $\vec{g}$ the gravity vector. The terms $\rho\vec{g}$ and $\vec{F}$ account for the gravitational and external body forces, respectively.

The above equation is applied and solved throughout the whole problem domain. Thus, the resulting velocity field is shared among the phases. The properties in the transport equations, such as density (ρ) and viscosity (μ) are determined by the volume fraction of the phases in each control volume:

$$\rho = \sum \alpha_q \rho_q \tag{5-4}$$

$$\mu = \sum \alpha_q \mu_q \tag{5-5}$$

where α_q is the volumetric fraction of the q^{th} phase. A value of unity for α indicates that the cell is full of the q^{th} fluid. The opposite is true for $\alpha = 0$.

As isothermal conditions have been assumed in the formulation of the problem, the energy equation has been neglected in the calculation process.

Using the equation for the conservation of mass, the volume fraction of the secondary phase, or in this case the phase representing the metal sphere, can be calculated, hence effectively tracking the interface between the phases:

$$\frac{1}{\rho_q}\left[\frac{\partial}{\partial t}\left(\alpha_q \rho_q\right) + \nabla \cdot \left(\alpha_q \rho_q \vec{v}_q\right) = \sum_{p=1}^{n}\left(\dot{m}_{pq} - \dot{m}_{qp}\right)\right] \tag{5-6}$$

The variable $\dot{m}_{pq}$ represents the mass transfer from phase p to q, whereas $\dot{m}_{qp}$ the mass transfer from phase q to p.

The volume fraction of the primary phase, which in this case represents the fluid medium, is then calculated by enforcing the following equation of conservation:

$$\sum_{q=1}^{n_{VOF}} \alpha_q = 1 \qquad (5\text{-}7)$$

where n_{VOF} is the total number of phases in the flow problem (n_{VOF} = 2 for the current case).

5.5 Numerical method

Having specified a mathematical formulation for the basis of the CFD analysis, the problem can now be completed with suitable initial and boundary conditions and solved with an appropriate numerical method.

5.5.1 Numerical grid generation

As the Finite Volume (FV) method has been selected for the numerical analysis of this problem, control volumes (CVs) within the 3D computational domain as defined in Section 5.4.1 need to be constructed. This was conducted by creating a numerical grid consisting of uniform hexahedral mesh using commercial meshing software package, GAMBIT 2.3. The differential equations are integrated over each control volume and all variables are defined at the centre of the control volume. This storage arrangement for the flow variables is commonly known as the 'collocated' grid arrangement (see Figure 5-3).

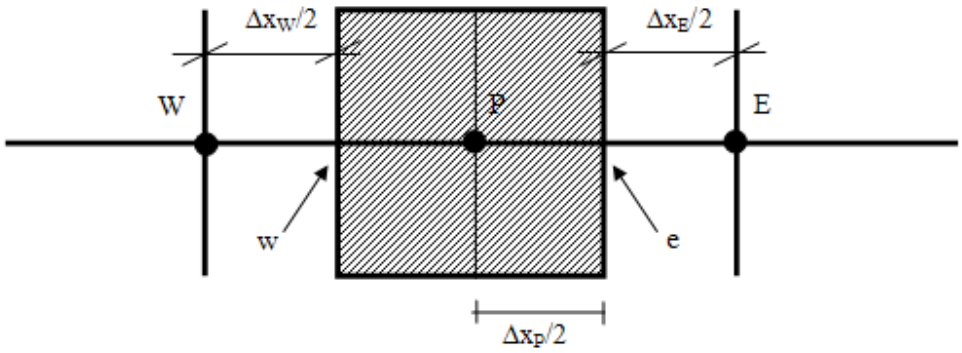

Figure 5-3: Collocated grid arrangement

The utilisation of the collocated grid arrangement has been recommended by Chen et al. (1998) in their numerical study of two-phase flow using VOF formulation. Although the collocated arrangement of the grid may reduce the accuracy of the diffusive terms of the governing equations, the advantage of this arrangement is that accurate representation of flux and source terms can be obtained (see Section 5.5.2). The inaccuracies induced by the use of the collocated grid arrangement and the utilisation of appropriate numerical schemes for the minimisation of these errors will be discussed in further detail in Section 5.5.2.

5.5.2 Discretisation methods: general equations

The FV method of discretisation is based on the integral form of the governing equations. For example, for a scalar quantity φ over a control volume v, the conservation of momentum equation can be written as follows:

$$\int_v \frac{\partial \rho\varphi}{\partial t} dv + \oint \rho\varphi \vec{V} \cdot d\vec{A} = \oint \Gamma_\varphi \nabla\varphi \cdot d\vec{A} + \int_v S_\varphi dv \qquad \textbf{(5-8)}$$

where $\vec{A}$ is the combined form of the direction vector and the surface area of the control volume, Γ_φ is the diffusion coefficient for φ, and $\nabla\varphi$ the gradient of φ. The

last term, S_φ accounts for any sources or sinks (per unit volume) that either create or destroy φ. The integrals in equation 5-8 are approximated as follows:

$$\underbrace{\frac{\partial \rho \varphi}{\partial t} v}_{\text{UNSTEADY}} + \underbrace{\sum_{f}^{N_{faces}} \rho_f \vec{V}_f \varphi_f \cdot \vec{A}_f}_{\text{CONVECTIVE}} = \underbrace{\sum_{f}^{N_{faces}} \Gamma_\varphi \nabla \varphi_f \cdot \vec{A}_f}_{\text{DIFFUSION}} + \underbrace{S_\varphi v}_{\text{SOURCE}} \qquad \textbf{(5-9)}$$

where N_{faces} is the number of faces enclosing control volume v, whereas f refers to any face of this particular cell. φ_f is the value of φ convected through face f, $\vec{A}_f$ is the combined form of the direction vector of φ_f with the surface area of face f, and $\nabla \varphi_f$ is the gradient of φ at face f. The term $\rho_f \vec{v}_f \cdot \vec{A}_f$ thus accounts for the mass flux through face f.

In order to evaluate equation 5-9, the face values of φ, φ_f, need to be evaluated for the convection term. This is conducted by interpolating the field variables stored at the cell centres to the faces of the control volumes. In FLUENT 6.3, various interpolation methods are available for this purpose, including the first- and second- order upwind methods, power law, quadratic upwind (QUICK), as well as the central-differencing method. For this thesis, the central-differencing method has been implemented to minimise the effects of numerical diffusion. With respect to the notations outlined in Figure 5-3, this numerical method can be written as follows:

$$\varphi_e = \frac{1}{2}(\varphi_P + \varphi_E) + \frac{1}{2}\left(\nabla \varphi_P . \vec{r}_P + \varphi_E . \vec{r}_E\right) \qquad \textbf{(5-10)}$$

where the indices P and E refer to the cells that share face e. φ_P and φ_E hence refer to the values of φ stored at the centres of cells P and E. $\nabla \varphi_P$ and $\nabla \varphi_E$ are the gradients of φ at the centres of these cells, whereas $\vec{r}$ is the displacement vector from the upstream cell centroid to the face centroid.

The gradient of φ at the centre of the cell, $\nabla\varphi$, is evaluated using the Green-Gauss theorem:

$$\nabla\varphi = \frac{1}{v}\sum_{f} \bar{\varphi}_f \vec{A}_f \qquad \textbf{(5-11)}$$

where v is the volume of the cell. The variable $\bar{\varphi}_f$ represents the value of φ at the centroid of the cell-face. This variable is evaluated as the average between the φ values at the centre of the adjacent cells (e.g. the value of $\bar{\varphi}_e$ is the average of φ_P and φ_E in Figure 5-3)

In equation 5-8, it can also be seen that an additional gradient form of φ needs to be evaluated for the approximation of the diffusion term. In this case, the gradient of φ at the face of the cell is needed, i.e. $\nabla\varphi_f$. By default, FLUENT 6.3 evaluates this variable through a central differencing method based on the values of the cell-centre gradient at the adjacent cells, thus ensuring second-order accuracy.

In addition to these approximation methods, several other numerical adjustments need to be incorporated, mainly due to the nature of calculation involved with the collocated arrangement of the grid. Due to this arrangement, a pressure field that is interpolated linearly would effectively be dependent on alternate nodal pressure values rather than adjacent ones. This can cause the pressure field to attain a 'checker-board' effect, where, in each of the dimension, alternate grid points would have the same value in pressure, but not adjacent ones. This can be seen in equation 5-12, where the one-dimensional pressure gradient in cell P is shown to be dependent on the cell-centre pressure values at cells W and E, according to the grid arrangement outlined in Figure 5-3:

$$\frac{\delta p}{\delta x} \approx \frac{p_w - p_e}{\Delta x} = \frac{1}{\Delta x}\left(\frac{p_W + p_P}{2} - \frac{p_P + p_E}{2}\right) = \frac{p_W - p_E}{2\Delta x} \qquad \textbf{(5-12)}$$

where p_w and p_e are the pressure values at the face between cells W-P and P-E, respectively, and p_W, p_P, and p_E the cell-centre pressure values of cells W, P, and E.

While the use of this numerical scheme (equation 5-12) may be acceptable for systems involving minimal variations in pressure, this calculation procedure can lead towards instability if there are large fluctuations in the pressure field. During the momentum calculation, these fluctuations would translate to large gradients in the source terms, often leading to overshoots/undershoots in the calculated velocity field. In this study, this difficulty was overcome by the incorporation of the PRESTO! (PREssure STaggering Option) scheme into the discretisation of the momentum equation. Using this scheme, the discrete continuity equation is applied to a 'staggered' cell whose cell-centre is incident with the face of the collocated cell. This scheme allows for the pressure field at the cell-face to be determined according to the values of adjacent cells, thus avoiding the 'checkerboard' effect (S. V. Patankar, 1980).

To further minimise the checkerboard effect associated with the use of the collocated grid arrangement, FLUENT 6.3 also employs an interpolation technique that was proposed by Rhie and Chow (1983) for the discretisation of the continuity equation. In this method, the face value of the velocity field is averaged using momentum-weighted factors. Both of the numerical schemes mentioned above are used widely in CFD analyses and have been found to be effective in ensuring mass conservation throughout problem domains that has been assigned with collocated grids.

Finally, a first-order approximation of the time integral is applied for any variable, φ, over a control volume P (Fluent, 2006):

$$\int_V \frac{\partial \rho \varphi}{\partial t} dv \approx \frac{\varphi_{i,j,k}^{n+1} - \varphi_{i,j,k}^{n}}{\Delta t} \Delta v_P \qquad \textbf{(5-13)}$$

Where φ^n is the φ value at the current time level, t, and φ^{n+1} is the value at the next time level, $t + \Delta t$. The interface between the phases is calculated based on equation 5-6, using the volume fraction values that were computed at the previous time step. For all other variables, the implicit temporal discretisation scheme is used, with all

of the convective, diffusion and source terms being evaluated at the future time level, n+1.

5.5.3 Discretisation methods: Fluid viscosity model

The fluid model used in the following sections is based on the semi-viscoplastic fluid model outlined in Section 4.4. To incorporate this model, a User Defined Function (UDF) had to be generated and loaded with the FLUENT solver.

The UDF used for the current study was based on the DEFINE_PROPERTY macro in FLUENT 6.3. In this macro, the fluid structure parameter (λ) is firstly calculated based on the numerical approximation of equation 4-3:

$$\frac{\Delta\lambda}{\Delta t} \approx \frac{1-\lambda}{\theta} - \kappa\dot{\gamma}\lambda \qquad \textbf{(5-14)}$$

where θ is characteristic relaxation time of the fluid viscous parameters, κ is a constant that reflects the rate of break-down in the fluid structure, and $\dot{\gamma}$ is the shear rate. The following approximation can thus be applied:

$$\Delta\lambda_{t+\Delta t} \approx \left(\frac{1-\lambda_t}{\theta} - \kappa\dot{\gamma}_t\lambda_t\right)\Delta t \qquad \textbf{(5-15)}$$

and

$$\lambda_{t+\Delta t} = \lambda_t + \Delta\lambda_{t+\Delta t} \qquad \textbf{(5-16)}$$

where the subscript t indicates the time step of the simulation. The calculation then progresses to calculate the resulting viscosity based on equation 4-5. At the start of the simulation, a starting value of unity is assigned for the λ values across the domain filled with the fluid phase.

In this study, the solutions of the discretised governing equations were obtained through the utilisation of the segregated pressure-based solver, which will be

discussed in more detail in section 5.5.5. At each iteration step, this calculation algorithm requires that the fluid properties be updated before the momentum equations are solved for the velocity and pressure fields. As a result, the DEFINE_PROPERTY UDF is effectively 'called' and updated at the beginning of each iteration step. To prevent FLUENT from updating the values of λ at each iteration step, another UDF, DEFINE_EXECUTE_AT_END, has to be incorporated. This macro is basically a general-purpose macro that is executed at the end of a time step in a transient run. In this macro, the values of λ across the fluid domain as well as the strain rate used in the calculation for the new values of λ, are updated.

The UDF code used in this study is presented in Appendix C.1.

5.5.4 Interface reconstruction scheme

One of the issues that are associated with the VOF model is the reconstruction of the interface between the phases. Since the development of the VOF method by Hirt and Nichols in 1981, many methods have been suggested for the reconstruction of interfaces in VOF problems, based on the α field at the face of a control volume. This process is commonly known as 'advection'. In the simplest form of VOF (SOLA-VOF), Hirt and Nichols used a scalar volume-fraction field representing the averaged volume fractions of fluids within each control volume (see Figure 5-4(b)). A cell is identified as a donor of an amount of fluid from one phase, while a neighbouring cell acts as the acceptor of the same amount of fluid, thus preventing numerical diffusion at the interface (Donor-Acceptor scheme). This method is remarkably simple to use and is effective in modelling flows with complex free-surface geometries. However, this method does not readily provide information about the interfaces between the fluids. As a result, the user of this method has to be cautious in advecting the volume fraction fields so as to preserve the sharpness of the interfaces.

An improvement of the Donor-Acceptor scheme was suggested by Youngs (1982), termed as the Piecewise Linear Interface Construction (PLIC), which has since been generalised for unstructured mesh and known as the Geometric Reconstruction Scheme. This method is able to reconstruct the interfaces more effectively, although it does require more computational time than the previous method. In this scheme, the interface between the fluids is assumed to have a linear slope within each cell. With this assumption, the position of the interface can be calculated based on the values of the volume fraction and its derivatives. Using this information and the normal and tangential velocity distribution on the face, the advection calculation for the fluid through the cell faces can then be conducted. The volume fraction in each cell can then be updated. The typical results of this method in comparison to the SOLA-VOF algorithm can be seen in Figure 5-4(c). Improvements on the PLIC method have also been recently suggested by Pillod and Puckett (2004) using least-square procedure and Lopez et al. (2004) using splines instead of linear slopes.

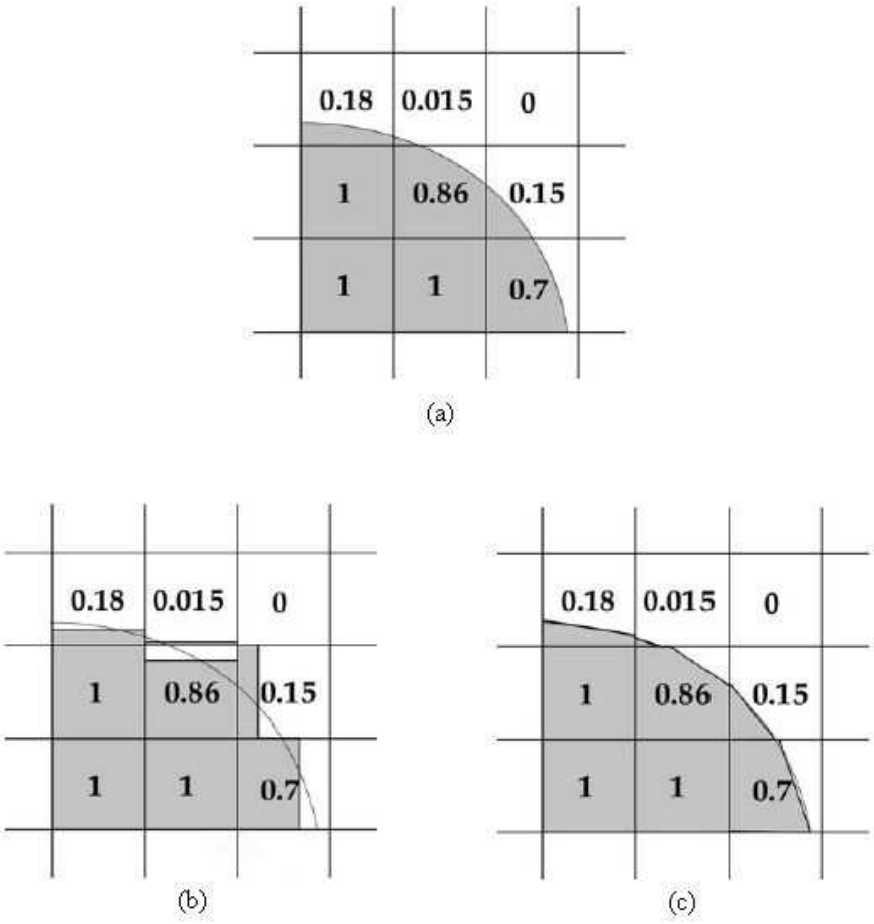

Figure 5-4: Comparison of Interface Reconstruction Schemes (Martinez, Chesneau, & Zeghmati, 2006): (a) True interface; (b) SOLA-VOF; (c) PLIC.

Other advection schemes have also recently been developed recently, including CICSAM (Ubbink & Issa, 1999) and HRIC (Muzaferija & Peric, 1999), which are based on high resolution differencing scheme. Özkan et al. (2007) have conducted a comparative study between several CFD codes and advection schemes for the interfacial simulation of bubble-train flow in a narrow channel. From this study, it was found that the VOF method with PLIC and donor-acceptor schemes that are offered by FLUENT 6.3 generally yield satisfactory results, whereas high-order difference schemes such as CICSAM and HRIC were found to give a higher level of smearing, resulting in alterations in the flow patterns.

Due to the above finding and the well-established nature of the PLIC method, this advection scheme was selected for the basis of the VOF calculation in this thesis.

5.5.5 Solving procedure

Once discretisation is applied, a large system of non-linear algebraic equations is produced. Numerous solution schemes are available for solving these equations, including those involving direct methods, such as the Gauss elimination and cyclic reduction. The iterative methods, however, are used much more commonly in the CFD community, as they are less sparse, require less memory space in storing the matrix problem, and can be used to solve highly non-linear equations. A set of convergence criteria, which will be discussed in Section 5.5.6, is then enforced during the calculation process, to optimise the balance between accuracy and efficiency of the calculation.

For the current study, the series of algebraic equations resulting from the discretisation of the governing equations were solved using the segregated pressure-based solver algorithm. As the name suggests, this algorithm considers a single variable (φ) at a time, over all cells simultaneously. The solution of each variable is found through a point implicit (Gauss-Seidel) linear solver in combination with the algebraic multi-grid (AMG) method. The calculation procedure involved with this calculation algorithm can be seen in Figure 5-5.

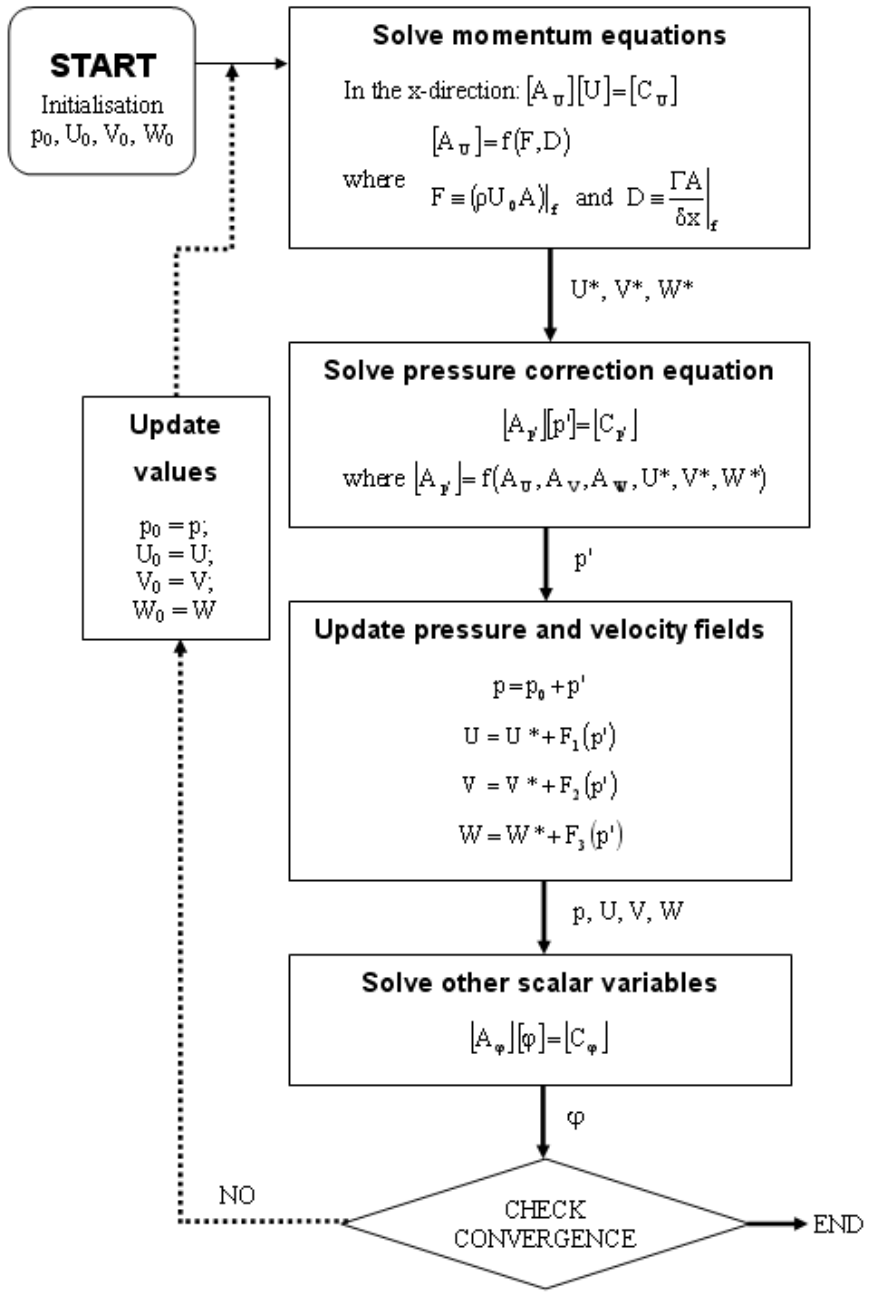

Figure 5-5: Segregated pressure-based solver with SIMPLE pressure-velocity coupling scheme. U, V, and W represent the velocity vector in the x-, y-, and z- directions. A and C represent the matrix resulting from the system of linearised equations obtained from considerations of the convection (F), diffusion (D) and source terms of each element of the calculation. F_1, F_2, and F_3 represent the momentum-weighted factors for the correction of the velocity field.

As can be seen in Figure 5-5, the pressure-based segregated solving algorithm involves the initial solution of the momentum equations, yielding a first 'guess' of the velocity field and mass-flux. A pressure correction equation is then applied, resulting in the 'corrected' values of face mass fluxes, pressure, and velocity field. Other scalars, such as turbulent quantities, energy, species and radiation intensity are then evaluated using the corrected pressure and velocity fields. Due to this segregated approach towards the solution of the governing equations, which are in fact highly coupled, a pressure-velocity coupling algorithm is required to ensure that the calculated pressure and velocity fields comply with the continuity equation. In this thesis, the SIMPLE pressure-velocity coupling algorithm (S. V. Patankar & Spalding, 1972), which has been developed based on the discretised continuity equation, has been implemented for the calculation of the pressure correction term.

5.5.6 Stability and convergence

Convergence criteria of $1x10^{-3}$ and $1x10^{-6}$ were enforced for the continuity and momentum equations, respectively, with a maximum number of iterations of 50 per time step.

For all of the governing equations, under-relaxation factors were incorporated in order to control the update of computed variables at each iteration step. For example, in the pressure-correction stage, an under-relaxation factor is incorporated to avoid large fluctuations in the pressure field:

$$p = p_0 + \varepsilon_p p' \qquad (5\text{-}17)$$

where p_0 is the initial guess of the pressure field, ε_p the under-relaxation factor for pressure, and p' the pressure-correction.

As can be seen from equation 5-17, higher values of under-relaxation factor ($0 < \varepsilon < 1$) allow for more aggressive calculation progression, resulting in possibly faster convergence. However, larger fluctuations in the calculation procedure may lead to unstable results and vice versa. Balance of the two aspects can lead to

optimum level of under-relaxation. In this thesis, under-relaxation factors of 0.3 and 0.7 have been assigned for the pressure and momentum calculations. The selection of these parameters were based on the recommendations of FLUENT (Fluent, 2006) and were found to give a good balance between solution stability and convergence.

FLUENT 6.3 also provides an optional "implicit body force" treatment for multiphase calculations, which is recommended for flows involving large body forces such as gravity and surface tension forces. In these cases, often the body force and pressure gradient terms in the momentum equation are nearly in equilibrium, with the contributions for convective and viscous terms minimal. This reduces the ability for segregated solvers to converge, and as a result the equilibrium between the pressure gradient and body forces needs to be taken into account. In the implicit body force mechanism, FLUENT introduces additional terms involving corrections to the body force, allowing the flow to achieve a realistic pressure field very early in the iterative process (Fluent, 2006). This numerical scheme was incorporated for the VOF-based simulations conducted for this study.

The stability of a numerical procedure is also highly dependent on the time step selected. In VOF calculations, where numerical diffusion has to be avoided as much as possible, the highly-unstable central differencing discretisation method for the momentum equation has to be used. Furthermore, as the sharpness of the interface is highly important, very fine uniform mesh is normally required. The Courant-Friedrichs-Lewy (CFL) criterion states that in the simulation of a wave crossing a discrete grid, for example, the selected value for time step should be less than the time for the wave to travel adjacent grid points:

$$\frac{V.\Delta t}{\Delta x} \leq CFL \qquad \textbf{(5-18)}$$

Where Δx is the size of the grid. Therefore, the smaller the grid size, smaller time steps should be used to maintain stable solutions.

The time step used in the simulations conducted for this thesis was selected based on the above considerations, and a maximum courant number (CFL) of 0.1 is enforced at all times during the calculation process.

5.5.7 Summary of numerical scheme

Overall, the features of the proposed numerical method for the mathematical problem presented in Section 5.4 can be summarised as follows:

- A 3D numerical grid consisting of uniform hexahedral control volumes has been constructed over the computational domain
- The motion of the sphere through the fluid medium was tracked through the PLIC interface-tracking scheme based on VOF method suggested by Youngs (1982)
- The semi viscoplastic fluid model discussed earlier in section 4.4 has been discretised. A code was written for the implementation of this equation into the solution procedure through the utilisation of the User Defined Functions (UDFs) available in FLUENT 6.3
- An implicit differencing scheme was used for the time derivative term of the governing equations
- The convective and diffusion terms of the governing equations were discretised using the standard central differencing scheme.
- The interpolation for the pressure field for the momentum equation was conducted using the PRESTO! Scheme (S. V. Patankar, 1980)
- The SIMPLE method (S. V. Patankar & Spalding, 1972) was adopted for the pressure-velocity coupling in conjunction with the segregated pressure-based solver used for the solution of the discretised equations.

In the development of this numerical formulation, careful consideration has been given for the minimisation of errors during the discretisation process. The solution

procedure, such as the selection of time step (CLF $\leq$ 0.1) and under relaxation factors, has been developed in such a way to attain good stability as well as rapid convergence during the calculation stage. The suitability and validity of this numerical scheme will be examined in the following section.

5.6 Newtonian results

In order to accurately represent the settling behaviour of solid particles in a fluid medium using the VOF method, careful consideration needs to be given towards the preservation of the interface between the liquid phase and the phase representing the solid material (i.e. the secondary or 'solid' phase), both in its shape and its sharpness, throughout the discretisation and numerical processes. Therefore, the level of deformation in the spherical profile of the 'solid' phase has to be adequately minimised so as not to affect the accuracy of the flow profile surrounding the sphere. Based on the mathematical formulation of the problem, this deformation is obviously highly dependent on the selection of a viscosity value assigned for the phase representing the solid sphere. As this parameter is unmeasurable in reality, its quantification has to be done through a process of trial and error. In this thesis, this process was conducted through a simulation study in Newtonian fluids, and will be discussed later in Section 5.6.2.

In addition to the selection of the 'solid' viscosity, the preservation of the shape and sharpness of the interface is also dependent on the formulation of the numerical scheme, particularly in the advection of the α (or volume fraction) field. The discretisation of the α equations in both the transient and spatial domains has to incorporate sufficient level of accuracy so as to minimise the effects of interface smearing associated with numerical diffusion. The formulation of the numerical scheme, as has been discussed previously in section 5.5, was developed with this concept in mind. The applicability of this numerical scheme and the capability of the interface-tracking method in reconstructing the interface for the specified discretised domain and numerical problem will be evaluated in Sections 5.6.2 and 5.6.3, using numerical simulations conducted in Newtonian fluids.

The parameters selected for the numerical study conducted in Newtonian fluids were assigned such that similar values in Reynolds number as those to be done in the semi-viscoplastic fluid model could be obtained. With the rate-of-shear estimated to be $\dot{\gamma}_R = V/D$ (Bot et al., 1998; Kemiha, Frank, Poncin, & Li, 2006), the Reynolds number for the rate equation, here represented by the steady-state form of the semi-viscoplastic model of equation 4-5, can be written as:

$$Re = \frac{\rho_f VD}{\mu_\infty + (\mu_0 - \mu_\infty)\left(1 + \kappa\theta\left(\frac{V}{D}\right)\right)^{-m}} \tag{5-19}$$

Equation 5-19 can be simplified by neglecting the term μ_∞, which has been found to be very small for all of the fluid solutions (~ 0.0001 Pa.s, see Table 4-2):

$$Re = \frac{\rho_f VD}{\mu_0\left(1 + \kappa\theta\left(\frac{V}{D}\right)\right)^{-m}} \tag{5-20}$$

where ρ_f is the density of the fluid, V the settling velocity of the sphere, and D the diameter of the sphere. For Newtonian fluids, the power-index m of the rate equation is zero. The Reynolds number for this case then becomes:

$$Re = \frac{\rho_f VD}{\mu_N} \tag{5-21}$$

where μ_N is the Newtonian viscosity. The range of μ_N was thus selected such that the resulting Reynolds number is similar to those conducted experimentally using the viscoplastic fluids ($0.1 < Re < 7.0$). For a spherical object of ρ_s = 8000 kg/m^3 and D = 0.01 m, this corresponds to fluid viscosity (μ_N) of 0.7 – 5.3 Pa.s (see Appendix C.2 for details of calculation).

5.6.1 Domain description

The geometry of the column has been selected such that the smallest distance between the ball and the wall is 4.5 D.

In VOF-based calculations, the efficiency of the numerical scheme depends highly on the effectiveness of the advection scheme for the α fluxes, which in turn is highly dependent on the position of the interface within each computational cell. As a result, VOF-based numerical schemes generally require the discretisation process to be conducted over highly structured (square) grids. In this study, to ensure the consistency of the advection scheme over all of the simulations, the size of the numerical mesh was related to the diameter of the spherical particle, rather than the intended dimensions of the column. As a result, simulations involving larger spheres would require less degree of finesse in grid dimensions than those involving smaller spheres. From the convergence study presented in Section 5.6.3, it will be shown that the number of mesh nodes required across the diameter of the sphere is approximately 11 for a grid independent solution.

In the numerical study involving the semi-viscoplastic fluid model, some consideration will be given towards the recovery characteristics of the fluid medium after it has been sheared by the motion of a settling sphere. As will be seen in Section 5.7.3, this aspect of the fluid characteristic can be examined by considering the flow field surrounding a sphere settling through a fluid medium that has previously been sheared by the movement of another sphere some time earlier. Any changes in the viscous parameters of the fluid in this region could then be identified. The results of this study are expected to be comparable to the set of experiments conducted in the Floxit solutions. In these experiments, a sphere that is released following the flow path of another sphere was found to exhibit much higher settling velocity than the preceding one.

The consideration stated above is highly relevant towards the architecture of the numerical grid for the CFD study. For the recovery of the viscous parameters to be

accurately simulated, the symmetry of the flow field as well as the accuracy of the advection scheme need to be sustained and conserved throughout the discretised domain. As a result, a uniform cubic mesh has to be assigned throughout the 3D column. The details of the resulting grid configurations have been outlined in Table 5-1. As can be seen in this Table, the simulations conducted for this study generally require large numbers of nodes. These calculations, therefore, are relatively computationally expensive.

Table 5-1: Grid configuration over the computational domain.

Mesh size (mm)	Column width (mm)	# mesh nodes (for H = 100 mm)	# mesh/sphere diameter
1.1	101.2	769,455	9.09
1	100	1,000,000	10.00
0.9	99.9	1,369,000	11.11
0.8	100	1,953,125	12.50

5.6.2 'Solid' viscosity

To examine the level of 'solid' viscosity required to maintain the sharpness of the interface between the 'solid' and liquid phases, simulations using a Newtonian fluid of $\mu_N = 1.0$ Pa.s were conducted. The results of this study have been shown in Figure 5-6. From this Figure, it can be seen that the all three simulations show minimal deformation in the shapes of the spheres as they settle over a distance of ~ 70 mm from rest. Furthermore, it can also be seen that all three simulations yield relatively similar predictions in the settling progression of the sphere. Based on these observations, it was concluded that for μ_N value of 1.0 Pa.s and a 'solid' viscosity value ranging from 100 to 400 Pa.s, the proposed numerical scheme is able to preserve the spherical shape of the secondary phase throughout the iteration process relatively satisfactorily. Moreover, the similarities in the settling progression of the solid phase also indicate that within the parameters of these simulations, the level of viscosity in the secondary or 'solid' phase does not greatly influence the flow field development of the primary phase. Therefore, given that the level of 'solid' viscosity is adequately high for the preservation of the sphericity of

the 'solid' phase, the selection of this parameter is not expected to greatly influence the prediction of the settling velocity of the particle.

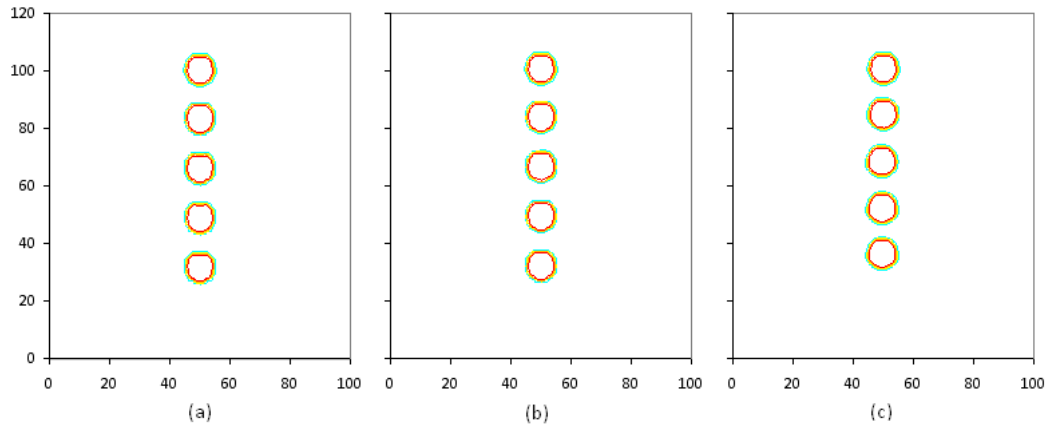

Figure 5-6: Translation of a sphere (D = 10mm, ρ_s = 8000 Kg/m^3) in a Newtonian fluid (1 Pa.s): (a) μ_s/μ_f = 100; (b) μ_s/μ_f = 200; (c) μ_s/μ_f = 400. The sphere at the top indicates the original position of the sphere, whereas the lowest sphere indicates its position after 800 iterations (mesh spacing = 0.9 mm; indicated distances are in mm).

From the observations outlined above, it was concluded that for the simulation of the settling behaviour of metal spheres in a fluid medium using the VOF model, a 'solid' to liquid viscosity ratio (μ_s/μ_f) of 100-400 is appropriate. All of the subsequent simulations conducted for this study were performed using μ_s/μ_f = 200.0.

5.6.3 Convergence study

A grid independence test was performed by comparing the predicted settling velocity after 800 iteration time steps for spheres (D = 0.01 m; ρ_s = 8000 kg/m^3) settling in Newtonian fluids of several different values in viscosity (0.72, 1.0, 2.5, and 5.3 Pa.s). The results of this analysis were illustrated in Figure 5-7 with four different grid sizes as outlined in Table 5-1.

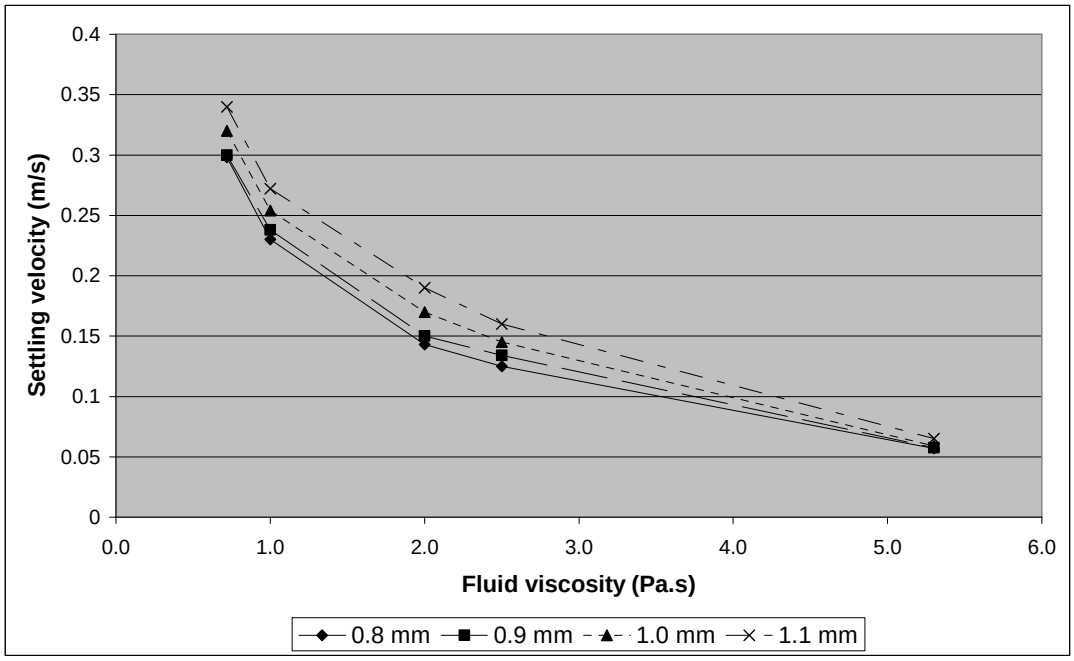

Figure 5-7: Terminal settling velocity of spheres predicted by the simulation using the VOF method, as a function of grid size.

From this Figure, it can be seen that notable differences in the values of the predicted settling velocity could be obtained by successively refining the numerical grid from 1.1 mm to 0.9 mm. This dependence on the grid size was found to be significantly reduced for cases where the fluid viscosity is relatively high (μ_N ~ 5.2 Pa.s). When the size of the grid was further decreased to 0.8 mm, minimal differences were obtained for all of the μ_N values being tested. Through this observation, it was concluded that the results generated by the 0.9 mm numerical grid were approximately grid independent. This grid size was therefore used in the following simulation runs.

Furthermore, the predicted settling velocities were then compared with the literature values, here calculated through the correlation suggested by Clift et al. (1978), incorporating the wall correction factors suggested by Francis (Francis, 1933) and Kehlenbeck and DiFelice (1999) (See details of calculation in Appendix C.3). The results of this comparison can be seen in Figure 5-8, where the predicted

values of settling velocity, here in the form of the drag coefficient (C_D), as a function of the Reynolds number, have been presented.

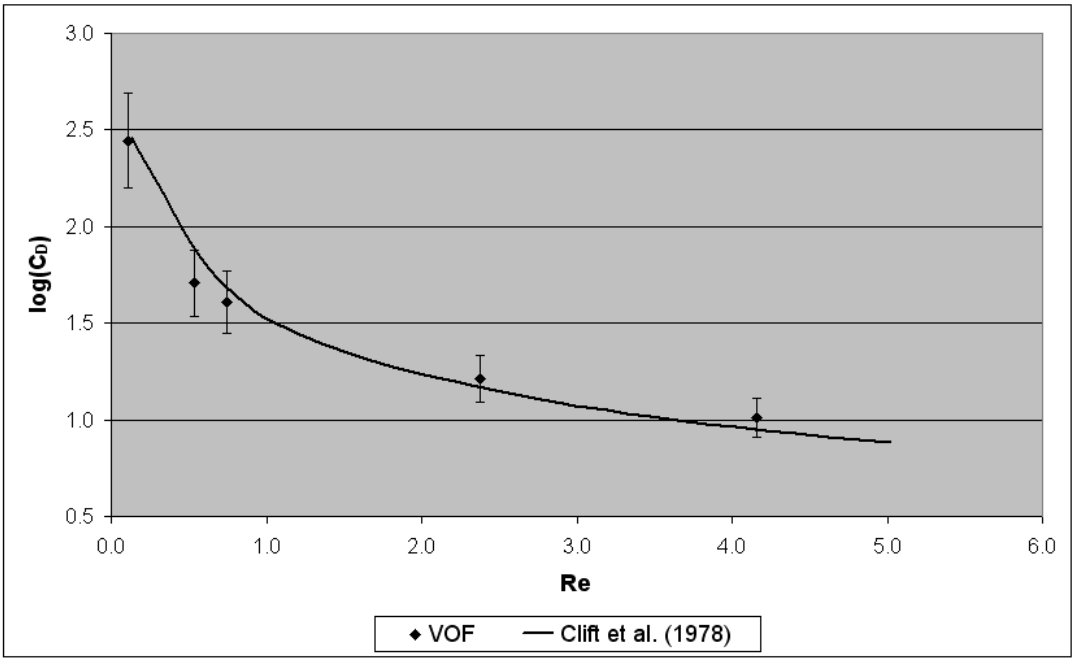

Figure 5-8: Predicted values of the drag coefficient (C_D), obtained through the VOF-based numerical scheme, in comparison to those obtained through the correlation suggested by Clift et al. (1978). The wall-correction factors suggested by Francis (1933) and Kehlenbeck and DiFelice (1999) were incorporated (see Appendix C.3). An error band of 10% on the VOF-based settling velocity has been included.

Based on the comparison presented in Figure 5-8, it was concluded that the VOF-based numerical scheme is able to emulate the prediction of drag experienced by a sphere settling through Newtonian fluids to within 10% accuracy of the values predicted through established correlations available in the literature. At lower values of Reynolds numbers, it can be seen that the VOF simulation tends to slightly under-predict the drag coefficient of the spheres when it is compared to the respective values calculated from the correlations. At the other end of the scale, i.e. at Re > 2.0, the predicted drag force was slightly higher than these calculated values. However, the difference between the predicted drag correlation and those

calculated based on the correlation suggested by Clift et al. (1978) were minimal and well within any experimental or numerical errors.

The relatively small margin of uncertainty (< 10%) shown in Figure 5-8 indicates that the proposed VOF-based numerical scheme presents a promising avenue for the prediction of the settling velocity of spheres in Newtonian fluids. In the following section, this numerical scheme will be used in conjunction with the discretised semi-viscoplastic fluid model, and the results of these simulations will be compared with the experimental data for aqueous polyacrylamide solutions.

5.7 Semi-viscoplastic results

Having established a VOF-based method for the simulation of the settling behaviour of spherical particles in fluids, the study can now be extended towards the implementation of the semi-viscoplastic model into the liquid phase. In doing so, it is hoped that a better understanding regarding the flow field surrounding a sphere settling in fluids exhibiting this flow behaviour can be obtained and factors affecting the settling velocity of the spheres can be determined.

The results of the numerical study conducted in Newtonian fluids indicate that for the simulation of the settling behaviour of spherical particles in a fluid medium, the use of a hypothetical parameter representing the viscosity of the solid material, which is approximately 200 times the viscosity of the fluid medium, is necessary. This parameter was selected such that the deformation of the interface between the liquid phase and the phase representing the solid particle is minimised.

To incorporate this approach in the numerical study of semi-viscoplastic fluids, the maximum fluid viscosity surrounding a sphere settling in this type of fluid needs to be estimated. This was conducted by estimating the particle terminal settling velocity (V_t), using the correlation suggested by Wilson et al. (2004; 2003). The minimum rate-of-shear resulting from the motion of the sphere is then estimated as follows:

$$\dot{\gamma}_{min} = \frac{V_t}{W_D} \qquad \textbf{(5-22)}$$

where W_D is the hydraulic diameter of the column.

The maximum viscosity of the fluid phase is then estimated based on the steady-state form of the rate equation (see equation 4-5). Based on this analysis (see Appendix C.4 for full details on the calculation), it can be seen that to minimise the level of deformation between the two phases, the range of solid viscosity that should be applied is 680 – 1940 Pa.s.

5.7.1 The effects of yield stress and fluid plasticity

The contours of the relative vertical velocity from simulations with the semi-viscoplastic fluid model are shown in Figure 5-9. In this Figure, the profiles of axial velocity distribution along the horizontal axis have been compared to the corresponding profiles from simulations with Newtonian fluids of similar Reynolds value. In this Figure, it can be seen that simulations with the semi-viscoplastic model tend to yield 'flatter' velocity profiles than those with the Newtonian models. This flatness indicates that in regions away from the sphere, the flow fields of semi-viscoplastic fluids have lower velocity gradients. This was expected, as the semi-viscoplastic model features high values of viscosity at the lower range of shear forces. Since the regions further away from the settling sphere generally experience much lower values of shear stresses than those closer to the settling sphere, the high values of viscosity in these regions causes a more severe reduction in the velocity gradients than in the case of the Newtonian fluids.

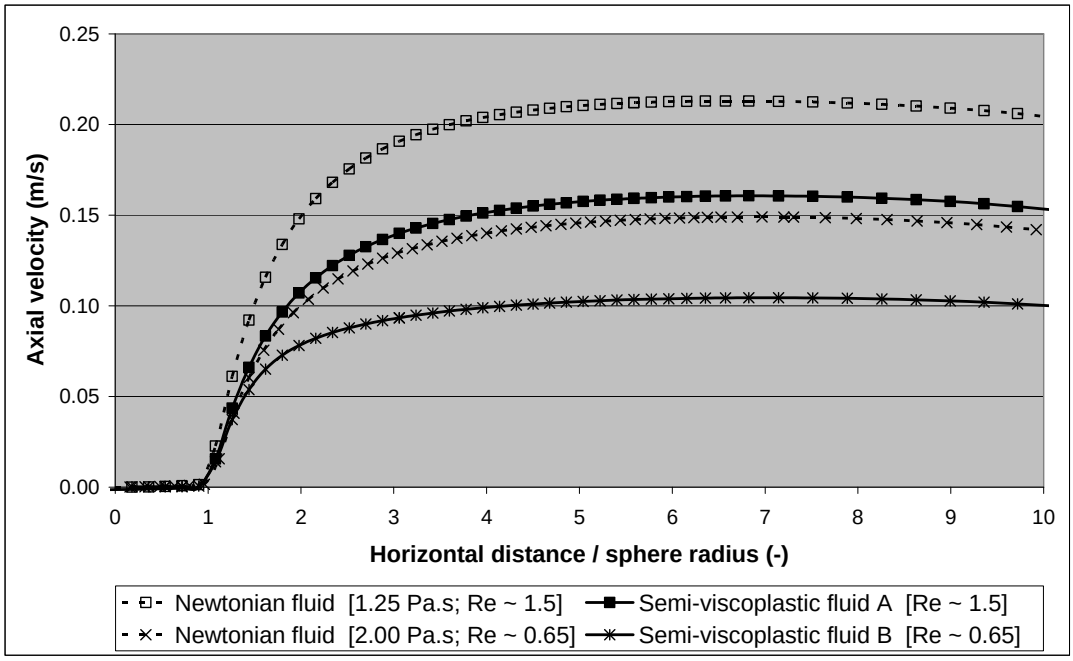

Figure 5-9: Distribution of the relative vertical velocity along the horizontal axis, at the cross-section of the sphere. The viscous parameters of the semi-viscoplastic fluids A and B are those of 0.9% and 1.0% Floxit solutions, respectively (see Tables 4-2 and 4-3). D = 10.0 mm, ρ_f/ρ_s = 8.016.

To further analyse the flow field of the semi-viscoplastic fluid, the distribution of relative axial velocity along the vertical axis has been presented in Figure 5-10. As can be seen in this Figure, all of the simulations show slower decay in the axial velocity in the region above the sphere (here indicated by negative values in vertical distance) than in the region below it. In the simulations with the semi-viscoplastic models, fluid regions below the sphere generally reach a near-constant velocity at a distance of approximately eight times the radius of the sphere, i.e. 8.0 R. This indicates that the fluid medium beyond this distance can be considered to be relatively undisturbed by the settling motion of the sphere. In the simulations with the Newtonian fluid model, on the other hand, the decay in the axial velocity in the region below the sphere continues to occur beyond a vertical distance of 9.0 R. This indicates that the disruption in the fluid medium caused by the settling motion of the sphere in Newtonian fluids extends over a longer vertical distance than in the case of semi-viscoplastic fluid of the same Reynolds value.

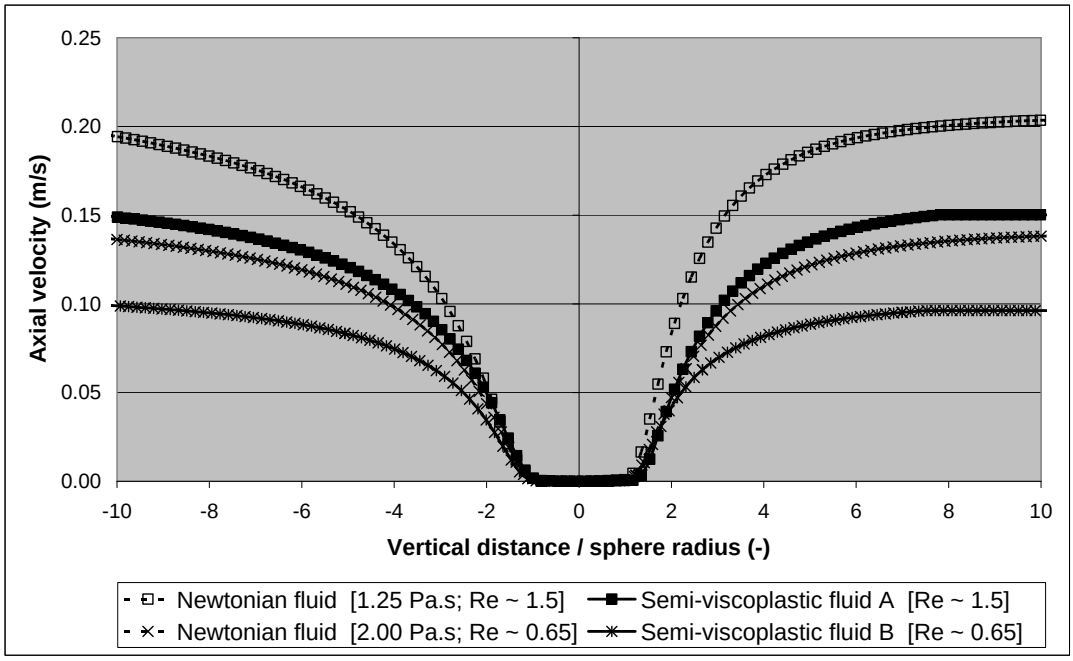

Figure 5-10: Distribution of the relative vertical velocity along the vertical axis. The origin of the x-axis indicates the centre of the sphere. The region above the sphere is represented by the negative values of vertical co-ordinates, and vice versa. The viscous parameters of the semi viscoplastic fluids A and B are those of 0.9% and 1.0% Floxit solutions, respectively (see Tables 4-2 and 4-3). D = 10.0 mm, ρ_f/ρ_s = 8.016.

Based on the observations stated above, it can be seen that the incorporation of the semi-viscoplastic fluid model generally causes a decrease in the distribution of velocity in the flow field surrounding a settling sphere. This decrease in velocity could be caused by the transient yield stress characteristics of the fluid model. In turn, this aspect of the fluid model is expected to induce the presence of distinct yielding and unyielding regions in the flow field surrounding the settling sphere, as observed by Atapattu (1989) and suggested by Beris et al. (1985) and Yoshioka et al. (1971) in their numerical studies of traditional viscoplastic fluid flows. The distinction of the yielding and unyielding regions is due to the yield stress of the viscoplastic model. Due to the presence of the yield stress, fluid regions experiencing pressure forces that are less than the yield stress essentially behave as elastic solids and do not experience any form of permanent deformation, and vice versa. In the studies discussed above, this unyielding phenomenon is generally

encountered in regions several radii away from the settling sphere (~ 3.0 – 4.0 R from the visualisation study conducted by Atapattu et al. (1989)), as well as in fluid zones immediately attached to the surface of the sphere, e.g. at the polar ends of the sphere (polar caps).

In the studies mentioned above, the transition between the yielding and unyielding regions surrounding a settling sphere has generally been depicted as relatively abrupt. This is due to the use of the idealised viscoplastic equations, such as Bingham and Herschel-Bulkley fluid models, which enable the location of the unsheared regions to be defined clearly. In comparison, as the semi-viscoplastic fluid model displays yield stress values that are temporary and variable in nature, the distinction between the yielding and unyielding regions is generally harder to determine.

The categorisation of the yielding and unyielding zones in the semi-viscoplastic fluid model can be performed by considering the magnitude of force or pressure that is required to overcome the 'structure' of the fluid. Based on the rate equation of the scalar parameter representing the structure of the fluid (λ), the yield process of the fluid can be defined as:

$$\frac{d\lambda}{dt} = \frac{1-\lambda}{\theta} - \kappa \lambda \dot{\gamma} < 0 \qquad \textbf{(5-23)}$$

The rate-of-change in structure at each time-step can thus be approximated as:

$$\frac{\Delta\lambda}{\lambda} = \left(\frac{1-\lambda}{\theta} - \kappa \lambda \dot{\gamma} \right) \frac{\Delta t}{\lambda} \qquad \textbf{(5-24)}$$

In fluid regions where yielding occurs, negative values in $\Delta\lambda/\lambda$ would be encountered, and vice versa.

Figure 5-11 shows the development of the yielding region around a sphere settling in a viscoplastic fluid. The extent of the yielding zone in this case has been defined as regions where the existing rate-of-shear induces a relative change of at least

0.05% in comparison to the fluid-structure parameter during the imposed time step. As can be seen in this Figure, the yielding region tends to expand as the flow field surrounding the settling sphere develops. This continues to occur, until a steady settling velocity is obtained. In the case presented in Figure 5-11, it can be seen that the yield zone of the fully-developed flow field, obtained after 400 iteration time steps, extends at approximately 4-5 times the sphere diameter in the vertical direction.

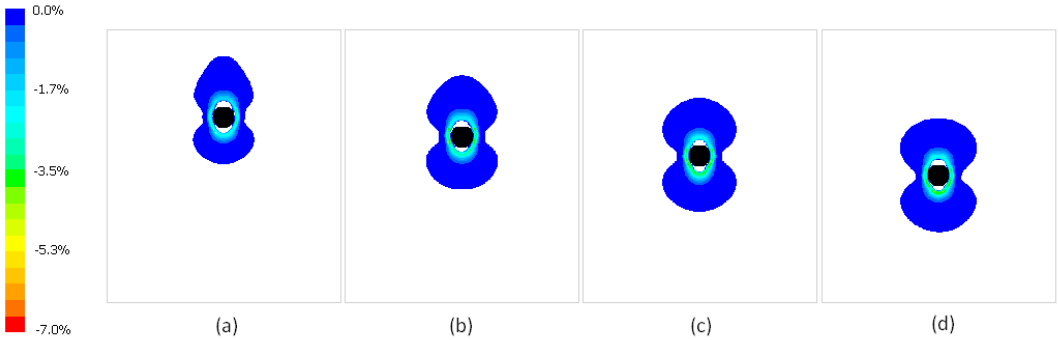

Figure 5-11: The development of yielded and unyielded zones in the flow field surrounding a settling sphere (D = 10.0 mm, ρ_s = 8000 kg/m³, Re = 1.5). The fluid medium is modelled using the semi-viscoplastic equation (ρ_f = 998.0 kg/m³, μ_0 = 54.9 Pa.s, μ_∞ = 0.0001 Pa.s, κ = 0.234 1/s, θ = 48.48 s, m = 0.7794): (a) after 200 iterations; (b) 300 iterations; (c) 400 iterations; (d) 500 iterations.

The shape of the yielding region surrounding the settling sphere is highly comparable to that suggested by Yoshioka et al. (1971) (cf. the flow fields of viscoplastic fluids presented in Figure 2-3). Furthermore, Figure 5-11 also shows the presence of high-shear regions with prominent yielding tendencies at the sides of the sphere. At the polar ends of the sphere, on the other hand, the flow fields seem to feature unyielding regions that are attached directly above and below the sphere. This is similar to the hypotheses of Yoshioka et al. (1971) and Beris et al.(1985), both of whom suggested the presence of 'polar caps', which are regions of unyielding fluids that are attached to the surface of the polar ends of the sphere.

In the current study, the polar-cap regions discussed above actually correspond to regions of sheared fluid that have very low values of fluid-structure parameters ($\lambda \sim 0.01$, see Figure 5-12(b)). The highly-sheared character of the fluid structure in this region causes the recovery term in the rate equation, i.e. $\left[(1-\lambda)/\theta\right]$, to become very large. As a result, very high values of shear-rate are required to further disrupt or yield the structure of the fluid in these regions. As the existing rate-of-shear is insufficient to overcome the rate of recovery of the fluid structure, the fluid structure in this region tends to recover (or increase in λ) rather than deteriorate. These fluid zones should therefore be termed more appropriately as 'apparently unyielding regions', due to the insufficiency of the pressure forces in these regions to further yield and destroy the structure, and hence decrease the viscous parameters of the fluid.

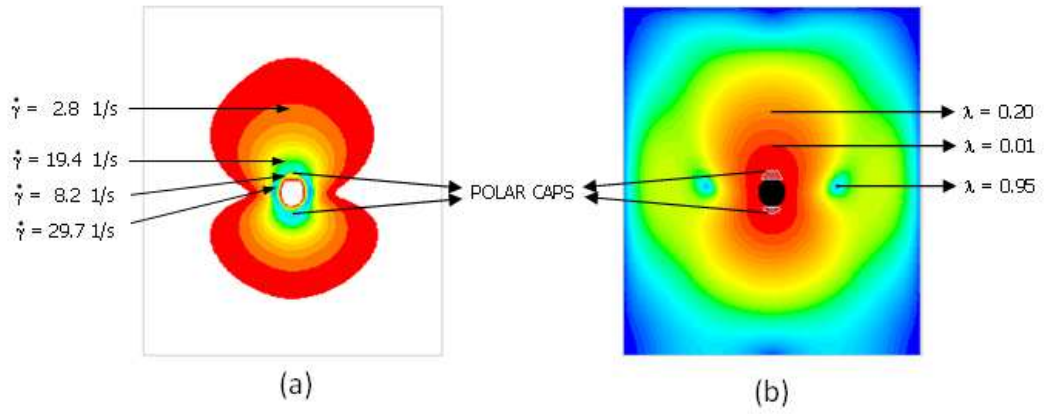

Figure 5-12: Profile of (a) shear rate and (b) fluid structure parameter (λ) surrounding a settling sphere (D = 10.0 mm, ρ_s = 8000 kg/m^3, Re = 1.5). The fluid medium is modelled using the semi-viscoplastic equation (ρ_f = 998.0 kg/m^3, μ_0 = 54.9 Pa.s, μ_∞ = 0.0001 Pa.s, κ = 0.234 1/s, θ = 48.48 s, m = 0.7794).

Contrary to the high-shear conditions evident in the region of the polar caps, the flow profiles presented in Figure 5-12 suggest that the region of unyielding fluid at the sides of the sphere is coincident with a region of fluid that is actually unsheared ($\lambda \sim 0.95$, see Figure 5-12(b)). This region occurs at a distance of ~ 4.0 R. The presence and location of this unyielding zone was found to be highly comparable to

the results of the visual study presented by Atapattu et al. (1989), who observed that the yielded region surrounding a sphere settling in a viscoplastic fluid extends to approximately 3.5 to 4.0 R in the horizontal direction from the centre of the sphere. Further away from the sphere, the structure parameter begins to decline slightly, as the fluid segment that is displaced due to the movement of the sphere recirculates back up to the top of the sphere.

Based on the observations stated above, it can be concluded that under conditions of a fully-developed velocity field, the flow patterns due to the transient yield-stress characteristics in the semi-viscoplastic fluid model are similar to those caused by the presence of permanent yield stress in traditional viscoplastic fluid models. The presence of unyielding regions around the sphere causes a decrease in the magnitude of velocity distribution in the flow field, as observed earlier in the comparisons of axial velocity distributions in semi-viscoplastic and Newtonian fluids (of similar Reynolds numbers), presented in Figure 5-9 and Figure 5-10.

5.7.2 Terminal settling velocity of spherical particles in semi-viscoplastic fluids

In Section 5.6.3, it has been demonstrated that within the parameters of the numerical study, the proposed numerical scheme is able to effectively predict the fall velocity of a sphere settling through Newtonian fluids to within 10% of the experimental values available in the literature. In this section, this analysis will be repeated using the semi-viscoplastic fluid model. The results of this analysis are expected to provide an understanding on the validity of the proposed fluid model in comparison to the rheological behaviour of the actual Floxit solutions used in the sphere-settling experiment.

To test the validity of the proposed fluid model, comparisons between the values of the predicted settling velocity from the numerical study to those obtained experimentally were conducted, using various combinations of viscous parameters (as listed in Table 4-2 and Table 4-3), sphere densities (6000, 7000, and 8000

kg/m^3), and diameters (5.94, 7.92, and 9.9 mm). This is presented in Figure 5-13, where, in the manner of the correlation suggested by Wilson et al. (2004; 2003), the variability of dimensionless velocity ration, Vt/V*, with respect to the shear Reynolds number (Re*, see equation 2-45) for both the VOF and experimental results were shown.

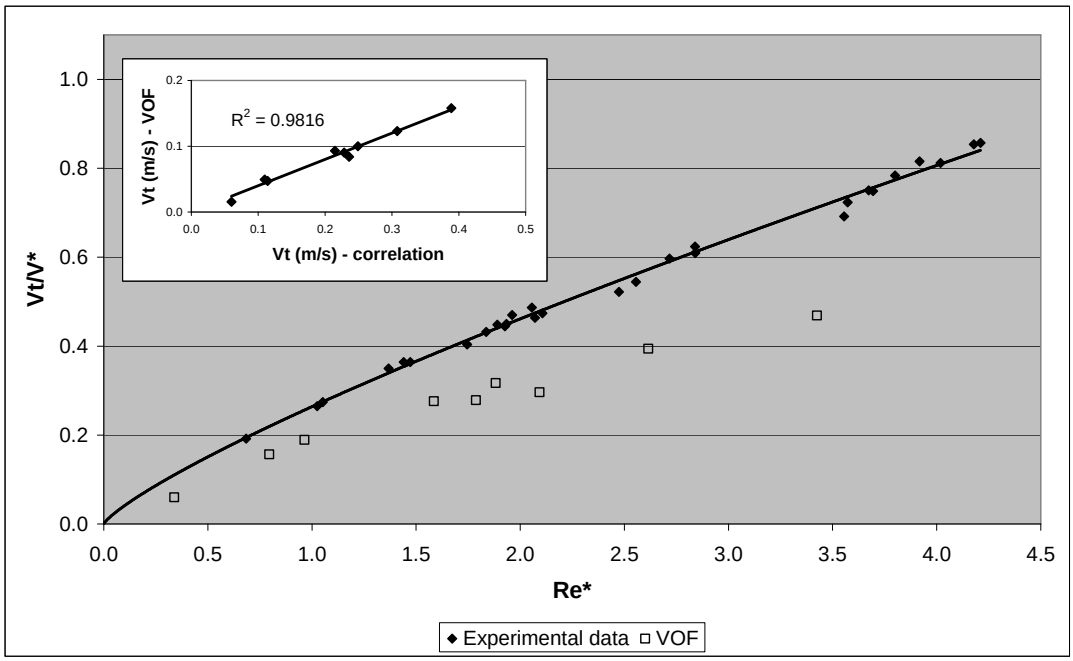

Figure 5-13: Graph of Vt/V* vs. Re* calculated based on the values of V_t obtained experimentally and numerically (VOF). The inset shows the direct comparison of V_t between the values obtained numerically and those calculated from the correlation of Wilson et al. (2003).

In Figure 5-13, it can be seen that the VOF-based numerical scheme tends to under-predict the settling velocity of the spheres. As expected, the same trend of under-prediction was encountered upon the direct comparison between the predicted values of V_t with those calculated from the correlation of Wilson et al. (2004; 2003) (see inset of Figure 5-13). However, the direct comparison also shows that there is a very strong regression between the two data sets ($R^2 = 0.9816$).

The excellent correspondence between the experimental and numerical results, as indicated by the high value of regression, suggests that the proposed semi-viscoplastic fluid model is able to adequately represent the rheological behaviour of the Floxit solutions. Furthermore, as the three Floxit solutions display slightly different levels of elasticity (as indicated by the differences in the relaxation times of the fluid solutions, see Section 4.6), this correspondence between the experimental and numerical results for all three fluid solutions indicates that the prediction of the settling behaviour of a single sphere in these solutions can be done by considering the shear viscosities alone. This suggests that within the parameters selected for this study, the elasticity of the Floxit solutions does not significantly contribute towards the settling behaviour of a sphere in the fluid solutions.

The poor quantitative agreement between the experimental and numerical results, despite the apparently high regression between the two data sets, indicates that such deviation in accuracy could be caused by the errors in the rheometric measurements used to determine the viscous parameters of the fluid solutions. Although great care has been employed during the rheometric measurement to uphold its accuracy and repeatability, it should be noted that such measurement involves a number of assumptions in flow profiles that may cause deviation in accuracy if the conditions are not met. In the cone-and-plate equipment, which was the rheometric geometry used in this study, an assumption of primary laminar flow across the whole geometry has been considered as the basis for the numerical formulations of shear stress and deformation rates. Additionally, the numerical formulations for these measurements were also developed under the assumptions of negligible edge effects and isothermal flow. Any deviations from these assumptions, therefore, could significantly reduce the accuracy of the rheological measurement.

The assumptions stated above are often not satisfied in actual rheometry, as have been noted by various researchers in the field (Cheng, 1966; Mewis & Moldenaers, 1999). Furthermore, the effects of yield stress and viscoelasticity on such measurement geometry are still not well established. In 1995, Petera and Nassehi

conducted a study on the flow patterns of shear-thinning fluids in cone-and-plate rheometers using finite element techniques. Through this examination, the researchers found that non-Newtonian fluids with relatively low viscosities have the tendency to develop secondary flows in cone-and-plate geometries even at shear rate values of 1 s^{-1}. This irregularity in flow was then found to significantly affect the uniformity of the stress distribution within the geometry. This is in agreement with the visual findings of Kulicke and Porter (1979) on the flow behaviour of polyacrylamide solutions in cone-and-plate geometries. In their study, Kulicke and Porter reported the formation of vortices at shear rates as low as 1-5 s^{-1}, which is considerably lower than the Newtonian transition from laminar to turbulent flows that normally occurs at shear rate values of about 1200 s^{-1}. Kulicke and Porter (1979) also reported that this behaviour is not noticeable on the rheogram of the tested material. The non-uniformity of the flow of viscoplastic/viscoelastic materials in the rheometer has also been reinforced in the report of Britton and Callaghan (1997), who used NMR techniques in combination with cone-and-plate rheometer to establish the velocity distribution across the cone-and-plate geometry. Based on these findings, Britton and Callaghan (1997) suggested that the use of NMR microscopy for the accurate velocity profiling is essential for a precise interpretation of rheometric data. Petera and Nassehi (1995), on the other hand, suggested corrective techniques that combine the utilisation of experimental data with finite element modelling in order to attain accurate rheometric data.

Based on the discussion above, it is clear that errors in the estimation of rheology parameters are the leading cause of the poor quantitative agreement between the numerical predictions of the settling velocity of spheres from the experimental data as seen in Figure 5-13. However, based on the high regression between the numerical predictions of V_t with those obtained experimentally, it can be concluded that the proposed VOF based numerical scheme can satisfactorily handle the highly non-linear nature of the governing equations for the semi-viscoplastic model.

5.7.3 The effects of viscous recovery

Having analysed the characteristics of the flow field surrounding a sphere settling in the semi-viscoplastic fluid under fully-developed conditions (see Section 5.7.1), another aspect of the proposed fluid model, i.e. the gradual recovery of the structure parameter after it is sheared by the movement of the sphere, can now be examined. In the experimentations conducted using the Floxit solutions, this aspect of the fluid characteristic is evident in the settling behaviour of two spheres settling one after the other in the same flow path. After being sheared by the movement of a preceding sphere, the fluid medium takes some time to regain its structure. As a result, when another sphere shears through the same fluid region, it is subjected to a fluid region that has lower values of viscous parameters, and hence settles at a higher velocity than the preceding sphere.

In the numerical study, this aspect of the fluid model is examined further by observing the flow field surrounding two spheres that are placed one above the other, but with a set distance apart, along the centre-line of the column (see Figure 5-14). The recovery of the fluid parameter can be examined as the upper sphere (sphere 2 in Figure 5-14) passes a region that has previously been passed by the lower sphere (sphere 1).

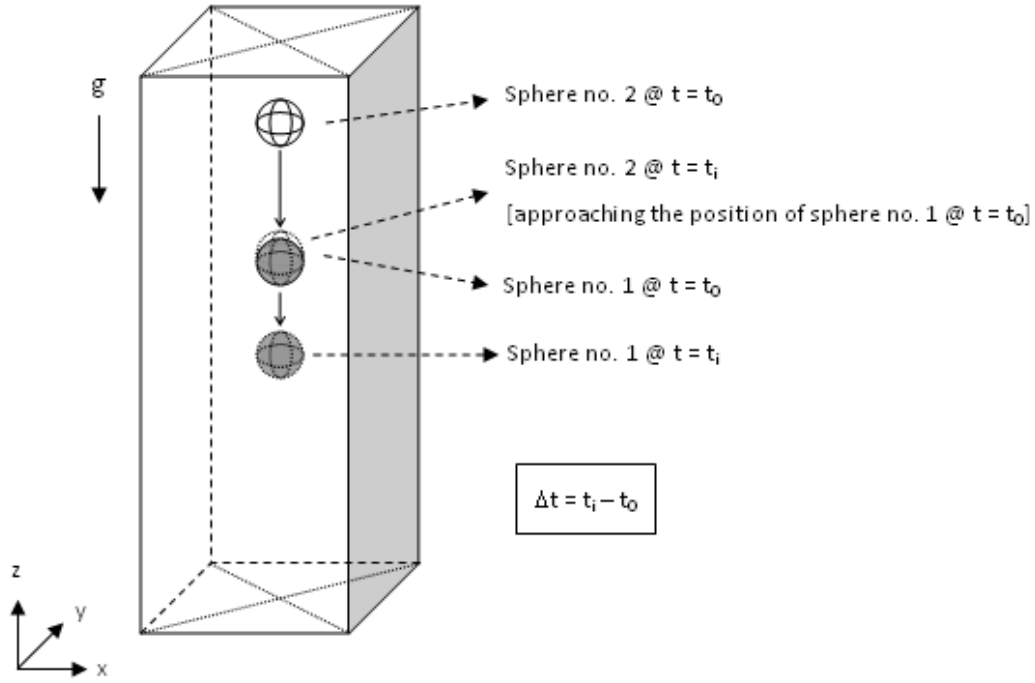

Figure 5-14: A schematic description of the problem involving two spheres settling along the centre-line of the column.

While the same column and grid configurations as that outlined in section 5.6.1 are used in this numerical study, the height of the column has to be considerably larger than that used for the study of the settling behaviour of a single sphere. This aspect of the problem domain has to be assigned such that the two spheres have sufficient path way to settle through and complete the development of the flow field that surrounds them. For two spheres (D = 9.9 mm) having an initial gap of 49.5 mm, for example, the required minimum height of the column was found to be 180 mm. As the VOF-based numerical formulation requires the use of a numerical grid consisting of a uniform fine mesh of 0.9 mm width, this height requirement causes the numerical analysis to be very computationally demanding. Using the case stated above as an example, a uniform grid of 112 x 112 x 200 node points is required. As a result of this high computational requirement, considerably smaller values of initial distance than those used experimentally (~ 5.0 – 7.0 D in comparison to 50 – 110 D in the settling-sphere experiments) had to be assigned.

For the solution of this numerical problem, the same discretisation and solving procedures as that outlined in section 5.5 are applied. Furthermore, comparable to the analysis of the experimental data, which will be presented later in chapter 6, the time difference between the two spheres, Δt, is defined as the time lapse since the preceding sphere passes through and shears the fluid medium that is currently occupied by the trailing sphere (see Figure 5-14).

As a result of the values of the initial distance between the two spheres being much smaller than those used experimentally, direct comparison between the results of this analysis with the experimental results would require the movement of the spheres to be tracked and measured over very small increments of space and time. This could be accomplished through two different approaches, with the first being the use of motion tracking photogrammetry system with much higher frame frequency than that used in the current experiment. This approach however requires major modifications to the current experimental setup and is highly expensive in practice. Modifications to the current experimental parameters can also be incorporated such that much slower settling movements are obtained. This can be accomplished either by using fluids with much higher values of apparent viscosity, or by using particles with much lower values of density and/or diameter. However, rheological analyses of viscoplastic fluids over very low values of shear rate have been known to be highly inaccurate, due to the effects of wall slip and elastic deformation (see Sections 4.2 and 4.3). These uncertainties may therefore significantly decrease the validity of the analysis of these experiments. Due to these difficulties, the two approaches mentioned above could not be incorporated in the current thesis. The incorporation of these approaches has been considered for the future development of this research project (see Section 8.2).

Additionally, the difficulties associated with the direct comparison between the numerical results with the experimental observations were also caused by the fact that the width of the column used in the numerical study is actually smaller than that used experimentally (0.2 m x 0.2 m in comparison to 0.1 m x 0.1 m for the numerical domain). Due to these dimensional differences, it is expected that the

settling velocity of the trailing sphere is heavily affected by the upwards velocity resulting from the flow recirculation that exists at the sides of the settling spheres, near the walls of the column. The upwards motion of this flow region is expected to impede the settling motion of the trailing sphere.

Nevertheless, although the results of this study are not expected to be quantitatively comparable to the experimental investigation, this numerical study is expected to provide a qualitative description of the flow field surrounding a sphere settling through a partially-recovered fluid and assist in the determination of important parameters that affect the settling velocity of the spheres in semi-viscoplastic fluids.

The typical distribution of axial velocity along the horizontal axis for various values of Δt has been presented in Figure 5-15. For comparison, the velocity field in the fluid medium surrounding a single sphere settling in a similarly-configured fluid model has been included. As can be seen in this Figure, the variation in the relative axial velocity in the fluid medium surrounding the leading sphere, denoted as sphere 1 in Figure 5-15, at Δt of 0.469 s generally resembles that of a single sphere settling through the same fluid medium. This similarity indicates that in an experiment involving two spheres settling one above the other in this type of fluid, the leading sphere (sphere 1) tends to possess a settling velocity that is comparable to the terminal settling velocity of a single sphere. The flow field surrounding the corresponding trailing sphere (or sphere 2), on the other hand, is shown to possess higher values in relative axial velocity than the fluid medium surrounding sphere 1. This pattern in axial velocity indicates that the trailing sphere possesses a settling velocity that is approximately 13.3% higher than the preceding sphere.

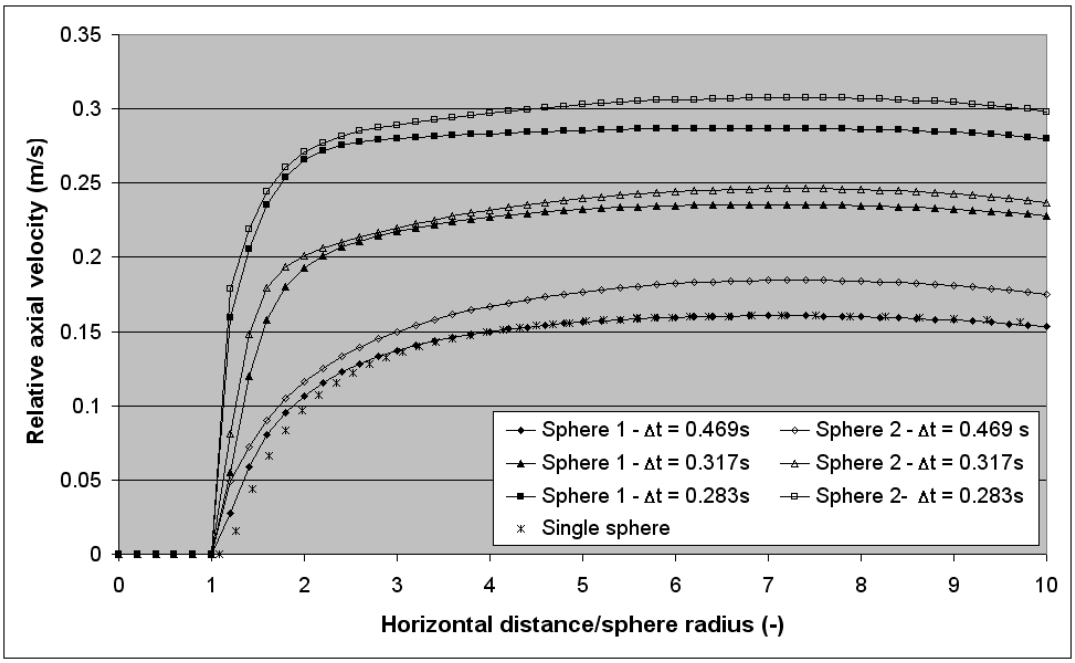

Figure 5-15: The variation of axial velocity, relative to the settling velocity of the spheres, along the horizontal axis of the column. The spheres (D = 10.0 mm, ρ_s = 8000 kg/m^3) were settling through a semi-viscoplastic fluid (ρ_f = 998.0 kg/m^3, μ_0 = 54.9 Pa.s, μ_∞ = 0.0001 Pa.s, κ = 0.234 1/s, θ = 48.48 s, m = 0.7794) with an initial inter-sphere distance of 50.0 mm.

The observations outlined above suggest that the results from the simulation at Δt value of 0.469 s are qualitatively similar to the settling pattern obtained from the experiments conducted in the Floxit solutions. As shown in the velocity trace presented in Figure 3-4, a sphere that falls through a properly-rested fluid medium tends to maintain a steady terminal settling velocity as it settles through the column, while another sphere that follows its path tends to possess a significantly higher settling velocity, leading to an eventual collision between the two particles.

Interestingly, at smaller values of Δt, Figure 5-15 shows that the values of the relative axial velocity increases dramatically, for both the preceding and trailing spheres. While the values of relative vertical velocity in the flow field surrounding sphere 2 is still generally higher than that of sphere 1 for both Δt values of 0.317 and 0.283 s, the flow fields surrounding sphere 1 at this stage of the experiment are considerably higher than those resulting from Δt of 0.469 s. This change in velocity

pattern indicates that at smaller separation distances, the leading sphere ceases to maintain its steady settling velocity and begins to accelerate.

In comparison with the experimental data, this increase in the settling velocity of sphere 1 at smaller values of Δt has been found to be comparable to the acceleration of the leading sphere that is commonly observed shortly before its collision with the sphere that follows behind it (see Figure 3-4). This increase in settling velocity could be caused by the acceleration of the trailing sphere, which induces a 'pushing' motion on the particle beneath it as the gap between the two spheres decreases, causing sphere 1 to accelerate considerably from its steady settling velocity.

The cause of the discrepancies in the magnitude of the flow field surrounding two spheres settling one after the other can be examined further by observing the fluctuations in the fluid-structure parameter (λ) as the two spheres settle through the fluid medium. In Figure 5-16, the variation of λ along the horizontal axis in the fluid medium surrounding the two spheres has been illustrated. As expected, the variation in the λ field surrounding sphere 1 at Δt of 0.469 s closely resembles that of a single sphere settling through a fluid medium of the same viscous parameters. In the flow field surrounding the corresponding trailing sphere, on the other hand, significantly lower values of λ in regions close to the surface of the sphere were evident. This observation enforces the hypothesis stated previously, that the acceleration evident in the fall behaviour of the trailing sphere is caused by the incomplete recovery of the fluid structure, after it is sheared by the motion of the sphere preceding it.

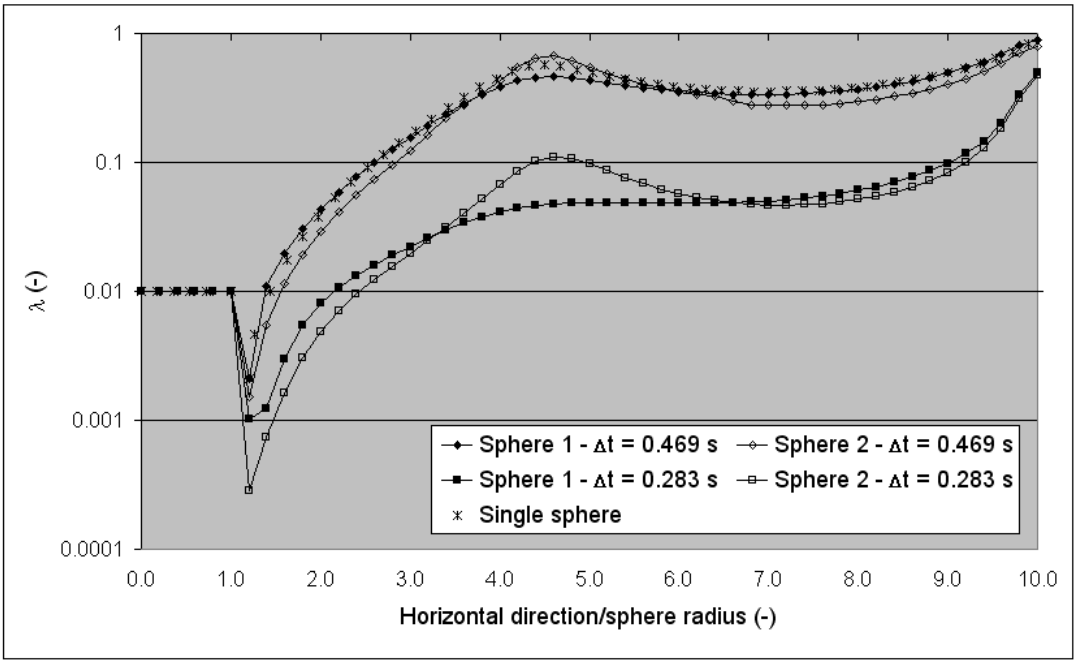

Figure 5-16: The variation of λ along the horizontal axis of the column, for the numerical results presented in Figure 5-15.

At even smaller values of Δt, the fluid medium has less time to recover its structure. This is indicated by the values of theλ field surrounding sphere 2 atΔt of 0.283 s, which were significantly lower than those obtained after the fluid has been rested for 0.469 s.

The 'pushing' effect that is assumed to cause the acceleration of the leading sphere as the gap between the two spheres decreases is also evident in the figures presented in Figure 5-16. The fluid-structure parameter along the horizontal axis of sphere 1 can be seen to be considerably lower in the instance of Δt = 0.283 s in comparison to when the gap between the two spheres is larger (Δt = 0.469 s). Based on this observation, it is considered that this change in settling pattern is caused by the extra shear forces induced by the acceleration of the particle settling above the flow field surrounding sphere 1. This additional force causes further structural damage to the velocity field surrounding the lower sphere, initiating a decrease in the magnitude of the viscous parameters in the fluid medium. This change in

viscous parameters results in the acceleration of the leading sphere when the two spheres are very close to colliding.

Another aspect of the velocity field that is apparent in the graphs presented in Figure 5-16 is that the flow fields surrounding the spheres show local maxima in λ values at a distance of ~ 4.5 R from the centre of the spheres. This suggests the presence of unsheared regions at the sides of the settling spheres. This observation is consistent with that stated in Section 5.7.1, where the presence of unyielded (and apparently unsheared) regions at the sides of a settling sphere has been noted (see Figure 5-11 and Figure 5-12). The existence of this region is characteristic of the flow field surrounding a particle settling in yield-stress fluids. As a result of this phenomenon, the decrease in the λ values in this area is significantly less than in any other area surrounding the settling sphere.

Figure 5-16 also shows that in the case of the trailing sphere, the increase in λ values with increasing horizontal distance is even steeper. This development is such that at a distance of 3.2 to 6.0 R, higher values of λ were obtained in the flow field surrounding sphere 2 than those of the corresponding leading sphere. This development in flow field enforces the hypothesis stated above that the fluid in this region is relatively unaffected by the shearing motion of the sphere. The fluid medium in this area thus continues to recover in structure, despite the existence of shear effects due to the settling movement of the sphere a few radii away. This causes the unyielding region surrounding the trailing sphere to possess even higher values of maxima in λ than in the case of the preceding sphere.

5.8 Conclusions

A numerical study of the settling behaviour of spheres in viscoplastic fluids has been performed and the resulting patterns in flow fields with the factors affecting the settling behaviour of the spheres have been determined and analysed.

The numerical scheme formulated for this study was based on the VOF (Volume of Fluid) model with finite volume (FV) method of discretisation. In doing so, the solid particle was likened to a fluid material with very high viscosity, ± 100 – 200 times the viscosity of the fluid medium. The discretisation process of the resulting mathematical problem was performed in such a way that the effects of numerical smearing and diffusion can be minimised. Furthermore, the advection of the field of volumetric fraction of the secondary (solid) phase was conducted using the PLIC method, such that the deformation of this phase throughout the calculation process can be kept to a minimum. Uniform fine grid was assigned throughout the problem domain to enhance the accuracy of the VOF-based numerical scheme.

The validity of the calculation and discretisation procedure was examined through a study of the settling behaviour of a sphere in Newtonian fluids. The viscous parameters of the Newtonian fluids were selected such that similar values in Reynolds number to the simulations to be conducted with the semi-viscoplastic fluid model were obtained. Through this assessment, it was found that within the parameters of the assessment, the proposed numerical and discretisation procedure was able to reasonably sustain the spherical shape of the particle throughout the iterative procedure. Furthermore, the resulting predictions in settling velocity were found to be within 10% of the experimental values available in the literature. Based on these observations, it was concluded that the proposed numerical scheme is able to provide adequate representation of the settling motion of spheres in fluids of $0.1 < Re < 7.0$.

A time-dependent estimation of the proposed rheological fluid model presented in section 4.3 was then developed and implemented into the numerical scheme. This was conducted through the implementation of a series of UDF (User Defined Function) codes into the numerical solver (FLUENT 6.3).

The results of this study suggest that the flow field surrounding a sphere settling in this fluid medium are comparable to the flow field reported in the literature for viscoplastic and yield-stress fluids. This suggests that the settling behaviour of

spheres in semi-viscoplastic fluids is highly dependent on the yield stress characteristics of the fluid model.

The hypothesis stated above was further supported through the examination of the settling behaviour of two spheres falling one behind the other. Through this study, it was found that a sphere that falls through a fluid medium that has earlier been sheared by the movement of another particle tends to possess a settling velocity that is greater than the preceding sphere. The motion of the preceding sphere causes the fluid medium in that region to temporarily lose its structure (λ). As the fluid medium is again sheared through the motion of the trailing sphere, the recovery in the fluid structure is still incomplete. As a result, the trailing sphere falls through a fluid medium with considerably weaker λ field, transpiring into considerably lower values of viscous parameters.

In comparing the numerical predictions of this study with those found experimentally, it was found that although the quantitative agreement with the experimental data was generally poor, the correspondence of the numerical results with the experimental data was found to be excellent ($R^2 = 0.9816$). This deviation from the experimental data could be caused by the errors involved with the rheological measurements of viscoelastic fluids and the uncertainties associated with the irregularities of flow patterns existing within the geometry of the rheometer. Nevertheless, the excellent correspondence between the numerical and experimental data suggests that the proposed numerical scheme is able to handle the non-linearity of the mathematical problem satisfactorily. Furthermore, it also suggests that within the parameters of this study, the settling behaviour of the spheres in the Floxit solutions can be modelled through considerations of the changes in structural parameters in the fluid medium and the effects of such changes on the viscous parameters of the fluid.

Chapter 6 The settling behaviour of two vertically-aligned spheres

6.1 Introduction

In this chapter, the results of experiments involving two vertically-aligned spheres, where one sphere is released into a fluid medium following the flow path of another (Category I, see Section 3.1), will be discussed. The details of the experimental procedures and equipment, along with the different parameters being tested (see discussion on cases A to F, classified based on the differences in the diameter and density of the two spheres being tested in Section 3.3), have been discussed in Chapter 3.

The settling behaviour of particles in viscoplastic fluids has been researched extensively in the past, but still presents many uncertainties. One of these uncertainties include the transient aspects, where the motion of a particle falling through a fluid that has previously been sheared by the motion of another particle was found to be significantly different to the settling behaviour of the preceding particle (Gumulya et al., 2007; Horsley et al., 2004). In this thesis, this phenomenon has been demonstrated in Section 3.3.2, where the typical settling behaviour of two identical spheres was discussed (see Figure 3-4). It was demonstrated that a sphere released into a viscoplastic medium that has been 'rested' for a set period of time (~ 15 minutes) attains a constant velocity almost immediately after it enters the solution. This constant velocity is considered to be equivalent to the terminal settling velocity, which is a unique value that depends on the viscous characteristics of the fluid solution and the configuration of the particle. On the other hand, a sphere that is released following this sphere shortly afterwards (~ 2 to 60 s), was found to possess a much higher settling velocity. Moreover, this sphere continues to accelerate as the gap between the two spheres decreases, until a collision between the two occurs. Due to this continual acceleration, it was concluded that the second sphere does not reach a terminal settling condition.

The fluid media used for the current experimental study are three aqueous solutions of polyacrylamide of different concentrations (0.9, 1.0, and 1.1% w/w). These solutions have previously been identified to possess significant yield stress and shear thinning characteristics (Horsley et al., 2004; Wilson & Horsley, 2004; Wilson et al., 2003). In the current study, these aspects of the fluid flow behaviour have been confirmed in the rheometric analysis presented in Chapter 4. Upon conducting a more thorough study of the rheometric characteristics of the experimental fluids, it was found that a level of time dependency, resulting from thixotropy (as well as elasticity), also exists in the flow behaviour of the fluids. To describe the viscous characteristics of these fluids, therefore, a new fluid model termed 'semi-viscoplastic', based on the scalar representation of the 'structure' of the fluid (λ), was developed. Although λ is not a direct measure of actual 'structure' existing within the fluid medium, it is expected that this variable reflects the level of hydrogen bonding that exists between the polyacrylamide and water molecules, a phenomenon that is believed to contribute significantly to the rheological characteristics of the solutions (Kulicke et al., 1982). The results of the rheology experiments using various different shear conditions suggest that there is a good correspondence between the experimental data and the proposed fluid model, which has been demonstrated to exhibit yield-stress-like behaviour that dissipates once the 'structure' of the fluid has been deformed due to the application of shear. Due to this feature, the fluid model is termed as semi-viscoplastic.

The rheological tests also revealed that the fluid solutions possess low to moderate levels of elasticity. Comparisons of the characteristic maximum relaxation times due to elastic deformation (~ 1.5 to 3 s), obtained based on the results of small-amplitude oscillation (SAOS) tests, with the average total measurement time of each experiment (t ~ 4-10 s), suggest that the contribution of the fluid elastic components (De ~ 0.2 to 0.75) should be relatively minor towards the dynamics of the sphere-settling experiments. Furthermore, these relaxation times were also found to be considerably lower than the values of the relaxation time parameter of the shear viscosity (θ ~ 44-53 s). Based on these figures, it is expected that the changes in the viscous parameters observed in the experiment of vertically-aligned

spheres is mainly caused by the thixotropy characteristics of the fluid and that the effects of the elastic deformations are overwhelmed by the effects of shear-thinning. This hypothesis was supported by the excellent qualitative agreement between results of the CFD analysis – conducted using the semi-viscoplastic fluid model under the assumption of zero normal stresses (representing the effects of elasticity) – with the experimental data obtained from the Floxit-based solutions (see Chapter 5).

In this study, the accuracy of the above statement and the implications of such assumption will be examined further through comparisons of the experimental data with the results of similarly-configured experiments that have been published in the literature (Section 6.2). A set of correlations that can be used to predict the settling behaviour of spheres in viscoplastic fluids will then be developed based on the results of this analysis.

6.2 Preliminary data analysis

The typical velocity profile obtained from an experiment involving two identical spheres settling in the same flow path in the test fluid solutions has been shown in Figure 3-4. As can be seen in this graph, a sphere that follows the flow path of another sphere exhibits much higher settling velocity than the preceding one. Furthermore, as the gap between the two spheres decreases, the trailing sphere continues on accelerating. This condition remains until a 'critical region' is obtained, where the interaction between the two spheres becomes highly significant that the movement of the trailing (or second) sphere seems to 'push' the leading (or first) sphere, resulting in the increase and decrease in the velocity of the first and second sphere, respectively. This condition, however, only occurs briefly and over a very short distance. A collision between the two spheres occurs, after which the two spheres attach and travel at the same velocity. This velocity profile is identical to that described by Gumulya et al. (2007) as well as Horsley et al. (2004).

Despite the simplicity of the experiment, several interesting fall patterns associated with the settling of consecutive spheres in viscoelastic and viscoplastic fluids have been reported in the literature, some of which seem to correspond well with the results of the experiments outlined above while some seem to contradict these observations. In a number of studies, for example, the formation of a stable distance between the two spheres has been reported (Bot et al., 1998), whereas others have observed a 'repulsion' effect, where the trailing sphere exhibit a lower settling velocity than the preceding one (Gheissary & van den Brule, 1996; Riddle, Narvaez, & Bird, 1977). These fall patterns and their associated causes will be discussed below.

In 1977, Riddle and co-workers conducted a study on the settling of vertically-aligned spheres in shear thinning viscoelastic fluids. Riddle et al. (1977) observed that an 'aggregation' tendency exists between two spheres that settle one after the other in the same path, given that their initial distance is less than a critical value. This implies that the second sphere, which travels through a fluid region that has been sheared some time earlier by the movement of another sphere, travels at a higher velocity than the preceding sphere, causing a considerable decrease in the gap between the spheres. This is similar to the results obtained from the solutions of polyacrylamide used for this study. Above the critical value of initial distance, however, the aggregation tendencies disappear and Riddle et al. (1977) commented that the two spheres tend to 'diverge' or increase in gap size. No such diverging effects were encountered with the current experimental parameters.

Gheissary and van den Brule (1996), who conducted their study in both shear thinning and constant viscosity elastic (Boger) fluids, did not observe any diverging effects in their shear thinning fluids and noted that a decrease in the distance between the two vertically-aligned spheres is always in effect. In their experiments using Boger fluids, however, Ghessary and van den Brule (1996) observed that the two spheres that are close to each other tend to display diverging effects, similar to that reported by Riddle et al. (1977). In this instance, the trailing sphere, which is

caught in the wake of the leading sphere, was found to move 'further away' from the leading sphere.

The observation of Gheissary and Van den Brule (1996) in Boger fluids is supported by the findings of Bot et al. (1998), who observed the formation of a 'stable distance' during the settling experiment, which prevents the two spheres from colliding. That is, although a higher settling velocity is initially obtained with the trailing sphere, resulting in a reduction from the initial gap size, a critical gap size is soon reached, at which point the fall velocity of the leading sphere starts to increase. The settling velocity of the two spheres soon become identical and a 'stable distance' is observed. Similar results have also been reported by Won and Kim (2004), who conducted their experiments in Xanthan solutions that possess typical rheological behaviour of Boger solutions.

Based on the studies discussed above, it becomes clear that the fall profiles obtained from an experiment involving two vertically-aligned spheres is highly dependent on the wake development behind the leading sphere. In Boger fluids, a significant increase in the drag experienced by a settling sphere has been associated with the development of 'birefringent strands' (Harlen, 1990). This is a phenomenon commonly observed in highly elongational polymers, where the application of shear forces changes the orientation of the polymer molecules from being isotropic to anisotropic. In optical experiments, this change in orientation is visible through the formation of bright birefringent lines over the severely elongated regions. In experiments involving two vertically-aligned spheres, where one sphere is in the wake of the sphere below it, the wake development of the leading (or lower) sphere becomes obstructed. This results in a decrease in the drag experienced by the leading sphere, causing it to accelerate and maintain a 'stable distance' with the trailing sphere (Bot et al., 1998).

Chhabra (2007) has noted that the 'stable distance' effect is generally nonexistent in fluids that inhibit the 'negative wake' effect (e.g. polymeric fluids), based on the observations of Liu and Joseph (1993) and Patankar and Hu (2000; 2001). The negative wake effect is a phenomenon that is commonly encountered in

shear-thinning elastic fluids, where a flow reversal behind a settling sphere is encountered, sometimes up to distance of 30 radii downstream. In agreement with the results of Gheissary and Van den Brule (1996) for their experiments in shear-thinning elastic fluids, the researchers listed above observed that despite the presence of a flow reversal, a sphere that trails the flow path of another sphere in these types of fluids still tends to maintain a higher velocity than the leading sphere. Based on these observations, it can be concluded that the phenomenon of 'stable distance' developed between two spheres that are settling consecutively in the same flow path only occurs in fluids with constant viscosity (Boger fluids), and that in shear-thinning fluids, the two spheres always tend to aggregate and combine. Gheissary and Van den Brule (1996) have suggested that the absence of stable distances in their experiments could be caused by the dominance of the 'hole' (or memory) effects in the shear thinning fluid over the elongation properties that causes the presence of the wake above the spheres.

The effects of negative wake on the settling behaviour of the spheres has recently been examined by Gueslin et al. (2006b; 2006a), who utilised the optical PIV (Particle Image Velocimetry) technique to characterise the flow fields surrounding spheres that are settling in aqueous suspensions of clay. In this study, spheres of two different specific gravities were used (SG = 2.7 and 8.7 for the aluminium and brass spheres, respectively). Interestingly, Gueslin et al. (2006a) reported that the presence of a negative wake is only encountered in cases where the heavier sphere is used. Furthermore, in their experiment on the aggregation tendencies of two spheres settling one above the other (Gueslin et al., 2006b), it was found that the presence of this negative wake tends to influence the lateral movement of the spheres. Through this study, it was found that in cases where the spheres possess tendencies to develop negative wakes, the lateral movement of the spheres causes them to settle slightly 'off-centre' with respect to each other. For cases where the negative wake effects are absent, no such lateral movement was detected and the trailing sphere tends to settle directly above the leading one. Nevertheless, Gueslin et al. (2006b) did not observe any effects of the presence of negative wakes on the development of the sphere settling velocities, as both cases (with and without

negative wake) demonstrate considerable reduction in gap size, causing the two spheres to collide.

In Figure 6-1, a series of snapshots taken before and after the collision of two spheres falling in the test fluid solutions used for this study has been presented. This figure represents the typical settling progression obtained from this experiment. As can be seen in this Figure, the spheres settling in the polyacrylamide solutions do not appear to possess any lateral movement, suggesting the absence of negative wake above the leading sphere (cf. snapshots of PIV experiment presented by Gueslin et al. (2006b)). Based on these observations, it can be concluded that within the parameters of the current experiment, the elastic characteristics of the fluid solutions do not appear to be determining factors in the settling behaviour of the spheres and that the acceleration of the trailing sphere appears to be largely dependent on the shear-thinning (or memory) effects of the fluid. This supports the evaluation stated earlier on the comparison of the characteristic relaxation times of the fluid solutions, as well as the observations of flow fields resulting from the numerical analysis of the settling-sphere experiment in semi-viscoplastic fluids (Chapter 5). As a result of the conclusion stated above, it was deduced that the fluid solutions for this experiment can be modelled based on considerations of their shear characteristics only.

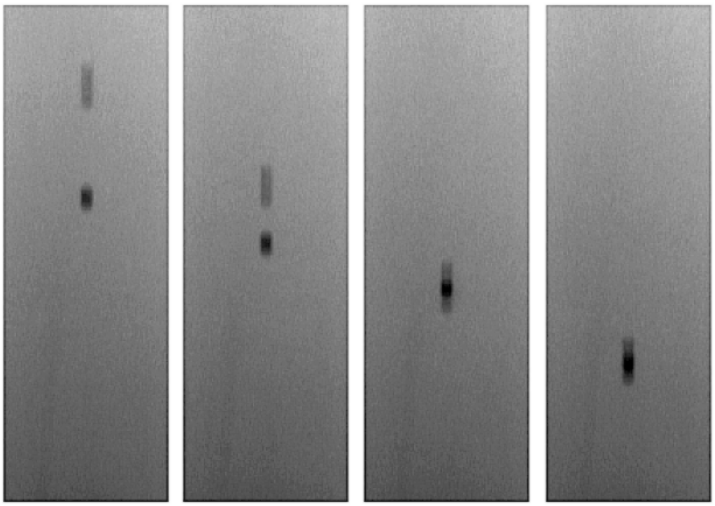

Figure 6-1: 2D pictorial capture of an experiment involving two vertically-aligned bronze spheres (7.94 mm) in 1.1% Floxit solution. The trailing sphere, which travels at a much higher velocity than the leading one, appears in a more distorted form than the lower sphere. The snapshots were captured at time interval of 0.1 s.

6.3 Correlation for the settling velocities of spheres in a viscoplastic fluid

The discrepancies observed in the settling behaviour of two spheres falling one above the other in a viscoplastic fluid have previously been attributed to the transient changes in the viscous parameters of the fluid solutions, which, as termed by Gheissary and van den Brule (1996), can also be known as the 'hole' or memory effects found in experiments involving shear-thinning fluids. Over the years, various correlations have been developed to predict the settling behaviour of these spheres. However, most of these were based on traditional viscoplastic correlations that do not incorporate the dynamic properties of the fluid. As a result, different correlations were required for the settling behaviour of the two spheres to account for the different fluid conditions (see correlations suggested by Wilson et al. (2004; 2003) and Gumulya et al. (2007)). By considering the dynamic properties of the fluid, which is achievable with the use of the semi-viscoplastic fluid model, it is hoped that more generalised correlations can be developed for the prediction of the settling behaviours of these spheres.

In this section, considerations of the changes in rheological properties due to the shearing motion of a sphere, as well as the recovery of the fluid region above the settling sphere, will be discussed. The effects of these changes on the settling behaviour of the spheres will then be examined, and a correlation will then be formulated based on these observations.

6.3.1 Rheology considerations

For a fluid solution modelled with the semi-viscoplastic rheology model depicted by equations 4-3 and 4-5, its fully-rested (or stabilised) state is represented by a structure parameter (λ) of 1.0. This condition of complete stabilisation occurs after the fluid has been left 'undisturbed' for some time. For the experiments conducted in this study, it has been assumed that this stabilised state can be achieved by 'resting' the fluid for 15 minutes in-between experiments (see Section 3.1). This assumption was based on the experimental results reported by Horsley et al. (2004), who conducted their experiments in a similar fluid solution (1.15% Floxit solution) as those used in the current study. In their experiment, it was observed that a sphere that is released 15 minutes after the release of another sphere possesses a settling velocity that is ~ 5.0 % higher than that released with a 100 minutes time-gap. This figure is noticeably lower than the ~ 15.7 % difference in settling velocity when a time gap of 5 minutes is set between the releases of the spheres. Based on this observation, it was concluded that a time gap of 15 minutes would be sufficient to attain a reliable representation of the terminal settling behaviour of a sphere falling through a fully stabilised Floxit solution.

The breakdown in the structure of the fluid medium, as it is sheared by the motion of the settling sphere, is represented by a decrease in the values of λ throughout the affected areas in the fluid medium. According to equations 4-3 and 4-4, the decrease in λ depends on the magnitude of the disturbance, quantified here by the rate-of-shear, $\dot{\gamma}$. Some time after the disturbance, the fluid recovers and regains its structure. This is accompanied by a general increase in the values of λ.

Through the considerations stated above, it can be seen that a large variation in the value of λ in the fluid medium surrounding a settling sphere can be expected. The region immediately above the sphere should theoretically feature the lowest values of λ in comparison to the whole region occupied by the fluid, due to the immediate impact of the shearing motion applied by the settling sphere on the fluid medium. Above this region, the fluid medium recovers, and thus higher values of λ can be expected. Furthermore, for a sphere is settling through a fluid medium that has previously been stabilised or 'rested', the values of λ below the sphere should be considerably higher than those above the sphere. Any deformation in this region could be caused by the dispersion of pressure exerted by the weight of the sphere on the fluid medium.

The variability in the values of λ around a settling sphere is evident in the results of the numerical analysis presented in Chapter 5 (see the illustrations presented Figure 5-13 and Figure 5-17). In these figures, the value of λ in the flow field surrounding a settling sphere can be seen to vary from 0.001 to 0.95 within a distance of ~ 4 sphere radii in the horizontal direction.

The theoretical distribution of λ in the fluid medium surrounding the sphere can be inspected further through the plot presented in Figure 6-2. In this Figure, the variability of λ along the vertical axis, in the regions above and below the spheres, has been illustrated. The origin of the x-axis indicates the centre of the settling sphere.

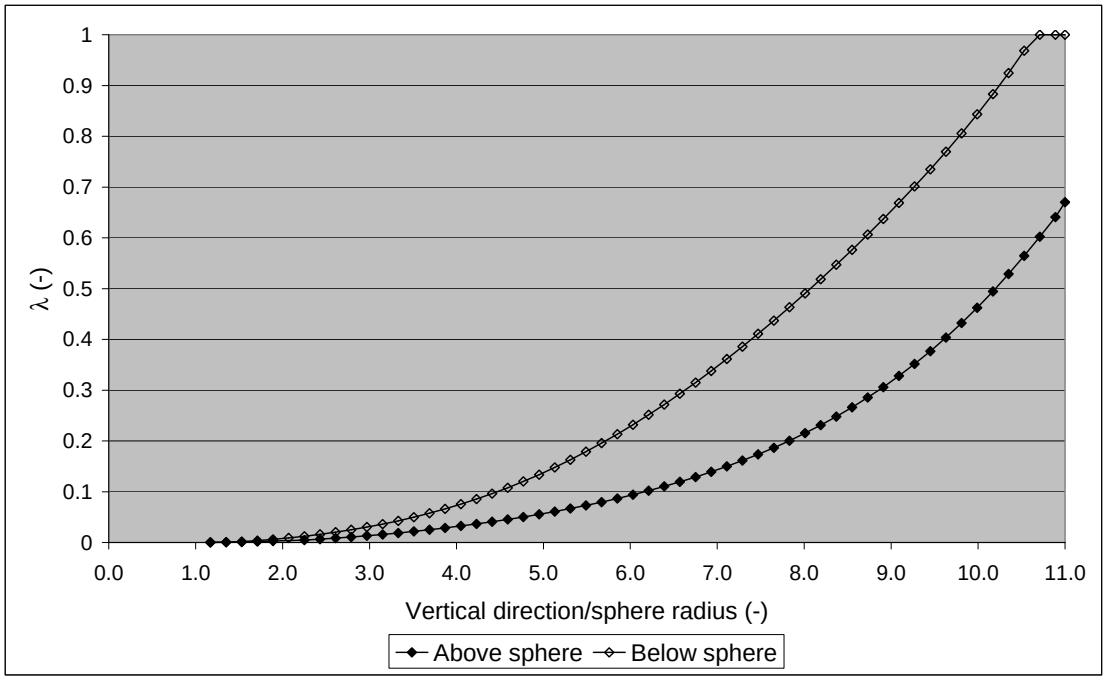

Figure 6-2: The variation of fluid structure parameter along the vertical axis of the column. The sphere (D = 10.0 mm, ρ_s= 8000 kg/m^3) is settling through a semi-viscoplastic fluid (ρ_f= 998.0 kg/m^3, μ_0= 54.9 Pa.s, μ_∞ = 0.0001 Pa.s, κ = 0.234 1/s, θ = 48.48 s, m = 0.7794).

Figure 6-2 shows that due to the mechanism of breakdown and recovery of the fluid structure, the values of λ in the fluid region above the sphere are considerably lower than those below the sphere. Furthermore, in the region below the sphere, the disturbance in the structure of the fluid due to the weight of the sphere extends to a distance of ~ 10.5 radii. Beyond this region, the fluid medium is practically undisturbed, as represented by λ values of 1.0. The variability of λ in the region below the sphere as shown in Figure 6-2 indicates that the disturbance in the fluid medium extends relatively extensively below the settling sphere. This deformation in structure that occurs even before the fluid medium gets directly sheared by the movement of the sphere is due to the recirculation motion of the fluid as it becomes displaced by the settling sphere.

Due to the variability of the viscous parameters throughout the problem domain, representative values that signify the average fluid structure parameter in the fluid

medium surrounding the spheres need to be selected and defined. These representative variables are symbolised by $\bar{\lambda}_{ss}$ and $\bar{\lambda}_0$ for the regions above and below the sphere, respectively. In the following few paragraphs, the estimation methods of these parameters and the associated assumptions required to obtain these estimates will be discussed.

The variable $\bar{\lambda}_{ss}$ represents the structure of the fluid immediately after it has been sheared by the motion of the sphere. Thus, its value is quantifiable by the application of equation 4-4, which is the steady-state form of the structural rate equation represented by equation 4-3. In this study, the rate of deformation ($\dot{\gamma}$) has been calculated by considering the reference point of shear-stress suggested by Wilson et al. (2004; 2003), as represented by equation 2-47.

Beneath the settling sphere, the representative fluid structure parameter is symbolised by $\bar{\lambda}_0$. For the preceding sphere, a value of unity has been assigned for this parameter ($\bar{\lambda}_0$ = 1.0), representing the fact that this sphere is settling through a completely stabilised fluid medium. The effects of fluid deformation due to the recirculation of fluid beneath the sphere as shown in Figure 6-2 have therefore been disregarded in this calculation. This assumption considerably simplifies the basic representation of the fluid rheology that is required for the development of a correlation for the settling velocity of particles in viscoplastic fluids. It will be demonstrated in the following sections that the implementation of this assumption provides an adequate platform for the representation of the changes in the viscous parameters in the fluid medium as it is sheared by the movement of the spheres.

To estimate the representative fluid structure parameter beneath the trailing sphere (sphere 2), the rate of recovery of the fluid structure after it has been sheared by the settling motion of the preceding sphere needs to be considered. This rate of recovery can be estimated by assuming that the fluid structure does not experience any form of disturbance unless it is subjected to the shear force of another (or trailing) sphere, i.e. $\dot{\gamma}$ = 0.0. Therefore, by applying the rate equation

presented in equation 4-3, the recovery in the fluid region between the two spheres can be estimated as follows:

$$\int_{\lambda_{ss-1}}^{\lambda_{0-2}} \frac{\partial\lambda}{1-\lambda} = \int_{0}^{t} \frac{t}{\theta} \qquad \textbf{(6-1)}$$

where subscripts 1 and 2 have been assigned to indicate the representative fluid structure parameters of the leading and trailing spheres, respectively. $\overline{\lambda}_{0-2}$ therefore is the representative fluid structure parameter below sphere 2, whereas $\overline{\lambda}_{ss-1}$ is the representative fluid structure parameter above sphere 1. t represents the amount of time lapse since the fluid was last sheared by the settling movement of the leading sphere. $\overline{\lambda}_{0-2}$ can therefore be estimated by the integration of equation 6-1:

$$\overline{\lambda}_{0\text{-}2} = 1 + \exp\left(\frac{-t}{\theta}\right)\left(\overline{\lambda}_{ss\text{-}1} - 1\right) \qquad \textbf{(6-2)}$$

Similar to the case with the preceding sphere, i.e. in the estimation of $\overline{\lambda}_{0-1}$, the deformation of the fluid structure below the sphere caused by the recirculation of fluid has been neglected in the estimation of $\overline{\lambda}_{0-2}$.

6.3.2 The effective fluid structure parameter

In the previous section, the parameters representing the level of structural integrity in the fluid medium surrounding the settling spheres have been defined. Furthermore, by defining these parameters, it became apparent that the disparity observed in the settling behaviour of two spheres settling one above the other in the test fluid solutions is due to the changes in the viscous parameters of the fluid surrounding the spheres. Any changes in these parameters are expected to be reflected in the settling velocities of the spheres.

In the study presented by Wilson et al. (2004; 2003), the settling velocity of the spheres has been correlated against a figure of equivalent viscosity (μ_{eq}). This parameter represents a calculated figure of Newtonian viscosity that would produce the same settling velocity as a particle (of the same density and dimensions) settling through a non-Newtonian fluid medium (see Section 2.4.3 and Figure 2-4). In the current analysis, this correlation has been used to examine the viscous parameters of the fluids as reflected by the settling velocities of the spheres. The observed values of μ_{eq} were used to determine the average value of λ in the fluid medium surrounding the spheres, represented here by the variable $\bar{\lambda}_{eff}$. The details of this calculation have been presented in Appendix D.1. The results of this analysis can be seen in Figure 6-3, where the observed values of $\bar{\lambda}_{eff}$ as a function of the representative fluid structure parameters above and below the spheres ($\bar{\lambda}_0$ and $\bar{\lambda}_{ss}$), have been illustrated.

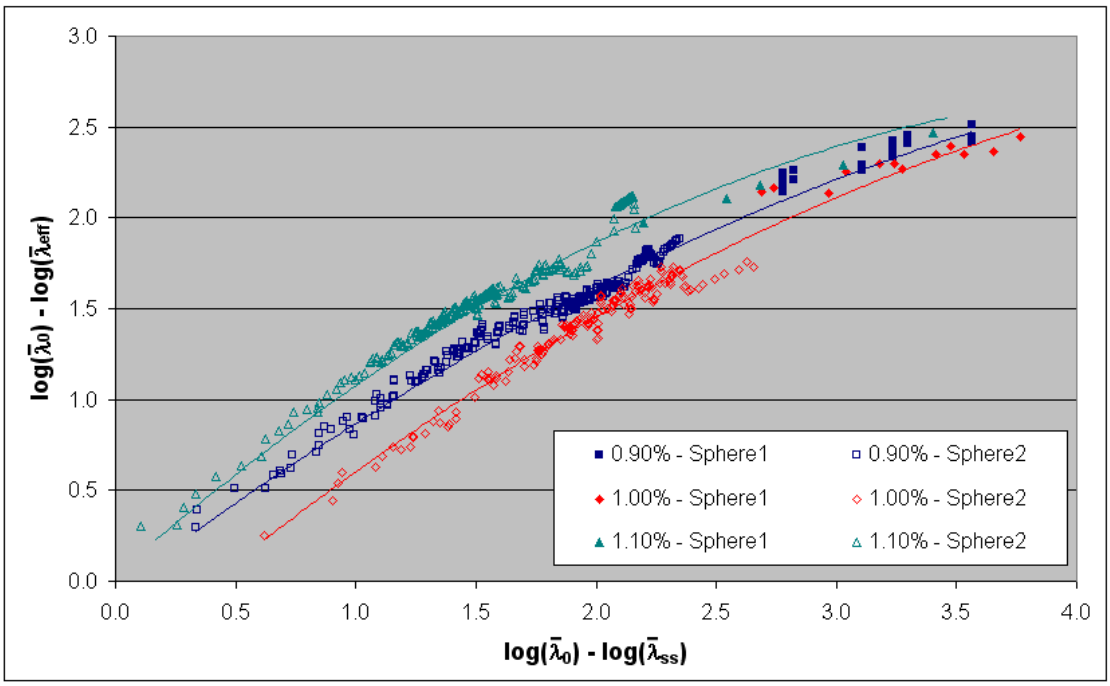

Figure 6-3: Observed values of fluid structure parameter based on the experimental data of vertically-aligned identical spheres in 0.9, 1.0, 1.1% Floxit solutions, as a function of the representative fluid structure parameters above and below the spheres.

As expected, Figure 6-3 shows that there is a strong dependency between $\bar{\lambda}_{eff}$ and the estimated fluid structure parameters at the polar ends of the spheres, represented here by the variable $\left[\log\left(\bar{\lambda}_0\right)-\log\left(\bar{\lambda}_{ss}\right)\right]$. Furthermore, Figure 6-3 also shows that the values of $\left[\log\left(\bar{\lambda}_0\right)-\log\left(\bar{\lambda}_{eff}\right)\right]$ for 1.0% Floxit solution are generally the lowest in comparison to those of 0.9% and 1.1%. The corresponding values resulting from the 1.1% Floxit solution, on the other hand, are the highest. This variability was found to reflect the degree of plasticity in the fluid media. This rheological parameter, as has previously been discussed in Section 4.5, is represented by the variable P. It describes the degree of viscoplasticity of the fluid medium and is dependent on the 'shape' of the rheogram, i.e. fluids that exhibit completely Newtonian flow characteristics has a P value of zero, whereas a completely plastic material has a P value of infinity. The values of P for each of the fluid solution used in this study have been presented in Table 4-4. In this Table, it was shown that the 1.1% Floxit solution possesses the lowest level of viscoplasticity (P = 1.632) in comparison to the other test solutions, whereas the 1.0% Floxit solution the highest (P = 1.837). This variation in P thus appears to be inversely proportional to the dependency of $\left[\log\left(\bar{\lambda}_0\right)-\log\left(\bar{\lambda}_{eff}\right)\right]$ on the concentration of Floxit in the fluid media.

Based on the comparative analysis outlined above, it can be concluded that the dependency of $\left[\log\left(\bar{\lambda}_0\right)-\log\left(\bar{\lambda}_{eff}\right)\right]$ on $\left[\log\left(\bar{\lambda}_0\right)-\log\left(\bar{\lambda}_{ss}\right)\right]$ is also a function of the level of fluid plasticity. This is in agreement with the hypothesis of Horsley et al. (2004), who suggested that for the prediction of the settling velocities of spheres falling consecutively in a viscoplastic solution, the level of fluid plasticity (this variable was also represented by the variable P in this study) needs to be considered. It also agrees with the correlation suggested by Gumulya et al. (2007), in which the settling velocity of the spheres is correlated with the degree of fluid plasticity, represented in this case by the variable α. The relation of P with α can be seen in equation 4-12.

In Figure 6-4, the variability of $\left[\log\left(\bar{\lambda}_0\right)-\log\left(\bar{\lambda}_{eff}\right)\right]$ with the plasticity of the fluid solutions, as well as the values of $\left[\log\left(\bar{\lambda}_0\right)-\log\left(\bar{\lambda}_{ss}\right)\right]$, has been illustrated. In this graph, it can be seen that by considering the plasticity of the fluid in this manner, the differences in the effective structure parameter ($\bar{\lambda}_{eff}$) in the three fluid solutions can be minimised, thus permitting the development of a generalised correlation for all the fluids.

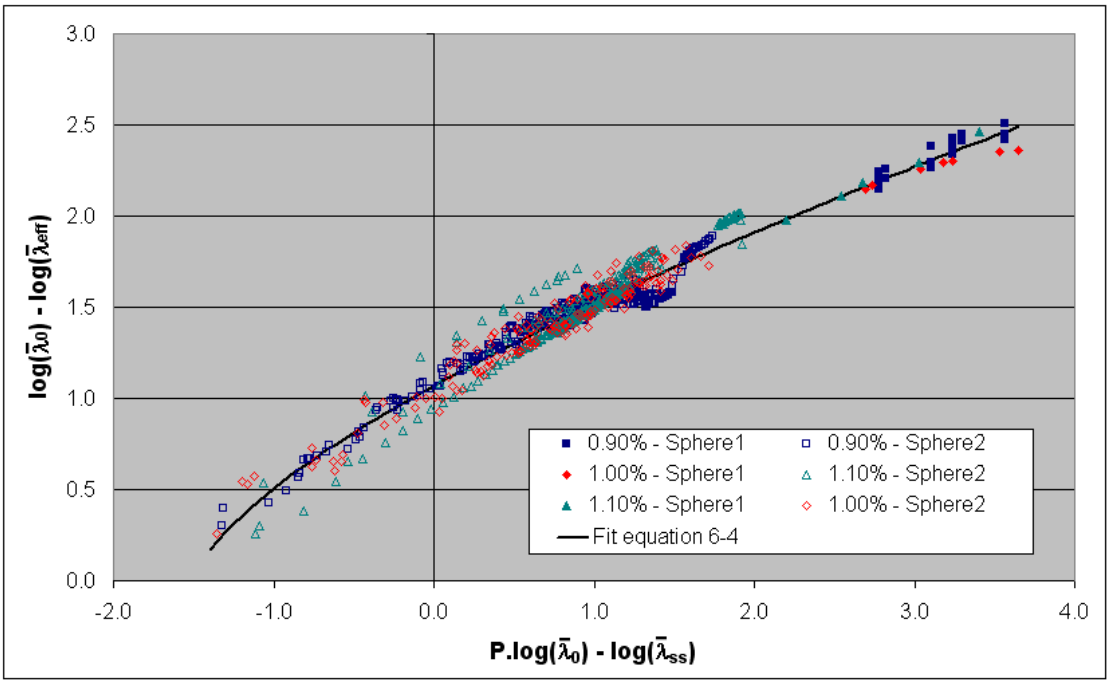

Figure 6-4: : Observed values of the fluid structure parameter based on the experimental data of vertically-aligned identical spheres in 0.9, 1.0, 1.1% Floxit solutions, as a function of the representative fluid structure parameters above and below the spheres, as well as the plasticity of the fluid solutions.

From Figure 6-4, it can be seen that the following equation is able to reflect the changes in the effective fluid structure parameters as a function of $\bar{\lambda}_0$ and $\bar{\lambda}_{ss}$:

$$\log\left(\bar{\lambda}_0\right) - \log\left(\bar{\lambda}_{eff}\right) = C_1 \left[P.\log\left(\bar{\lambda}_0\right) - \log\left(\bar{\lambda}_{ss}\right) + C_2\right]^N \quad \textbf{(6-3)}$$

where C_1, C_2, and N are constants.

The constants C_1, C_2, and N were evaluated by using 662 experimental data points obtained from consecutive drops of spheres with the same diameter and density (case A). A linear regression evaluation method was used, and the results of this analysis are $C_1 = 0.81$, $C_2 = 1.5$ and $N = 0.685$. Thus, equation 6-3 can be rewritten as:

$$\log\left(\bar{\lambda}_0\right) - \log\left(\bar{\lambda}_{eff}\right) = 0.81\left[P.\log\left(\bar{\lambda}_0\right) - \log\left(\bar{\lambda}_{ss}\right) + 1.5\right]^{0.685} \quad \textbf{(6-4)}$$

The results of equation 6-4 are evaluated in Figure 6-5 and Figure 6-6, where the predicted settling velocities of the first and second spheres are compared to the observed values. In Figure 6-5, it can be seen that there is a good correspondence between the calculated and observed values of terminal settling velocity of the first sphere. High regression and proportionality between the calculated and observed settling velocity of the second sphere is also evident in Figure 6-6. This suggests that the considerations and assumptions discussed above are valid and that equation 6-4 can be used for the prediction of the settling velocities of two identical spheres falling consecutively in Floxit solutions with concentrations of 0.9 – 1.1%.

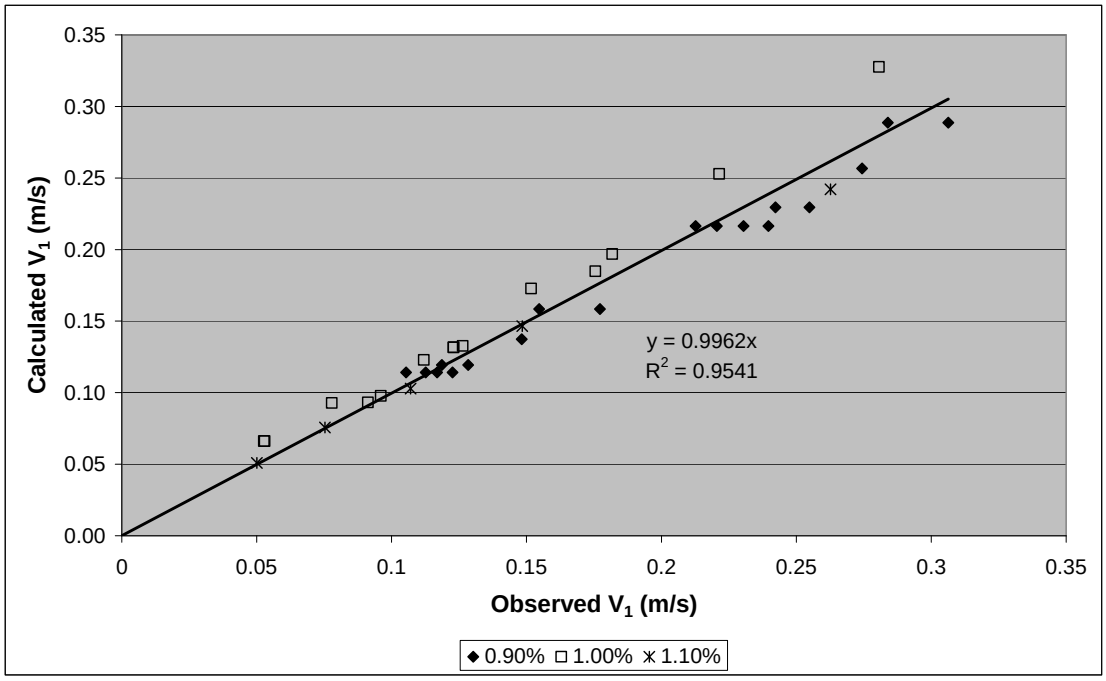

Figure 6-5: Calculated values of the terminal settling velocity (V_1) as a function of the observed values in 0.9, 1.0, and 1.1% Floxit solutions.

The uncertainties of the proposed correlation as reflected by the standard error between the calculated and the observed values of settling velocity were found to be 0.0149 (over 37 data points) and 0.0317 (over 625 data points) for the fall velocity of the leading and trailing spheres, respectively, equivalent to 9.3% and 11.8% relative to the mean value of settling velocities. Higher uncertainties in the settling velocity of the trailing sphere were generally found in cases where the amount of time lapse between the two spheres, represented by the variable t in equation 6-2, is small ($t < 1$ s). Based on this observation, it is suspected that one of the major contributors to error is the uncertainties involved in taking the average velocity between the sensors. This view is supported by the fact that the discrepancy between the level of uncertainties in the prediction for the fall velocities of the leading and trailing spheres reflects the estimated % errors in the settling-sphere experiment (1.8% and 6.7% for the terminal and second-sphere settling velocities, respectively. See the experimental error analysis presented in Section 3.3.3). Additionally, the difference between the levels of uncertainties involved with the proposed correlation and the settling-sphere experiment may have been due to

errors in rheometry, which, as has been discovered in the numerical (CFD) study presented in Chapter 5, are often inevitable due to the complexity of the shear behaviour of viscoplastic and viscoelastic fluids. Nevertheless, the level of uncertainties presented by the proposed correlation was deemed to be highly satisfactory.

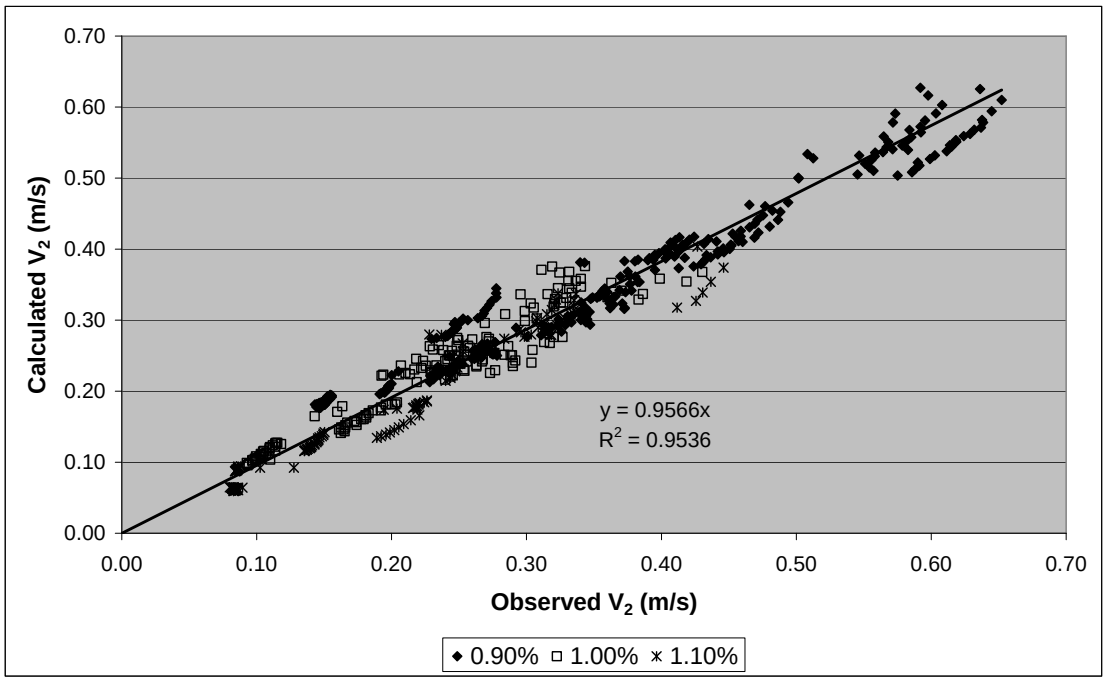

Figure 6-6: Calculated values of the settling velocity of the second sphere (V_2) as a function of the observed values in 0.9, 1.0, and 1.1% Floxit solutions.

It should also be noted that the Reynolds number (Re*) of the experiments conducted for this study (calculated based on the terminal velocity of the spheres) ranges from 0.5 to 5.0. Beyond this region of Re*, the accuracy of this correlation is still unknown. It is speculated that the accuracy of the correlation would decrease significantly beyond this region, due to difficulties in obtaining accurate rheology measurements at high rates of shear.

6.4 Characteristics of correlation: its applicability and limitations

The basis of the proposed method for the prediction of the settling velocity of a sphere with a given time lapse since the fluid was sheared by the movement of another sphere some time earlier is the integrated form of the rate equation, which is presented by equation 6-2. In Section 6.3, it was demonstrated that by applying this equation, the level of structural recovery of the fluid medium as a function of time can be quantified, and therefore, a successful prediction of the fall behaviour of a sphere moving through this partially-recovered fluid medium can be obtained. However, the proposed correlation has so far only been applied on cases where the two spheres have identical parameters, i.e. diameter and density, and the velocity profiles associated with two vertically-aligned spheres of different densities and diameters are yet to be examined.

The different parameters of the spherical particles being tested for this study have been outlined in Section 3.3. By conducting these experiments, the effects of different levels of shear stresses asserted by the trailing sphere on a partially-recovered fluid structure can be examined. In this study, this investigation will be performed by firstly considering the effects of differences in sphere densities on the fall velocity of the trailing sphere, using results from experimental cases B and C. The effects of differences in sphere diameters will then be examined by considering results from experimental cases D and E.

6.4.1 Effects of the density of the spheres on fluid-structure recovery

In Figure 6-7, the velocity profiles resulting from several experiments featuring different levels of discrepancies in sphere densities (representing cases A, B, and C) have been presented. In this Figure, the settling velocities of the two spheres (V_2/V_{t1}) have been presented in comparison to the amount of time lapse between the two spheres (t). As can be seen in this Figure, the experiment where the density of

the trailing sphere is higher than that of the leading sphere (case B, $\rho_1 < \rho_2$), the velocity of the trailing sphere is significantly higher than that of the leading sphere. High values of velocity ratio in comparison to cases where $\rho_1 = \rho_2$ were obtained. On the contrary, for the experiment classified under case C, which features lower trailing-sphere density ($\rho_1 > \rho_2$), significantly lower values of velocity ratio were displayed. In general, this class of experiment features velocity ratios exceeding 1.0, unless the initial distance between the spheres is very large (t > 15 s). Based on this observation, it can be concluded that in experiments where the trailing sphere possesses a lower density than the leading sphere, a collision between the two spheres can still occur, provided that the time lapse between the releases of the two spheres is relatively short. This critical figure was found to be ~ 1.5 s for the parameters of the current experiment.

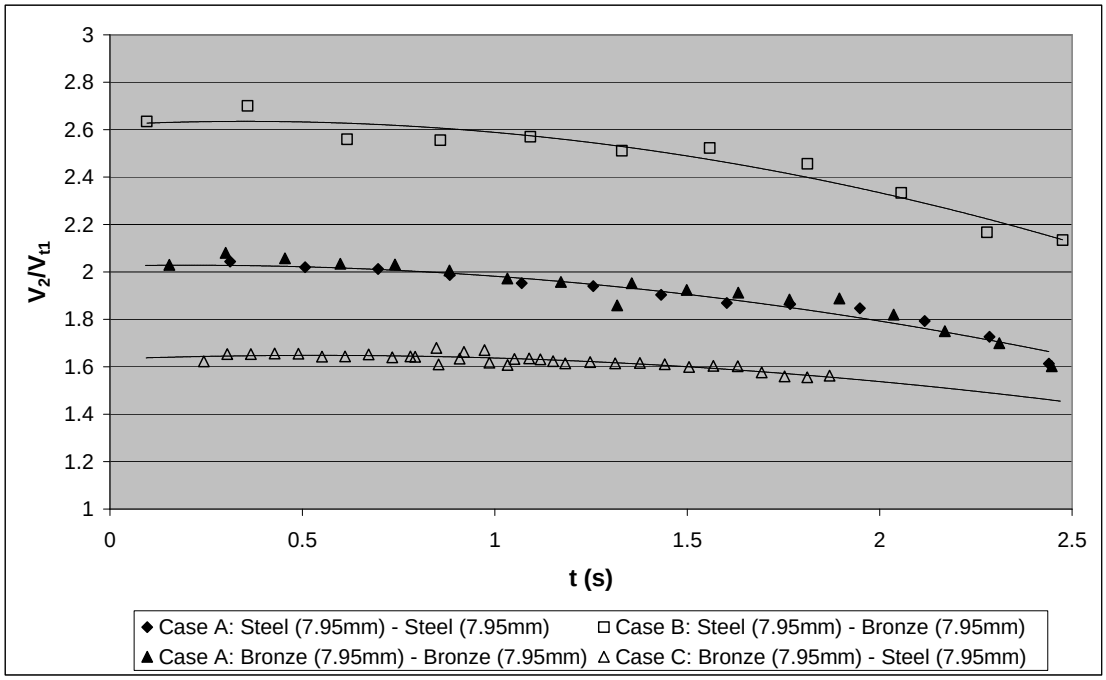

Figure 6-7: The profile of the variations in settling velocity, as a function of the time lapse since the fluid was sheared by another sphere (t). Data acquired from the 0.9% Floxit solution was used.

In contrast to the experiment involving two identical spheres, the differences in the density of the two particles involved with experiments of cases B and C are expected to cause an inequality in the amount of stress applied to the fluid medium. As a result, different levels of breakdown in the fluid structure surrounding the two spheres would be generated i.e. $\lambda_{ss-1} \neq \lambda_{ss-2}$. To obtain an appropriate representation of the settling conditions of the two spheres, therefore, care must be implemented in assigning the appropriate figure of shear stresses, represented by the variable $\bar{\tau}$ (or $[(\rho_s - \rho_f)gD/6]$ as represented by equation 2.47), as well as $\bar{\lambda}_{ss}$. The details of this calculation are presented in Appendix D.1.

The resulting outline of the effective structural parameter, $\bar{\lambda}_{eff}$, calculated based on the observed settling velocities obtained from experimental cases B and C, in comparison with the predicted values of $\bar{\lambda}_{eff}$ predicted through equation 6-4, is presented in Figure 6-8. From this Figure, it can be seen that a good correspondence between the observed and predicted values of structural parameter exists for both cases B and C, indicating that the proposed correlation can be applied for both cases.

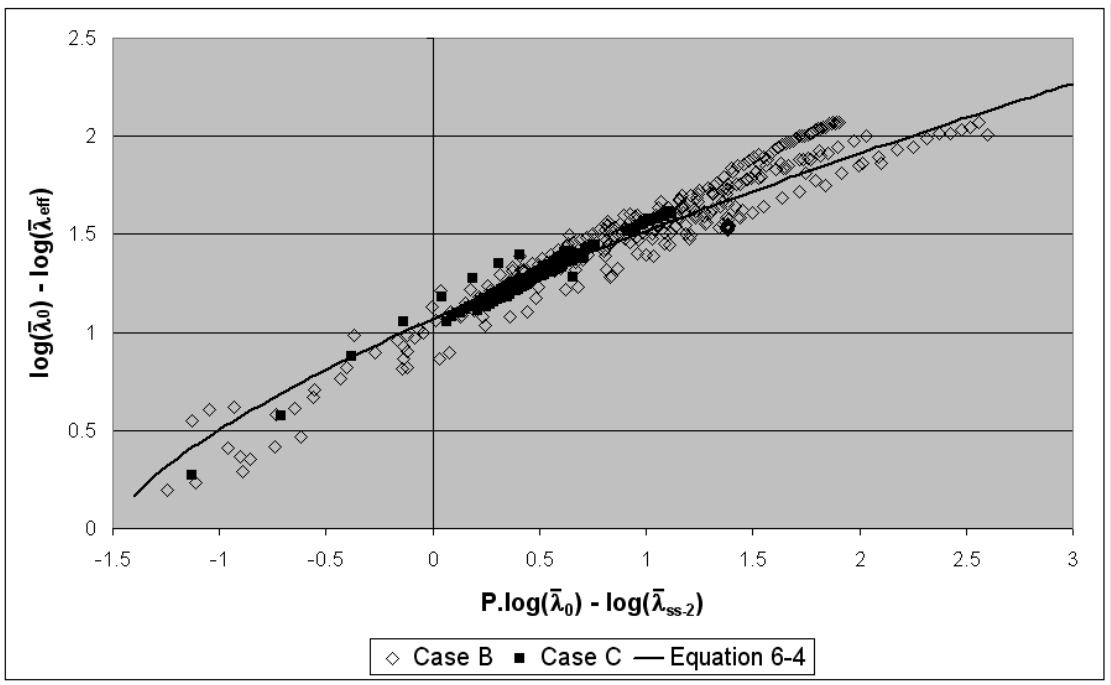

Figure 6-8: Observed values of fluid structure parameter based on the experimental data of vertically-aligned spheres in the Floxit solutions, as a function of the representative fluid structure parameters above and below the spheres, as well as the plasticity of the fluid solutions. In case B, $\rho_1 < \rho_2$, whereas in case C, $\rho_1 > \rho_2$.

The applicability of equation 6-4 on cases B and C is further enforced in Figure 6-9, where strong regression and proportionality between the calculated and observed values of the settling velocity of the second sphere are evident. The level of uncertainty involved with this calculation, as reflected by the standard error between the observed and predicted values of settling velocities was found to be 0.0490 over 399 data points (or 20.0% relative to the mean value of settling velocity). Although the standard error in this case is slightly higher than those found for the case of identical spheres, this figure is still deemed to be highly satisfactory, indicating that the proposed correlation applies for cases where the ratio of the density of the two spheres (ρ_{s2}/ρ_{s1}) varies by a factor of 0.86 to 1.16. Similar to the case of identical spheres discussed previously, higher level of uncertainties was found in cases where the time difference between the spheres is small ($t < 1$ s).

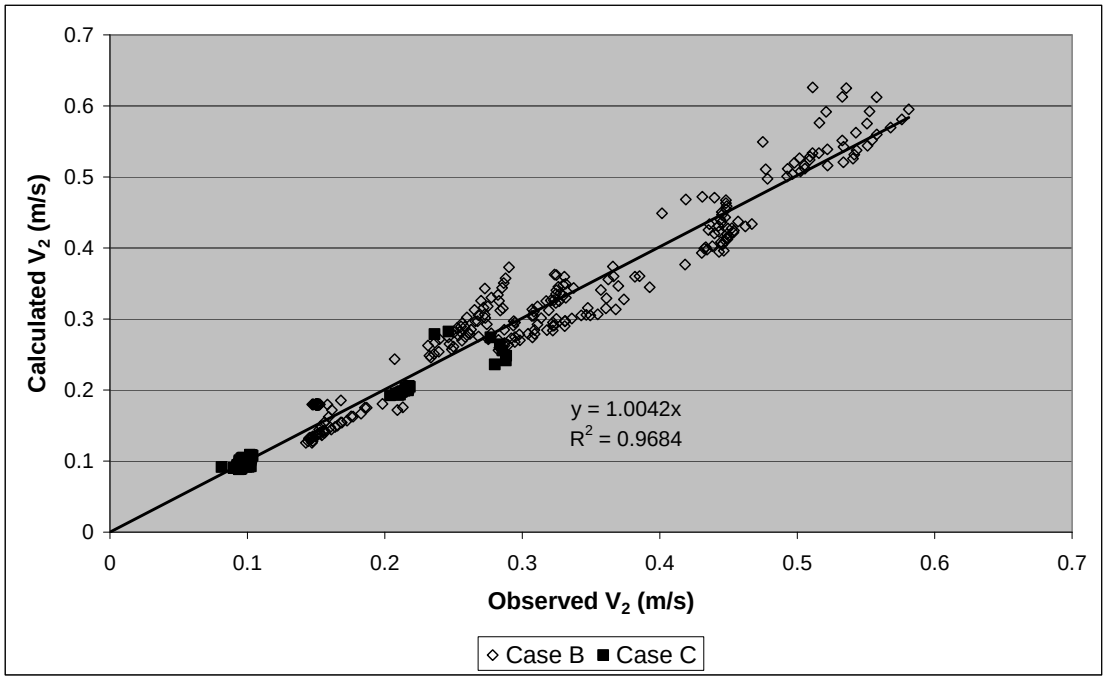

Figure 6-9: Calculated values of the settling velocity of the second sphere (V_2) as a function of the observed values from experiments of cases B and C in the Floxit solutions.

6.4.2 Effects of the diameter of the spheres on fluid-structure recovery

The typical velocity profiles obtained from experiments of cases D and E were presented in Figure 6-10. In this Figure, it can be seen that for cases where the trailing sphere has a larger diameter than the leading sphere (case D, $D_1 < D_2$), very high ratios in the settling velocities of the two spheres were encountered. On the contrary, experiments of case E ($D_1 > D_2$) presents much lower values of velocity ratios, although their values are still greater than 1.0, indicating that the gap between the two spheres reduces over time. At larger values of initial distances, lower trailing sphere velocity could be obtained, i.e. $V_2/V_1 < 1.0$, as demonstrated in the velocity trace presented in Figure 6-11. In this Figure, the settling velocity of the trailing sphere is shown to be significantly lower than that of the leading sphere, although conditions at the start of the experiment show a slightly higher

trailing-sphere velocity. As the gap between the two spheres increases, the trailing sphere continues to decelerate as it settles through the column.

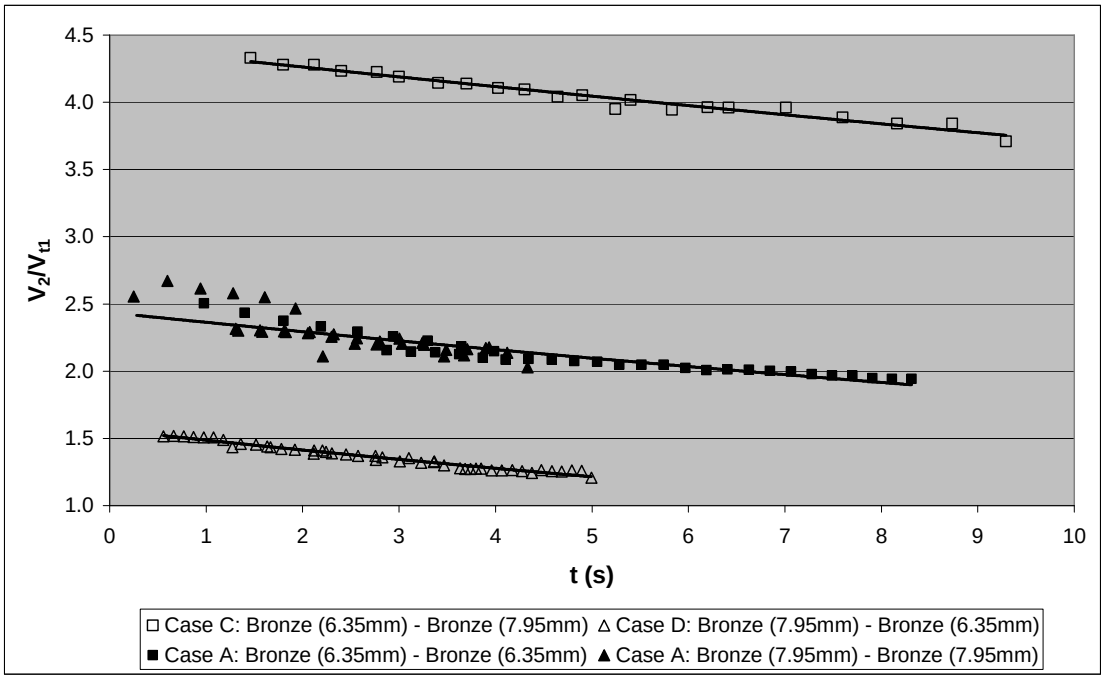

Figure 6-10: Profile of the settling velocity, as a function of the time lapse since the fluid was sheared by another sphere (t). Data acquired from the 1.1% Floxit solution was used.

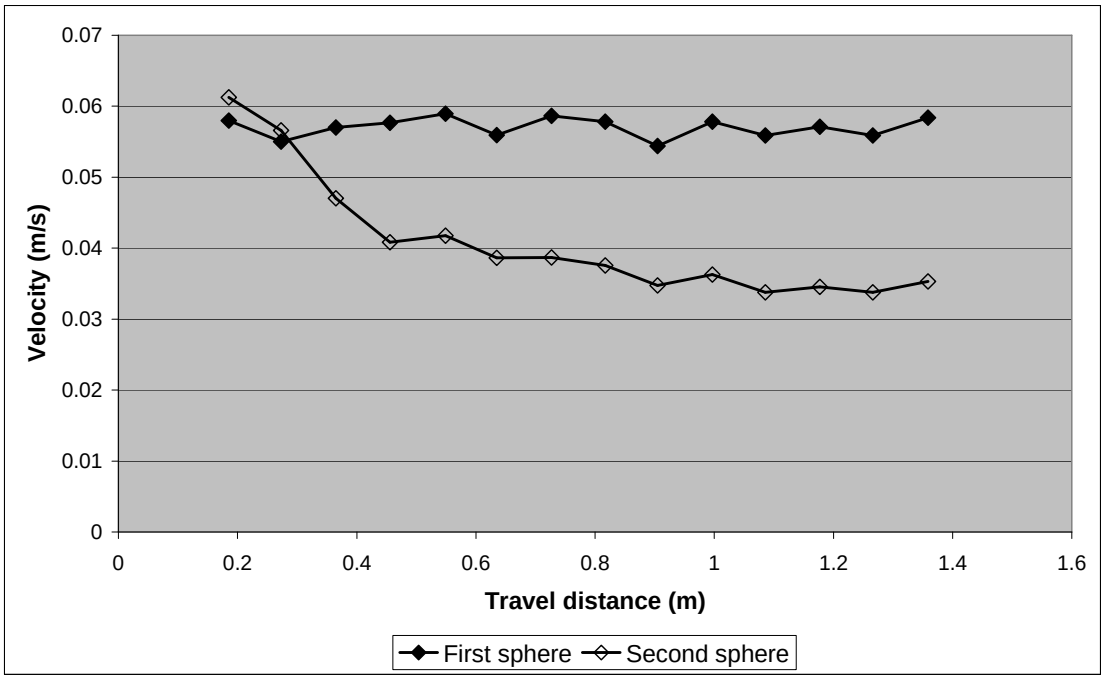

Figure 6-11: Velocity trace of a stainless sphere (7.95 mm) followed by another stainless steel sphere (6.25 mm) with approximately 2 s release time difference travelling in a 1.0% Floxit 5250L solution.

Similar to the experiments involving spheres of different densities (see previous section), an accurate description of the settling experiment of cases D and E, where two spheres of different diameters are used, requires a careful assignment of figures in the calculation for shear stresses and structural parameters. The details of this calculation are shown in Appendix D.1. The resulting outline of $\overline{\lambda}_{eff}$, calculated based on the observed settling velocities obtained from experimental cases D and E, in comparison with the corresponding values of $\overline{\lambda}_{eff}$ predicted based on equation 6-4, is presented in Figure 6-12.

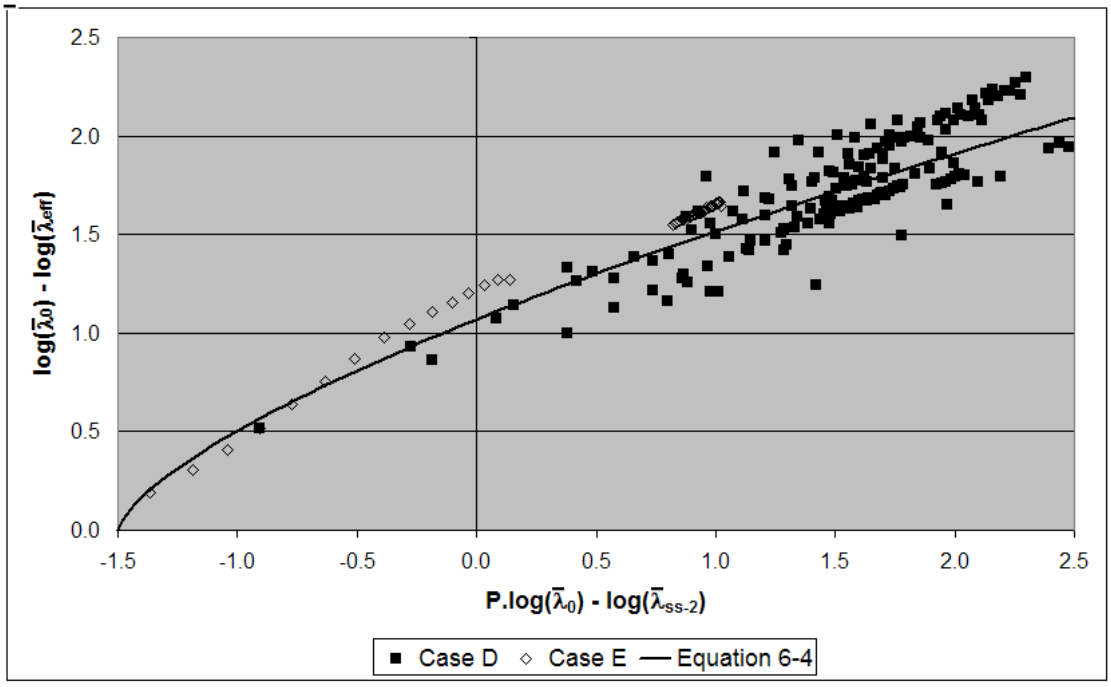

Figure 6-12: Observed values of fluid structure parameter based on the experimental data of vertically-aligned spheres in the Floxit solutions, as a function of the representative fluid structure parameters above and below the spheres, as well as the plasticity of the fluid solutions. In case D, $D_1 < D_2$, whereas in case E, $D_1 > D_2$.

The comparison of fluid structure parameters presented in Figure 6-12 suggests that there is a good agreement between the correlation and the experimental data. This view is further reinforced by the strong correspondence and satisfactory regression displayed in Figure 6-13, where a comparison between the calculated values of the trailing sphere velocity with the corresponding observed values is presented. Figure 6-13, however, also shows that the correlation slightly tends to under-estimate the second ball velocity. The level of uncertainty of this calculation as reflected by the standard error between the observed and calculated values of settling velocity was found to be 0.0717 over 202 data points, equivalent to 21.6% relative to the average value of settling velocity. Although this figure is slightly higher than that for the case of identical spheres, it is still deemed to be highly satisfactory, indicating that the proposed correlation applies for cases where the diameter of the spheres differ by ± 3.7 mm.

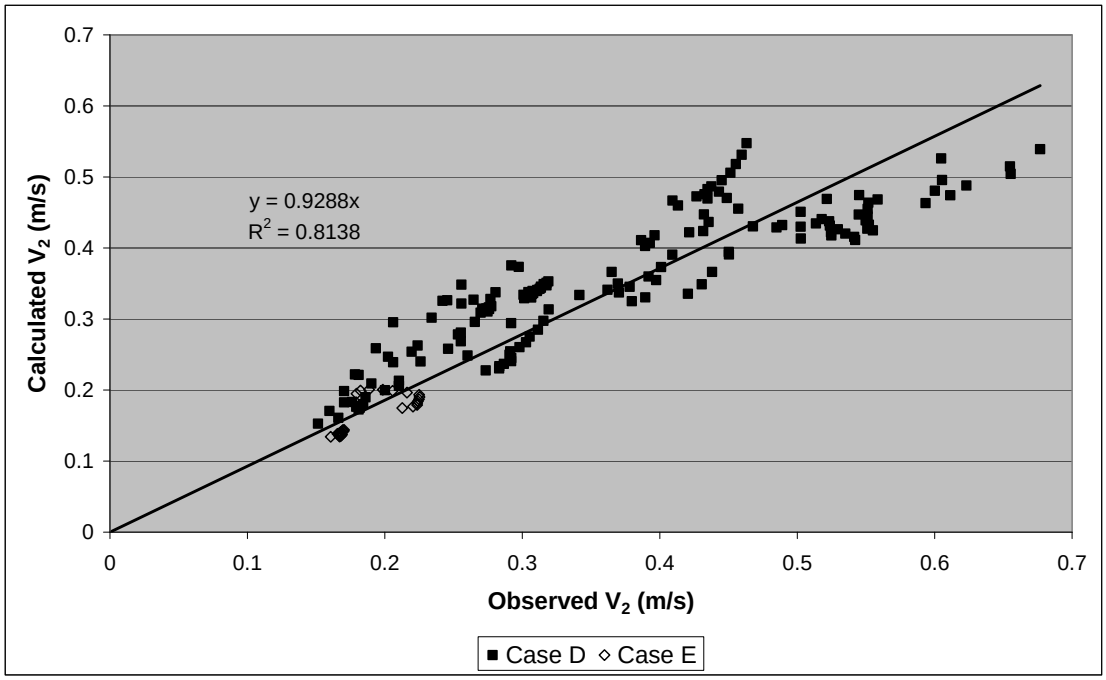

Figure 6-13: Calculated values of the settling velocity of the second sphere (V_2) as a function of the observed values from experiments of cases D and E in the Floxit solutions.

6.4.3 Effects of inter-sphere interaction

In earlier discussions on the velocity profiles obtained from the experiments of vertically-aligned spheres (see Sections 3.3.2 and 6.2.1), the presence of a critical sphere-to-sphere distance, below which there is a marked decrease in the velocity of the trailing sphere accompanied by an acceleration of the leading sphere, was noted. A more apparent depiction of this condition is presented in Figure 6-14, where the variation of the velocity ratio between the two spheres (V_2/V_1), as a function of the ratio between the inter-sphere distances with the diameter of the spheres (d/D), is shown. From this Figure, it can be seen that as the distance between the two spheres decreases, the velocity of the trailing sphere continues to increase. This occurs until a d/D ratio of ~ 10 is reached, upon which the velocity ratio starts to decrease, indicating the start of the critical condition.

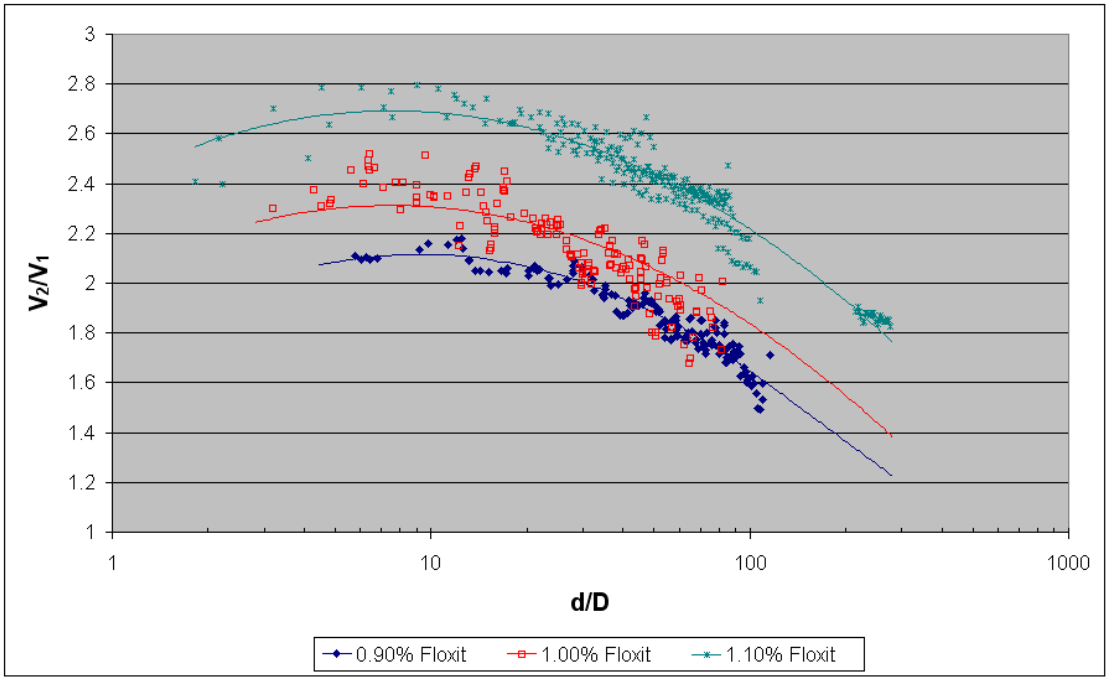

Figure 6-14: The variation of the velocity ratio between the leading and trailing spheres (V_2/V_{t1}), as a function of the distance-to-diameter ratio for experimental results of Case A (identical spheres) in 0.9%, 1.0%, and 1.1% Floxit solutions.

In the error analysis presented in Section 3.3.3, the accuracy of data collected during this critical condition has been noted to be relatively low. As a result, accurate values of distance-to-diameter ratio, upon which the onset of the critical condition occurs, could not be evaluated. A critical distance-to-diameter ratio of 10.0, based on the velocity profiles presented in Figure 6-14, is generally accepted for the experimental configurations used for this study.

In Figure 6-15, the hypothetical variation of the velocity ratio of two spheres settling through solutions of 0.9, 1.0, and 1.1% Floxit, calculated based on the proposed correlation outlined in Section 6.3, was presented as a function of the distance between the spheres. As can be seen from this Figure, the correlation appears to predict the decline in the settling velocity of the trailing sphere as it draws near to the leading one, and the resulting velocity profiles are similar to those presented in Figure 6-14. The proposed correlation, however, is not able predict the increase in the velocity of the leading sphere. This was as expected, as

this phenomenon is likely to be dominated by the interaction between the spheres, rather than changes in the structural parameter in the fluid medium. The momentum of the trailing sphere induces a 'pushing' effect on the leading sphere, which results in a temporary acceleration of the leading sphere, prior to the collision.

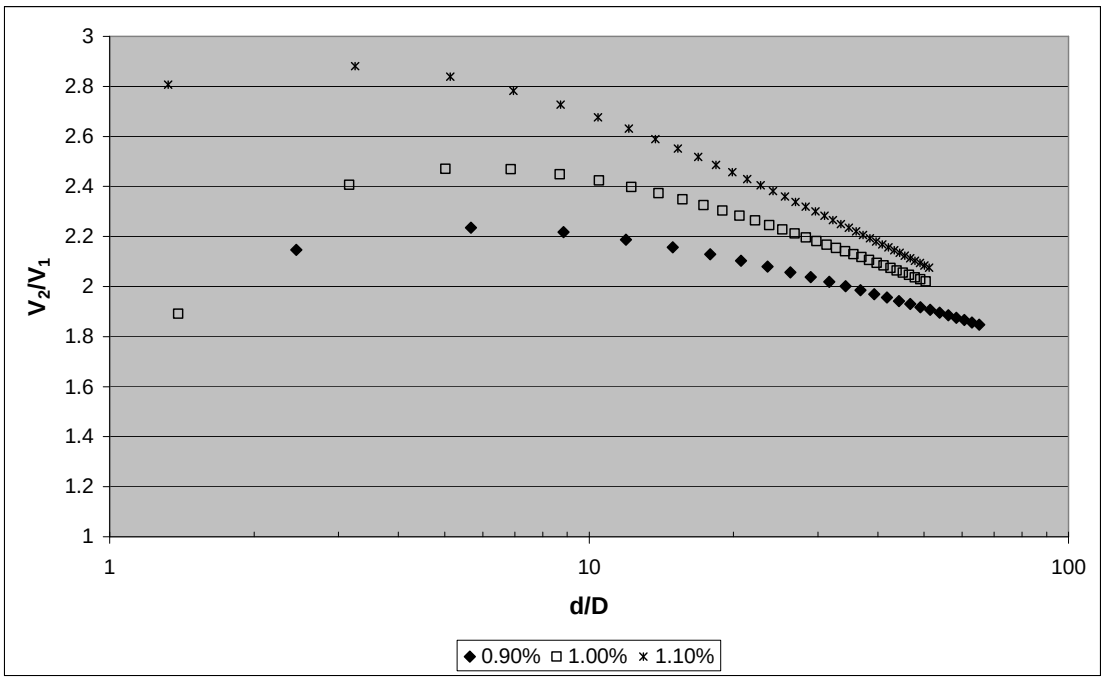

Figure 6-15: The hypothetical velocity ratio of two vertically-aligned bronze spheres (6.35mm), with an initial distance of 0.9 m, settling through a 0.9% Floxit solution.

The predicted critical distance for the sphere parameters presented in Figure 6-15 are approximately 4.0 – 6.0 D. Considering the level of accuracy involved with the analysis of the critical condition in the settling-sphere experiments, combined with the inability of the correlations to predict the onset of acceleration in the fall behaviour of the leading sphere, these values can be considered to be in relatively good agreement with the experimental data presented in Figure 6-14. This suggests that the proposed correlation can be used as a predictive tool for the estimation of the extent of inter-sphere interaction in the study of the settling of vertically-aligned spheres.

6.5 The settling velocity of aggregated spheres

Figure 3-4 and Figure 6-1 show that after colliding, the two spheres combine and travel at the same velocity. As the fluid region underneath the spheres is undisturbed, the aggregated spheres soon reach a terminal velocity. In this work, the correlation represented by equation 6-4 will be used as the basis for the development of a correlation for the prediction of this terminal settling velocity.

In a similar manner to the analysis conducted by Wilson et al. (2003), the stress asserted by the aggregated spheres on the fluid medium is represented by the mean surficial shear stress ($\bar{\tau}$).This parameter is a function of the submerged weight of the aggregated spheres (FW_{12}):

$$FW_{12} = g\frac{\pi}{6}\left[D_1^3(\rho_{s1}-\rho_f)+D_2^3(\rho_{s2}-\rho_f)\right] \qquad \textbf{(6-5)}$$

The effective surface area of the combined spheres (A_{12}) should be less than the total surface area because of the path interference between the two spheres:

$$A_{12} = A_1 + \beta.A_2 \qquad \textbf{(6-6)}$$

where A_1 and A_2 are the surface areas of the first and second spheres and β is a variable that is less than unity. The variable β takes into account the path interference of the two spheres as they combine.

The mean surficial shear stress caused by the combination of the spheres can be then be calculated as follows:

$$\bar{\tau}_{12} = \frac{g\left[(\rho_{s1}-\rho_f)D_1^3+(\rho_{s2}-\rho_f)D_2^3\right]}{24\left[\left(\frac{D_1}{2}\right)^2+\beta.\left(\frac{D_2}{2}\right)^2\right]} \qquad \textbf{(6-7)}$$

For an experiment involving two identical spheres (i.e. case A), equation 6-7 can be simplified to:

$$\bar{\tau}_{12} = \frac{2\bar{\tau}}{1+\beta} \tag{6-8}$$

By calculating the mean surficial stress of the combined spheres, the effective shear stress can be calculated by considering the reference point of shear-stress suggested by Wilson et al. (2003) (see equation 2.46). The structural parameter above the aggregated spheres ($\bar{\lambda}_{ss-12}$) can then be calculated, followed by the averaged effective structural parameter ($\bar{\lambda}_{eff}$), which is estimated by equation 6-4. This can then be used to determine the shear Reynolds number, and hence the ratio of the settling velocity to the shear velocity (V_t/V^*).

Based on the experimental results of case A, the average value of β was found to be 0.541 ± 30%. Using this averaged value, the settling velocities of the combined spheres were calculated, and the comparison with the experimental values can be seen in Figure 6-16. In this graph, it can be seen that there is a good agreement between the calculated and observed values of the terminal settling velocity. The standard error of this correlation was found to be less than 0.0247 over 40 data points, equivalent to 11.6% relative to the average value of settling velocity. Furthermore, no trends in error have been detected with this correlation.

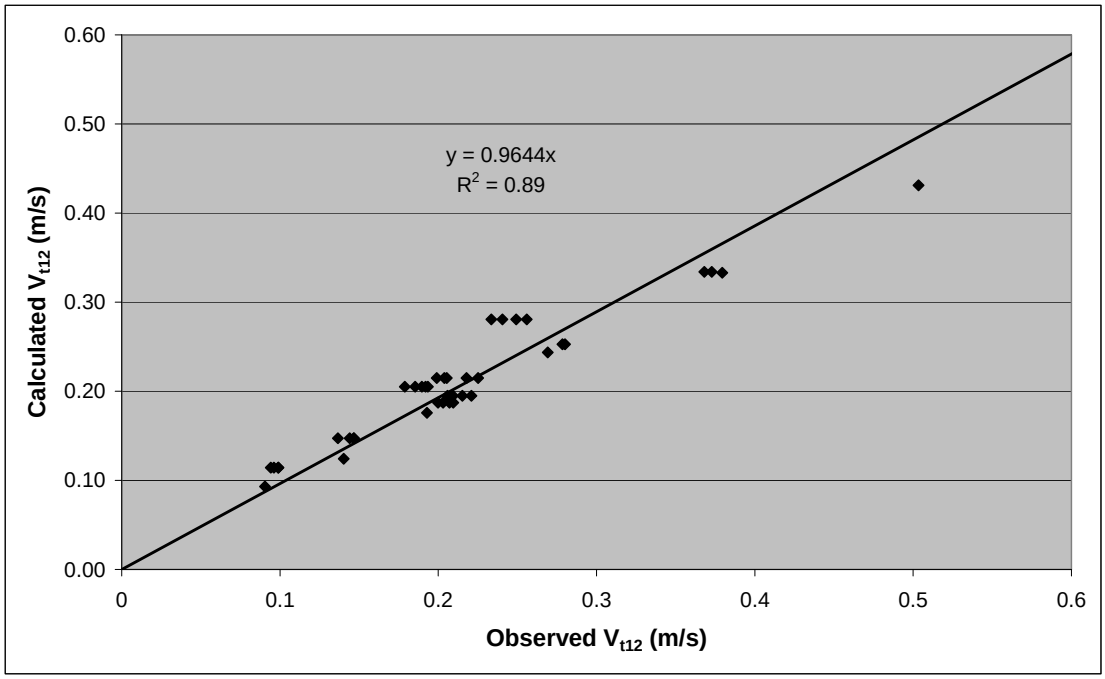

Figure 6-16: Calculated values of the terminal settling velocity of two aggregated spheres (V_{12}) as a function of the observed values from experiments of case A in the Floxit solutions. A β factor of 0.541 was used in the calculation.

A similar calculation procedure was applied to the observed settling velocities obtained from experiments involving two spheres of different densities (Case B). The average value of β in this case was found to be 0.521 ± 20%. The similarity of the averaged β values between case A and B was expected, as the considerations presented by equations 6-5 to 6-8 appear to suggest that β should only be a function of the difference in the diameters of the two aggregated spheres.

Thus, by combining the results of case A and B, a new averaged β value of 0.534 was obtained. The results of this calculation can be seen in Figure 6-17. Similar to the previous calculation, a good agreement between the calculated and observed values of the terminal settling velocity is obtained. The standard error of this correlation was found to be 0.0246 over 62 data points, comprising of results from experiments of cases A and B, equivalent to 10.8% relative to the average value of settling velocity. This indicates that within the limits of the experimental

conditions, the average value of 0.534 for β can be used for an effective prediction of the settling velocity of two aggregated spheres of identical dimensions.

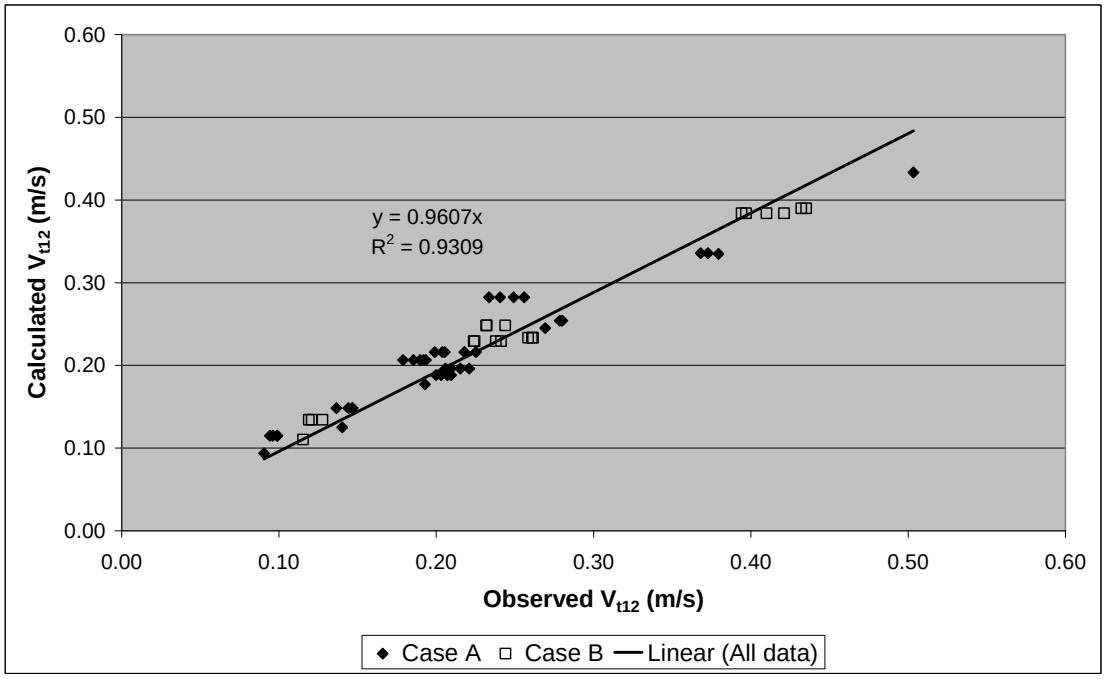

Figure 6-17: Calculated values of the terminal settling velocity of two aggregated spheres (V_{12}) as a function of the observed values from experiments of cases A and B in the Floxit solutions. A β factor of 0.534 was used in the calculation.

The dependency of β on the dimensional differences of the first and second spheres was evaluated using the experimental data of cases D and F, which are experiments that involve spheres of different diameters (as well as density for case F). For these experiments, several possibilities exist for the calculation of the parameter representing the effective diameter of the two spheres (D_{eff}), which in turn is used in the calculation of the shear Reynolds number (Re*). The first possibility is to use the diameter of the first sphere (D_1) and regard β as an adjustment parameter for the difference in the diameter of the second sphere. Another possibility is to use the average diameter of the two spheres (D_{ave}) and regard β as an adjustment parameter for the difference in the diameters of the first and second spheres. Based on the experimental data obtained from cases D and F, it was found that a stronger correlation can be obtained when the shear Reynolds

number is based on the second option, i.e. $D_{eq} \sim D_{ave}$. This correlation is presented in Figure 6-18, which shows the dependence of $\left[\beta/\beta_{identical}\right]$ on $\left[P.\frac{D_2 - D_1}{D_1}\right]$.

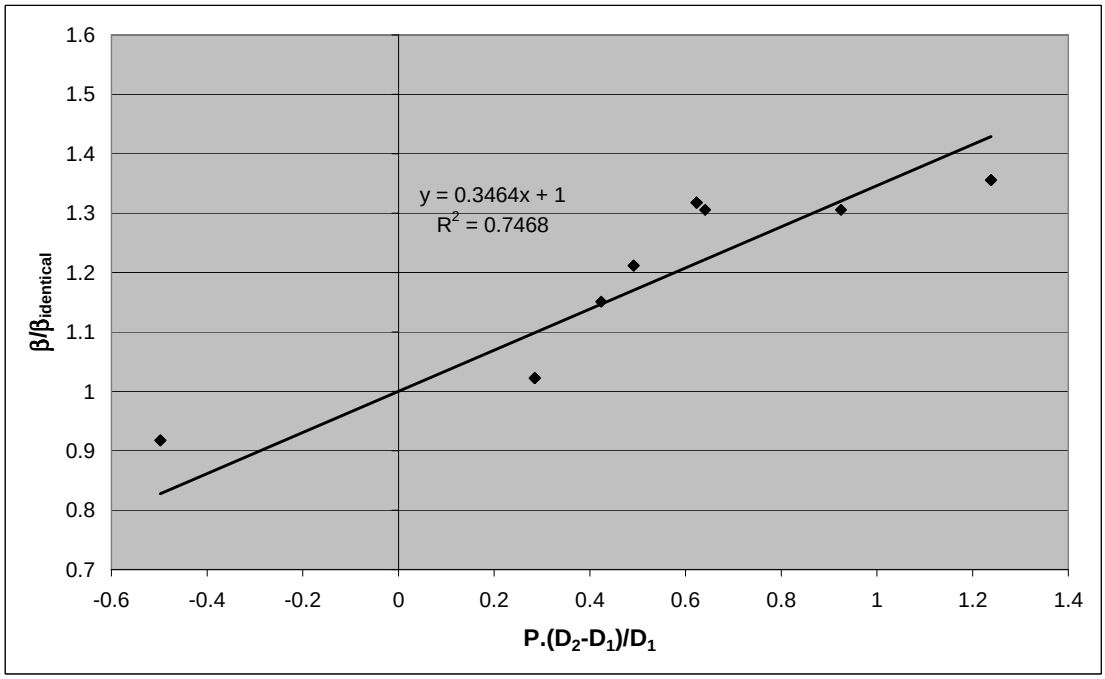

Figure 6-18: Calculated values of β as a function of fluid plasticity (P) and the difference in the diameters of the spheres (D_1 and D_2). β was calculated based on the observed settling velocity of aggregated spheres of cases D and F, and the average diameters of the spheres were used to calculate Re*.

Based on this finding, a correlation of β as a function of the dimensional differences between the first and second sphere can be obtained:

$$\beta = 0.534 \times \left[1 + 0.3464 \times \left(P.\frac{D_2 - D_1}{D_1}\right)\right] \qquad \textbf{(6-9)}$$

The results of this calculation can be seen in Figure 6-19, where a high proportionality and regression between the calculated and observed values of settling velocities can be observed. The relative standard error of this calculation was found to be 15.8% and no trends were found in the calculation error. This

promising result suggests that equation 6-9 can be used to effectively predict the settling velocity of two aggregated spheres, within the parameters of the experiment.

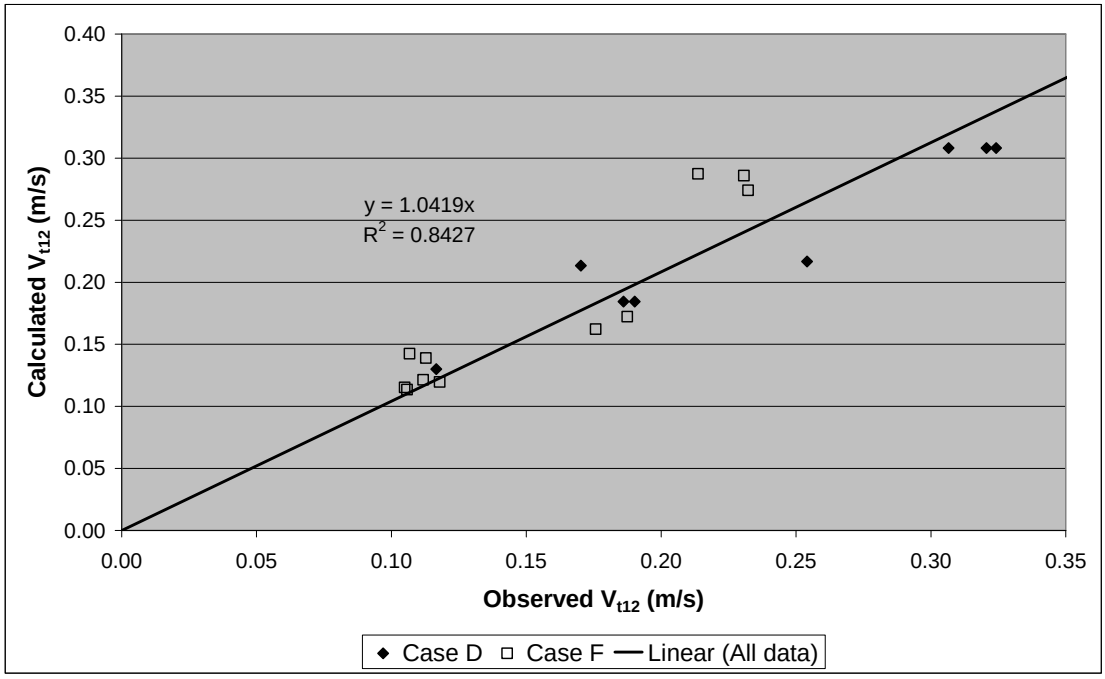

Figure 6-19: Calculated values of the settling velocity of aggregated spheres for cases D and F, as a function of the corresponding observed values. Equation 6-9 was used to calculate the path interference between the two spheres as they combine and form an aggregate. The average values of the sphere diameters were used to calculate Re*.

6.6 Conclusions

In this chapter, an experimental study of the settling behaviour of spherical particles in aqueous solutions of polyacrylamide has been presented. In particular, the effects of the dynamic properties of the fluid viscous parameters were examined. The parameters of the experiment were carefully controlled such that prior the commencement of each test, sufficient time is allowed for the fluid to recover its original viscous parameters after being disrupted by the movement of the spheres in the previous test. It was found that a sphere that falls through this fluid medium is able to attain a constant (terminal) settling velocity almost instantaneously upon

its release. On the other hand, a sphere that is released into the same flow path shortly afterwards tends to travel at a velocity that is much higher than the preceding sphere. Furthermore, the trailing sphere tends to continually accelerate as the gap between the two particles decreases. This decrease in gap leads to a collision between the two spheres, after which they combine and travel at the same (constant) velocity.

The results of these experiments were compared with those of other studies, namely the works of Gheissary and van den Brule (1996) and Gueslin et al. (2006b). The determining parameters of the fluid rheology on the settling experiment were then identified based on this analysis. The settling behaviour of the spheres was found to be highly dependent on be the shear characteristics of the fluids. Furthermore, within the parameters of the experiment, the elasticity of the fluids was not found to greatly influence the settling velocity of the spheres. This view was supported by the results of the numerical studies (see Chapter 5). It also agrees with the dynamic analysis discussed earlier in Chapter 4, in which it was found that the characteristic relaxation times of the fluids due to elastic deformation were relatively short in comparison to the relaxation times due to viscous deformation.

The discrepancy in the settling behaviour of the two spheres can therefore be attributed towards the changes in the structure of the fluid, which, as has been discovered earlier in Chapter 4, correlates directly with the fluid viscous parameters. The presence of this structure has been attributed to the inter- and intra- molecular interactions in the fluid, resulting from the hydrogen bonding between the polyacrylamide and water molecules. In the fluid model developed in Chapter 4, i.e. the semi-viscoplastic model, a correlation was made between the viscous properties of the fluids with the integrity of this fluid structure, here represented by the scalar variable, λ. The fluctuation of λ depends highly on the amount of shear that the fluid is subjected to. Therefore, in the settling-sphere experiment, the shearing movement of the spheres induces processes of breakdown and recovery in the fluid structure, resulting in large fluctuations in the values of the λ. Based on this fluid model, two new parameters, $\overline{\lambda}_{ss}$ and $\overline{\lambda}_{0}$, were developed

to represent the structural conditions of the fluid medium above and below the spheres, respectively.

Using a set of 662 data points, comprising of the settling velocities of both the leading and trailing spheres, a correlation was developed between the representative figures of fluid structure parameter ($\overline{\lambda}_{ss}$ and $\overline{\lambda}_{0}$), the plasticity of the fluid solutions (P), and the average fluid structure parameter surrounding the spheres ($\overline{\lambda}_{eff}$). The latter variable determines the equivalent viscosity of the fluid (μ_{eq}), which, as has been proposed by Wilson et al. (2004; 2003), represents a calculated figure of Newtonian viscosity that would produce the same settling velocity for a particle settling in a non-Newtonian medium.

The resulting correlation can therefore be viewed as an extension to the correlation suggested by Wilson et al. (2004; 2003). Through this correlation, the settling velocity of spherical particles falling through fluid media of various structural conditions, i.e. whether it is completely stabilised or is undergoing processes of recovery after being subjected to shear, can be predicted with much higher accuracy than previously. It is also more widely applicable than the correlation proposed by Gumulya et al. (2007), in which different equations were used for fluids of different structural conditions. Subsequent tests indicate that this generalised correlation is capable of providing satisfactory predictions for the settling velocity of spheres in experiments where the two spheres possess different diameter and/or density. Furthermore, in cases where two spheres have collided and aggregated, a satisfactory prediction of the value of their terminal settling velocity can be obtained, by considering the effects of path interference induced by the arrangement of the spheres and calculating the effective shear stress resulting from this settling orientation. The applicability of the correlation towards these cases supports the validity of the analysis outlined in this study.

Chapter 7 The settling behaviour of two horizontally-aligned spheres

7.1 Introduction

Having developed a suitable correlation for the settling behaviour of spheres in viscoplastic fluids (see discussion in Chapter 6), the focus of the work now turns towards the nature of interaction that exists between spheres that are settling in close proximity to each other in the test fluids. By conducting this study, it is hoped that the settling behaviour of spheres in these types of fluids can be further characterised and the parameters influencing this behaviour can be determined.

In Chapter 4, a detailed study on the rheology of the test solutions, which are essentially polyacrylamide (commercially known as Floxit) solutions in water (0.9, 1.0, and 1.1 % w/w), have been presented. Through this study, it was established that the fluid solutions exhibit thixotropic and elastic characteristics in addition to their viscoplasticity. To describe the shear properties of the test solutions, a fluid model that correlates the viscosity of the fluid with a scalar variable that represents its 'structure' was developed. Although this variable is certainly not a direct measure of the actual 'structure' that exists within the fluid medium, it is considered to reflect the level of hydrogen bonding that exists between the polyacrylamide and water molecules. It is this phenomenon of hydrogen bonding that is believed to contribute significantly to the rheological characteristics of the solutions (Kulicke et al., 1982). The resulting fluid model, which was developed based on the structural kinetics approach commonly used to describe the flow behaviour of thixotropic fluids, was found to be able to satisfactorily describe the steady and time-dependent shear properties of the fluid. Furthermore, upon examining the dynamic properties of the fluid model, it was found that a fluid medium that is fully intact in structure requires the application of stresses that are significantly larger in magnitude for the initiation of its deformation than in cases where the structure of the fluid is already partially-deformed. Due to this dynamic characteristic, in which the fluid model seems to exhibit a temporary yield

stress-like quality, the fluid model becomes known as the 'semi-viscoplastic' model. The first normal stress differences arising from the elasticity of the fluids have been correlated with the rate-of-shear through a set of power-law equations.

To examine the effects of inter-sphere interaction on the settling behaviour of spheres in viscoplastic fluids, experiments involving the simultaneous release of two identical spheres positioned side-by-side, but with a set distance apart (25.0, 37.5, and 50.0 mm), were conducted. The equipment and procedures surrounding this study have been discussed in detail in Chapter 3. In this chapter, the trajectory of the particles resulting from this experiment will be discussed. Possible factors that may affect the interaction of the particles will then be identified, and the results of a numerical study conducted using the semi-viscoplastic fluid model will be compared to those obtained experimentally. Finally, a correlation between the parameters of the experiments and the interaction tendencies of the particles, based on the observations resulting from the experiment and the CFD simulations, will be developed.

7.2 Analysis of experimental data

7.2.1 Primary observations: flow profiles

In Figure 7-1, the typical flow profiles obtained from experiments of side-by-side spheres in the test fluid solutions have been presented. In this Figure, the variation of the polar coordinates of the horizontal axis, i.e. $r=\sqrt{x^2+y^2}$, of each sphere as they settle through the column can be inspected.

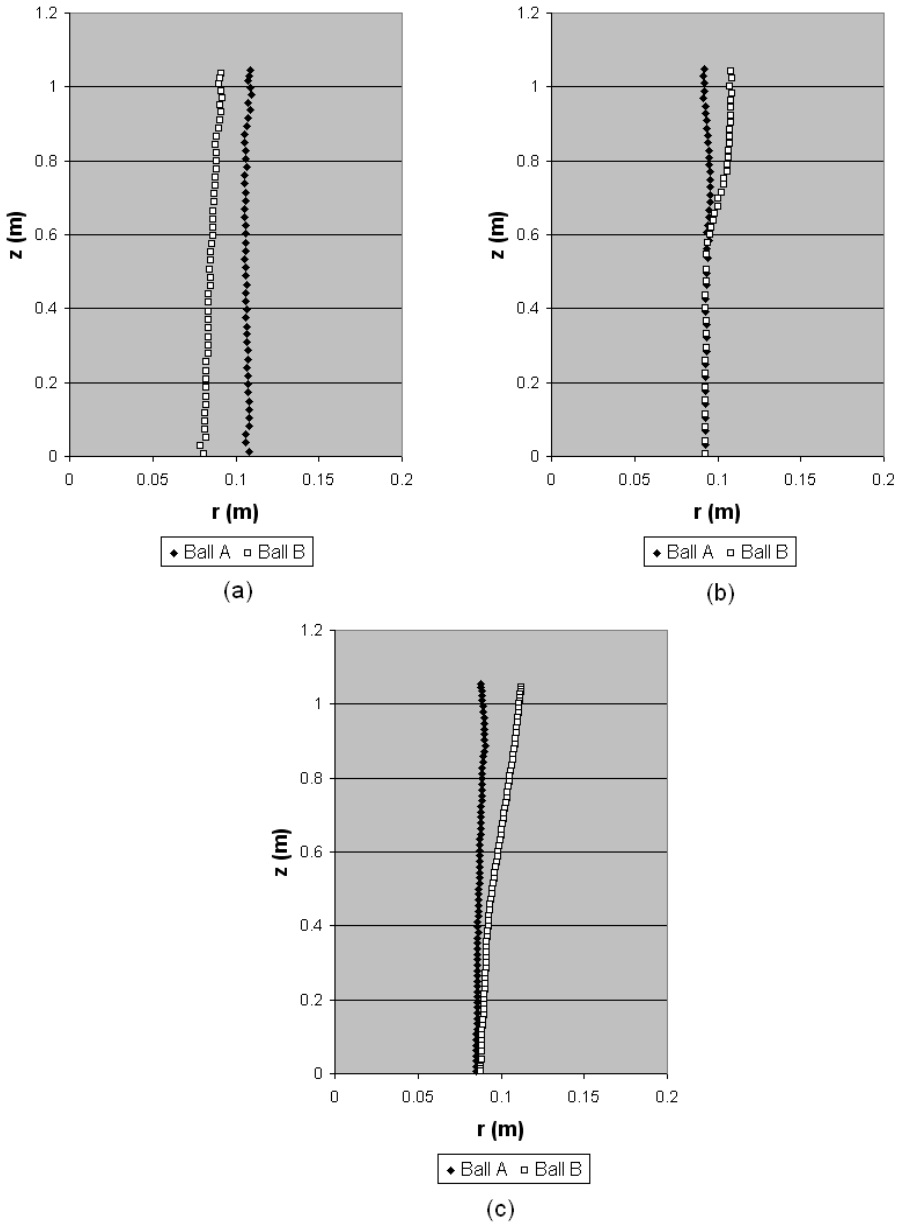

Figure 7-1: Typical settling trajectories of two horizontally-aligned spheres, with an example for each case: (a) slight repulsion between the spheres [ρ_s = 7792.2 kg/m^3, D = 7.95 mm, 0.9% Floxit, initial separation distance (d_0) = 25 mm]; (b) strong inter-sphere attraction [ρ_s = 7638 kg/m^3, D = 6.35 mm, 1.1% Floxit, d_0 = 25 mm]; (c) weak inter-sphere attraction [ρ_s = 7638 kg/m^3, D = 9.95 mm, 1.1% Floxit, d_0 = 25 mm].

Three general types of flow profile were obtained in this experiment. In the first type of the flow profile, represented here by Figure 7-1(a), the two spheres tend to

repel very slightly as they settle. In Figure 7-1(b), on the other hand, the two spheres tend to strongly attract. This interaction results in a collision between the two spheres, after which, much like the flow path obtained for the experiment involving two vertically-aligned spheres, the two particles appear to become attached and settle at the same pace. In the third type of flow trajectory (Figure 7-1(c)), the two spheres can be seen to display similar tendencies to attract as that shown in Figure 7-1(b). In this case, however, the reduction in the horizontal distance between the two spheres appears to be less rapid than that shown in Figure 7-1(b). As a result, the two spheres do not undergo any collision within the duration of the settling experiment.

Interestingly, in both cases where the two spheres show tendencies to attract and converge (see Figure 7-1(b) and Figure 7-1(c)), non-symmetrical flow trajectories were obtained. For example, in Figure 7-1(b), it can be seen that ball B travels more towards ball A than vice versa. As a result, the path travelled by ball B prior to the collision appears to be longer than that of ball A. Similar non-symmetrical pattern is also evident in the interaction between the spheres in the case presented in Figure 7-1(c).

The non-symmetrical trajectory of the two particles can be further inspected in Figure 7-2, where snapshots of the paths taken by the two particles as they interact and collide are presented. In this Figure, it can be seen that although ball B appears to possess more side-movement than ball A, it also settles at a slightly lower pace. In fact, at this particular instance, the settling velocity of ball B has been found to be ~ 5.4% lower than that of ball A. This results in ball B emerging towards the flow path of ball A, with ball B placed slightly higher than ball A. As the flow paths of the two spheres converge, ball B starts to behave much like the second sphere in the experiment of two consecutive releases in the fluid, where the trailing sphere starts to increase in velocity and collides with the leading sphere.

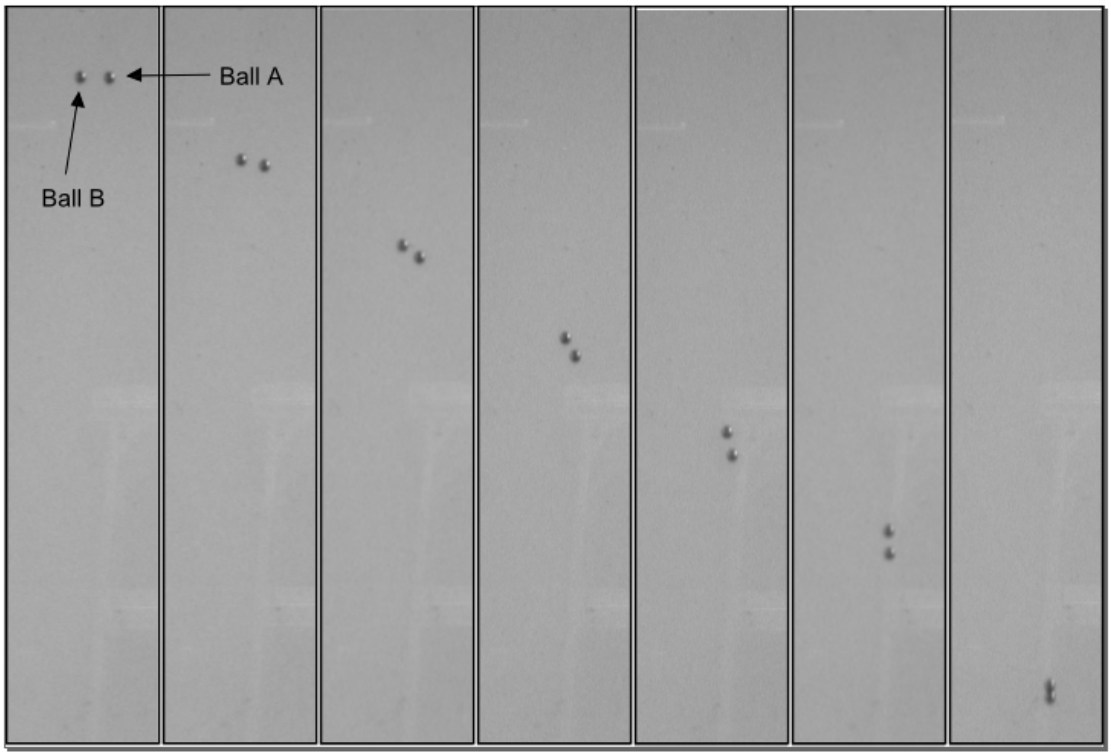

Figure 7-2: Snapshots of the experiment of two horizontally-aligned stainless steel spheres (6.35 mm) in 1.1% Floxit solution with initial distance of 25 mm.

The re-orientation between two interacting spheres as they settle through the Floxit solution is likely to be caused by the interaction of the wakes behind them, as well as the effects of shear thinning in the region surrounding the spheres. Unfortunately, this aspect of the settling experiment cannot be examined with the current experimental setup, as its investigation would require the flow fields surrounding the spheres to be visualised. This examination would therefore require the incorporation of flow-visualisation techniques, such as Particle Image Velocimetry (PIV), into the sphere-settling experiment. This development of the experimental technique has been considered for future studies (see Section 8.2).

7.2.2 Velocity profile

Except for cases where the two spheres rapidly converge and are about to collide, upon which the trailing sphere would start to accelerate towards the leading

sphere, no significant deviations in the settling velocity of the spheres from the value of their terminal velocity (± 6 %) were detected. The interaction between the spheres, therefore, does not appear to significantly affect their settling velocities.

The onset of the acceleration observed in the settling behaviour of the trailing sphere as the horizontal distance between the two spheres diminishes can be examined further in Figure 7-3 and Figure 7-4. In these Figures, the orientations of two interacting spheres with respect to each other, as indicated by their separation distance, have been presented. To aid this analysis, the separation distance between the two spheres has been divided into two components: horizontal (d_H) and vertical (d_V). At the beginning of the side-by-side sphere-settling experiment, i.e. time = 0 s, the value of d_V is zero, reflecting the fact that two spheres are horizontally-aligned. The value of d_H at this point equals to d_0, which is the set value of initial separation distance between the two spheres.

In Figure 7-3, the typical fluctuation in the separation distance between the spheres in experiments that feature weak inter-sphere attraction (an example of this is the experiment featured in Figure 7-1(c)) has been presented. In this Figure, the fluctuations in d_H and d_V, starting from the commencement of the experiment (time = 0 s) to the instance at which the two spheres exit the column (time = 3.6 s) have been shown. As can be seen in this Figure, the decrease in d_H is relatively slow, with the final value of d_H being found to be ~ 0.0032 m. Interestingly, Figure 7-3 also shows that this decrease in d_H is accompanied by significant increase in d_V. This reflects the observation stated earlier in Section 7.3.1, where the tendency of the spheres to 're-orientate' while converging towards each other has been noted.

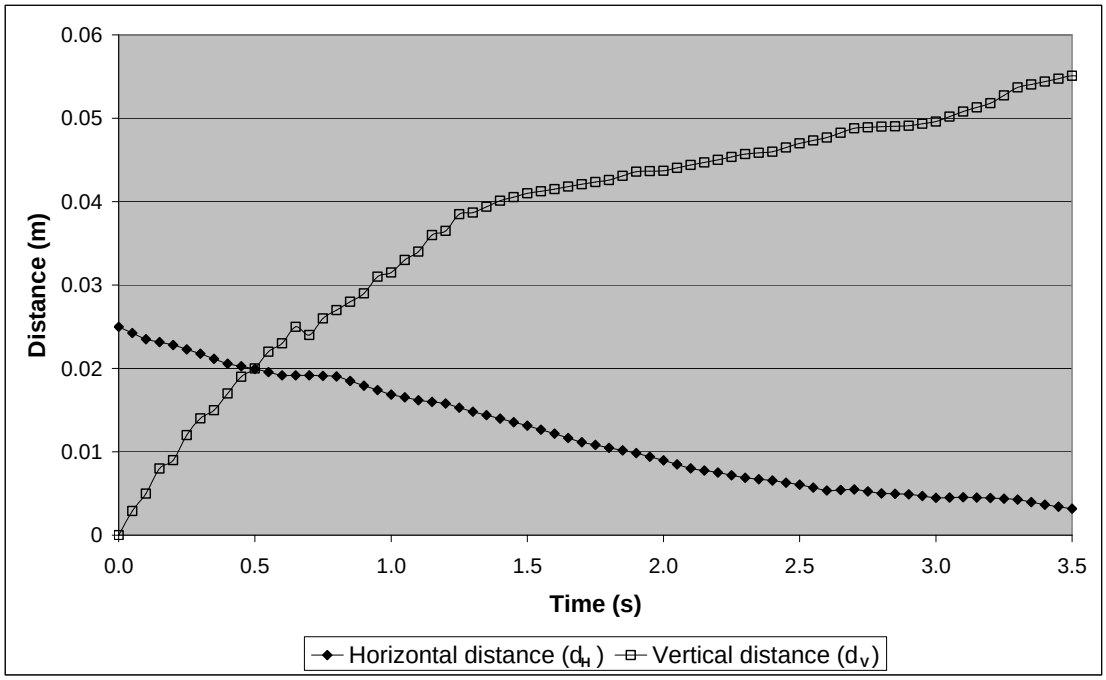

Figure 7-3: Variation of the horizontal and vertical distances between two stainless steel spheres (9.95 mm) released side by side with an initial distance of 25.0 mm in a 1.0% Floxit solution, as a function of the time of the experiment since their time of release.

In Figure 7-4, the fluctuations in the separation distance between the spheres for cases where strong inter-sphere attraction, such as that shown in Figure 7-1(b), have been presented. As expected, the decline in d_H for this case is more rapid than in the case presented in Figure 7-3. Due to this strong interaction, the two spheres converge and collide at time ~ 5.2 s, prior to the two spheres exiting the column at time ~ 6.0 s. Similar to the case presented in Figure 7-3, Figure 7-4 also shows increasing trends in d_V that occurs in conjunction with the decrease in d_H. This reflects the re-orientation motion that occurs as the two spheres converge, where one sphere appears to possess a slightly higher settling velocity than the other, forcing the slower sphere to trail behind. In Figure 7-4, this increase in d_V continues to occur, until a d_H value of ~ 0.0015 m is reached, upon which the trailing sphere starts to accelerate and catches up with the leading sphere.

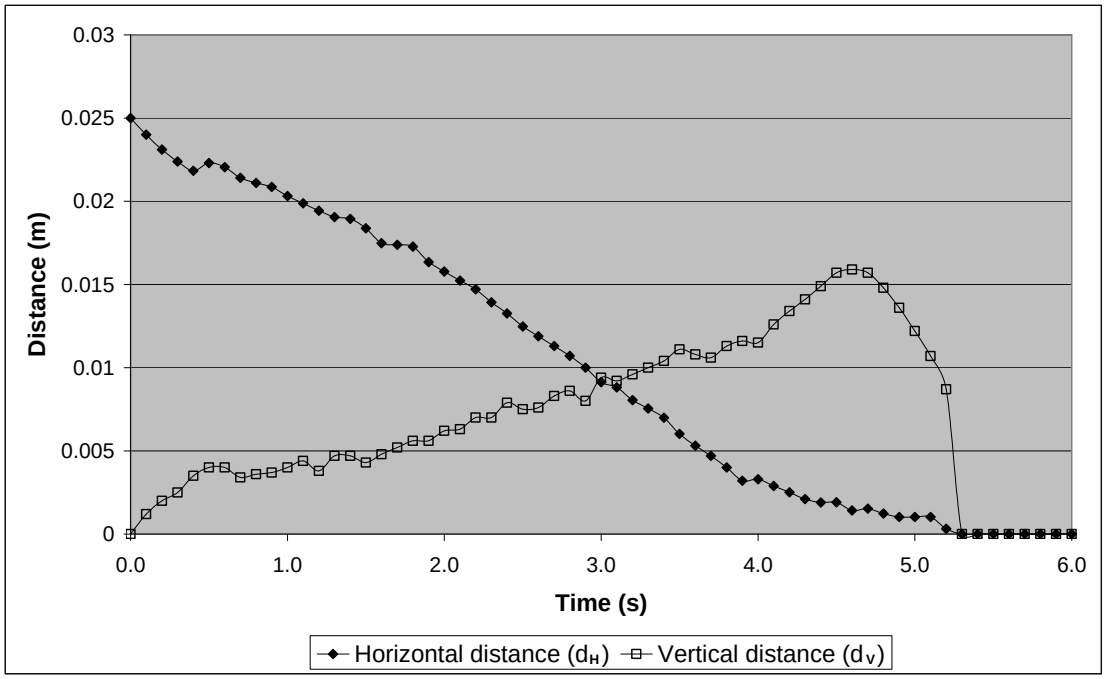

Figure 7-4: Variation of the horizontal and vertical distances between two chrome steel spheres (6.35 mm) released side-by-side with an initial distance of 25 mm in a 1.0% Floxit solution, as a function of the time of the experiment since their time of release.

The patterns of fluctuation in d_H and d_V as described above, in which the vertical separation distance between the two spheres increases as they rearrange their orientation towards each other, were observed in all of the cases that display convergent behaviour between the two spheres. In cases where the interaction between the two spheres is relatively strong, the two spheres may converge significantly such that their horizontal separation distance reduces to ~ 1–2 mm. At this instance, the sphere that is positioned behind the leading sphere would start to accelerate, causing a collision between the two. This behaviour is viewed to be similar to the settling behaviour of spheres settling one behind the other, i.e. vertically aligned. The parameters affecting the settling pattern of these spheres have been discussed thoroughly in Chapter 6, where the acceleration observed in the settling pattern of the trailing sphere was found to be caused by the changes in the viscous parameters of the fluid solutions.

7.2.3 Comparison with other flow profiles

Several studies that examine the interaction of spheres that are settling close-by each other in different types of fluids have been conducted in the past. These studies include those of Wu and Manasseh (1998) and Joseph et al. (1994) (see review in Section 2.4.5.2), through which it has been discovered that the interaction of spheres settling in Newtonian fluids always tend to produce an effect of repulsion between the spheres. Furthermore, Joseph et al. (1994), who conducted their experiments in a variety of fluids (namely Newtonian, non-elastic shear-thinning, Boger, and viscoelastic fluids), reported that the tendencies of spheres attract and converge were only found in fluids that exhibit elastic properties. Joseph et al. (1994) also noted that this tendency to attract and converge is only obtained in cases where the set value of initial separation distance between the two spheres is relatively small. Through this observation, Joseph et al. (1994) suggested that a critical parameter of initial separation distance should be used for the analysis of this experiment. That is, in cases where the d_0 values are below this critical parameter, convergent sphere behaviour would be observed, whereas beyond this region of criticality, the two spheres would appear to slightly diverge. As will be demonstrated later in Section 7.4, this analytical approach of the sphere-settling experiment has been adopted and developed further in this thesis.

In agreement with the observations obtained from the current project, Joseph et al. (1994) also noted that in cases where the two spheres do attract and converge, the interaction between the spheres tend to be non-symmetrical. Furthermore, the re-orientation motion of the two spheres, where one of the spheres tends to move towards the flow-path, i.e. behind, the other sphere, was also observed. No explanations were given towards flow mechanisms responsible for this behaviour.

Based on this comparative analysis, it was concluded that the interaction of particles settling in the Floxit solutions depends highly on the elasticity of the fluid and that the attraction between two settling spheres as observed earlier in Section 7.2.1 is mainly caused by the elasticity of the test fluids. The accuracy of this

statement and the effects of other rheological properties of the fluids in the current study will be assessed in the next section.

7.2.4 Parameters governing the extent of inter-sphere interactions

The tendency of spheres to attract and converge has previously been identified by Joseph et al. (1994) to be highly dependent on the initial separation distance that has been set between them. In this thesis, the tendency of spheres to attract and converge has been quantified through the parameter ℓ_C, which signifies the vertical distance that has to be travelled by the spheres prior to their convergence. This point of convergence has been defined as the instance where the trailing sphere starts to accelerate towards the leading one, i.e. when the horizontal separation distance between the spheres reaches levels that are below 0.002 m. According to this definition, the point of convergence in the case presented in Figure 7-4 occurs at experimental time of ~ 4.6 s. In Table 7-1, the values of ℓ_C resulting from some selected data points have been presented. The values of ℓ_C in this Table has been normalised against the terminal settling velocity and shear-rate of the spheres. In this Table, the tendencies of the spheres to diverge or slowly converge (in which cases no collision would be observed) can also be inspected, as symbolised by (x) and (-), respectively.

Table 7-1: The effects of sphere diameter on the tendency of spheres to interact and attract, as indicated by the dimensionless vertical distances that have to be travelled by the spheres prior to their collision. Data resulting from bronze spheres was used.

D (mm)	d_0 (mm)	Interaction parameter = $\left[(\ell_C/V_t)\dot{\gamma}\right]$		
		0.9% Floxit	1.0% Floxit	1.1% Floxit
6.35	25.0	673.3	306.5	115.5
6.35	37.5	x	-	317.8
6.35	50.0	x	-	-
7.95	25.0	x	x	444.4
7.95	37.5	x	x	-
7.95	50.0	x	x	x
9.95	25.0	x	x	518.7
9.95	37.5	x	x	x
9.95	50.0	x	x	x

Note: (x) Spheres diverge
(-) Spheres slowly converge and do not undergo collision

As expected, Table 7-1 shows that strong interaction between spheres generally occurs in cases where the set values of initial separation distance are small (25.0 mm). As the value of initial separation distance is increased, the tendencies of spheres to attract and collide appear to decrease rapidly. This trend is clearly demonstrated in the comparison of the interaction of bronze spheres of 7.95 mm diameter that are settling in the 1.1% Floxit solution.

Table 7-1 also shows that the tendencies for spheres to attract and converge are more prominent in the solutions containing higher concentrations of Floxit, i.e. spheres settling in the 1.1% Floxit solution would show higher tendencies to converge and collide than those settling in the 0.9% Floxit solution. Moreover, Table 7-1 also shows that the value of the interaction parameter $\left[(\ell_C/V_t)\dot{\gamma}\right]$ generally decreases with increasing Floxit concentration. This suggests that for the same configurations of settling experiment, spheres settling in 1.1% Floxit solution would require shorter travelling distance to converge than those settling in 1.0% and 0.9% Floxit solutions.

The tendency of spheres to attract and converge while settling in the more concentrated Floxit solutions was compared to the elastic properties of the fluids. The contribution of the fluid elasticity on the settling-sphere experiment has earlier been assessed based on the values of their characteristic relaxation times (due to elastic deformations). Through this analysis, it was discovered that the 1.1% Floxit solution possesses the longest relaxation time among the three test solutions, while the 0.9% Floxit solution the shortest (1.63, 2.15, and 2.99 s, for the 0.9, 1.0, and 1.1% Floxit solutions, respectively, see discussion in Section 4.6). The tendency of the spheres to interact and attract, therefore, appears to reflect the elastic properties of the test fluids. It was thus concluded that for the interaction of spheres to be examined thoroughly, the elastic properties of the fluid needs to be taken into consideration.

The interaction parameters presented in Table 7-1 also suggest that the tendencies of spheres to attract and converge decreases significantly with increasing particle size (or sphere diameter). Moreover, in cases where the spheres do attract, higher values of interaction parameters are obtained in the case of the larger spheres, suggesting that the spheres have to travel over longer distances prior to their convergence.

In Table 7-2, the dependency of the inter-sphere interaction on the density of the spheres has been assessed. From this Table, it can be seen that lower interaction parameters are generally encountered in cases where lighter spheres were used ($\rho_{steel} < \rho_{chrome} < \rho_{bronze}$). This suggests that, with respect of the settling velocities of the spheres, interacting particles with lower values of specific gravity would require shorter travelling distance to converge. Based on this observation and the observation stated earlier regarding the dependency of the sphere interaction on the diameter of the sphere, it was concluded that spheres having lower values of shear stress, which is a parameter that is determined by the density and diameter of the sphere (see equation 2-47), would have higher tendencies to attract and converge while settling side-by-side.

Table 7-2: The effects of sphere density on the tendency of spheres to interact and attract, as indicated by the dimensionless vertical distances that have to be travelled by the spheres prior to their collision. Data resulting from bronze spheres was used.

Sphere	D (mm)	Interaction parameter = $\left[(\ell_c / V_t)\dot{\gamma}\right]$		
		0.9% Floxit	1.0% Floxit	1.1% Floxit
Bronze	6.25	673.3	306.5	148.8
Chrome	6.25	318.1	234.3	123.2
Steel	6.25	239.4	139.7	110.8
Bronze	7.95	x	x	444.4
Chrome	7.95	-	730.6	204.7
Steel	7.95	-	349.9	192.3

Note: (x) Spheres diverge
(-) Spheres slowly converge and do not undergo collision

7.3 Numerical study

In Section 7.2, the settling behaviour of spheres positioned side-by-side in the test fluid solutions has been studied and parameters that influence the movement of the spheres have been identified. Complete assessment of the factors influencing the divergent and convergent flow profiles obtained during the experiment, however, could not be conducted based solely on these observations. This is mainly caused by the rheological complexity of the fluid solutions, which, as have been discussed thoroughly in Chapter 4, possess elastic characteristics in addition to their viscoplasticity and thixotropy. This combination of flow characteristics makes it difficult to isolate the effects of each contributing element, i.e. viscous and elastic, on the experiment.

Traditionally, the contribution of the rheological characteristics mentioned above can be determined by conducting a series of comparative experiments, which are performed in various types of fluids, such as Newtonian, viscous, and Boger fluids. An example of this approach is the study conducted by Joseph et al. (1994), where the effects of shear thinning and fluid elasticity on the interaction of spheres settling side-by-side were evaluated by conducting the experiments in fluids of various elasticity and viscous characteristics.

In the current study, a different approach has been adopted for this analysis, i.e. through numerical methods (CFD). The basis of this approach has been discussed thoroughly in Chapter 5, where the settling behaviour of a sphere in fluid solutions modelled with a non-elastic shear thinning fluid model that features a temporary yield stress-like characteristics, i.e. the semi-viscoplastic fluid model, was studied numerically. Through this examination, it was found that an excellent qualitative agreement exists between the values of settling velocity predicted numerically with those obtained experimentally in all three Floxit solutions. Given that the three Floxit solutions actually exhibit slightly distinct levels of elasticity (as evident in the fit parameters for the normal stresses outlined in Table 4-5), the findings stated above indicate that the fall behaviour of these spheres is largely dependent on the viscous parameters of the fluid solutions, and that the elasticity of the fluid solutions does not greatly affect the settling velocity of the particles.

Using the approach previously outlined in Chapter 5, it is hoped that similar assessments on the contributions of the various rheological elements can be conducted for the analysis of the fall behaviour of spheres settling side-by-side in the Floxit solutions. This numerical approach will be discussed briefly in the next section, followed by the resulting flow profiles predicted through this numerical analysis.

7.3.1 Mathematical formulation and solving strategy

The numerical strategy employed for this study is based on the particle-tracking method, in which the Volume-of-Fluid (VOF) algorithm is used. In this numerical scheme, the spherical particles are represented by a 'solid' phase, which in turn is represented by a highly viscous fluid material (~ 1000-2000 Pa.s). These spherical particles settle through a primary fluid phase that represents the viscosity of the test fluid solutions. To minimise the deformation of the 'solid' phase, in addition to assigning a very high value of the viscosity of the secondary 'solid' phase (~ 200 times the liquid viscosity), appropriate methods of discretisation have to be

employed. The methods of approximation and discretisation utilised for this study have been discussed in detail in chapter 5.

The numerical grid used for the current study follows the same dimensioning and meshing principles as that described in section 5.6.1. A structured grid was employed to minimise the level of interface smearing, and the size of the mesh was determined based on the diameter of the sphere, such that there are 12 or more node points across its diameter. As this problem involves two spheres that are settling side-by-side, the numerical domain has to be wider than that used in section 5.6.1, to allow for the spheres to settle freely with minimum wall effects. As a result, simulations involving horizontally aligned spheres generally require more node points and are more computationally expensive.

7.3.2 Results and discussion

Figure 7-5 shows the typical settling trajectory predicted numerically for two spheres settling side-by-side in a fluid solution modelled with the semi-viscoplastic equation. As can be seen, divergent sphere behaviour is evident, with the horizontal distance between the spheres increasing throughout the settling process. This behaviour was observed in all of the simulations, which were conducted under various values of initial-distance-to-sphere-diameter ratio (d_0/D = 1.5, 2.0, and 2.5), as well as three different viscous parameters, modelled after solutions of 0.9%, 1.0%, and 1.1% Floxit.

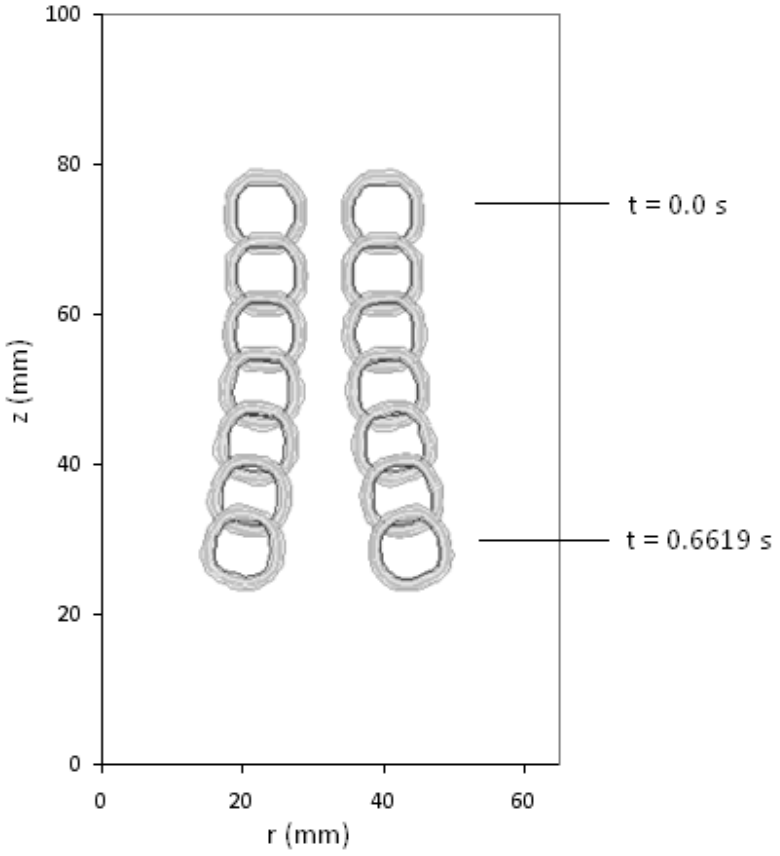

Figure 7-5: The settling trajectory of side-by-side spheres (D = 9.90 mm) in a 0.9% Floxit solution, with a d_0/D value of 1.5.

The interaction between the spheres under different values of initial distances and Reynolds numbers can be inspected further in Figure 7-6. In this figure, it can be seen that simulations involving higher values of Re, here calculated as per equation 5-20, generally predict stronger inter-sphere repulsion than those involving lower values of Re. This is similar to the observations of Wu and Manasseh (1998), who conducted their experiments in Newtonian fluids. In their study, it was observed that for cases where $Re > 0.1$, spheres that are placed in close proximity to each other always tend to repulse and diverge. For cases where $Re < 0.1$, on the other hand, no interaction tendencies were detected, and the spheres tend to maintain a constant distance between each other.

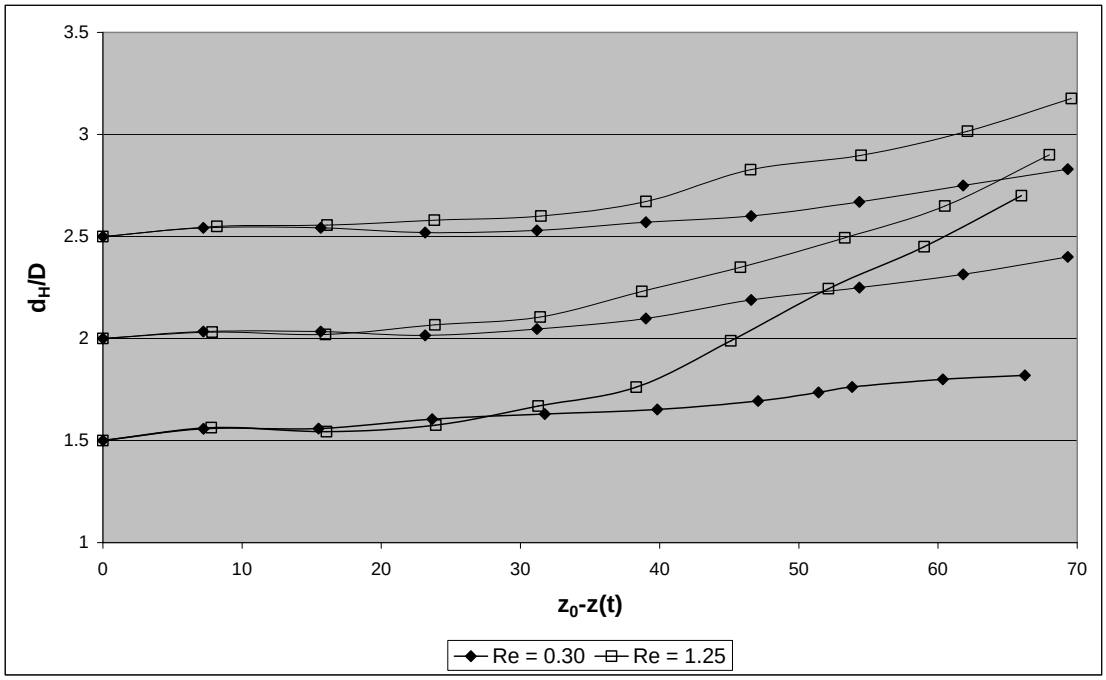

Figure 7-6: Development of inter-sphere distance as the spheres settle through the semi-viscoplastic fluid. In the simulations featuring Re ~ 0.3, the viscous parameters resulting from the 1.1% Floxit solution were utilised. On the other hand, in cases where Re ~ 1.25, the viscous parameters of 0.9% Floxit were used.

The repulsive behaviour predicted through this numerical study can also be examined by observing the development of velocity field in the fluid medium surrounding the spheres. This is presented in Figure 7-7, where the development of the relative axial velocity along the horizontal axis has been illustrated. The origin of the x-axis in this figure indicates the centre line of the computational domain. The positions of the spheres in this Figure can be determined through the values of relative velocity, with V/V_t values of 1.0 indicating regions that are occupied by the spheres. In this Figure, the repulsion between the two spheres is evident in the widening of the gap between the two spheres as the simulation progresses from t = 0.10 s to t = 0.75 s.

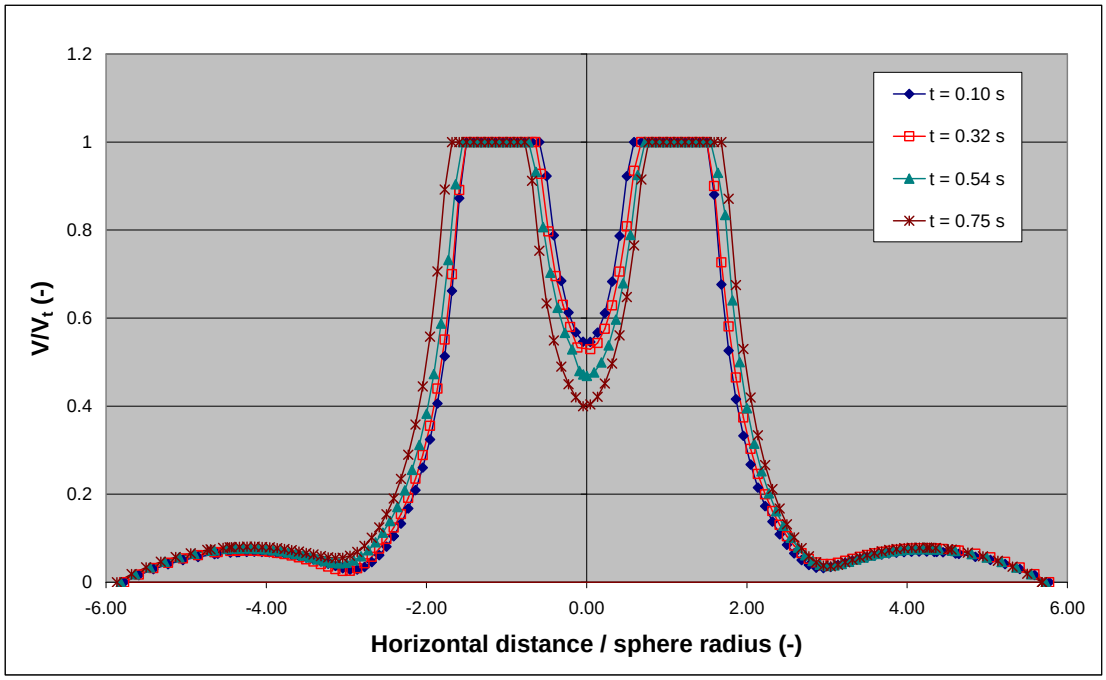

Figure 7-7: The distribution of axial velocity, relative to the terminal settling velocity of the spheres. The origin of the horizontal axis indicates the centre line of the computational domain.

In Figure 7-7, it can be seen that there is a negative shift, both in terms of position and magnitude, in the point of local velocity minimum in the gap between the two settling spheres. This negative shift continues to occur as the simulation is extended from simulation times of 0.10 to 0.75 s. It thus reflects the widening of the gap between the two spheres during the course of the simulation. The decrease in the magnitude of the minimum velocity in this region indicates that the inter-sphere repulsion evident in this numerical study is caused by the effects of the dynamic pressure between the two spheres. Due to the inability of the fluid medium in this region to deform elastically, the minimisation of pressure in this case occurs through the widening of the gap between the two spheres, which in turn decreases the magnitude of velocity within the gap.

Outside this region of interaction, i.e. in the area encompassing the outer side of the sphere and the walls of the column (0.5 – 4.7R), the changes of the distribution of velocity were found to be minimal throughout the simulation process. The local

velocity maximum that can be observed at a distance of ~ 3.2R to the right of the sphere is due to the recirculation of flow, as the region of fluid that has been displaced by the movement of the sphere recirculates back to regions above the settling spheres.

Based on the observations outline above, it can be concluded that the decrease in the horizontal distance between two spheres that are settling closely side-by-side in the Floxit solutions are largely caused by the elastic properties of the fluid solutions, which is an aspect of the fluid rheology that has not been captured by the semi-viscoplastic fluid model. To develop a method of predicting the interaction between the spheres being studied in this experiment, therefore, considerations need to be given towards the elastic characteristics of the fluid solutions.

7.4 Correlation for the prediction of inter-particle interaction

So far in this discussion, it has been demonstrated that the experimental and numerical observations of the fall behaviour of spheres settling side-by-side generally agree with the findings presented by other studies, namely those by Joseph et al. (1994) and Wu and Manasseh (1998) for the settling behaviour of spheres in viscoelastic and non-elastic fluids, respectively. Based on this agreement, it was concluded that the unique interactive behaviour of spheres observed in the current experiment, in which two spheres that are initially placed in close proximity to each other demonstrate tendencies to attract and converge, are due to the elastic properties of the fluids that the spheres are released into.

To develop a correlation for the prediction of the interaction tendencies of the settling spheres, therefore, the extent of elastic deformation in the fluid medium during this experiment needs to be examined. In this section, a parameter that represents the interactive tendencies of the spheres will be firstly developed, followed by an assessment on the factors influencing these interactions. A correlation will then be developed and assessed based on these observations.

7.4.1 Interaction parameter

The tendency of two settling spheres to interact and attract can be quantified by considering the distance required for the spheres to converge, ℓ_C . The dimensionless form of this parameter was developed by considering the terminal settling velocity of the spheres (V_t), as well as the effective rate-of-shear ($\dot{\gamma}$) due to the effective shear stress of the spheres ($\bar{\tau}$, see equations 2-46 and 2-47):

$$\frac{V_t}{\ell_C \dot{\gamma}} \tag{7-1}$$

Another form of quantification for the tendency of the spheres to interact can be derived by estimating the rate of convergence between the two spheres, V_H:

$$V_H = \frac{\Delta d_H}{\Delta t} \tag{7-2}$$

As can be seen in the above equation, the rate of convergence has been estimated by taking the average rate-of-change in the horizontal component of the separation distance between the spheres, d_H.

Based on the approximated value of V_H, the vertical distance that needs to be travelled by spheres placed side-by-side with an initial spacing of d_0 can be estimated as follows:

$$\ell_C = d_0 \frac{V_t}{V_H} \tag{7-3}$$

The dimensionless form of V_H can thus be written as:

$$\frac{V_t}{\ell_C \dot{\gamma}} \approx \frac{V_H}{d_0 \dot{\gamma}} \tag{7-4}$$

In order to obtain a complete representation of the interactive behaviour of spheres settling side-by-side in the fluid solutions, the two forms of dimensionless interaction parameter presented in equation 7-4 are used in conjunction with each other for the analysis of the experimental data. In doing so, the first form of the dimensionless parameter is generally regarded to be more reliable, as the uncertainties involved with the calculation of the variables involved in this parameter are lower (~ 2%, see Appendix D.2) than those involved with the second form of the dimensionless parameter. In the second form, uncertainties arose with the estimation of V_H, in which the rate-of-change in d_H has been assumed to be approximately constant. Based on the variance of the experimental data, the level of uncertainty associated with V_H has been approximated to be ~ 3%, causing the total level of uncertainty for the second form of dimensionless parameter to be ~ 9% (see Appendix D.2).

As a result of the discrepancy in the level of uncertainties involved with the calculations of the dimensionless interaction parameter, the first form of this parameter was implemented for cases where a collision between the two spheres occurs. Additionally, in analysing the experimental data, the discrepancies in the level of uncertainties involved with the calculation of the dimensionless interaction parameter had to be taken into consideration. This aspect of the calculation procedure will be addressed in detail in Section 7.4.4.

7.4.2 Effects of fluid elasticity

To estimate the extent of elastic deformation that occurs during the sphere-settling experiment, the average rate-of-shear experienced by the fluid medium in the region between the spheres needs to be approximated. This is done by considering the amount of fluid displaced due to the movement of one sphere, Q:

$$Q = \frac{\pi D^2}{4} V_t \qquad \textbf{(7-5)}$$

Assuming that the fluid flow rate is independent of the size of the gap (~ d_H), the average shear rate within this gap, $\dot{\gamma}_G$, can then be approximated:

$$\dot{\gamma}_G = \frac{Q}{d_H \, x \, D^2} = \frac{\pi V_t}{4 d_H} \qquad \textbf{(7-6)}$$

Based on this equation, it can be seen that an increase in the effective shear rate can be expected as the gap between the spheres is decreased.

Having approximated the representative value of shear rate in the fluid region between the two settling spheres, the level of elastic deformations that are associated with this shear rate can be estimated. As has been discussed previously in chapter 2, the development of normal stresses in fluid solutions is often associated with the elastic characteristics of the fluid rheology. Therefore, the quantification of fluid elasticity is often accomplished through the measurement of the development of normal-stress differences when the fluid is subjected to shear forces. In this study, this aspect of the fluid rheology is quantified through the first normal-stress difference (N_1), as well as its corresponding coefficient (ψ_1). The development of first normal-stress difference due to the settling movement of two closely-situated spheres is therefore quantified using the power-law fit for the first normal-stress growth coefficient (ψ_1) presented in equation 4-15 and Table 4-5, with the shear rate approximated through equation 7-6.

Using the formulation of the average shear-rate across the gap presented in equation 7-6, it can be seen that at low values of inter-sphere distance, an increase in N_1 is predicted, indicating that the level of elastic deformation at this stage is higher than in cases where the inter-sphere gap is wider. This is in agreement with the experimental observations presented earlier in section 7.2.1, in which it was noted that in experiments where the initial separation distance between the spheres is small (d_0 ~ 25 mm), there is a higher probability that the spheres would converge and collide than in experiments that feature larger values of initial separation distances (d_0 > 37.5 mm).

The influence of other parameters on the interaction between spheres settling in the test fluid solution has been examined earlier in section 7.2.4, where the variation of the interaction parameter $\left[\left(\ell_C/V_t\right)\dot{\gamma}\right]$ for various configurations of spheres and fluid solutions was presented. The results of this analysis show the dependency of the inter-sphere interaction on the density and diameter of the spheres, which are parameters that largely determine the level of stress exerted by the spheres on the fluid medium. For example, the values of $\left[\left(\ell_C/V_t\right)\dot{\gamma}\right]$ presented in Table 7-2 have been shown to be generally smaller for lighter spheres, or spheres having lower values of ρ_s. This indicates that in cases where these spheres exhibit convergent interactive behaviour during their settling process, the lighter spheres would have to travel over shorter distances than in cases where the heavier spheres are used. That is, the lighter spheres tend to possess higher rate-of-convergence than the heavier spheres. Similar observations could be made in comparing the values of critical initial distances in experiments using different sphere diameters.

The dependence of the inter-sphere interaction on the density and diameter of the spheres indicates that a complete assessment of the interactive behaviour of spheres in the fluid solution requires the elastic effects of the fluid to be compared with the corresponding viscous effects. This can be examined by considering the viscosity of the fluid in the region immediately above the settling spheres, μ_{ss}, which can be calculated based on the rate of deformation caused by the mean surficial stress of the sphere ($\bar{\tau}$). In this study, the reference point of shear-stress suggested by Wilson et al. (2004; 2003) (see equations 2-46 and 2-47) were incorporated for the completion of this calculation. Due to the similarity of the comparison between ψ_1 with the viscous properties of the fluid to the Weissenberg analysis presented by Arigo and McKinley (1997), the figure of comparison in this study is termed as We_G:

$$We_G = \frac{\psi_1\left(\dot{\gamma}_G\right)}{2\,\mu\left(\lambda_{ss}\right)}\dot{\gamma}_{ss} \qquad \textbf{(7-7)}$$

where $\psi_1(\dot{\gamma}_G)$ is the coefficient of first normal-stress, evaluated based on the average value of shear-rate across the gap between the spheres. The terms $\mu(\lambda_{ss})$ and $\dot{\gamma}_{ss}$ represent the fluid viscosity and shear rate, respectively, above the settling sphere. These terms are therefore calculated based on the mean surficial stress of the sphere, $\bar{\tau}$.

7.4.3 Effects of initial separation distance

In Figure 7-8, the development of the dimensionless interaction parameter $V_H/(d_0\dot{\gamma})$ with We_G for several different configurations of d_0/D has been presented. In this figure, it can be seen that $V_H/(d_0\dot{\gamma})$ tends to decay rapidly with increasing values of We_G. Furthermore, a general decrease in $V_H/(d_0\dot{\gamma})$ was also obtained with increasing values of d_0/D.

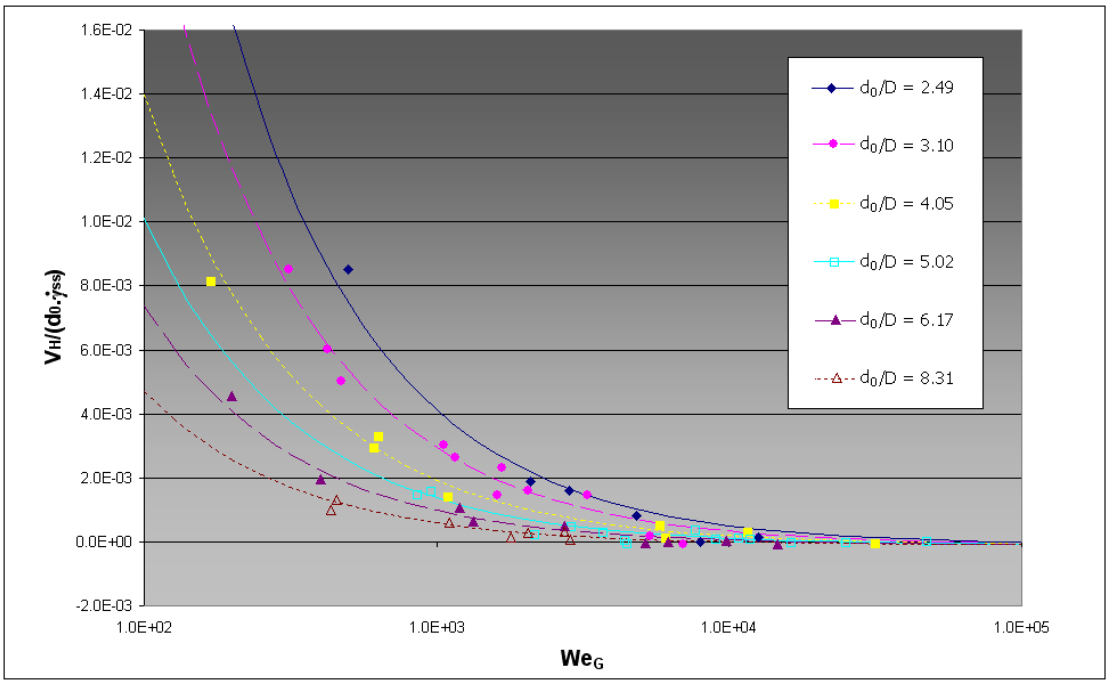

Figure 7-8: Variation of the interaction parameter as a function of We_G and the ratio of the initial sphere-to-sphere distance (d_0) to the diameter of the spheres (D), d_0/D.

Based on the experimental observations outlined in Section 7.2.4, the dependence of the interaction parameter on We_G and d_0/D as seen in Figure 7-8 was as expected. With a reduction in the size of the gap between the two spheres, an increase in the value of $\dot{\gamma}_G$, and hence also in the effective first normal-stress difference (N_1), can be expected. This increase in N_1 causes an apparent decrease in the growth coefficient of the normal stress, ψ_1 (see equation 4-17). As a result, We_G tends to decrease with the size of the gap between the spheres. The increase in $V_H/(d_0\dot{\gamma})$ with decreasing values of We_G thus agrees with the experimental observations, where probability of spheres to attract and converge has been noted to be higher in cases where the initial value of separation distance (d_0) is small.

7.4.4 Assessment of the proposed correlation

The downward shift of the $V_H/(d_0\dot{\gamma})$- We_G curves with increasing values of d_0/D as shown in Figure 7-8 suggests that the following form of generalisation can be applied:

$$\frac{V_H}{d_0\dot{\gamma}}\left(\frac{d_0}{D}\right)^N = f\left(We_G\right) \qquad (7\text{-}8)$$

N is a generalisation constant for the $V_H/(d_0\dot{\gamma})$- We_G curves shown in Figure 7-8 and f is a We_G-based function that can be evaluated through regression analysis. The efficiency of this method of generalisation can be inspected in Figure 7-9, where a value of N = 1.5 has been applied on the experimental data. As can be seen from this Figure, the variation of $V_H/(d_0\dot{\gamma})$ - We_G with d_0/D appears to have been minimised. This indicates that a fit parameter of N = 1.5 is appropriate for the implementation of equation 7-8. This figure has therefore been adopted for the evaluation of function f.

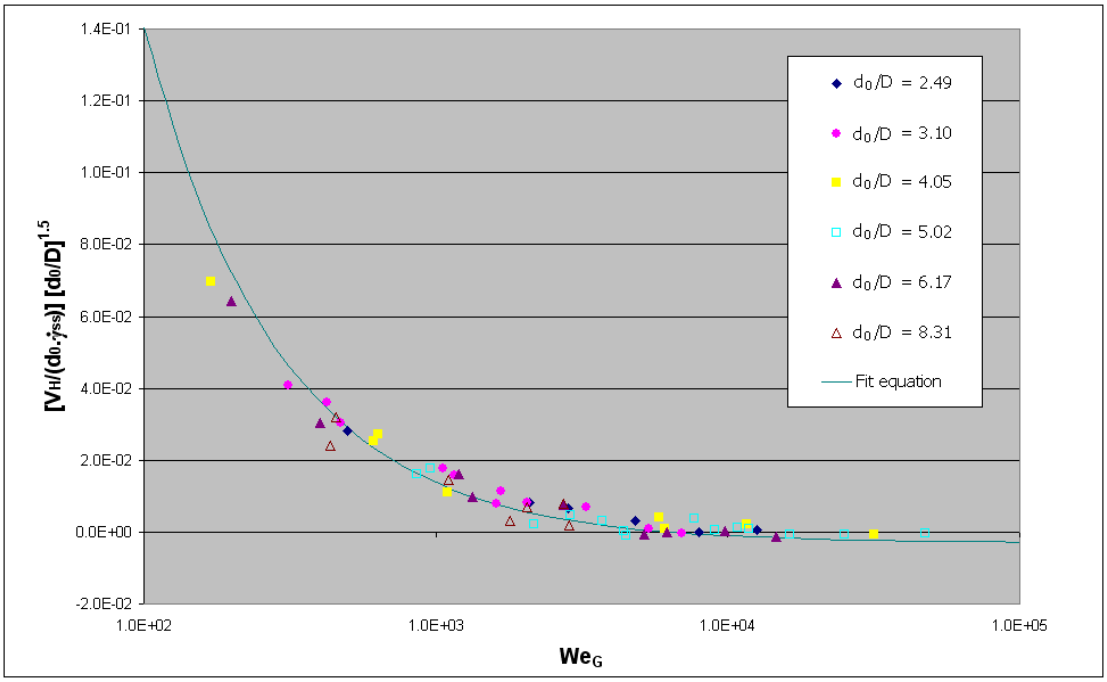

Figure 7-9: The variation of the generalised interaction parameter as a function of We_G and d_0/D. Fit equation 7-11 has been included in the plot.

Figure 7-9 also shows that the following equation of fit can be implemented on the experimental data:

$$\frac{V_H}{d_0\dot{\gamma}}\left(\frac{d_0}{D}\right)^{1.5} = a\left(We_G\right)^b - c \qquad \textbf{(7-9)}$$

The constants of equation 7-9, i.e. a, b, and c were evaluated using 72 experimental data points through a multiple linear regression evaluation method. To highlight the discrepancies in the levels of uncertainty between the two calculation methods presented for the interaction parameter (see the discussion presented in section 7.4.1 and equations 7-1 and 7-4), weighted formulations of the sum-of-squared errors (SSE) were used:

$$SSE=\sum_{i=1}^{i} w_i\left[a\left(We_G\right)_i^b - c - \left(\frac{V_H}{d_0\dot{\gamma}}\right)\left(\frac{d_0}{D}\right)^{1.5}\right] \qquad \textbf{(7-10)}$$

The parameter w_i represents the 'weight' value applied to data point i, i.e. it indicates the level of uncertainties that are associated with the measurement of a particular data point (Mosteller & Tukey, 1977). The values of this parameter were determined iteratively. First approximations of these values were obtained through the use of the Ordinary Least Squares method (i.e. $w_i = 1.0$) over data points where the first form of interaction parameter, i.e. equation 7-1, has been applied. The weight parameters, here defined as the inverse of the resulting variance in residuals, were then calculated for all of the remaining data points. These parameters were substituted into equation 7-9, upon which the minimisation calculation of the SSE can be repeated, and better values of the fit parameters can be obtained. The results of this analysis were: a = 10.48, b = − 0.931, and $c = 3x10^{-3}$. Equation 7-9 can thus be rewritten as follows:

$$\frac{V_H}{d_0\dot{\gamma}} = \left[10.48\left(We_G\right)^{-0.931} - 3x10^{-3}\right]\left(\frac{d_0}{D}\right)^{-1.5} \qquad \textbf{(7-11)}$$

The fit correlation as outlined in equation 7-11 has been featured in Figure 7-9, where its satisfactory agreement with the experimental data is highly apparent. Furthermore, in this Figure, it can also be seen that the fit correlation crosses the x-axis at $We_G \sim 6310$, indicating that the predicted values of $V_H/(d_0\dot{\gamma})$ beyond this point tend to become negative. As a result, it can be expected that attraction and convergence between the settling spheres beyond this value of We_G would cease to occur. The limiting value of $V_H/(d_0\dot{\gamma})$ as We_G tends towards infinity is -0.003, indicating that spheres settling in conditions of high We_G would possess very slight tendencies to repel each other during the course of the experiment.

The shift in the interaction tendencies of the spheres as discussed above was considered to be analogous to the condition of critical initial separation distance that have been suggested by Joseph et al. (1994) in their analysis of the settling behaviour of side-by-side spheres. In their analysis, this critical parameter was found to determine the types of interaction that occurs between spheres that are settling side-by-side, i.e. if the initial separation distance between the two spheres

is less than this critical figure, the two spheres would possess tendencies to attract and converge. If the opposite is true, the two spheres would either diverge very slightly or do not undergo any significant interaction. In the current study, such conditions of criticality have been generalised based on the rheology of the fluid, i.e. through the calculation of We_G. Using this parameter, as well as the correlation outlined in equation 7-11, critical values of initial separation distance below which the spheres would possess tendencies to interact and attract (and vice versa) can be predicted.

The correspondence of the correlation presented above can be examined by testing their applicability towards the prediction of whether certain configurations of spheres would attract or repel under various parameters of fluid rheology. Furthermore, in cases where the two spheres do attract, the rate of their convergence predicted through equation 7-11 can be compared with the experimental data. The results of these analyses can be seen in firstly in Figure 7-10, where comparisons of the estimated values of interaction parameters with those observed experimentally have been presented, and also in Figure 7-11, where the estimated distances required for two settling spheres to attract and converge (L_C) have been compared with the experimental data.

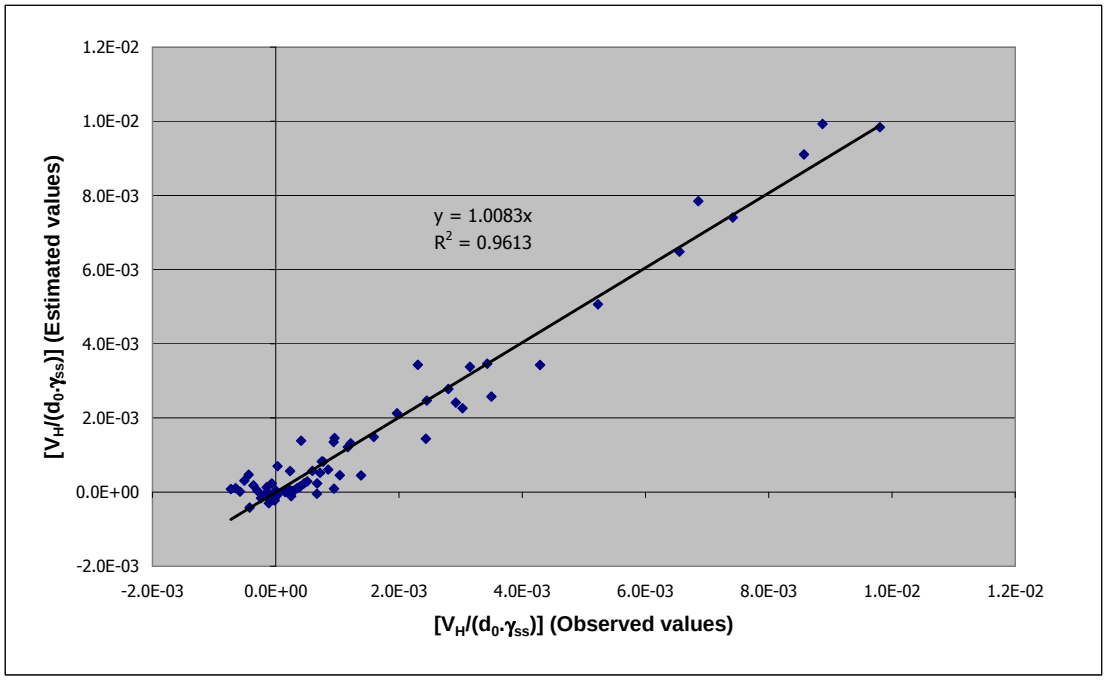

Figure 7-10: A comparison of the observed values of dimensionless interaction parameter with the corresponding values, calculated based on the proposed correlation (equation 7-11).

Both Figure 7-10 and Figure 7-11 show that the correspondence and regression between the observed and calculated values of interaction parameters were excellent. This suggests that by using the proposed correlation, predictions of whether two spheres that are released side-by-side into a viscoelastic fluid would attract or repel can be made with high level of accuracy.

The standard error resulting from the analysis outlined above was found to be ~ 0.1 m, which is equivalent to 16% of the mean value of ℓ_C. This figure suggests that the proposed correlation is able to provide a relatively good indication of the level of inter-sphere interaction that occurs in an experiment of two spheres released side-by-side into viscoplastic fluids possessing low to medium levels of elasticity. The simplicity of the correlation, in combination with the straightforward method of measurement of the first normal-stress difference and shear viscosity, makes this method easily applicable for the prediction of whether two spheres would attract or repel in the fluid solution.

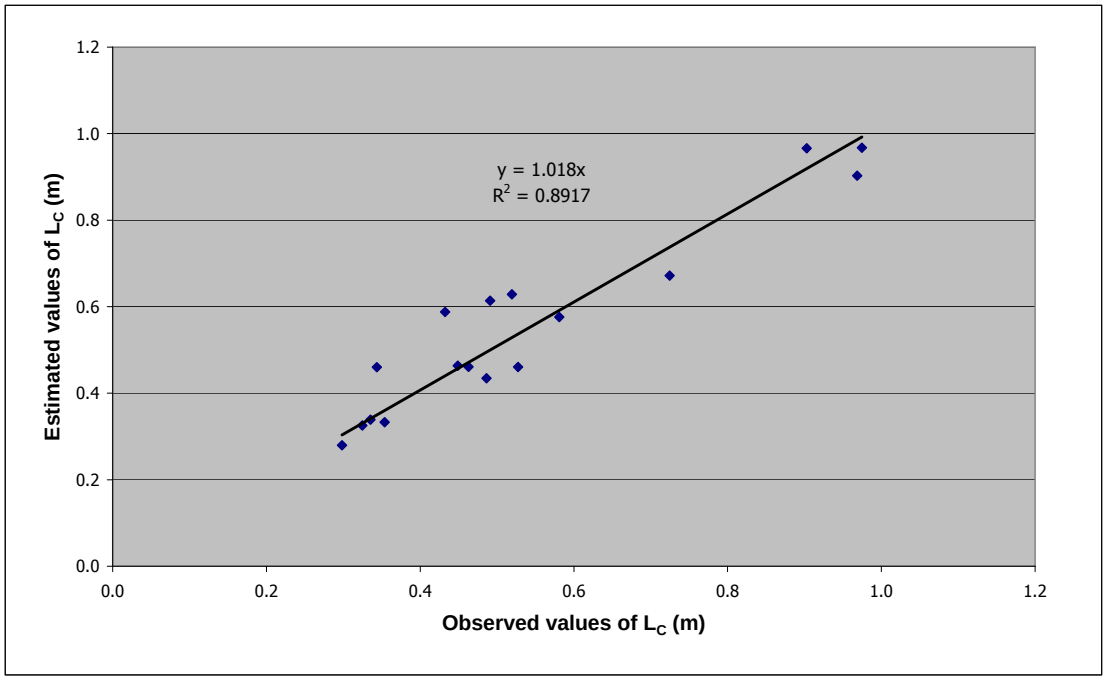

Figure 7-11: A comparison of the observed settling distance required for two spheres settling side-by-side to attract and converge with the corresponding values, calculated based on the proposed correlation (see equation 7-11).

7.5 Conclusion

Through an examination of the settling behaviour of spheres released simultaneously in a side-by-side arrangement – but with a set distance apart – into dilute solutions of polyacrylamide, it was found that two different types of settling trajectory could be obtained. In the first type, the two spheres show strong tendency to attract and converge. This behaviour contrasts with that found in the second type of trajectory, where the horizontal separation distance between the spheres was found to undergo minimal level of changes throughout the experiment.

Interestingly, in the first type of settling trajectory, it has been observed that one of the spheres tend to decelerate slightly while their horizontal separation distance decreases. This causes a re-orientation in the position of the spheres, with the slower sphere showing tendencies to settle towards the flow path of the faster sphere. Upon converging, which is an instance where the horizontal distance

between the two reaches a very low level (~ 0.001 – 0.002 m), the trailing sphere starts to experience the shear-thinning effects induced by the shearing movements of the leading sphere, causing it to accelerate towards the leading sphere and collide. This motion of re-orientation was found to be comparable to that reported by Joseph et al. (1994) in their study of viscoelastic fluids. The cause of this phenomenon, however, could not be determined with the current experiment, and a flow visualisation study, e.g. Particle Image Velocimetry, would be required to further assess this behaviour.

Upon comparing the interaction tendencies of the settling spheres in three different aqueous solutions of polyacrylamide (0.9, 1.0, and 1.1 w/w %), it was found that higher incidence of convergence, i.e. inter-sphere attraction, tends to occur in the solution of highest polymer concentration, i.e. 1.1%. The opposite is true with the 0.9% polyacrylamide solution. This trend of inter-sphere interaction was found to reflect the elastic properties of the fluids, which, as indicated by the values of characteristic relaxation time of the fluids (see Chapter 4), are the most severe in the 1.1% polyacrylamide solution. This observation was found to agree with the results presented by Joseph et al. (1994).

Comparisons were also made with the results of the numerical study (CFD) conducted using the semi-viscoplastic fluid model. In this fluid model, the changes in the viscous parameters of the fluid solutions are described to be a function of λ, which is a scalar variable that reflects the integrity of the structural network configuration of the fluid solutions due to the existence of hydrogen bonding between the polyacrylamide and water molecules. The normal stresses arising from the elasticity of the fluids have been assumed to be negligible, i.e. this fluid model represents purely viscous flow behaviour. In an earlier CFD study (see Chapter 5), it has been demonstrated that this fluid model is able to represent the viscous characteristics of the experimental fluid solutions, as indicated by the close agreement of the terminal settling behaviour of spheres predicted numerically to that observed experimentally. In the current study, however, the simulations conducted using this fluid model did not detect any inter-particle interaction that

results in convergent sphere behaviour. This was as expected due to the absence of elastic effects in the fluid model.

Based on the findings discussed above, it was concluded that the tendencies of spheres to attract and converge are highly influenced by the elastic properties of the fluids. A correlation was thus developed between the observed interaction tendencies of the spheres with the viscous and elastic properties of the fluids. The latter figure was quantified through the coefficient of first normal stress differences (ψ_1) determined through rheometric analyses (see Chapter 4). The result is a parameter that compares the normal stresses of the fluid medium within the gap between the spheres with the viscous parameters that exist above the settling spheres, We_G. Through this correlation, the attraction tendencies of spheres settling through the fluid solutions can be predicted based on the rheology of the fluids.

Chapter 8 Conclusions and recommendations

In an effort of improving the efficiency of tertiary grinding circuits, a fundamental study of the fall behaviour of solid bodies in these highly resource-demanding unit operations have been conducted. In most grinding circuits, the fine mineral particles are suspended in a fluid medium, thus forming slurries and suspensions that typically have viscoplastic flow characteristics. The work in this thesis has therefore been focused on the settling behaviour of particles (specifically spheres) in fluids with this type of flow behaviour.

Viscoplastic flow behaviour is characterised by the presence of a yield stress, which denotes a critical level of stress that is required to deform the structure of the medium before it starts to flow. The influence of this flow behaviour on the terminal settling of spherical particles has recently been captured by the correlation suggested by Wilson et al. (2004; 2003). A further review of past studies, however, revealed that many aspects of this flow problem are still unsolved. These include the interaction of spheres settling in close proximity to each other, as well as the effects of the fluid recovery on the viscous parameters of the fluid (Gumulya et al., 2007). Both of these aspects are critical for the understanding of the motion of solid bodies in grinding circuits.

Three studies have been performed in accordance to the objective of this thesis:

1. To experimentally and numerically study the settling behaviour of two vertically-aligned spheres, i.e. one sphere following the flow path of another sphere.
2. To experimentally and numerically study the settling behaviour of two horizontally-aligned spheres, with a set distance apart, released simultaneously into the fluid.

The experiments were performed in aqueous solutions of polyacrylamide (0.9 – 1.1 w/w Floxit 5250L), which have been known to possess viscoplastic fluid behaviour.

The conclusions obtained from these studies are addressed in the following section, followed by recommendations for future work.

8.1 Conclusions

This thesis makes a significant contribution to the understanding of the effects of fluid rheological properties on the settling behaviour of particles.

The first contribution goes to the systematic analysis of the rheological properties of the test fluid solutions, through which a new rheological model that can provide better characterisation of the changes in the viscosity, both as functions of shear and time, was developed.

The second contribution was the development of the stereo-photogrammetry measurement system. In this system, two low-cost video cameras and a combination of commercially-available and custom-built software were assembled for the measurement and tracking of spheres settling in clear viscoplastic fluids. Through an extensive testing regime, it was found that the resulting measurement system is able to track the 3D motion of spheres to within 1 mm accuracy.

The third contribution was the development of a VOF-based numerical (CFD) scheme, through which a detailed analysis of the flow fields surrounding the settling particles can be obtained. In the future, this numerical scheme can be used as the basis of the analysis of flow fields affecting the movement of solid bodies in grinding circuits.

Fourthly, by using the newly-developed fluid model to highlight the changes in the structural conditions of the fluid throughout a settling-sphere experiment, predictions of the settling velocity of spheres in fluids of various structural conditions (e.g. disturbed or undisturbed), can be made with far greater accuracy than before.

Finally, contributions were also made towards the knowledge of the interaction tendencies between spheres that are settling in close proximity to each other. Correlations were developed in order to relate the elastic and viscous properties of the fluid solutions with the tendencies of the spheres to attract and converge.

8.1.1 Fluid rheology

- The new fluid model includes a scalar structural parameter (λ). This parameter reflects the integrity of the structural network configuration that exists in the fluid solutions due to the existence of hydrogen bonding between the polyacrylamide and water molecules (Kulicke et al., 1982). The viscosity of the fluid is directly correlated with λ. The rate-of-change in λ is dependent on the magnitude of shear that the fluid experienced.
- Under steady-state conditions, the new fluid model resembles the model suggested by Cross (1965) for pseudo-plastic fluids, i.e. it does not explicitly feature a yield stress value. Instead, the model features very prominent shear-thinning behaviour, where significant reduction in viscosity is obtained with increasing values of shear stress. This reflects the changes in viscosity observed experimentally when the fluids are subjected to shear forces that exceed the apparent yield stress value.

- The response of the fluid model predicted numerically under conditions of continually-increasing shear rate (i.e. ramp testing) was found to reflect the experimental observations of the fluid rheometry. Under this testing condition, fluids that initially possess fully-intact structures were found to exhibit stress overshoot at the beginning of the ramp-testing. This was followed by a temporary region of negative slope, indicating the temporary existence of unstable flow. This flow instability was not encountered in cases where the structure of the fluid has previously been destroyed due to the application of shear.

- The flow instability discussed above was compared to the definition of yield stress suggested by Møller et al. (2006), who proposed that this parameter be

defined as the critical stress value below which no permanent (stable) flow occurs. The presence of a temporary negative slope in the numerical response of the fluid indicates that the fluid model features temporary yield-stress characteristics that dissipate once the structural network of the fluid is destroyed due to the application of shear. Once the structure is destroyed, the fluid model features shear-thinning flow behaviour only.

- As the fluid model used in this thesis does not explicitly feature a yield stress value, and due to the fact that the yield stress characteristics dissipates once the fluid has been sheared, the term 'semi-viscoplastic' was used to describe the fluid model.

- The elastic properties of the fluids were examined using a series of Small Amplitude Oscillatory Shear (SAOS) testings. The resulting values of the characteristic relaxation time were found to be relatively short in comparison with the measurement time of the experiments, as well as the values of relaxation parameter (θ) in the semi-viscoplastic fluid model. This indicates that the elasticity of the fluid solutions should be of low consequence to the dynamics of the settling-sphere experiments and that the fluids may be modelled as viscous liquids.

- The resulting normal-stresses caused by the elasticity of the fluids were characterised through the measurement of first normal-stress difference (N_1), which was then correlated with the shear rate through power-law equations.

8.1.2 Numerical modelling

- A numerical scheme based on the VOF (Volume of Fluid) model, in which the solid particle is likened to a fluid material with very high viscosity (~ 400 –1000 Pa.s), has been formulated and developed. By implementing appropriate discretisation strategies and approximation methods, the effects of numerical smearing and diffusion, which are issues that are particularly relevant in VOF-based calculations, can be minimised. A time-dependent estimation of the

semi-viscoplastic fluid model was developed and implemented into the numerical scheme using a series of User Defined Functions (UDF).

- The numerical scheme was validated through a study conducted in Newtonian fluids ($0.1 < Re < 7.0$).

- The flow field of the semi-viscoplastic fluid surrounding a settling sphere in this fluid medium was found to be comparable to the flow fields reported in the literature for viscoplastic and yield-stress fluids.

- Excellent qualitative agreement ($R^2 \sim 0.98$) was found between the results of the numerical analysis with the experimental results. This suggests that the settling behaviour of the spheres in these experiments can be modelled through considerations of the changes in the structural parameters of the fluid, and the effects of such changes on its viscous parameters. It also confirms the assumption stated earlier that the elastic properties of the Floxit solutions are of low consequence to the dynamics of the settling experiment.

- The quantitative agreement between the numerical predictions and experimental data was found to be generally poor. This deviation, in addition to the excellent qualitative agreement, indicates that the rheological analyses of the fluids are subject to large errors. These errors are likely to be caused by the irregularities of flow patterns within the geometry of the cone-and-plate rheometer. In future work, the impact of these flow irregularities may be addressed by incorporating computational techniques into the rheometric analysis. Nevertheless, these results show that, through the incorporation of a calibration factor, the proposed numerical scheme can be used for the prediction of terminal settling velocity of spheres settling in viscoplastic fluids.

8.1.3 The settling behaviour of two vertically-aligned spheres

- In this experiment, a sphere that falls through an undisturbed medium was found to attain a constant (terminal) settling velocity almost instantaneously upon its release. The sphere that follows this initial release tends to possess a much higher settling velocity. It also continues to accelerate as the gap between

the two particles decreases, leading to a collision between the two, after which they combine and travel at the same (constant) velocity.

- The structural changes of the fluid as it is sheared by the movement of the spheres were considered. A correlation of the settling velocities of the leading and trailing spheres was then developed based on this consideration. In this correlation, the representative structural parameter above the sphere was calculated based on the mean surficial stress of the sphere (see equations 2-40 and 2-41). Below the sphere, the representative structural parameter was estimated through the integration of the rate equation of λ, over the time that has lapsed since the fluid was sheared by the movement of the previous sphere (see equation 6-2).

- Through consideration of 662 data points, comprising of the settling velocities of the leading and trailing spheres in the experiment of vertically-aligned spheres, a correlation was developed, relating the changes in the structure of the fluid with a figure of equivalent viscosity (μ_{eq}). This parameter represents a calculated figure of Newtonian viscosity that produces the same settling velocity for a particle (of the same density and dimension) that falls through a non-Newtonian fluid medium (Wilson & Horsley, 2004; Wilson et al., 2003). The resulting correlation (see equation 6-4) can be viewed as an extension of the correlation suggested by Wilson et al. (2004; 2003), enabling the settling velocity of spheres falling through fluid media of various structural conditions and shear history to be predicted with much greater accuracy than before.

- Subsequent tests using data points resulting from experiments using two spheres of different diameter and/or density revealed that the new correlation was able to satisfactorily predict the settling velocity of both the leading and trailing spheres. The applicability of this correlation towards these cases supports the validity of the presented analysis.

- After the collision, the effective shear stress induced by the settling motion of the combined or aggregated spheres can be examined by considering the effects of path interference induced by the settling arrangement of the spheres. The

same correlation as that outlined above applies for the prediction of the terminal settling velocity of these aggregated spheres.

8.1.4 The settling behaviour of two horizontally-aligned spheres

- Two different types of settling trajectory were obtained from this experiment: Firstly, the two spheres show strong tendency to attract and converge. Secondly, the two spheres show minimal level of interaction and the horizontal distance between them changes very slightly throughout the settling experiment.
- In cases where the two spheres tend to interact, one of the spheres tends to undergo slight deceleration. This causes the two spheres to re-orientate their position towards each other, i.e. the slower sphere tending to settle towards the flow path of the faster sphere. When the horizontal distance between the two reaches a very low level (~ 0.001–0.002 m), the trailing sphere starts to accelerate and collide with the leading sphere. This acceleration is due to the same effects as those that cause the acceleration of the trailing sphere in the experiment of two vertically-aligned spheres, i.e. structural deformation.

- With the current experimental setup, the cause of the re-orientation motion observed in cases where the two spheres converge could not be determined. A flow visualisation study, e.g. Particle Image Velocimetry, would need to be conducted to characterise this phenomenon.

- The results of the numerical analysis indicates that in the non-elastic semi-viscoplastic fluid model, two spheres settling side-by-side always tend to diverge and repulse, regardless of the value of initial separation distance. This indicates that in cases where the interactions between the particles are of primary concern, the elasticity of the fluid medium needs to be considered. This finding was supported by the experimental data and the results of other studies, e.g. Joseph et al. (1994)

- A correlation was developed between the interaction tendencies of the spheres with the viscous and elastic properties of the fluid (see equations 7-7 and 7-11). The latter figure was quantified through the coefficient of first normal-stress

differences (ψ_1). The result of this analysis is a parameter (We_G) that compares the normal-stresses of the fluid medium within the gap between the spheres, with the viscous parameters surrounding the spheres. Through this correlation, the tendencies of settling spheres to attract and converge can be predicted based on the rheology of the fluid.

8.2 Recommendations

By thoroughly examining the settling behaviour of spheres of two different initial configurations in viscoplastic fluids, the effects of the recovery of fluid structure after being sheared by the motion of the sphere have been characterised, along with the effects of the presence of a neighbouring particle on the settling behaviour of the spheres. Aided by this knowledge, the motion of spheres falling through viscoplastic fluids can be predicted with much higher certainty than previously. The objectives of this research, as outlined in Section 1.3, have therefore been completed.

Despite this progress, considerable amount of work is still required towards the accomplishment of the fundamental aim of this research project, which is to attain a greater understanding of the motion of solid bodies in tertiary grinding circuits. The tasks that need to be completed for the achievement of this goal have been outlined in the following sections.

8.2.1 The extension of the current experimental work

The experiment involving the settling behaviour of two side-by-side spheres has so far been confined to the study of spheres having identical diameter and density. This can be extended towards the study of the motion of horizontally-aligned spheres having different diameter and/or density.

The scope of the settling experiment can then be extended by studying the settling behaviour of three (or more) spheres of various initial configurations in viscoplastic

fluids. In particular, experiments involving the simultaneous release of two side-by-side spheres followed by another simultaneous release of two side-by-side spheres can be seen as the direct extension of the current experimental configurations.

Similar experiments can also be conducted using other viscoplastic fluids, e.g. solutions of Carbopol and Separan, as well as some Newtonian fluids with high viscosity, e.g. Silicone oils. In doing so, greater overview of the effects of the fluid rheology on the settling behaviour of the spheres can be obtained.

8.2.2 Flow visualisation study

Further insights of the flow field surrounding the settling sphere, as well as the interaction between the spheres as they settle through the fluids, can be gained by the utilisation of flow-visualisation techniques, such as Particle Image Velocimetry (PIV), in conjunction with the sphere-settling experiments.

8.2.3 Numerical study

The value of numerical analysis on the study of the settling behaviour of spheres in viscoplastic fluids has been demonstrated in this thesis. In conducting the experiments outlined in Section 8.2.1, therefore, it is expected that valuable insights can be obtained by conducting numerical analyses that are analogous to these experiments.

Furthermore, it has also been demonstrated that rheometric analysis involving viscoplastic and viscoelastic fluids are highly prone to measurement errors. This is due to the fact that the interpretation of rheometric measurements using cone-and-plate geometry has generally been based on several assumptions, e.g. primary laminar flow across the flow geometry and negligible edge effects, which are often not met with the measurements of these non-Newtonian fluids. In the current study, the effects of these errors can be observed by the lack of quantitative agreement between the numerical predictions of the settling behaviour of spheres

in semi-viscoplastic fluids with those observed experimentally, despite the fact that the two data sets show excellent qualitative agreement. To overcome the difficulties associated with the attainment of accurate rheometric data, such measurements need to be conducted in conjunction with a study in *computational rheometry*. In this field of rheometry, simulations of the rheometric experiments are conducted, with the aim of attaining better understanding of the flow and velocity fields that are developed during the measurement process. The attainment of this knowledge will aid the development of better methods of translating the measurement data (forces, torques, and deformations) into useful rheological information (shear stress, shear rate, first normal-stress, etc.) (Keunings, 2000).

8.2.4 Settling experiments in slurries

With the successful completion of the tasks outlined above, simulations of the settling behaviour of solid bodies in slurries can be commenced. Two different approaches can be adopted in conducting this study. First, the simulations can be conducted using the VOF-based particle tracking scheme that has been developed in this thesis. While this approach allows the flow problem to be analysed through fundamental principles of fluid mechanics, it possesses a drawback in being very computationally expensive. As a result, with the current computational resources, the large-scale simulations that would be required for the flow analysis of milling processes would be unachievable. This approach should therefore be used in conjunction with a second approach, in which the simulations are conducted using the empirical equations and correlations, such as ones that have been developed in this thesis. The utilisation of this approach will allow for large-scale simulations of the milling process to be conducted using less computational resources.

The simulations outlined above have to be conducted in conjunction with a series of experimentations conducted in industrial slurries, through which the validity of the models can be assessed and confirmed.

REFERENCES

Acharya, A., Mashelkar, R. A., & Ulbrecht, J. (1976). Flow of inelastic and viscoelastic fluids past a sphere. *Rheologica Acta, 15*(9), 471-478.

Acierno, D., La Mantia, F. P., Marrucci, G., & Titomanlio, G. (1976). A non-linear viscoelastic model with structure-dependent relaxation times. *Journal of Non-Newtonian Fluid Mechanics, 1*, 125-146.

Agrawal, M., Bakker, A., & Prinkey, M. T. (2004). *Macroscopic particle model - Tracking big particle in CFD.* Paper presented at the AIChE 2004 Annual Meeting, Austin, Texas.

Ambeshkar, V. D., & Mashelkar, R. A. (1990). On the role of stress-induced migration on time dependent terminal velocities of falling spheres. *Rheologica Acta, 29*, 182-191.

Ambeskar, V. D., & Mashelkar, R. A. (1990). On the role of stress-induced migration on time dependent terminal velocities of falling spheres. *Rheologica Acta, 29*, 182-191.

Andres, U. T. (1960). Equilibrium and motion of spheres in a viscoplastic fluid. *Soviet Physics Doklady (USA) 5*, 723-726.

Ansley, R. W., & Smith, T. N. (1967). Motion of spherical particles in a Bingham plastic. *AIChE Journal, 13*, 1193-1196.

Arigo, M. T., & McKinley, G. H. (1997). The effects of viscoelasticity on the transient motion of a sphere in a shear-thinning fluid. *Journal of Rheology, 41*(1), 103-128.

Arigo, M. T., & McKinley, G. H. (1998). An experimental investigation of negative wakes behind spheres settling in a shear-thinning viscoelastic fluid. *Rheologica Acta, 37*(4), 1435-1528.

Arigo, M. T., Rajagopalan, D., & McKinley, G. H. (1995). The sedimentation of a sphere through an elastic fluid: Part 1. Steady motion. *Journal of Non-Newtonian Fluid Mechanics, 60*(2-3), 225-257.

Atapattu, D. D. (1989). *Ph.D Dissertation.* Monash University, Australia.

Atapattu, D. D., Chhabra, R. P., Tiu, C., & Uhlherr, P. H. T. (1986). *The effect of cylindrical boundaries for spheres falling in fluids having a yield stress.*

Paper presented at the 9th Australasian Fluid Mechanics Conference, Auckland.

Atapattu, D. D., Chhabra, R. P., & Uhlherr, P. H. T. (1990). Wall effects for spheres falling at small Reynolds number in a viscoplastic medium. *Journal of Non-Newtonian Fluid Mechanics, 38*, 31-42.

Atapattu, D. D., Chhabra, R. P., & Uhlherr, P. H. T. (1995). Creeping sphere motion in Herschel-Buckley fluids: flow field and drag. *Journal of Non-Newtonian Fluid Mechanics, 59*, 245-265.

Baaijens, F. P. T. (1998). Mixed finite element methods for viscoelastic flow analysis: a review. *Journal of Non-Newtonian Fluid Mechanics, 79*(2-3), 361-385.

Barnes, H. A. (1997). Thixotropy - a review. *Journal of Non-Newtonian Fluid Mechanics, 70*, 1-33.

Barnes, H. A. (1999). The yield stress—a review or 'παντα ρει'—everything flows? *Journal of Non-Newtonian Fluid Mechanics, 81*(1-2), 133-178.

Barnes, H. A., & Walters, K. (1985). The Yield Stress Myth? *Rheologica Acta, 24*(4), 323-326.

Bauer, W. H., & Collins, E. A. (1967). Thixotropy and Dilatancy. In F. R. Eirich (Ed.), *Rheology: Theory and Applications* (Vol. 4). New York: Academic Press.

Bavarian, C., Quemada, D., & Parker, A. (1996). *A new methodology for rheological modelling of thixotropy application to hydrocolloids.* Paper presented at the XIIth International Congress on Rheology, Laval University, Quebec City, Canada.

Beaulne, M., & Mitsoulis, E. (1997). Creeping motion of a sphere in tubes filled with Herschel-Bulkley fluids. *Journal of Non-Newtonian Fluid Mechanics, 72*(1), 55-71.

Becker, L. E., McKinley, G. H., Rasmussen, H. K., & Hassager, O. (1994). The unsteady motion of a sphere in a viscoelastic fluid. *Journal of Rheology, 38*(2), 377-403.

Bercovier, M., & Engleman, M. (1980). A finite-element method for incompressible non-Newtonian flows. *Journal of Computational Physics, 36*, 313-326.

Beris, A. N., Tsamopoulos, J., Armstrong, R. C., & Brown, R. A. (1985). Creeping motion of a sphere through a Bingham plastic. *Journal of Fluid Mechanics, 158*, 219-244.

Beverly, C. R., & Tanner, R. I. (1992). Numerical analysis of three-dimensional Bingham plastic flow. *Journal of Non-Newtonian Fluid Mechanics, 42*, 85-115.

Bingham, E. C. (1922). *Fluidity and Plasticity*. New York: McGraw-Hill.

Bisgaard, C. (1983). Velocity field around spheres and bubbles investigated by laser Doppler anemometry. *Journal of Non-Newtonian Fluid Mechanics, 12*, 283-302.

Blackery, J., & Mitsoulis, E. (1997). Creeping motion of a sphere in tubes filled with a Bingham plastic material. *Journal of Non-Newtonian Fluid Mechanics, 70*(1-2), 59-77.

Bodart, C., & Crochet, M. J. (1994). The time-dependent flow of a viscoelastic fluid around a sphere. *Journal of Non-Newtonian Fluid Mechanics, 54*, 303-329.

Bot, E. T. G., Hulsen, M. A., & van den Brule, B. H. A. A. (1998). The motion of two spheres falling along their line of centres in a Boger fluid. *Journal of Non-Newtonian Fluid Mechanics, 79*, 191-212.

Britton, M. M., & Callaghan, P. T. (1997). Nuclear magnetic resonance visualizaion of anomalous flow in cone-and-plate rheometry. *Journal of Rheology, 41*(6), 1365-1386.

Broadman, G., & Whitmore, R. I. (1961). The static measurement of yield stress. *Laboratory Practice, 10*, 782-785.

Bush, M. B. (1993). The stagnation flow behind a sphere. *Journal of Non-Newtonian Fluid Mechanics, 49*(1), 103-122.

Bush, M. B., & Phan-Thien, N. (1984). Drag force on a sphere in creeping motion through the Carreau model fluid. *Journal of Non-Newtonian Fluid Mechanics, 16*(3), 303-313.

Carreau, P. J. (1972). Rheological equations from molecular network theories. *Transactions of the Society of Rheology, 16*, 99-127.

Casson, N. (1959). *Rheology of Disperse Systems*. New York: Pergamon Press.

Ceylan, K., Herdem, S., & Abbasov, T. (1999). A theoretical model for estimation of drag force in the flow of non-Newtonian fluids around spherical solid particles. *Powder Technology, 103*, 286-291.

Chan Man Fong, C. F., & De Kee, D. (1994). Yield stress and small amplitude oscillatory flow in transient networks. *Industrial Engineering Chemistry Research, 33*, 2374-2376.

Chen, L., Reizes, J. A., Leonardi, E., & Li, Y. (1998). *Ball falling through viscoplastic fluid in a cylinder.* Paper presented at the 13th Australasian Fluid Mechanics Conference, Monash University, Melbourne, Australia.

Chen, R. C., & Wu, J. L. (2000). The flow characteristics between two interactive spheres. *Chemical Engineering Science, 55*(6), 1143-1158.

Cheng, D. C.-H. (1966). Cone-and-plate viscometry: explicit formulae for shear stress and shear rate and the determination of inelastic thixotropic properties. *British Journal of Applied Physics, 17*, 253-263.

Chhabra, R. P. (2007). *Bubbles, Drops, and Particles in Non-Newtonian Fluids*. Boca Raton, FL: CRC Taylor & Francis.

Chhabra, R. P., & Uhlheer, P. H. T. (1980). Creeping motion of spheres through shearthinning elastic fluids described by the Carreau viscosity equation. *Rheologica Acta, 19*(2), 187-195.

Chilcott, M. D., & Rallison, J. M. (1988). Creeping flow of filute polymer solutions past cylinders and spheres. *Journal of Non-Newtonian Fluid Mechanics, 29*, 381-432.

Chmielewski, C., Nichols, K. L., & Jayaraman, K. (1990). A comparison of the drag coefficients of spheres translating in corn syrup based and polybutene based Boger fluids. *Journal of Non-Newtonian Fluid Mechanics, 35*(1), 37-49.

Cho, Y. I., Hartnett, J. P., & Lee, W. Y. (1984). Non-Newtonian viscosity measurements in the intermediate shear rate range with the falling sphere viscometer. *Journal of Non-Newtonian Fluid Mechanics, 15*(1), 61-74.

Clift, R., Grace, J. R., & Weber, M. E. (1978). *Bubbles, Drops, and Particles*. New York: Academic.

Colebrook, C. F. (1938-1939). Turbulent flow in pipes, with particular reference to the transition region between the smooth and rough pipe laws. *Journal of the Institute of Civil Engineers, 11*, 133-156.

Crochet, M. J., Davies, A. R., & Walters, K. (1984). *Numerical Simulations of Non-Newtonian Flow*. Amsterdam: Elsevier.

Cross, M. M. (1965). Rheology of non-Newtonian fluids: A new flow equation for pseudoplastic systems. *Journal of Colloid Science, 20*(5), 417-437.

de Besses, B. D., Magnin, A., & Jay, P. (2004). Sphere drag in a viscoplastic fluid. *AIChE Journal, 50*(10), 2627-2629.

De Kee, D., Code, R. K., & Turcotte, G. (1983). Flow properties of time-dependent foodstuffs. *Journal of Rheology, 27*(6), 581-604.

Debae, F., Legat, V., & Crochet, M. J. (1994). Practical evaluation for mixed finite element methods for viscoelastic flow. *Journal of Rheology, 38*(2), 421-442.

Debbaut, B., & Crochet, M. J. (1988). Extensional effects in complex flows. *Journal of Non-Newtonian Fluid Mechanics, 30*(2-3), 169-184.

Delvaux, V., & Crochet, M. J. (1990). Numerical prediction of anomalous transport properties in viscoelastic flow. *Journal of Non-Newtonian Fluid Mechanics, 37*, 297-315.

Devenish, M. (1998). *Proposal for a system to measure particle flow in a slurry flow test rig*. Perth: Slurry Research Group, Curtin University of Technology.

Dullaert, K., & Mewis, J. (2006). A structural kinetics model for thixotropy. *Journal of Non-Newtonian Fluid Mechanics, 139*, 21-30.

Dunand, A., Guillot, D., & Soucemarianadin, A. (1984). *Viscous properties of glass bead suspensions and falling sphere experiments in hydroxypropyl guar solutions.* Paper presented at the Proceedings of the IXth International Congress in Rheology, Acapulco, Mexico.

duPlessis, M. P., & Ansley, R. W. (1967). Settling parameter in solids pipelining. *Journal of Pipeline Division, ASCE, 93*(PL2), 1-17.

El Kayloubi, A., Kiddioui, N., & Sigli, D. (1987). Structure of the rate of deformation field of Newtonian and viscoelastic fluids in a falling ball experiment. *Journal of Non-Newtonian Fluid Mechanics, 22*(3), 335-357.

Elliott, J., & Ganz, A. J. (1977). Salad dressings - Preliminary rheological characterisation. *Journal of Texture Studies, 8*, 359-371.

Elliott, J., & Green, C. E. (1972). Modification of food characteristics with cellulose hydrocolloids, II. The modified Bingham body - a useful rheological model. *Journal of Texture Studies, 3*, 195-201.

Ellis, S. C., Lanham, A. F., & Pankhurst, K. G. A. (1955). A rotational viscometer for surface films. *Journal of Scientific Instruments, 32*(2), 70-73.

Ferry, J. D. (1980). *Viscoelastic Properties of Polymers* (3rd ed.). New York: John Wiley & Sons.

Ferziger, J. H., & Perić, M. (1999). *Computational Methods for fluid dynamics* (2nd ed.). Berlin; New York: Springer.

Fluent, Inc. (2006). FLUENT 6.3 User's Guide. Lebanon, NH.

Fornberg, B. (1988). Steady viscous flow past a sphere at high Reynolds number. *Journal of Fluid Mechanics, 190*, 471-489.

Francis, A. W. (1933). Wall effect in falling ball method for viscosity. *Physics, 4*(11), 403-406.

Fraser, C. S. (1997). Digital camera self-calibration. *ISPRS Journal of Photogrammetry and Remote Sensing, 52*(4), 149-159.

Freundlich, H. (1935). *Thixotropie*. Paris: Hermann.

Frigaard, I. A., & Nouar, C. (2005). On the usage of viscosity regularisation methods for visco-plastic fluid flow computation. *Journal of Non-Newtonian Fluid Mechanics, 127*(1), 1-26.

Gaston, M. J., Reizes, J. A., & Evans, G. M. (2002). *Numerical modelling of multiple three dimensional gas bubbles in a quiescent liquid using a volume of fluid method.* Paper presented at the 2nd International Conference on Computational Fluid Dynamics, Sydney, Australia.

Gervang, B., Davies, A. R., & Phillips, T. N. (1992). On the simulation of viscoelastic flow past a sphere using spectral methods. *Journal of Non-Newtonian Fluid Mechanics, 44*, 281-306.

Ghannam, M. T., & Esmail, M. N. (1998). Rheological properties of aqueous polyacrylamide solutions. *Journal of Applied Polymer Science, 69*, 1587-1597.

Gheissary, G., & van den Brule, B. H. A. A. (1996). Unexpected phenomena observed in particle settling in non-Newtonian media. *Journal of Non-Newtonian Fluid Mechanics, 67*, 1-18.

Glowinski, R., Lions, J. L., & Tremolieres, R. (1981). *Numerical Analysis of Variational Inequalities*. Amsterdam: Dunod.

Green, H., & Weltmann, R. (1943). Analysis of thixotropy of pigment-vehicle suspensions - basic principles of the hysteresis loop. *Industrial and Engineering Chemistry Analytical Edition, 15*(3), 201-206.

Gueslin, B., Talini, L., Herzhaft, B., Peysson, Y., & Allain, C. (2006b). Aggregation behaviour of two spheres falling through an aging fluid. *Physical Review E, 74*(042501), 1-4.

Gueslin, B., Talini, L., Herzharft, B., Peysson, Y., & Allain, C. (2006a). Flow induced by a sphere settling in an aging yield-stress fluid. *Physics of Fluids, 18*(103101), 1-8.

Gumulya, M. M., Horsley, R. R., & Wilson, K. C. (2007). The settling of consecutive spheres in viscoplastic fluids. *International Journal of Mineral Processing, 82*(2), 106-115.

Happel, J., & Pfeffer, R. (1960). The motion of two spheres following each other in a viscous fluid. *AIChE Journal, 6*, 129-133.

Hariharaputhiran, M., Subramanian, R. S., Campbell, G. A., & Chhabra, R. P. (1998). The settling of spheres in a viscoplastic fluid. *Journal of Non-Newtonian Fluid Mechanics, 79*, 87-97.

Harlen, O. G. (1990). High-deborah-number flow of a dilute polymer solution past a sphere falling along the axis of a cylindrical tube. *Journal of Non-Newtonian Fluid Mechanics, 37*, 157-173.

Harlen, O. G., Rallison, J. M., & Chilcott, M. D. (1990). High Deborah number flow of dilute polymer solutions. *Journal of Non-Newtonian Fluid Mechanics, 34*(3), 319-349.

Hassager, O. (1979). Negative wake behind bubbles in non-Newtonian liquids. *Nature, 279*(May), 402-403.

Heider, A., & Levenspiel, O. (1989). Drag coefficient and terminal velocity of spherical and non-spherical particles. *Powder Technology, 58*, 63-70.

Herbst, J. A., Yi, C. L., & Flintoff, B. (2003). Size reduction and liberation. In M. C. Fuerstenau & K. N. Han (Eds.), *Principles of Mineral Processing*. Littleton, Colorado: Society for Mining, Metallurgy, and Exploration, Inc.

Herschel, W. H., & Bulkley, R. (1926). Measurement of consistency as applied to rubber-benzene solutions. *Proceedings of the American Society for Testing Materials, 26*, 621-633.

Heymann, L., & Aksel, N. (2007). Transition pathways between solid and liquid state in suspensions. *Physical Review E, 75*, 021505.

Higbie, J. (1991). Uncertainty in the linear regression slope. *American Journal of Physics, 59*(2), 184-185.

Hirt, C. W., & Nichols, B. D. (1981). Volume of fluid method for dynamics of free boundaries. *Journal of Computational Physics, 39*, 201-221.

Hopke, S. W., & Slattery, J. C. (1970). Upper and lower bounds on the drag coefficient of a sphere in an Ellis model fluid. *AIChE Journal 16*, 224-229.

Horsley, M. R., Horsley, R. R., & Wilson, K. C. (2004). Non-Newtonian effects on fall velocities of pairs of vertically aligned spheres. *Journal of Non-Newtonian Fluid Mechanics, 124*, 147-152.

Hsu, J. P., Hsieh, Y. H., & Tseng, S. (2005). Drag force on a rigid spheroidal particle in a cylinder filled with Carreau fluid. *Journal of Colloid and Interface Science, 284*, 729-741.

Jenson, V. G. (1959). Viscous flow around a sphere at low Reynolds number (<40). *Proceedings of the Royal Society London, Series A, Mathematical and Physical Sciences, 249*(1258), 346-366.

Jin, H., Phan-Thien, N., & Tanner, R. I. (1991). A finite element analysis of the flow past a sphere in a cylindrical tube: PIT fluid model. *Computational Mechanics, 8*(6), 409-422.

Jones, W. M., Prince, A. H., & Walters, K. (1994). The motion of a sphere falling under gravity in a constant-viscosity elastic liquid. *Journal of Non-Newtonian Fluid Mechanics, 53*, 175-196.

Joseph, D. D., Liu, Y. J., Polleto, M., & Feng, J. (1994). Aggregation and dispersion of spheres falling in viscoelastic fluids. *Journal of Non-Newtonian Fluid Mechanics, 54*, 45-86.

Kato, H., Tachibana, M., & Oikawa, K. (1972). On the drag of a sphere in polymer solutions. *Bulletin of JSME, 15*, 1556-1565.

Kawase, Y., & Moo-Young, M. (1986). Approximate solutions for power law fluid flow past a particle at low Reynolds number. *Journal of Non-Newtonian Fluid Mechanics, 21*(2), 167-177.

Kehlenbeck, R., & DiFelice, R. (1999). Empirical relationships for the terminal settling velocity of spheres in cylindrical columns. *Chemical Engineering & Technology, 21*(4), 303-308.

Kelessidis, V. C. (2004). An explicit equation for the terminal velocity of solid spheres falling in psudoplastic fluids. *Chemical Engineering Science, 59*, 4473-4445.

Kelessidis, V. C., & Mpandelis, G. (2004). Measurements and prediction of terminal velocity of solid spheres falling through stagnant pseudoplastic fluids. *Powder Technology, 147*, 117-125.

Kemiha, M., Frank, X., Poncin, S., & Li, H. Z. (2006). Origin of the negative wake behind a bubble rising in non-Newotnian fluids. *Chemical Engineering Science, 2006*, 4041-4047.

Keunings, R. (2000). *A Survey of Computational Rheology.* Paper presented at the Opening Session of the XIIIth International Congress on Rheology, Cambridge, UK.

Khan, A. R., & Richardson, J. F. (1987). The resistance to motion of a solid sphere in a fluid. *Chemical Engineering Communications, 62*, 135-150.

King, M. J., & Waters, N. D. (1972). The unsteady motion of a sphere in an elasto-viscous liquid. *Journal of Physics. D, Applied Physics, 5*, 141-150.

Kulicke, W. M., Kniewske, R., & Klein, J. (1982). Preparation, characterisation, solution properties and rheological behaviour of polyacrylamide. *Progress in Polymer Science, 8*, 373-468.

Kulicke, W. M., & Porter, R. S. (1979). Irregularities in steady flow for non-Newtonian fluids between cone and plate. *Journal of Applied Polymer Science, 23*(4), 953-965.

Kutschmann, E. M. (1997). *Yield Point Determination - a Critical Discussion of Different Methods* (No. (Paper also presented in the 1997 Nordic Rheology Conference in Reykjavik, Iceland)): Gebruder HAAKE GmbH.

Lapasin, R., Grassi, M., & Pricl, S. (1996). Fractal approach to rheological modeling of aggregate suspensions. In A. Ait-Kadi, J. M. Dealy, D. F. James & M. C. Williams (Eds.), *Proceedings of the XIIth International Congress on Rheology* (pp. 524). Quebec City, Canada.

LeClair, B. P., Hamielec, A. E., & Pruppacher, H. R. (1970). A theoretical and experimental study on the internal circulation in water drops falling at terminal velocity in air. *Journal of the Atmospheric Sciences, 29*(4), 728-740.

Lee, S. W., Ryu, S. H., & Kim, C. (2003). Studies on the axisymmetric sphere-sphere interaction problems in Newtonian and non-Newtonian fluids. *Journal of Non-Newtonian Fluid Mechanics, 110*(1), 1-25.

Li, R., Tao, C., Curran, T. A., & Smith, R. G. (1997). A digital photogrammetric system for large scale underwater spatial information acquisition. *Marine Geodesy, 20*(2/3), 163-173.

Lichti, D. D., Gumulya, M. M., & Horsley, R. R. (2009). Determination of trajectories of metallic spheres settling in non-Newtonian fluids. *The Photogrammetric Record, 24*(125), 37-50.

Liu, B. T., Muller, S. J., & Denn, M. M. (2002). Convergence of a regularization method for creeping flow of a Bingham material about a rigid sphere. *Journal of Non-Newtonian Fluid Mechanics, 102*(2), 179-191.

Liu, B. T., Muller, S. J., & Denn, M. M. (2003). Interactions of two rigid spheres translating collinearly in creeping flow in a Bingham material. *Journal of Non-Newtonian Fluid Mechanics, 113*(1), 49-67.

Liu, Y. J., & Joseph, D. D. (1993). Sedimentation of particles in polymer solutions. *Journal of Fluid Mechanics, 255*, 565-595.

Lopez, J., Hernandez, J., Gourez, P., & Faura, F. (2004). A volume of fluid method based on multidimensional advection and spline interface reconstruction. *Journal of Computational Physics, 195*, 718-742.

Lörstad, D., & Fuchs, L. (2001). A volume of fluid (VOF) method for handling solid objects using fixed Cartesian grids. In B. Sarler & C. A. Brebbia (Eds.), *Moving Boundaries VI - Computational Modelling of Free and Moving Boundary Problems* (pp. 143-152). UK: Wessez Institute of Technology, WIT Press.

Luo, X. L. (1998). An incremental difference formulation for viscoelastic flows and high resolution FEM solutions at high Weissenberg numbers. *Journal of Non-Newtonian Fluid Mechanics, 79*(1), 57-75.

Maalouf, A., & Sigli, D. (1984). Effects of body shape and viscoelasticity on the slow flow around an obstacle. *Rheologica Acta, 23*(1984), 497-507.

Machac, I., Siska, B., & Machacova, L. (2000). Terminal falling velocity of spherical particles moving through a Carreau model fluid. *Chemical Engineering and Processing, 39*, 365-369.

Marchal, J. M., & Crochet, M. J. (1987). A new mixed finite element for calculating viscoelastic flow. *Journal of Non-Newtonian Fluid Mechanics, 26*, 77-114.

Marin, G. (1998). Oscillatory rheometry. In A. A. Collyer & D. W. Clegg (Eds.), *Rheological Measurement, 2nd ed.* London: Chapman & Hall.

Marquardt, W., & Nijman, J. (1993). Experimental errors when using rotational rheometers. *Rheology 93, June 1993*.

Martinez, J. M., Chesneau, X., & Zeghmati, B. (2006). A new curvature technique calculation for surface tension contribution in PLIC-VOF method. *Computational Mechanics, 37*, 182-193.

McKinley, G. H. (2002). Steady and transient motion of spherical particles in viscoelastic liquids. In *Transport Processes in Bubbles, Drops and Particles* (2nd ed., pp. 338). New York: Taylor & Francis.

Media Cybernetics, Inc. (1999). *Optimas 6.5 User Guide and Technical Reference*: Media Cybernetics, L.P.

Mena, B., Manero, O., & Leal, L. G. (1987). The influence of rheological properties on the slow flow past spheres. *Journal of Non-Newtonian Fluid Mechanics, 26*(2), 247-275.

Mendelson, M. A., Yeh, P. W., & Brown, R. A. (1982). Finite element calculation of viscoelastic flow in a journal bearing: I. Small eccentricities. *Journal of Non-Newtonian Fluid Mechanics, 10*, 31-54.

Mewis, J., & Moldenaers, P. (1999). Rheometry of complex fluids. *Korea-Australia Rheology Journal, 11*(4), 313-320.

Mewis, J., & Wagner, N. J. (2009). Thixotropy. *Advances in Colloid and Interface Science, 147-148*, 214-227.

Missirlis, K. A., Assimacopoulos, D., Mitsoulis, E., & Chhabra, R. P. (2001). Wall effects for motion of spheres in power-law fluids. *Journal of Non-Newtonian Fluid Mechanics, 96*, 459-471.

Møller, P. C. F., Mewis, J., & Bonn, D. (2006). Yield stress and thixotropy: on the difficulty of measuring yield stresses in practice. *Soft Matter, 2*, 274-283.

Moore, F. (1959). The rheology of ceramic slips and bodies. *Transactions of the British Ceramic Society, 58*, 470-494.

Mosteller, F., & Tukey, J. W. (1977). *Data Analysis and Regression - a second course in statistics*. Reading, Massachusetts: Addison-Wesley Publishing Company.

Mujumdar, A., Beris, A. N., & Metzner, A. B. (2002). Transient phenomena in thixotropic systems. *Journal of Non-Newtonian Fluid Mechanics, 102*(2), 157-178.

Muzaferija, S., & Peric, M. (1999). Computation of free surface flows using interface-tracking and interface capturing methods. In O. Mahrenholtz & M. Markiewicz (Eds.), *Nonlinear Water Wave Interaction* (pp. 59-100). Southampton: WIT Press.

Nguyen, Q. D., & Boger, D. V. (1992). Measuring the Flow Properties of Yield Stress Fluids. *Annual Review of Fluid Mechanics, 24*, 47-88.

Ockendon, J. R., & Evans, G. A. (1972). The drag on a sphere in low Reynolds numbers flow. *Journal of Aerosol Science, 3*(4), 237-242.

Ookawara, S., Agrawal, M., Street, D., & Ogawa, K. (2005). *Modeling the motion of a sphere falling in a quescent Newtonian liquid in a cylindrical tube by using the macroscopic particle model.* Paper presented at the 7th World Congress of Chemical Engineerings, Glasgow, Scotland.

Oseen, C. W. (1927). *Neuere Methoden und ergebnisse in der hydrodynamik*. Leipzig: Akademische Verlagsgesellschaft.

Ourieva, G. N. (1999). *Instability in sterically stabilized suspensions.* Unpublished PhD, Katholicke Universiteit Leuven, Belgium.

Owens, R. G., & Phillips, T. N. (2002). *Computational Rheology*. London: Imperial College Press.

Özkan, F., Wörner, M., Wenka, A., & Soyhan, H. S. (2007). Critical evaluation of CFD codes for interfacial simulation of bubble-train flow in a narrow channel. *International Journal for Numerical Methods in Fluids, 55*, 537-564.

Papanastasiou, T. C. (1987). Flows of materials with yield. *Journal of Rheology, 31*(5), 385-404.

Patankar, N. A., & Hu, H. H. (2000). A numerical investigation of the detachment of the trailing particle from a chain sedimenting in Newtonian and viscoelastic fluids. *Journal of Fluids Engineering (ASME), 122*(3), 517-521.

Patankar, N. A., & Hu, H. H. (2001). Rheology of a suspension of particles in viscoelastic fluids. *Journal of Non-Newtonian Fluid Mechanics, 96*(3), 427-443.

Patankar, S. V. (1980). *Numerical Heat Transfer and Fluid Flow*. Washington DC: Hemisphere.

Patankar, S. V., & Spalding, D. B. (1972). A calculation procedure for heat, mass, and momentum transfer in three-dimensional parabolic flows. *International Journal of Heat and Mass Transfer, 15*, 1787-1806.

Pazwash, H., & Robertson, J. M. (1971). Fluid dynamic consideration of bottom materials. *Journal of Hydraulics Division, ASCE, 97*(9), 1317-1329.

Petera, J. (2002). A new finite element scheme using the Lagrangian framework for simulation of viscoelastic fluid flows. *Journal of Non-Newtonian Fluid Mechanics, 103*(1), 1-43.

Petera, J., & Nassehi, V. (1995). Use of the finite element modelling technique for the improvement of viscometry results obtained by cone-and-plate rheometers. *Journal of Non-Newtonian Fluid Mechanics, 58*(1), 1-24.

Peterfi, T. (1927). Die Abhebung der Befruchtungsmembran bei Seeigeleiern - Eine kolloidchemische Analyse des Befruchtungsvorganges. *Wilhelm Roux' Archiv für Entwicklungsmechanik der Organismen, 112*, 660-695.

Phan-Thien, N., Safari-Ardi, M., & Morales-Patino, A. (1997). Oscillatory and simple shear flows of a flour-water dough: a constitutive model. *Rheologica Acta, 36*(1), 38-48.

Photometrix, Pty Ltd. (2004). Australis 6.01 Users Manual. Retrieved September 21st, 2007, from www.photometrix.com.au

Pilate, G., & Crochet, M. J. (1981). Plane flow of a second-order fluid past submerged boundaries. *Journal of Rheology, 32*(6), 621-654.

Pillod, J. E., & Puckett, E. G. (2004). Second order-accurate volume-of-fluid algorithms for tracking material interfaces. *Journal of Computational Physics, 199*, 718-742.

Prahl, L., Holzer, A., Arlov, D., Revstedt, J., Sommerfeld, M., & Fuchs, L. (2007). On the interaction between two fixed spherical particles. *International Journal of Multiphase Flow, 33*(7), 707-725.

Prandtl, L. (1933). Neuere Ergebnisse Turbulenzforschung. *Z. Ver. Deutsch. Ing., 77*(5), 105-114.

Putz, A. M., Burghelea, T. I., Frigaard, I. A., & Martinez, D. M. (2008). Settling of an isolated spherical particle in a yield stress shear thinning fluid. *Physics of Fluids, 20*, 1-11.

Rae, D. (1962). Yield stress exerted on a body immersed in a Bingham fluid. *Nature 194*, 272.

Reddy, J. N., & Gartling, D. K. (2001). *The Finite Element Method in Heat Transfer and Fluid Dynamics* (2nd ed.). Boca Raton, Fl: CRC Press.

Reizes, J. A., & Leonardi, E. (2005). Numerical and experimental investigations of laminar natural convective flows. In A. J. Nowak, R. A. Bialecki & G. Wecel (Eds.), *Numerical Heat Transfer* (Vol. 82, pp. 21-46). Gliwice-Cracow, Poland: Institute of Thermal Technology, Silesial University of Technology.

Rhie, C. M., & Chow, W. L. (1983). Numerical study of the turbulent flow past an airfoil with trailing edge separation. *AIAA Journal, 21*(11), 1525-1532.

Riddle, M. J., Narvaez, C., & Bird, R. B. (1977). Interactions between two spheres falling along their line of centers in a viscoelastic fluid. *Journal of Non-Newtonian Fluid Mechanics, 2*, 23-35.

Sastry, N. V., Dave, P. N., & Valand, M. K. (1999). Dilute solution behaviour of polyacrylamides in aqueous media. *European Polymer Journal, 35*, 517-525.

Scott-Blair, G. W. (1943). *A Survey of General and Applied Rheology*. London: Pitman.

Shah, S. N., Fadili, Y. E., & Chhabra, R. P. (2007). New model for single spherical particle settling velocity in power law (visco-inelastic) fluids. *International Journal of Multiphase Flow, 33*, 51-66.

Sigli, D., & Coutanceau, M. (1977). Effect of finite boundaries on the slow isothermal flow of a viscoelastic fluid around a spherical obstacle. *Journal of Non-Newtonian Fluid Mechanics, 2*(1), 1-21.

Sigli, D., & Kaddioui, N. (1988). Combined influence of elasticity and inertia on the flow around a rigid sphere. *Progress and Trends in Rheology II*, 122.

Sisko, A. Q. (1958). Flow of lubricating greases. *Industrial and Engineering Chemistry 50*(12), 1789-1792.

Slatter, P. T. (1997). The rheological characterisation of sludges. *Water Science and Technology, 36*(11), 9-18.

Slibar, A., & Palsay, P. R. (1964). On the technical description of the flow of thixotropic materials. In M. Reiner & D. Abir (Eds.), *Second Order Effects in Elasticity, Plasticity, and Fluid Dynamics* (pp. 314-330). Oxford: Pergamon Press.

Solomon, M. J., & Muller, S. J. (1996). Flow past a spheres in polystyrene-based Boger fluids: the effect on the drag coefficient of finite extensibility, solvent quality and polymer molecular weight. *Journal of Non-Newtonian Fluid Mechanics, 62*(1), 81-94.

Stokes, G. G. (1851). On the effect of the internal friction of fluids on the motion of pendulums. *Transactions of the Cambridge Philosophical Society, 9*, 48-57.

Suetsugu, Y., & White, J. (1984). A theory of thixotropic plastic viscoelastic fluids with a time-dependent yield surface and its comparison to transient and steady state experiments on small particle filled polymer melts. *Journal of Non-Newtonian Fluid Mechanics, 14*, 121-140.

Sun, J., Smith, M. D., Armstrong, R. C., & Brown, R. A. (1999). Finite element method for viscoelastic flows based on the discrete adaptive viscoelastic stress splitting and the discontinuous Galerkin method: DAVSS-G/DG. *Journal of Non-Newtonian Fluid Mechanics, 86*(3), 281-307.

Thermo Fisher Scientific, Inc. (2009). Thermo Scientific HAAKE MARS Rheometer. Retrieved March 2, 2009, from www.thermo.com

Tirtaatmadja, V., Uhlherr, P. H. T., & Sridhar, T. (1990). Creeping motion of spheres in Fluid M-1. *Journal of Non-Newtonian Fluid Mechanics, 35*(2-3), 327-337.

Townsend, P. (1980). A numerical simulation of Newtonian and viscoelastic fluid flow past stationary and rotating cylinders. *Rheologica Acta, 6*, 219-243.

Tsuji, Y., Morikawa, Y., & Terashima, K. (1982). Fluid-dynamic interaction between two spheres. *International Journal of Multiphase Flow, 8*, 71-82.

Turian, R. M. (1967). An experimental investigation of the flow of aqueous non-Newtonian high polymer solutions past a sphere. *AIChE Journal, 13*(5), 999-1006.

Turton, R., & Clark, N. N. (1987). An explicit relationship to predict spherical particle terminal velocity. *Powder Technology, 53*, 127-129.

Tyabin, N. V. (1953). Discussion - some questions of the theory of viscoplastic flow of disperse systems. *Colloid J. U.S.S.R., 15*, 325.

Ubbink, O., & Issa, R. I. (1999). Method for capturing sharp fluid interfaces on arbitrary meshes. *Journal of Computational Physics, 153*, 26-50.

Uhlherr, P. H. T. (1986). *A novel method of measuring yield stress in static fluids.* Paper presented at the Proceedings of the 9th National Conference of Rheology, Adelaide.

Volarovich, M. P., & Gutkin, A. M. (1953). Theory of flow in a viscoplastic fluid. *Colloid Journal U.S.S.R., 15*, 153.

Walters, K., & Tanner, R. I. (1992). The motion of a sphere through an elastic liquid. In R. P. Chhabra & D. De Kee (Eds.), *Transport Processes in Bubbles, Drops, and Particles*. New York: Hemisphere.

Warichet, V., & Legat, V. (1997). Adaptive high-order prediction of the drag correction factor for the upper-convected Maxwell fluid. *Journal of Non-Newtonian Fluid Mechanics, 73*(1-2), 95-114.

Whitmore, R. L., & Boardman, G. (1962). Reply to Rae. *Nature, 194*, 272.

Wildemuth, C. R., & Williams, M. C. (1985). A new interpretation of viscosity and yield stress in dense slurries: coal and other irregular particles. *Rheologica Acta, 24*, 75-91.

Wilson, K. C., Addie, G. R., Sellgren, A., & Clift, R. (2006). *Slurry transport using centrifugal pumps, 3rd ed.* New York: Springer Science & Business.

Wilson, K. C., & Horsley, R. R. (2004). *Calculating fall velocities in non-Newtonian (and Newtonian) fluids: a new view.* Paper presented at the 16th International Conference on Hydrotransport of Solids, BHR Group, Cranfield, UK.

Wilson, K. C., Horsley, R. R., Kealy, T., Reizes, J. A., & Horsley, M. R. (2003). Direct prediction of fall velocities in non-Newtonian materials. *International Journal of Mineral Processing, 71*, 17-30.

Winter, H. H., Mours, M., & Baumgartel, M. (1998). Computer-aided methods in rheometry. In A. A. Collyer & D. W. Clegg (Eds.), *Rheological Measurement, 2nd ed.* London: Chapman & Hall.

Won, D., & Kim, C. (2004). Alignment and aggregation of spherical particles in viscoelastic fluid under shear flow. *Journal of Non-Newtonian Fluid Mechanics, 117*(2-3), 141-146.

Wu, G. H., Wu, B. Y., Ju, S. H., & Wu, C. C. (2003). Non-isothermal flow of a polymeric fluid past a submerged circular cylinder. *International Journal of Heat and Mass Transfer, 46*, 4733-4739.

Wu, J., & Manasseh, R. (1998). Dynamics of dual particle settling under gravity. *International Journal of Multiphase Flow, 24*, 1343-1358.

Yang, B., & Khomami, B. (1999). Simulations of sedimentation of a sphere in a viscoelastic fluid using molecular based constitutive models. *Journal of Non-Newtonian Fluid Mechanics, 82*(2-3), 429-452.

Yasuda, K. Y., Armstrong, R. C., & Cohen, R. E. (1981). Shear-flow Properties of Concentrated-solutions of linear and Star Branched Polystyrenes. *Rheological Acta, 20*(2), 163-178.

Yoshioka, N., Adachi, K., & Ishimura, H. (1971). On creeping flow of a viscoplastic fluid past a sphere. *Kagaku Kogaku, 10*, 1144-1152.

Youngs, D. L. (1982). Time-dependent multi-material flow with large fluid distortion. *Numerical Methods for Fluid Dynamics, 1982*, 273-285.

Zhu, C., Lam, K., Chu, H. H., Tang, X. D., & Liu, G. (2003). Drag forces of interacting spheres in power-law fluids. *Mechanics Research Communications, 30*, 651-662.

Appendix A. Experimental setup and data analysis

A.1 First Optical system

The settling velocity of the spheres in this experiment is measured by considering the average velocity between the sensors. The maximum % error, therefore, should be encountered at the high range of velocity values. The settling velocities obtained through the experiment ranges from 0.05 – 0.6 m/s.

Consider a sphere settling at a terminal velocity of 0.6 m/s. The average distance between the optical sensors is 0.0906 ± 0.001 m. The time taken for the sphere to travel this distance is then 0.151 s. The uncertainties involved with the time measurement is 0.01s.

The percentage error involved with the estimation of settling velocities over two optical sensors is thus:

$$\%\,\text{error} = \sqrt{\left(\frac{\Delta\text{distance}}{\text{distance}}\right)^2 + \left(\frac{\Delta t}{t}\right)^2}$$

$$= \sqrt{\left(\frac{0.001}{0.0906}\right)^2 + \left(\frac{0.01}{0.0151}\right)^2} = 6.71\%$$

In comparison, the % error of a sphere settling at 0.3 m/s is 3.49%.

In the estimation of the terminal settling velocity, an average velocity value over a set of optical sensors is normally taken, thus considerably reducing the maximum potential percentage error. Considering a velocity measurement over a set of 15 sensors, the maximum % error of a sphere settling at 0.6 m/s is thus:

$$\%\,\text{error} = \frac{\%\,\text{error}_{(2\,\text{sensors})}}{\sqrt{\text{number of sensors} - 1}} = \frac{6.71\%}{\sqrt{14}} = 1.79\%$$

A.2 Second optical system

A.2.1 Principles of photogrammetry

The set of collinearity equations presented in equation 3-1 represents an idealisation of the actual optical geometry found in real cameras. In the equation, no accounts of the distortions caused by the imperfections of the lenses were provided. The main distortions in cameras can generally be classified into 2 categories: radial and decentring (or tangential).

In close-range photogrammetry, these imperfections are typically signified by the use of analytical correction models:

$$\Delta X = \overline{X}\left(k_1 r^2 + k_2 r^4 + k_3 r^6\right) + p_1\left(r^2 + 2\overline{X}^2\right) + 2p_2 XY + a_1\overline{X} + a_2\overline{Y}$$

$$\Delta Y = \overline{Y}\left(k_1 r^2 + k_2 r^4 + k_3 r^6\right) + p_2\left(r^2 + 2\overline{Y}^2\right) + 2p_1 XY$$

where k_1, k_2, and k_3 are the radial lens distortion parameters, p_1 and p_2 the decentring distortion parameters, a_1 the x-axis scale term, and a_2 the shear term. The variables $\overline{X}$ and $\overline{Y}$ represent the distance between the photo-coordinates in the image frame from the perspective centre:

$$\overline{X} = X - X_p$$

$$\overline{Y} = Y - Y_p$$

The variable r represents the radial distance between the photo-coordinates in the image from perspective centre:

$$r^2 = \overline{X}^2 + \overline{Y}^2$$

The constants for this model have been characterised for each camera during the calibration process. This analytical model is then incorporated into the calculation algorithm written by Lichti (Lichti et al., 2009).

It should also be noted that other forms of distortion exist, namely instabilities in interior orientation, out-of-plane distortion, and in-plane distortion, however their significance are generally very low that their effects are normally omitted from general close-range photogrammetry applications not requiring triangulation accuracies of beyond 1:100,000 (Fraser, 1997). In this study, the satisfactory results of the calibration indicate that these effects can be disregarded.

A.2.2 Details of stereo-photogrammetry system

The stereo-photogrammetry measurement system consists of:

- 2 x Jai CVM4+CL cameras (see details in Table A-1)
- 2 x PC-Camlink PCI frame grabbers
- 2 x CL cables
- 2 x Camera power supplies
- 2 x Tamron 25-HB/12 lenses
- Labjack U12 (sync generator)

The two video cameras were synchronised and triggered through a USB-based automation device (LabJack U12), capable of acquiring digital input from the computer and generating low voltage differential signals for the automated start-up and triggering of the cameras. The cameras feature the Camera Link standardised interface, allowing the use of a PC-CamLink PCI Frame Grabber, which are plug-in boards for a computer's expansion slots, used for the acquisition and storage of individual, digital still frames recorded by the video cameras. The details of the parameters obtained from the calibration of the cameras have been listed in Table A-1.

Table A-1: The calibration parameters of the cameras used for the stereo-photogrammetry system.

Camera		
Model		Jai CV-M4
Scanning system		Progressive scan
Picture elements		1300 (h) x 1300 (v) effective pixels
Cell size		6.7 (h) x 6.7 (v) μm
Camera1 - Calibration results		
Principal distance, c		12.5683 mm
Principal point		(0.1752, -0.0174) mm
Radial lens distortion	k_1	1.19E-03
	k_2	1.26E-06
	k_3	5.78E-08
Decentring lens distortion	P_1	-9.93E+00
	P_2	1.16E-04
Camera2 - Calibration results		
Principal distance, c		12.5572 mm
Principal point		(0.1564, -0.0793) mm
Radial lens distortion	k_1	1.21E-03
	k_2	3.79E-06
	k_3	-3.94E-08
Decentring lens distortion	P_1	-2.68E-05
	P_2	-6.82E-05

A.2.3 Error analysis

The contribution of the uncertainties associated with the manual 2D measurement of sphere positions from the perspectives of the two cameras was examined by considering the settling experiment of two chrome steel spheres (6.35 mm diameter) with an initial distance of 25.0 mm in 1.0% Floxit solution. The level of uncertainty in the 2D measurement is estimated to be a quarter of the sphere diameter, ± 1.5875 mm. To determine the maximum level of error obtained from this uncertainty, the X- and Y- co-ordinates of one of the spheres (sphere A) from both cameras are alternately combined with the uncertainty figure. The resulting discrepancy of the triangulation results (x, y, z) is then used as a gauge for the effects of this uncertainty on the integrity of the experimental results. The results of this calculation are presented in Tables A-2 to A-4.

Table A-2: The resolved 3D co-ordinates (x, y, z) of one of the spheres (sphere A) in an experiment involving two chrome steel spheres (6.35 mm diameter) in 1.0% Floxit solution. (X_1, Y_1) and (X_2, Y_2) represent the 2D co-ordinates of sphere A from the perspectives of cameras 1 and 2, respectively.

Camera 1		Camera 2		Triangulation + refraction		
X_1 (mm)	Y_1 (mm)	X_2 (mm)	Y_2 (mm)	x (m)	y (m)	z (m)
79.000	445.667	12.333	578	1.6415	1.2159	1.4544
178.000	443.333	127.061	576.025	1.6405	1.216	1.3548
277.000	442.333	240.618	570.398	1.6409	1.2191	1.2579
377.667	441.333	357.254	560.879	1.6416	1.2251	1.1605
479.333	438.667	476.178	550.452	1.6409	1.2319	1.0624
581.522	438.131	595.569	544.4	1.6416	1.2349	0.9645
675.078	436.661	705.499	540.286	1.6412	1.2365	0.8748
785.842	435.304	836.576	536.155	1.6409	1.2377	0.7683
883.233	434.614	950.914	533.306	1.641	1.2381	0.6747
984.815	433.696	1069.33	530.09	1.6409	1.2387	0.5767
1087.207	433.015	1189.338	527.823	1.6407	1.2385	0.4765

Table A-3: Error analysis of the stereo-photogrammetry system, indicated by the discrepancies in the resolved 3D co-ordinates presented in Table A-1 with the co-ordinates calculated based on: (I) (X_1+1.5875, Y_1) and (X_2, Y_2); (II) (X_1, Y_1) and (X_2+1.5875, Y_2); (III) (X_1+1.5875, Y_1) and (X_2+1.5875, Y_2).

Case I. $x_1 + \delta x$			Case II. $x_2 + \delta x$			Case III. $x_1 + \delta x$, $x_2 + \delta x$		
dx (mm)	dy (mm)	dz (mm)	dx (mm)	dy (mm)	dz (mm)	dx (mm)	dy (mm)	dz (mm)
-0.25	0.25	-0.65	0.25	-0.25	-0.75	0.00	0.00	-1.45
-0.25	0.25	-0.65	0.20	-0.20	-0.75	-0.05	0.05	-1.45
-0.20	0.20	-0.60	0.15	-0.15	-0.70	-0.05	0.00	-1.40
-0.10	0.15	-0.65	0.10	-0.10	-0.75	0.00	0.00	-1.40
-0.10	0.10	-0.65	0.05	-0.05	-0.75	-0.05	0.00	-1.40
-0.05	0.05	-0.65	0.00	-0.05	-0.75	0.00	0.00	-1.40
0.00	0.05	-0.60	-0.05	0.00	-0.70	0.00	0.00	-1.35
0.05	0.00	-0.65	-0.05	0.05	-0.75	0.00	0.00	-1.40
0.15	-0.05	-0.65	-0.10	0.05	-0.75	0.05	0.00	-1.40
0.20	-0.10	-0.65	-0.15	0.10	-0.75	0.05	0.00	-1.40
0.25	-0.10	-0.65	-0.15	0.15	-0.75	0.05	0.00	-1.40

Table A-4: Error analysis of the stereo-photogrammetry system, indicated by the discrepancies in the resolved 3D co-ordinates presented in Table A-1 with the co-ordinates calculated based on: (I) (X_1, Y_1+1.5875) and (X_2, Y_2); (II) (X_1, Y_1) and (X_2, Y_2+1.5875); (III) (X_1, Y_1+1.5875) and (X_2, Y_2+1.5875).

Case IV. $y_1 + \delta y$			Case V. $y_2 + \delta y$			Case VI. $y_1 + \delta y$, $y_2 + \delta y$		
dx (mm)	dy (mm)	dz (mm)	dx (mm)	dy (mm)	dz (mm)	dx (mm)	dy (mm)	dz (mm)
1.45	-0.20	0.30	-0.20	-1.30	-0.10	1.25	-1.45	0.15
1.45	-0.15	0.20	-0.20	-1.25	-0.10	1.25	-1.40	0.10
1.45	-0.20	0.20	-0.20	-1.25	-0.05	1.25	-1.45	0.10
1.50	-0.20	0.15	-0.15	-1.25	-0.05	1.35	-1.45	0.05
1.45	-0.15	0.10	-0.20	-1.25	-0.05	1.30	-1.45	0.05
1.50	-0.20	0.05	-0.15	-1.25	0.00	1.35	-1.50	0.05
1.50	-0.20	0.05	-0.15	-1.25	0.05	1.35	-1.45	0.05
1.50	-0.15	-0.05	-0.15	-1.25	0.05	1.35	-1.45	0.00
1.50	-0.15	-0.10	-0.15	-1.25	0.05	1.35	-1.45	-0.05
1.50	-0.15	-0.10	-0.15	-1.25	0.10	1.35	-1.45	-0.05
1.50	-0.15	-0.15	-0.15	-1.25	0.10	1.35	-1.40	-0.05

Based on the data presented in Tables A-3 and A-4, it was concluded that the largest discrepancy in the resolved 3D co-ordinates resulting from this uncertainty is 1.50 mm.

Appendix B. Rheology of test fluids

B.1 Steady-state rheological properties of Floxit solutions

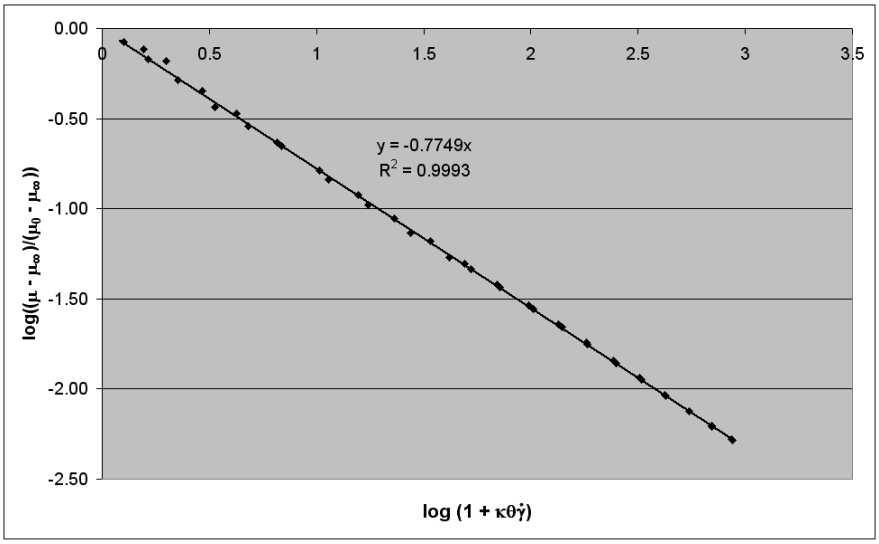

Figure B-1: Determination of the power constant, m, using the steady-state viscosity data of 0.9% Floxit solution.

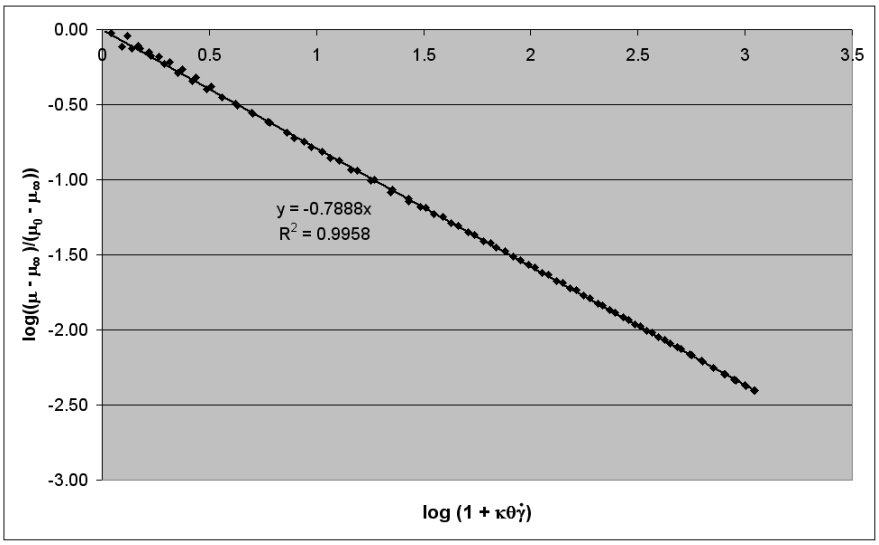

Figure B-2: Determination of the power constant, m, using the steady state viscosity data of 1.0% Floxit solution.

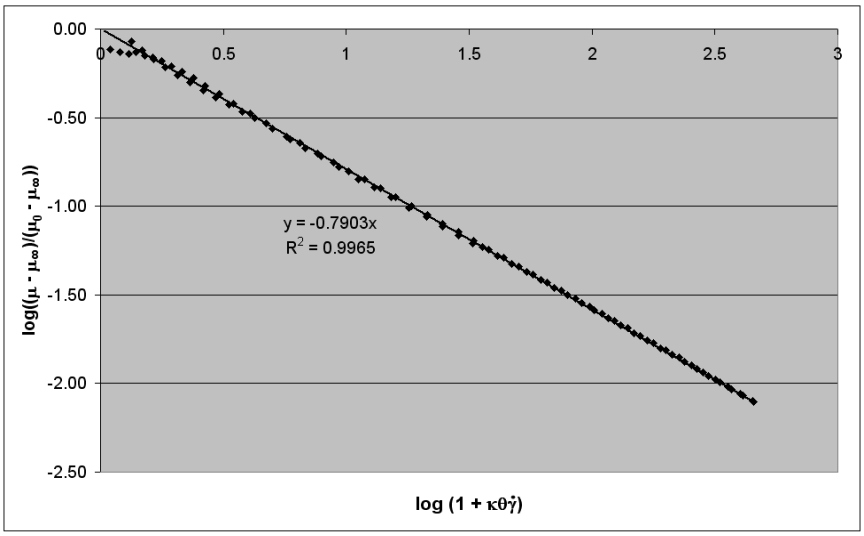

Figure B-3: Determination of the power constant, m, using the steady state viscosity data of 1.1% Floxit solution.

B.2 MATLAB numerical codes

B.2.1 Controlled-rate ramp

```
f = inline('(1-lambda)/48.48 - 0.2343*lambda*0.02*t', 't', 'lambda')
[t,lambda] = ode45(f, [0 1250], 1)
mu = 0.0001+(54.9-0.0001).*power(lambda, 0.7749)
gammadot = 0.02*t
tau = mu.*gammadot
plot(gammadot,tau)
```

B.2.2 Controlled-stress ramp

```
f = inline('(1-lambda)/48.48 - 0.2343*lambda*(0.1*t)/(0.0001+(54.9-
0.0001)*power(lambda,0.7749))', 't', 'lambda')
[t,lambda] = ode45(f, [0 220], 1)
mu = 0.0001+(54.9-0.0001).*power(lambda, 0.7749)
tau = 0.1*t
gammadot = tau./mu
```

B.3 More results of oscillatory (SAOS) testings

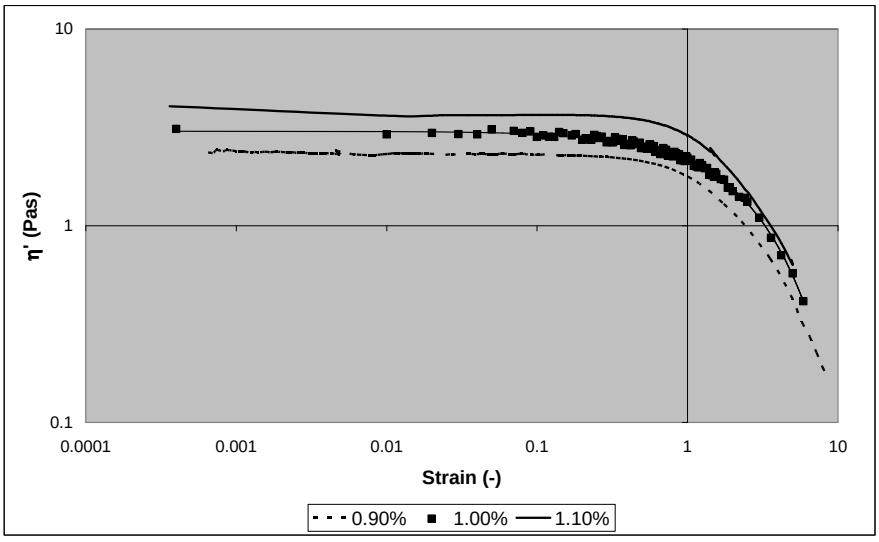

Figure B-4: SAOS amplitude sweep test, conducted at a frequency of 1.0 Hz, of 1.0% Floxit solution.

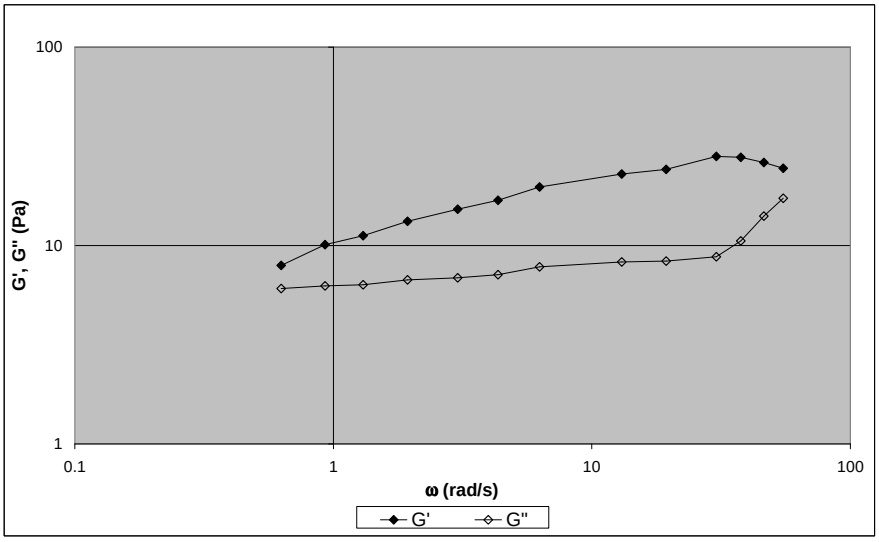

Figure B-5: SAOS frequency test, conducted at a shear stress of 1.0 Pa of 1.0% Floxit solution.

B.4 First normal stress difference

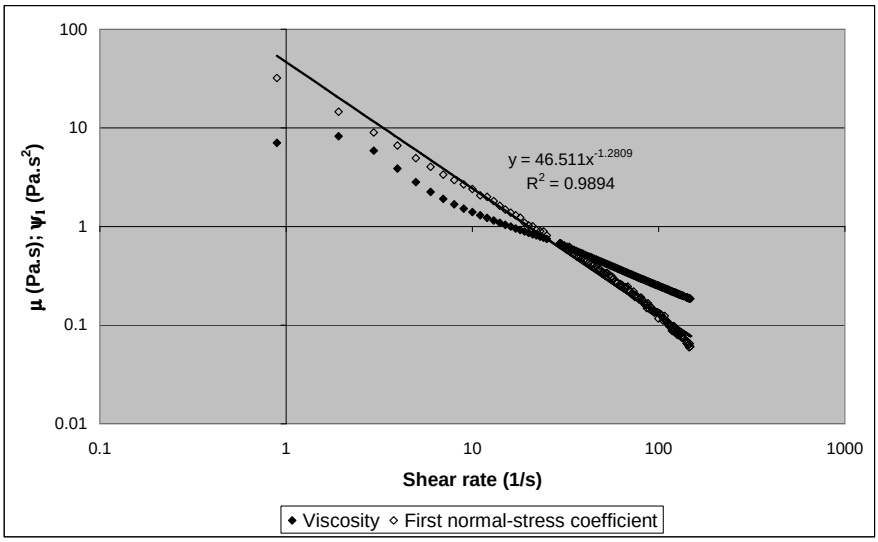

Figure B-6: Shear viscosity and first normal stress coefficient of 1.0% Floxit solution.

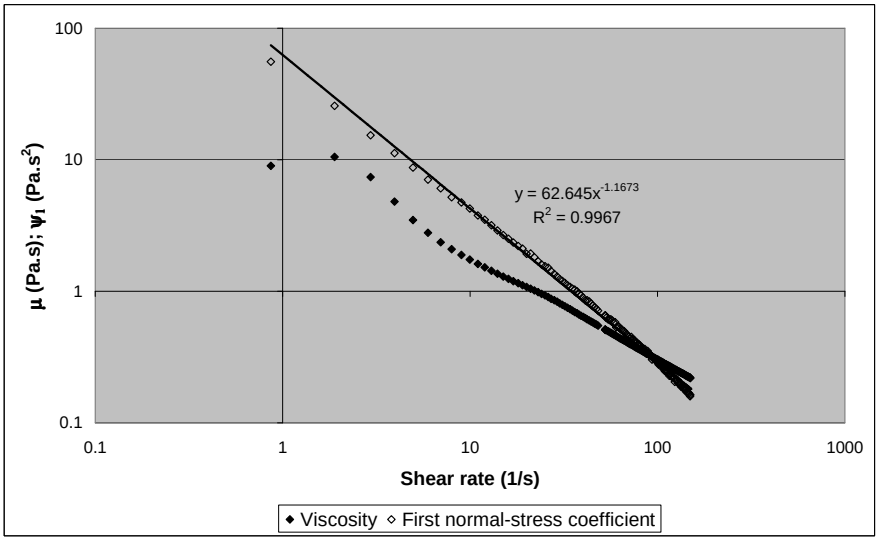

Figure B-7: Shear viscosity and first normal stress coefficient of 1.1% Floxit solution.

Appendix C. CFD analysis

C.1 UDF code for the semi-viscoplastic fluid model

```
#include <udf.h>
#include <mem.h>
#include <unsteady.h>

static real lambda_old_1 = 1.0;
real lambda_old, s_dot;
real lambda_new;

DEFINE_PROPERTY(carreau_viscosity,c,t)
{
/*
* lambda_new = lambda_old + t_step*((1-lambda)/r - alpha*lambda_old*s_dot)
* mu = muinf+(mu0-muinf)*lambda_new^m
*/

real t_step,r,alpha,mu0,muinf,m,real_time,mu;
real NV_VEC(cell_position);

/* Get cell centroid location:
cell_position[0] = x
cell_position[1] = y
cell_position[2] = z in 3D only */
C_CENTROID(cell_position,c,t);

mu0 =  54.9;
muinf =  0.0001;
alpha = 0.234323;
r =  48.48;
m =  0.7749;

/* time&timestep */
real_time = CURRENT_TIME;
t_step = CURRENT_TIMESTEP;
s_dot = C_STRAIN_RATE_MAG(c,t);

/*lambda calculation */
if (real_time > 0.)
        {
        lambda_new = lambda_old + t_step*((1-lambda_old)/r -
alpha*lambda_old*s_dot);
        }
else
        {
        lambda_new = lambda_old_1 + t_step*((1-lambda_old_1)/r -
alpha*lambda_old_1*s_dot);
        }

/* mu */
mu = muinf+(mu0-muinf)*pow(lambda_new,m);

/*
CX_Message("Sdot is %10.3e\n", s_dot);
CX_Message("Viscosity is %10.3e\n", mu);
CX_Message("lambda is %10.3e\n", lambda_new);
*/

return mu;
}
```

```
DEFINE_EXECUTE_AT_END(update_lambda_sdot_values)
{

#if !RP_HOST /* Execute on Node or serial process */

  Domain *d;
  Thread *t;
  cell_t c;


   d = Get_Domain(2);

thread_loop_c (t,d)
  {

   if (FLUID_THREAD_P(t))
     {
      begin_c_loop_int(c,t)
         {
         C_UDMI(c,t,0) = lambda_new;
         C_UDMI(c,t,1) = s_dot;
         lambda_old = lambda_new;
         }
      end_c_loop_int(c,t)
      }
   }
# endif
}
```

C.2 Selection of the viscous parameters for the numerical study in Newtonian fluids

Using equation 5-20, the Reynolds numbers of all the experiments conducted in the Floxit solutions were calculated. These values were found to range from 0.13 to 5.0.

In the case of spheres settling in a Newtonian fluid, the following C_D-Re correlation for $0.01 \leq Re \leq 20$ was applied (Clift et al., 1978):

$$C_D = \frac{24}{Re}\left[1 + 0.1315\,Re^{0.82 - 0.05\log Re}\right] \qquad \textbf{(C-1)}$$

where C_D is the drag coefficient:

$$C_D = \frac{4Dg(\rho_s - \rho_f)}{3\rho_f V^2} \qquad \textbf{(C-2)}$$

Based on the drag correlation suggested by Clift et al. (1978), the drag coefficient corresponding to the range of Reynolds number obtained experimentally is thus

$7.1 \leq C_D \leq 186.9$. The corresponding settling velocities could then be calculated, and were found to be 0.36 and 0.07 m/s for the minimum and maximum values of drag coefficient, respectively. Based on these figures, the values of μ_N were determined to be $0.72 \leq \mu_N \leq 5.33$ Pa.s (using equation 5-21).

C.3 Theoretical settling velocities of particles in Newtonian fluids

In calculating the terminal settling velocity of spheres in Newtonian fluid, the correlation presented in equation C-1 was applied. Furthermore, to account for the effects of the bounding walls in the simulation, the following correlations were applied for spheres settling under creeping conditions (Re < 1.0, Francis (1933)):

$$\frac{V_w}{V} = \left(\frac{1 - D/W_D}{1 - 0.475\, D/W_D} \right)^4$$

where V_W is the settling velocity of the sphere, taking into account the effects of the walls surrounding it, V the velocity of sphere settling in an unbounded environment, and W_D the hydraulic diameter of the column.

Beyond the creeping region (Re > 1.0), the correlation for wall correction factor suggested by Kehlenbeck and DiFelice (1999) was used:

$$\frac{V_w}{V} = \frac{1 - (D/W_D)^P}{1 + \left[(D/W_D)/(D/W_D)_0 \right]^p}$$

where p and $(D/W_D)_0$ were calculated as follows:

$$p = 1.44 + 0.5466 \mathrm{Re}^{0.434}$$

$$\frac{(D/W_D)_0 - 0.283}{1.2 - (D/W_D)_0} = 0.041 \mathrm{Re}^{0.524}$$

C.4 'Solid' viscosity for the numerical study in semi-viscoplastic fluids

The estimated values of maximum fluid viscosity for each configuration of the numerical simulation conducted, using the proposed semi-viscoplastic fluid model, have been listed in Table C- 1. The terminal settling velocities of the spheres were approximated using the correlation suggested by Wilson et al. (2004; 2003) (see details of calculation in Section D.1) and the minimum values of the shear-rate experienced by the fluid were then estimated as per equation 5-22. Equation 4-6 was applied to determine the corresponding values of fluid viscosity. The representative value of viscosity for the phase representing the solid sphere is then calculated as follows:

$$\mu_s = 200\mu_f$$

Table C- 1: The estimated values of maximum fluid viscosity, as well as the required values of 'solid' viscosity, for each configuration of numerical simulations (see equation 5-22).

Sphere		Fluid					Viscosity (Pa.s)	
D (mm)	ρ_s (kg/m^3)	μ_0 (Pa.s)	$\kappa.\theta$	m	V_t (m/s)	$\dot{\gamma}_{min}$ (1/s)	μ_f	μ_s
9.90	8000	54.9	11.36	0.7749	0.389	3.86	2.88	576.6
7.92	8000	54.9	11.36	0.7749	0.236	2.92	3.55	710.8
5.94	8000	54.9	11.36	0.7749	0.110	1.81	5.08	1015.5
9.90	7000	54.9	11.36	0.7749	0.308	3.05	3.44	687.8
9.90	6000	54.9	11.36	0.7749	0.229	2.27	4.30	859.9
9.90	8000	70.18	12.74	0.7888	0.349	3.46	3.48	696.0
5.94	8000	70.18	12.74	0.7888	0.089	1.48	6.65	1330.4
9.90	8000	101.8	14.55	0.7903	0.215	2.13	6.58	1315.2
7.92	8000	101.8	14.55	0.7903	0.114	1.42	8.98	1795.9

Appendix D. Data analysis

D.1 Analysis of particle settling velocity

The equivalent viscosity of the fluid surrounding a settling sphere was calculated based on the correlation suggested by Wilson et al. (2004; 2003):

$$\text{For} \quad \mathrm{Re}^* << 1 \qquad \frac{V_t}{V^*} = \frac{\mathrm{Re}^*}{3}$$

$$\mathrm{Re}^* \le 10 \qquad \frac{V_t}{V^*} = \frac{\mathrm{Re}^*}{3\left(1 + 0.08\,\mathrm{Re}^{*1.2}\right)} + \frac{2.80}{1 + 3.0\left(10^4\right)\left(\mathrm{Re}^{*-3.2}\right)}$$

$$10 < \mathrm{Re}^* \le 260 \qquad \log\left(\frac{V_t}{V^*}\right) = 0.2069 + 0.500\log\left(\frac{\mathrm{Re}^*}{10}\right) - 0.158\left[\log\left(\frac{\mathrm{Re}^*}{10}\right)\right]^{1.72}$$

$$\mathrm{Re}^* > 260 \qquad \frac{V_t}{V^*} = 4.24$$

where V* is the shear velocity of the particle (see equation 2-38) and Re* the particle Reynolds number (equation 2-39).

The representative fluid structure parameter above a settling sphere ($\overline{\lambda}_{ss}$) was calculated based on the shear stress caused by the submerged weight of the particle, as defined by Wilson et al. (2004; 2003) (equations 2-40 and 2-41). Below the sphere, the representative fluid structure parameter ($\overline{\lambda}_0$) was calculated based on the amount of time that has lapsed since the fluid was sheared by the preceding sphere (t) (see equation 6-2).

For two spheres of different densities, the following calculation procedure was utilised:

- Sphere 1: ρ_s = 7792.2 kg/m^3; D = 0.00635 m
- Sphere 2: ρ_s = 8876.0 kg/m^3; D = 0.00635 m
- Fluid (0.9% Floxit solution): μ_∞ = 0.0001Pa.s, μ_0 = 54.9 Pa.s; m = 0.7749, θ = 48.48 s, κ = 0.2343 s-1, α = 1.625, P = 1.667
- Time lapse between the two spheres: t = 4.56 s.

Table D-1: Mean surficial shear stress of the spheres.

Parameter	Sphere 1	Sphere 2
V* (m/s)	0.2659	0.2863
$\bar{\tau}$ (Pa)	70.54	81.79
τ (Pa)	21.16	24.54
μ_{ss} (Pa.s)	0.3394	0.2046
λ_{ss}	1.41 x 10^{-3}	7.34 x 10^{-4}

The representative fluid structure parameter below the first sphere is 1.0. On the other hand, the representative fluid structure parameter below the second sphere is:

$$\bar{\lambda}_0 = 1 + \exp\left(\frac{-t}{\theta}\right)\left(\bar{\lambda}_{ss\text{-}1} - 1\right) = \mathbf{9.147 \times 10^{-2}}$$

Equation 6-4 can then be used to determine the effective fluid structure parameter, and hence also the equivalent viscosity, of the fluid surrounding each sphere:

- Sphere 1: $\bar{\lambda}_{eff}$ = 4.833 x 10^{-3}, μ_{eq} = 0.8813 Pa.s
- Sphere 2: $\bar{\lambda}_{eff}$ = 1.907 x 10^{-3}, μ_{eq} = 0.4287 Pa.s

Sample results of this calculation have been presented in Tables D-2 to D-4.

Table D-2: Selected data points of the settling velocity of the first sphere in an experiment of two vertically-aligned spheres.

% Floxit	ρ_s (kg/m^3)	D (mm)	$\bar{\lambda}_{ss}$	$\bar{\lambda}_{eff}$	μ_{eq} (Pa.s)	Re*	V/V*	V (m/s) observed	% error
0.9	8876	6.35	7.34E-04	4.83E-03	0.881	2.06	0.577	0.155	-6.4%
0.9	8876	7.95	2.73E-04	3.46E-03	0.680	3.73	0.902	0.284	-1.6%
0.9	7792.2	6.35	1.41E-03	6.06E-03	1.050	1.60	0.469	0.128	2.9%
0.9	7792.2	7.95	5.07E-04	4.26E-03	0.800	2.98	0.769	0.242	5.6%
0.9	7638	6.35	1.56E-03	6.28E-03	1.079	1.54	0.454	0.123	2.8%
0.9	7638	7.95	5.81E-04	4.46E-03	0.828	2.81	0.737	0.213	-1.7%
1.0	8876	6.35	8.48E-04	5.08E-03	1.088	1.67	0.485	0.126	-9.0%
1.0	8876	7.95	2.95E-04	3.55E-03	0.821	3.09	0.790	0.221	-12.4%
1.0	7792.2	6.35	1.70E-03	6.47E-03	1.316	1.28	0.386	0.096	-6.3%
1.0	7792.2	7.95	5.72E-04	4.44E-03	0.978	2.44	0.660	0.182	-7.7%
1.0	7638	6.35	1.89E-03	6.72E-03	1.356	1.23	0.372	0.091	-6.5%
1.0	7638	7.94	6.61E-04	4.66E-03	1.017	2.29	0.629	0.176	-5.0%
1.0	7638	9.53	2.79E-04	3.49E-03	0.809	3.79	0.911	0.281	-4.3%
1.1	8876	6.35	2.66E-03	7.58E-03	2.173	0.84	0.278	0.075	-5.5%
1.1	8876	7.95	9.34E-04	5.25E-03	1.627	1.56	0.458	0.148	1.3%
1.1	8876	9.53	3.96E-04	3.92E-03	1.293	2.58	0.691	0.263	8.5%
1.1	7638	6.35	6.31E-03	1.04E-02	2.778	0.59	0.195	0.050	-1.6%
1.1	7638	7.95	2.08E-03	6.95E-03	2.028	1.15	0.350	0.107	4.1%

Table D-3: Selected data points of the settling velocity of the combined spheres in an experiment of two vertically-aligned spheres.

	Sphere 1		Sphere 2								V (m/s)	
% Floxit	ρ_s (kg/m^3)	D (mm)	ρ_s (kg/m^3)	D (mm)	β	$\bar{\lambda}_{ss}$	$\bar{\lambda}_{eff}$	μ_{eq} (Pa.s)	Re*	V/V*	observed	% error
0.9	8876	6.35	8876	6.35	0.5341	2.45E-04	3.34E-03	0.662	3.06	0.784	0.278	-8.7%
0.9	8876	7.95	8876	7.95	0.5341	8.41E-05	2.35E-03	0.505	5.75	1.185	0.503	-13.9%
0.9	7792.2	6.35	7792.2	6.35	0.5341	4.72E-04	4.16E-03	0.785	2.39	0.651	0.206	-4.7%
0.9	7638	6.35	7638	6.35	0.5341	5.23E-04	4.31E-03	0.806	2.30	0.632	0.200	-5.8%
0.9	7638	7.95	7638	7.95	0.5341	1.80E-04	3.01E-03	0.611	4.36	1.000	0.368	-8.8%
0.9	7638	6.35	8876	6.35	0.5341	3.30E-04	3.69E-03	0.714	2.78	0.731	0.224	2.1%
0.9	7638	7.95	8876	7.95	0.5341	1.22E-04	2.65E-03	0.554	5.03	1.094	0.397	-3.3%
0.9	7792.2	6.35	8876	6.35	0.5341	3.14E-04	3.63E-03	0.706	2.83	0.740	0.258	-9.7%
0.9	7792.2	7.95	8876	7.95	0.5341	1.16E-04	2.61E-03	0.547	5.12	1.105	0.435	-10.4%
0.9	7638	6.35	7638	7.95	0.6125	1.35E-04	2.74E-03	0.568	4.06	0.954	0.307	0.5%
1.0	8876	6.35	8876	6.35	0.5341	1.52E-04	2.86E-03	1.299	1.56	0.457	0.147	1.0%
1.0	8876	7.95	8876	7.95	0.5341	4.83E-05	1.97E-03	0.969	3.00	0.772	0.256	10.3%
1.0	7792.2	7.95	7792.2	7.95	0.5341	9.80E-05	2.47E-03	1.159	2.33	0.637	0.218	-0.8%
1.0	7638	7.94	7638	7.94	0.5341	1.10E-04	2.57E-03	1.194	2.23	0.615	0.193	6.7%
1.0	7638	7.95	8876	6.35	0.4421	9.60E-03	1.21E-02	2.040	1.15	0.351	0.105	9.8%
1.0	7792.2	7.95	8876	6.35	0.4421	8.43E-03	1.15E-02	1.953	1.21	0.367	0.112	8.6%
1.0	8876	6.35	8876	7.95	0.5868	4.64E-04	4.14E-03	1.403	1.81	0.519	0.186	-0.9%
1.0	8876	6.35	7792.2	7.95	0.6494	8.76E-03	1.17E-02	1.978	1.19	0.362	0.118	1.4%
1.0	8876	6.35	7792.2	9.53	0.7633	4.31E-03	9.02E-03	1.566	1.74	0.502	0.187	-8.1%
1.0	8876	6.35	7638	9.53	0.7633	5.07E-03	9.56E-03	1.650	1.64	0.477	0.176	-7.7%
1.0	7638	7.95	8876	7.95	0.5341	5.41E-04	4.36E-03	1.464	1.90	0.541	0.172	10.3%
1.0	7792.2	6.35	8876	6.35	0.5341	1.99E-04	3.12E-03	1.393	1.43	0.426	0.128	5.1%
1.0	7792.2	7.95	8876	7.95	0.5341	6.82E-05	2.20E-03	1.057	2.65	0.704	0.244	1.8%
1.1	8876	6.35	8876	6.35	0.5341	8.37E-04	5.06E-03	1.579	1.28	0.386	0.140	-10.8%
1.1	8876	7.95	8876	7.95	0.5341	2.70E-04	3.45E-03	1.168	2.49	0.671	0.269	-8.9%
1.1	7638	6.25	7638	6.25	0.5341	1.87E-03	6.68E-03	1.967	0.94	0.315	0.090	3.5%
1.1	7638	7.95	7638	7.95	0.5341	6.03E-04	4.52E-03	1.446	1.84	0.527	0.193	-8.2%
1.1	7638	6.35	8876	6.35	0.5341	1.15E-03	5.64E-03	1.720	1.16	0.352	0.115	-4.4%

Table D-4: Selected data points of the settling velocity of the second sphere in an experiment of two vertically-aligned spheres.

	Sphere 1			Sphere 2										
% Floxit	ρ_s (kg/m^3)	D (mm)	$\bar{\lambda}_{ss}$	ρ_s (kg/m^3)	D (mm)	$\bar{\lambda}_{ss}$	t (s)	$\bar{\lambda}_0$	$\bar{\lambda}_{eff}$	μ_{eq} (Pa.s)	Re*	V/V*	V (m/s) observed	% error
0.9	8876	6.35	7.34E-04	8876	6.35	7.34E-04	2.97	6.03E-02	1.66E-03	0.386	4.70	1.050	0.292	2.8%
0.9	8876	6.35	7.34E-04	8876	6.35	7.34E-04	2.01	4.14E-02	1.48E-03	0.353	5.14	1.108	0.333	-4.8%
0.9	8876	6.35	7.34E-04	8876	6.35	7.34E-04	0.99	2.10E-02	1.24E-03	0.307	5.91	1.203	0.349	-1.3%
0.9	8876	7.95	2.72E-04	8876	7.95	2.72E-04	1.60	3.29E-02	9.13E-04	0.242	10.49	1.648	0.512	3.0%
0.9	8876	7.95	2.72E-04	8876	7.95	2.72E-04	0.72	1.52E-02	7.30E-04	0.204	12.47	1.787	0.592	-3.3%
0.9	8876	7.95	2.72E-04	8876	7.95	2.72E-04	0.37	7.82E-03	6.27E-04	0.181	14.03	1.882	0.608	-0.9%
0.9	7638	7.95	5.78E-04	8876	7.95	2.72E-04	2.05	4.21E-02	9.89E-04	0.258	9.85	1.597	0.493	3.8%
0.9	7638	7.95	5.78E-04	8876	7.95	2.72E-04	1.78	3.68E-02	9.47E-04	0.249	10.20	1.626	0.534	-2.4%
0.9	7638	7.95	5.78E-04	8876	7.95	2.72E-04	1.05	2.21E-02	8.10E-04	0.221	11.50	1.722	0.554	-0.5%
0.9	7638	6.35	1.56E-03	7638	7.95	5.77E-04	6.51	1.27E-01	1.95E-03	0.436	5.35	1.135	0.342	-2.3%
0.9	7638	6.35	1.56E-03	7638	7.95	5.77E-04	3.91	7.92E-02	1.65E-03	0.383	6.08	1.224	0.392	-8.1%
0.9	7638	6.35	1.56E-03	7638	7.95	5.77E-04	1.16	2.52E-02	1.16E-03	0.293	7.98	1.422	0.396	5.5%
1.0	7792.2	7.95	3.44E-04	7792.2	7.95	3.44E-04	3.81	7.04E-02	1.55E-03	0.803	2.94	0.762	0.230	-1.3%
1.0	7792.2	7.95	3.44E-04	7792.2	7.95	3.44E-04	1.86	3.52E-02	1.32E-03	0.704	3.35	0.838	0.248	0.4%
1.0	7792.2	7.95	3.44E-04	7792.2	7.95	3.44E-04	1.05	2.02E-02	1.19E-03	0.648	3.64	0.887	0.257	2.7%
1.0	7638	7.95	3.85E-04	7638	7.95	3.85E-04	2.06	3.88E-02	1.40E-03	0.739	3.16	0.802	0.225	4.6%
1.0	7638	7.95	3.85E-04	7638	7.95	3.85E-04	1.62	3.08E-02	1.33E-03	0.712	3.28	0.824	0.240	1.0%
1.0	7638	7.95	3.85E-04	7638	7.95	3.85E-04	4.34	7.98E-02	1.67E-03	0.851	2.74	0.723	0.219	-2.7%
1.0	7792.2	7.95	3.44E-04	8876	7.95	1.70E-04	2.22	4.18E-02	1.02E-03	0.576	4.41	1.008	1.013	-0.5%
1.0	7792.2	7.95	3.44E-04	8876	7.95	1.70E-04	1.28	2.44E-02	8.99E-04	0.521	4.88	1.073	1.053	1.9%
1.0	7792.2	7.95	3.44E-04	8876	7.95	1.70E-04	0.78	1.50E-02	8.19E-04	0.484	5.25	1.123	1.193	-5.9%
1.0	7638	6.35	3.83E-04	8876	7.95	1.70E-04	13.01	2.20E-01	1.68E-03	0.856	2.97	0.767	0.233	5.3%
1.0	7638	6.35	3.83E-04	8876	7.95	1.70E-04	6.16	1.11E-01	1.34E-03	0.716	3.55	0.871	0.262	6.6%
1.0	7638	6.35	3.83E-04	8876	7.95	1.70E-04	2.94	5.48E-02	1.09E-03	0.607	4.18	0.974	0.284	9.9%
1.1	7792.2	6.35	5.87E-03	7792.2	6.35	5.87E-03	11.04	2.24E-01	5.56E-03	1.701	0.98	0.326	0.083	3.4%
1.1	7792.2	6.35	5.87E-03	7792.2	6.35	5.87E-03	9.98	2.05E-01	5.38E-03	1.659	1.00	0.310	0.082	-1.0%
1.1	7792.2	6.35	5.87E-03	7792.2	6.35	5.87E-03	8.23	1.74E-01	5.07E-03	1.582	1.05	0.324	0.084	1.8%
1.1	8876	7.95	9.31E-04	8876	7.95	9.31E-04	4.33	9.35E-02	1.92E-03	0.736	3.46	0.855	0.283	-3.3%
1.1	8876	7.95	9.31E-04	8876	7.95	9.31E-04	3.67	8.00E-02	1.81E-03	0.702	3.62	0.883	0.296	-4.4%
1.1	8876	7.95	9.31E-04	8876	7.95	9.31E-04	2.06	4.60E-02	1.48E-03	0.600	4.23	0.981	0.319	-1.4%
1.1	8876	7.95	9.31E-04	8876	6.35	2.66E-03	0.56	1.34E-02	1.73E-03	0.678	2.68	0.710	0.225	-9.7%
1.1	8876	7.95	9.31E-04	8876	6.35	2.66E-03	0.37	9.29E-03	1.65E-03	0.652	2.78	0.731	0.206	1.7%
1.1	8876	7.95	9.31E-04	8876	6.35	2.66E-03	0.30	7.60E-03	1.62E-03	0.644	2.82	0.738	0.199	6.4%
1.1	7792.2	6.35	5.28E-03	7792.2	7.95	1.86E-03	9.42	1.95E-01	3.34E-03	1.139	2.07	0.581	0.181	-4.5%
1.1	7792.2	6.35	5.28E-03	7792.2	7.95	1.86E-03	8.31	1.75E-01	3.20E-03	1.101	2.14	0.597	0.180	-1.6%
1.1	7792.2	6.35	5.28E-03	7792.2	7.95	1.86E-03	7.18	1.53E-01	3.04E-03	1.058	2.23	0.616	0.176	4.0%

D.2 The interaction of two horizontally-aligned spheres

The horizontal distance between the two spheres, d_H, was calculated as follows:

$$d_H = \sqrt{(x_B - x_A)^2 + (y_B - y_A)^2}$$

where (x_A, y_A) and (x_B, y_B) are the co-ordinates of sphere A and sphere B, respectively, according to the horizontal axes. The results of this calculation for one of the experiments have been shown in Table D-5.

The distance required for the spheres to converge, ℓ_C, is defined as the vertical distance that has to be travelled by the spheres prior to their convergence. This point of convergence has been defined as the instance where the trailing sphere starts to accelerate towards the leading one, i.e. when the horizontal separation distance between the spheres reaches levels that are below 0.002 m. In the sample results presented in Table D-5, this point of convergence occurs at time of 9.6 s. Therefore, ℓ_C = 0.4518 m.

The rate of convergence between the two spheres, V_H,, is estimated by taking the average rate-of-change in d_H, prior to the convergence of the spheres:

$$V_H \approx \frac{\partial d_H}{\partial t} = \textbf{- 0.00238}$$

The regression of this linear fit, i.e. the Pearson correlation coefficient (R^2), was found to be 0.9737. The error involved with this analysis can therefore be estimated as follows (Higbie, 1991):

$$\text{error in linear slope} = (\text{slope})\frac{\tan\left(\cos^{-1}\left(R^2\right)\right)}{\sqrt{N-2}} \quad \textbf{= 7.94 x 10-5 ~ 3.3\%}$$

where N is the number of data points used to determine the slope.

Table D-5: Sample results of an experiment involving two horizontally-aligned spheres (6.35 mm stainless steel spheres in 1.1% Floxit solution). All distances are in meters.

time	A			B			dH
(s)	x	y	z	x	y	z	
0	1.6405	1.212	1.4625	1.645	1.2366	1.4625	0.02501
0.2	1.6407	1.2126	1.4513	1.6446	1.2365	1.4495	0.02422
0.4	1.6417	1.2119	1.4475	1.6444	1.2357	1.4413	0.02395
0.6	1.6407	1.2126	1.4379	1.6446	1.2365	1.4322	0.02422
0.8	1.6406	1.213	1.4289	1.6448	1.2357	1.4218	0.02309
1.0	1.6403	1.2133	1.4189	1.6447	1.2358	1.4115	0.02293
1.2	1.6408	1.213	1.4091	1.644	1.2346	1.4012	0.02184
1.4	1.6408	1.2137	1.3989	1.6435	1.2354	1.3916	0.02187
1.6	1.6406	1.2138	1.3888	1.6447	1.2362	1.3818	0.02277
1.8	1.64	1.2138	1.3784	1.6442	1.2351	1.3715	0.02171
2	1.6398	1.214	1.3682	1.6447	1.2355	1.3621	0.02205
2.2	1.64	1.214	1.3596	1.6446	1.2355	1.3522	0.02199
2.4	1.641	1.2144	1.3487	1.6445	1.2352	1.3429	0.02109
2.6	1.6401	1.2148	1.3384	1.6445	1.2351	1.3328	0.02077
2.8	1.6403	1.2148	1.3284	1.6446	1.2348	1.3233	0.02046
3	1.6405	1.2153	1.3185	1.6452	1.235	1.3133	0.02025
3.2	1.6412	1.2154	1.3085	1.6449	1.2349	1.3034	0.01985
3.4	1.6408	1.2157	1.2986	1.6444	1.2347	1.2941	0.01934
3.6	1.6408	1.2158	1.288	1.6443	1.2344	1.285	0.01893
3.8	1.6411	1.2162	1.2785	1.6441	1.2344	1.2753	0.01845
4.0	1.6408	1.2164	1.268	1.6447	1.2341	1.2657	0.01812
4.2	1.6403	1.2169	1.2581	1.6446	1.2338	1.2566	0.01744
4.4	1.6407	1.2168	1.2482	1.6445	1.2338	1.2466	0.01742
4.6	1.6415	1.2172	1.2381	1.6446	1.2336	1.237	0.01669
4.8	1.641	1.2173	1.2282	1.644	1.2335	1.2274	0.01648
5	1.6403	1.2179	1.2184	1.6445	1.2331	1.2184	0.01577
5.2	1.6404	1.2181	1.2088	1.6449	1.2329	1.2087	0.01547
5.4	1.6409	1.2183	1.1987	1.6453	1.2324	1.1995	0.01477
5.6	1.6404	1.2186	1.1888	1.6444	1.2323	1.19	0.01427
5.8	1.6403	1.2188	1.1791	1.6448	1.2317	1.1807	0.01366
6	1.6407	1.2189	1.169	1.6452	1.2311	1.1716	0.01300
6.2	1.6407	1.219	1.159	1.6441	1.2309	1.1626	0.01238
6.4	1.6405	1.2191	1.149	1.6428	1.2307	1.1531	0.01183
6.6	1.6407	1.2193	1.1389	1.6431	1.23	1.1437	0.01097
6.8	1.6408	1.2194	1.1292	1.6438	1.2291	1.1346	0.01015
7.0	1.6399	1.2193	1.1185	1.6426	1.2285	1.1251	0.00959
7.2	1.6407	1.2193	1.1086	1.6428	1.2277	1.1152	0.00866
7.4	1.6411	1.2193	1.0983	1.6429	1.2269	1.1062	0.00781
7.6	1.6409	1.219	1.0877	1.642	1.2263	1.0965	0.00738
7.8	1.6407	1.2191	1.0774	1.6419	1.2255	1.0862	0.00651
8	1.6402	1.219	1.067	1.6426	1.2245	1.0769	0.00600
8.2	1.6408	1.2187	1.0565	1.642	1.2236	1.067	0.00504
8.4	1.6404	1.2184	1.0468	1.642	1.2228	1.057	0.00468
8.6	1.6404	1.2184	1.0361	1.6408	1.2224	1.0472	0.00402
8.8	1.6399	1.2185	1.0254	1.6418	1.2215	1.0381	0.00355
9	1.6402	1.2183	1.0152	1.6417	1.2211	1.027	0.00318
9.2	1.6397	1.2177	1.0056	1.6409	1.2207	1.018	0.00323

Sample results of an experiment involving two horizontally-aligned spheres (continued)

9.4	1.6401	1.2176	0.9952	1.6403	1.2202	1.0083	0.00261
9.6	1.6408	1.2176	0.9846	1.6406	1.2193	1.0007	0.00171
9.8	1.64	1.2175	0.974	1.6397	1.2188	0.989	0.00133
10.0	1.6398	1.2175	0.9628	1.6398	1.2184	0.9764	0.00090
10.2	1.6402	1.2173	0.9508	1.6399	1.2181	0.9609	0.00085
10.4	1.6409	1.2173	0.9379	1.6396	1.2173	0.9451	0.00130
10.6	1.6403	1.217	0.9238	1.6403	1.217	0.9238	0
10.8	1.6402	1.2166	0.9068	1.6402	1.2166	0.9068	0
11	1.6403	1.2164	0.8896	1.6403	1.2164	0.8896	0
11.2	1.64	1.2163	0.8722	1.64	1.2163	0.8722	0
11.4	1.6401	1.2162	0.8547	1.6401	1.2162	0.8547	0
11.6	1.6401	1.2157	0.837	1.6401	1.2157	0.837	0
11.8	1.6402	1.216	0.8192	1.6402	1.216	0.8192	0
12	1.6403	1.2158	0.8017	1.6403	1.2158	0.8017	0

Considering that the level of uncertainty involved with the measurement of terminal settling velocity, V_t, is 2.0% (this was calculated based on the difference in the average settling velocity of the two spheres), the total uncertainty of the first dimensionless interaction parameter (see equation 7-1) can be calculated as follows:

$$\text{error in first dimensionless parameter} = \frac{\Delta \ell_C}{\ell_C} + \frac{\Delta V_t}{V_t} = \mathbf{2\ \%}$$

In comparison, the total uncertainty of the second dimensionless interaction parameter (see equation 7-4) is:

$$\text{error in first dimensionless parameter} = \frac{\Delta d_0}{d_0} + \frac{\Delta V_H}{V_H} = \mathbf{9\ \%}$$

Sample results of this analysis have been presented in Table D-6.

Table D-6: Select data of the interaction between two horizontally-aligned spheres

% Floxit	ρ_s (kg/m^3)	D (mm)	d0 (mm)	V_H (m/s)	V_t (m/s)	$\dot{\gamma}_G$ (1/s)	μ_{ss} (Pa.s)	WeG	$\left[\frac{V_H}{d_0\dot{\gamma}}\right]_{calculated}$	$\left[\frac{V_H}{d_0\dot{\gamma}}\right]_{observed}$	% error
0.9	7792.2	6.35	25.0	4.92E-03	0.116	4.86	0.358	599.4	3.78E-03	3.43E-03	10.1%
0.9	7792.2	6.35	37.5	2.43E-03	0.117	2.93	0.358	1439.4	1.02E-03	1.11E-03	-8.1%
0.9	7638.0	6.35	37.5	2.88E-03	0.102	2.55	0.387	1531.1	9.78E-04	1.46E-03	-33.0%
0.9	7792.2	6.35	50.0	1.18E-03	0.116	2.08	0.358	2608.6	4.39E-04	4.04E-04	8.8%
0.9	7638.0	6.35	50.0	1.11E-03	0.109	1.96	0.387	2409.2	4.63E-04	4.21E-04	9.8%
1.0	7638.0	7.95	25.0	7.26E-03	0.180	8.30	0.218	1685.5	2.40E-03	2.92E-03	-17.7%
1.0	8876.0	6.35	37.5	3.52E-03	0.128	3.23	0.281	3178.3	5.97E-04	1.09E-03	-45.2%
1.0	7792.2	6.35	37.5	3.13E-03	0.097	2.44	0.486	1307.6	1.10E-03	1.95E-03	-43.5%
1.0	8876.0	6.35	50.0	1.26E-03	0.129	2.31	0.281	4871.3	3.05E-04	2.92E-04	4.1%
1.0	7792.2	6.35	50.0	1.01E-03	0.097	1.74	0.486	2014.4	5.22E-04	4.70E-04	11.1%
1.0	7638.0	6.35	50.0	1.01E-03	0.093	1.67	0.529	1751.3	5.77E-04	5.24E-04	10.1%
1.1	7792.2	6.35	25.0	2.56E-03	0.052	2.18	1.695	179.6	1.08E-02	8.87E-03	21.9%
1.1	7638.0	6.35	25.0	2.57E-03	0.049	2.06	1.843	158.5	1.21E-02	9.80E-03	23.5%
1.1	7792.2	7.95	25.0	1.15E-04	0.008	0.39	0.696	9964.8	8.99E-04	7.70E-04	16.8%
1.1	7638.0	7.95	25.0	4.13E-03	0.119	5.49	0.762	371.2	8.16E-03	6.86E-03	19.0%
1.1	8876.0	9.95	25.0	8.44E-03	0.247	12.89	0.208	2636.1	2.48E-03	1.97E-03	26.0%
1.1	7792.2	6.35	37.5	1.31E-03	0.053	1.32	1.695	320.9	3.52E-03	2.90E-03	21.0%
1.1	8876.0	7.95	37.5	3.65E-03	0.148	3.93	0.243	7409.9	5.51E-04	6.86E-04	-19.7%
1.1	8876.0	6.35	50.0	8.84E-04	0.076	1.36	0.981	1068.0	8.35E-04	7.39E-04	13.1%

Appendix E. Photos of the experimental apparatus and equipment

Figure E-1: Setup of column.

Figure E-2: Assembled ball dropper

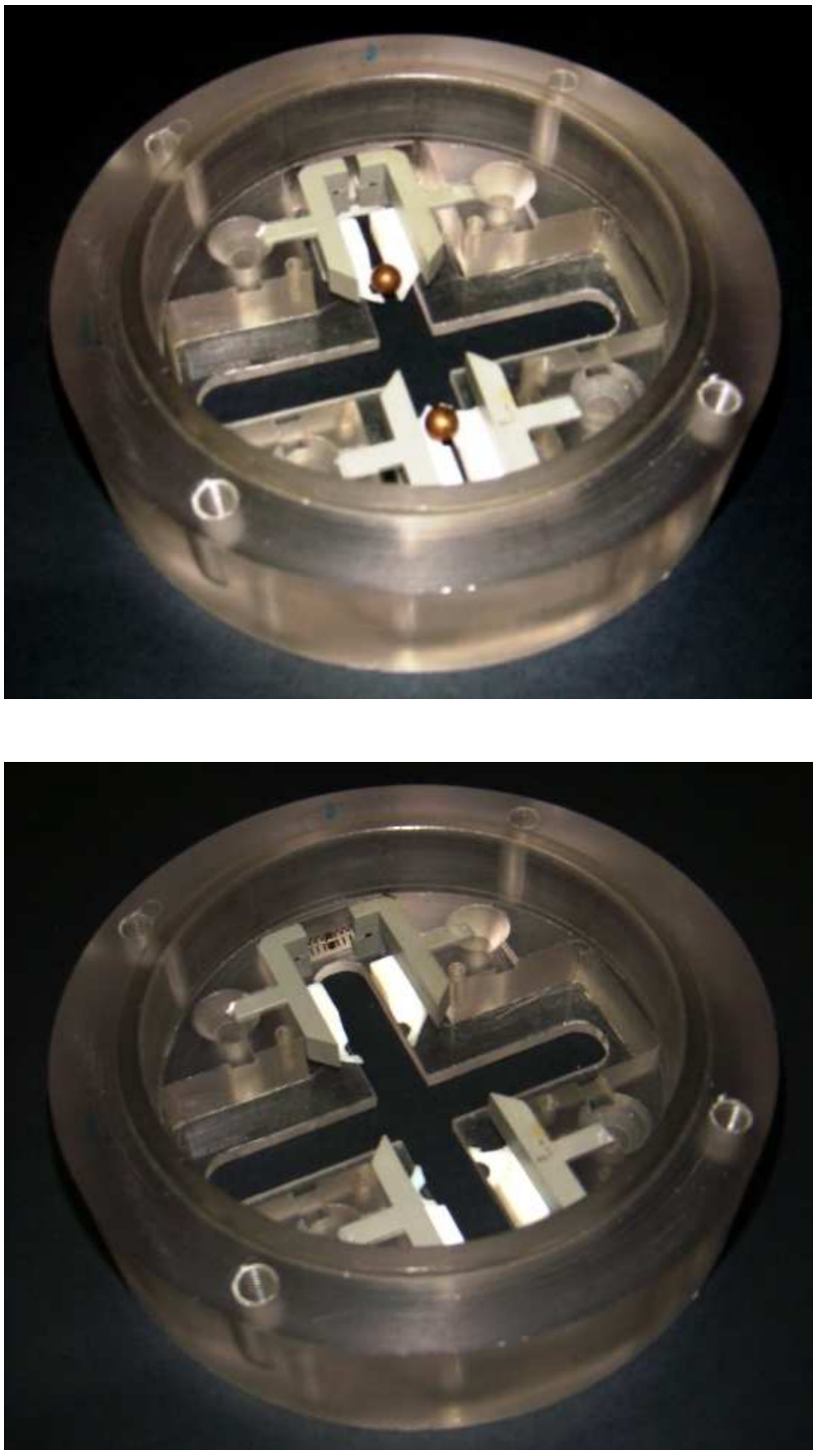

Figure E-3: The bottom part of the ball dropper, showing its ball-release mechanism.